Polymer Aluminophosphate Mixed Matrix Membranes for Gas Separations

By

Benjamin R. Vaughan

Dissertation submitted to the Faculty of

Virginia Polytechnic Institute and State University

in partial fulfillment of the requirements for the degree of

DOCTOR OF PHILOSOPHY

in

Chemical Engineering

Dr. Eva Marand, Chair

Dr. William Koros
Dr. S. Ted Oyama
Dr. Richey Davis

April 3, 2007

Blacksburg ,VA

Keywords: layered aluminophosphates, mixed matrix membranes, gas separations

Polymer Aluminophosphate Mixed Matrix Membranes for Gas Separations

Benjamin R. Vaughan

(Abstract)

It is well known that clays dispersed in a polymer matrix decrease the permeability of all gases through that membrane. Our objective was to explore the effects on transport when a microporous layered aluminophosphate was added to a polymer matrix. The clay like layered aluminophosphate used contains sheets with 8MR ring openings in the size range of 3-4 Å. The molecular level dispersion of this material into a polymer matrix is theorized to increase selectivity by molecular sieving. A previous study performed in our laboratory showed an increase in He/CH_4 selectivity when this aluminophosphate (8MR-AlPO) was dispersed in a fluorinated polyimide. The increase in selectivity was explained as size sieving by the aluminophosphate sheets where small gas species can pass through the microstructure and large gas species have to take a tortuous path around the sheets.

We performed several studies with different polymer materials in the attempt to make composite membranes that corroborated the previously seen increases in gas selectivity. In some cases different surfactants were used to swell 8MR-AlPO. In the first set of studies the methods used to produce the fluorinated polyimide composites were repeated using polydimethyl siloxane (PDMS), a copolymer of a fluorinated polyimide and PDMS, polysulfone, Matrimid, and cellulose acetate as the matrix materials. In general gas permeation studies of these materials showed an overall decrease in permeability with increasing addition of 8MR-AlPO but no substantial increase in selectivity. In an attempt to increase the chances of exfoliating and dispersing the layered aluminophosphate, an in-situ method using poly(etherimide) (PEI) was polymerized in the presence of 8MR-AlPO was employed. Mixed matrix membranes of PEI with 5wt% 8MR-AlPO were successfully fabricated and the transport properties measured. Microscopy revealed that the composites made with the 8MR-AlPO treated with a reactive surfactant showed better dispersion than those treated with the nonreactive surfactants. The permeability of gases changed very little as the result of adding 8MR-AlPO to PEI and no substantial increase in selectivity was observed. Finally, we incorporated a similar layered aluminophosphate with larger 12MR (6-7Å) openings into polysulfone. These composites showed barrier behavior but no increases in selectivity.

Acknowledgements

The research presented in this dissertation was performed with the assistance, input, and encouragement of many people.

A special thanks to my advisor Dr. Eva Marand who encouraged me to pursue my PhD, and provided me guidance and many opportunities to grow as a scientist. Thank you to my committee Dr. Koros, Dr. Davis, and Dr. Oyama who provided helpful input and guidance on my project. Thanks to Dr. Mirosalav Bleha, Jakub Peter, and Dr. Zdenka Sedlakova for good scientific interaction as well as friendship and hospitality during my times in the Czech Republic.

I would like to thank many of the staff including Mike Vaught, Riley Chan, Diane Cannaday, and Chris Moore who helped me in many ways to complete my work here at Virginia Tech. I would also like to thank my lab mates Sangil Kim, Will James, and Jose Hurrera-Alonso who were fun to work with, good friends, and helped me on a daily basis. Thanks also to the guys in my incoming class who were a great encouragement, to many other students and faculty in the department who made my endeavor possible, and to Dr. Cox who guided and helped me to transition into the chemical engineering department.

Thank you to Steve McCartney for a lot of help collecting SEM and TEM for my project. Thanks also to Tom Glass who ran solid state NMR for my project, and Tomonori Saito who performed TGA on 8MR-AlPO. Thank you to Dr. Tsapatisis of the University of Minnesota who provided me with 12MR-AlPO for one of my experiments. Also a thanks to Vadim Guliants for running our samples for porosity.

A special thanks to my wife Amy who supported me in many ways and made it possible for me to finish my PhD. I would not have been able to stay the course without her help with life's daily needs and loving support. Thanks to my little girls Mary and Sarah for understanding when daddy had to work instead of playing with them. Also, a sincere thanks to my mother Lynn who watched our girls for many hours making it possible for me to pursue school and to my father the original Dr. Vaughan for also helping with the girls and giving me good advice and words of encouragement that helped me finish.

Finally, all praise honor and glory goes to the triune God who makes all things possible. "For from him and through him and to him are all things. To him be the glory forever! Amen"

Table of Contents

List of Figures

Chapter 1

Chapter 2

Chapter 3

Chapter 4

Chapter 5

Chapter 6

Chapter 7

Chapter 8

List of Tables

Chapter 8

Chapter 1

Introduction and Objectives

1.1 Introduction and Objectives

It is known that polymeric materials can separate gas mixtures using a solution diffusion mechanism. In general, polymeric materials with high permeability have low selectivity, and polymeric materials that display high selectivity have low permeability. This trade off was documented by Robeson in a paper which correlated the permeability vs. selectivity of many of the available polymeric materials.[1] Robeson established an "upper-bound" for gas pairs which is illustrated in Figure 1. This upper-bound line represents the limit of polymeric materials to both permeate and separate gas species effectively.

Zeolites are another class of materials that can be made into membranes and are known to separate mixed gases.[2] Many of the properties of zeolite membranes surpass those of polymeric membranes including better chemical and thermal stability, higher flux, and better separation coefficients. The limitation of zeolite membranes is in the processing of the material. It is expensive to fabricate them into membrane modules and the membranes themselves are often fragile mechanically.

An ideal membrane would combine the durability and processability of polymers with the separation properties of zeolite membranes. One strategy to overcome the individual limitations of these materials and use them for gas separations is to combine them together. This type of hybrid material has been called a "mixed matrix membrane". A number of papers have been written on the benefits and challenges associated with making zeolite polymer mixed matrix membranes.[3-9]

The objective of this work was to develop a mixed matrix material using an aluminophosphate dispersed in a polymeric matrix that has improved gas separation properties when compared to the neat polymer. The aluminophosphate $[Al_3P_4O_{16}]^{3-} \cdot 3[NH_3CH_2CH_3]^+$ (8MR-AlPO) has some unique properties that may allow it to be used as a molecular sieve. We aimed to create a material with high selectivity and versatile processability by combining 8MR-AlPO with a variety of polymers. The project involved very basic research in fabrication of polymer aluminophosphate membranes and measuring the resulting transport properties.

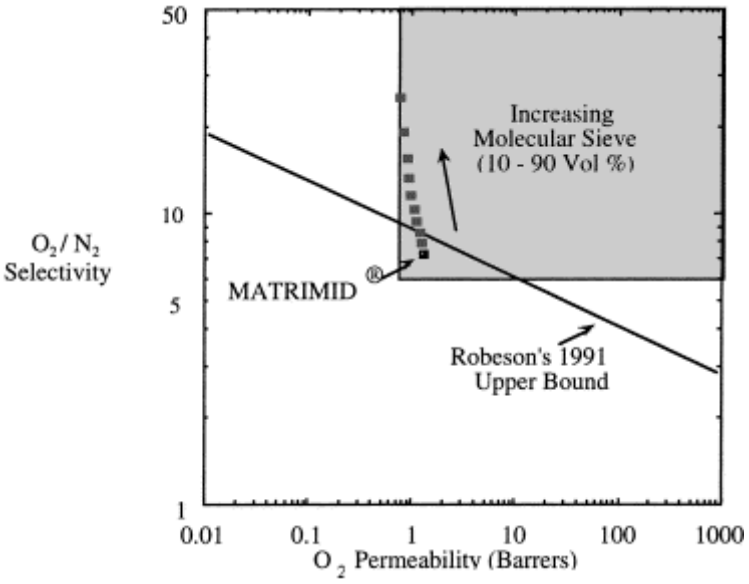

Figure 1.1 Permeability vs. Selectivity plot showing an example of potential improvements predicted for the high performance polyimide Matrimid containing zeolite 4A (grey area is the commercially attractive region) adapted from Koros and Mahajan. [4]

The predicted trend seen in Figure 1.1 is the general trend we expect to see when 8MR-AlPO is added to a polymer matrix. The permeability of the fast gas should decrease slightly but a substantial increase in selectivity should accompany the decrease in permeability. Jeong et al. performed some preliminary work in this area with positive results.[10] They used a simple solvent mixing technique to combine cetyltrimethyl ammonium modified 8MR-AlPO (5wt%, 10wt%) with 6FDA-6FpDA-8%-DABA. The composite membranes produced showed a reduction in permeability along with an increase in selectivity. They reported a 200% increase in CO_2/CH_4 selectivity and a 240% increase in He/CH_4 selectivity when 8MR-AlPO was dispersed in the hexafluorinated polyimide. The gas pair selectivities reported for the composites tested by Jeong et al. can be seen in Table 1.1 below. We hope to repeat the results reported above with other more common commercially available polymer materials, optimize the tradeoff between permeability drop and selectivity, and probe some of the fundamental factors effecting transport through these 2-D inorganic structures.

Table 1.1 Ideal selectivity values reported by Jeong et al. for their composites

	Ideal Selectivity									
	He/O_2	He/N_2	He/CH_4	He/CO_2	O_2/N_2	O_2/CH_4	N_2/CH_4	CO_2/O_2	CO_2/N_2	CO_2/CH_4
6FDA-6FpDA-8%-DABA 56K (Krych)	4.93	17.69	28.66	2.14	3.59	5.81	1.62	2.31	8.28	13.42
PANC 5wt% 30°C	6.07	23.99	41.56	2.25	3.95	6.85	1.73	2.70	10.68	18.50
PANC 10wt% 30°C	5.10	45.40	76.15	1.85	8.91	14.94	1.68	2.76	24.60	41.26
PANC 10wt% 60°C	7.29	54.85	96.37	2.39	7.53	13.23	1.76	3.05	22.98	40.39

Following this section a brief summary of the current state of commercial membrane systems is presented. This should give the reader an idea of where new materials like the one being studied in this work could be implemented for current applications.

1.2 Commercial gas separations with membranes

Polymeric membrane systems for gas separations have only recently become economically attractive to industry. Historically, gas purification as a unit operation has been dominated by cryogenic distillation and pressure swing adsorption (PSA). As recently as the 1970's polymeric gas separations began to gain a share of the market. Commercial gas separation with polymeric membranes has grown into a 150 million/year business.[11] These membrane systems have an economic advantage over these traditional systems when the volume of gas produced, and purity needed is low. The economic savings comes from low initial capital startup cost, low maintenance costs, and simplicity of the membrane units. The units themselves can be modular and therefore units can simply be added if a process needs to be scaled up or the purity needs to be increased.

Currently, the most common commercial applications for membrane units are hydrogen recovery from ammonia purge gas streams and various petrochemical processes, removal of acid gases from methane, air separation, and removal of helium from natural gas.[12] Even though

several hundred new polymeric materials for gas separations have been reported in the past few years, only about eight or nine polymer materials make up 90% of commercially used membranes.[11] Below are some examples of where polymer membrane systems are currently being used to give the reader an idea of the available market for development of improved polymer based membranes.

Air Separations

The third and fifth largest bulk chemicals produced worldwide are O_2 and N_2. Currently the O_2 market is dominated by cryogenic distillation (99.999%) and pressure swing adsorption (95%).[4] Using the best polymeric gas separations technology to date, O_2 purity from air results in only about 40% for single-stage membranes, and 60% purity for multi-stage systems.[12] These low purity gas streams are due to the fact that oxygen appears on the permeate side during separation, and some nitrogen always crosses over with it. Because of the low purities obtained the market for membrane separated oxygen is limited. The major potential markets are in combustion enhancement and medical uses as a respiratory aide.[12] Nitrogen however, can be produced with up to 99.5% purity and 25% recovery using polymeric membranes.[4, 11] It is estimated that 30% of the nitrogen produced utilizes membrane separations and a large part of the production comes from polymeric membranes.[4] The primary use for nitrogen at this level of purity is inert gas blanketing. Purities of 95%-97% can be used for blanketing fresh fruits and vegetables and flammable liquids. The military uses nitrogen blanketing for the fuel in their aircraft. Because membrane nitrogen producing systems are compact and portable they are an ideal technology for use aboard ships, airplanes and other remote locations.[13]

Hydrogen recovery

Hydrogen when recovered is worth three times more as a chemical feed stock than if it is burned. Currently, the cheapest sources new of hydrogen are from refinery fuel gas streams, which produce 30-80% hydrogen mixed with hydrocarbons (C_1-C_5). [11] Other important recovery and separation operations are hydrogen recovery from ammonia purge gas streams, and syngas ratio adjustment using recovered hydrogen.

Because hydrogen is small in comparison to most gases it is an ideal candidate for separation with polymeric membranes. Hydrogen can pass through a membrane with both high selectivity and flux. The first large scale use of polymeric membranes for gas separation was hydrogen recovery. In 1980 Permea premiered their Prism membrane for separating hydrogen from nitrogen, methane and argon in ammonia purge gas streams.[11] When compared with cryogenic separation, membranes used in ammonia purge gas streams have proven economically competitive.[12] Membrane systems used to recover hydrogen in refineries have increased due to stricter environmental regulations and heavier crude. Currently, as many as 100 membrane plants have been installed in refineries, but wide spread usage has been limited. Problems with reliability of the membrane units due to fouling, plasticization, and hydrocarbon condensation are an issue.[11] Adjusting syngas ratios of H_2 and CO for the production of methanol and other oxygenated chemicals has been another niche market for gas separation membranes. Raw syngas has a ratio of around 3:1 however, petrochemical processes need a ratio closer to 2:1. Membranes selective for H_2, can adjust this ratio closer to 2:1 while maintaining the feed pressure to the reactor since H_2 is the permeate. Maintaining the feed pressure during the unit operation gives membranes an economic advantage over PSA and cryogenic separation which produce low feed gas pressures.[13]

Natural Gas separations

The largest worldwide industrial gas separation application is natural gas separations. It is estimated that the world wide market for natural gas separations equipment is around $5 billion/year.[11] Raw natural gas is obtained from high pressure wells. It usually contains 75-90% CH_4, mixed with a variety of impurities depending on the source. These impurities including CO_2, H_2S, and water must be removed before natural gas can be passed into a pipeline.

Membrane gas separations are an ideal technology for the separation of acid gas impurities from raw natural gas streams. The high pressure feed from the well is the driving force for in membrane separation module. The methane is retained at high pressure in the treated feed because CO_2 and H_2S permeate much faster through polymer membranes.[13] This can cut down on compression costs for both the feed and product gas. Membranes also have low capital and operating costs when compared with traditional acid gas removal technology such as amine plants. Despite these inherent advantages, membrane separations processes represent only 1% of the total market.[11] Most of the commercial membrane processes are cellulose acetate hollow-fiber based units installed in small gas processing plants (less than 5 million scfd). Currently, the CO_2/CH_4 selectivity of these commercially used membranes is only 12-15.[11] There is a market for high flux membranes with increased selectivity that do not plasticize due to CO_2 partial pressure.

An emerging technology is the dehydration of natural gas streams using polymeric membranes. All natural gas is currently dried before use, most by glycol adsorption. Water is a fast gas in many membranes and offers some competitive advantage over traditional methods. There is a potentially large market for membrane units which are simpler, less energy intensive, and more environmentally friendly. Selectivities of water/methane membranes are in the range of

several hundred. A few successful units have been reported for commercial use; however, glycol adsorption is inexpensive and well accepted by the industry. Membranes must be developed that offer dehydration with minimal loss of CH_4.

(1) Robeson, L. M., Correlation of separation factor versus permeability for polymeric membranes. *Journal of membrane science* **1991,** 62, (2), 165-185.

(2) Karger, J.; Ruthven, D. M., *Diffusion in Zeolites and Other Microporous Solids*. ed.; John Wiley & Sons, Inc.: 1992; 'Vol.' p 605.

(3) Zimmerman, C. M.; Singh, A.; Koros, W. J., Tailoring mixed matrix composite membranes for gas separations. *Journal of Membrane Science* **1997,** 137, (1-2), 145-154.

(4) Koros, W. J.; Mahajan, R., Pushing the limits on possibilities for large scale gas separation: which strategies? *Journal of membrane science* **2000,** 175, (2), 181-196.

(5) Mahajan, R.; Koros, W. J., Factors Controlling Successful Formation of Mixed-Matrix Gas Separation Materials. *Industrial & Engineering Chemistry Research* **2000,** 39, (8), 2692-2696.

(6) Mahajan, R.; Koros, W. J., Mixed matrix membrane materials with glassy polymers. Part 1. *Polymer engineering and science* **2002,** 42, (7), 1420 - 1431.

(7) Mahajan, R.; Koros, W. J., Mixed matrix membrane materials with glassy polymers. Part 2. *Polymer engineering and science* **2002,** 42, (7), 1432 - 1441.

(8) Rajiv, M.; Ryan, B.; Michael, S.; Koros, W. J., Challenges in Forming Successful Mixed Matrix Membranes with Rigid Polymeric Materials. *Journal of Applied Polymer Science* **2002,** 86, 881-890.

(9) Vu, D. Q.; Koros, W. J.; Miller, S. J., Mixed matrix membranes using carbon molecular sieves I. Preparation and experimental results. *Journal of membrane science* **2003,** 211, (2), 311-334.

(10) Jeong, H.-K.; Krych, W.; Ramanan, H.; Nair, S.; Marand, E.; Tsapatsis, M., Fabrication of Polymer/Selective-Flake Nanocomposite Membranes and Their Use in Gas Separation. *Chemistry of Materials* **2004,** 16, (20), 3838 -3845.

(11) Baker, R. W., Future Directions of Membrane Gas Separation Technology. *Industrial & engineering chemistry research* **2002,** 41, (6), 1393 -1411.

(12) Kohl, A. L.; Nielsen, R., *Gas purification*. 5th ed. ed.; Gulf Pub.: Houston, Tex., 1997; 'Vol.' p.

(13) Ghosal, K.; Freeman, B. D., Gas separation using polymer membranes: an overview. *Polymers for advanced technologies* **1994,** 5, (11), 673-697.

Chapter 2

Literature review of layered materials modification, polymer clay nanocomposites, $Al_3P_4O_{16}$, and barrier membrane models

Introduction

The current work involves the combination of layered aluminophosphates and polymers into nanocomposites for gas separations. There is already a large body of information available on polymer clay nanocomposites (PCN) used as barrier membranes, which is a similar area of research. Conversely, there is currently only one publication about polymer aluminophosphate nanocomposites.[1] Because the technical challenges related to polymer-clay nanocomposites are similar to polymer-aluminophosphate nanocomposites, a large part of this literature review will focus on a review of the polymer clay nanocomposites literature.

Polymer clay nanocomposites combine the properties of engineering polymers and inorganic layered materials. A nanocomposite can refer to materials with one, two or three dimensions on the nanoscale. The current work pertains to molecular dispersion of clay-like platelets with one dimension on the nanoscale (< 1nm in thickness) into a polymer matrix. The main advantage of layered materials over conventional fillers is the large surface area which is created if they can be dispersed at a molecular level. Because exfoliated clay has such a large aspect ratio, small amounts (2wt%-5wt %) can give major property enhancements. When these layered materials are dispersed at a molecular level they display properties beyond micro and conventional composites. Theses properties include increased tensile strength[2-15], increased modulus[9, 13-22], thermal stability[2-8, 22], char or fire resistance[23, 24], reduced thermal expansion[3, 5, 10, 12, 16-18, 20, 25, 26], and increased moisture/gas barrier properties[2-9, 14, 25, 27-29].

2.1 Layered Materials

The inorganic portion of the nanocomposite discussed here can be naturally occurring clay or synthetic clay. The definition of a clay given by Auerbach et al.[30] states that all clays include an octahedral and tetrahedral sheet. While this is true of the natural clays, the layered material of interest in this study $[Al_3P_4O_{16}]^{3-}$ does not follow this rule but maintains many of the other properties of natural clays. Research and literature has focused largely on the area of naturally occurring layered silicate compounds and specifically on the clay montmorillonite. This clay was used early in the development of polymer clay nanocomposites by a group of researchers from Toyota Central Research & Development Laboratories[2-8]. It serves as a good case study for understanding the properties of layered materials used in polymer-clay nanocomposites. Figure 2.1 shows a view of the layers of montmorillonite and 8MR-AlPO including the counter ions in the gallery space.

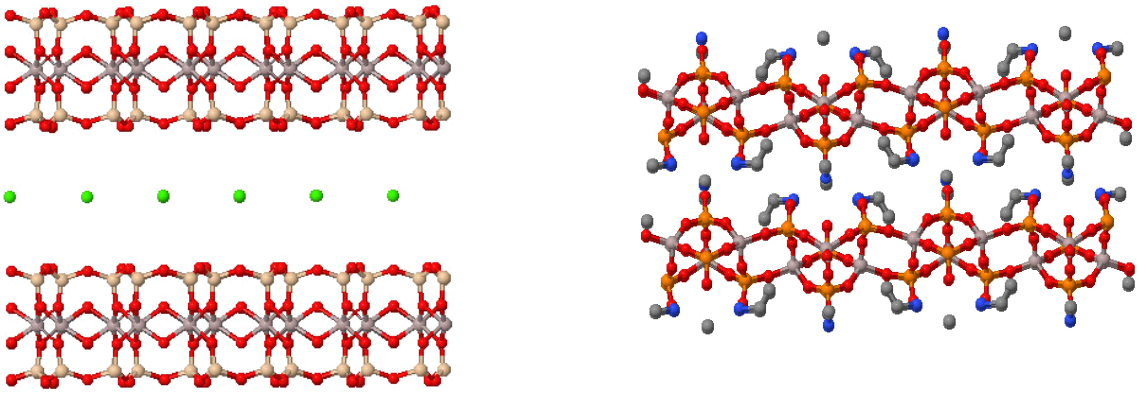

Figure 2.1. left) idealized view of montmorillonite along the plane of the layer. right) idealized view of $[Al_3P_4O_{16}]^{3-}\cdot 3[NH_3CH_2CH_3]^{+}$ along the plane of the layer.

Montmorillonite (MMT) belongs to the smectite group of naturally occurring clays. It is a 2:1 TOT clay which means that it has a structure composed of a single alumina AlO_6 octahedral sheet sandwiched between two tetrahedral silica SiO_4 sheets[30]. The sheets of montmorillonite contain mostly SiO_4 and AlO or Al(OH) units but also includes other minerals like Mg. There is a net negative charge on the sheets of the montmorillonite brought about by isomorphous substitution of metal atoms for Si, Al, or Mg. This charge is counter balanced by positively charged ions such as Na^+ or Ca^{2+} which reside in the gallery space between sheets (Figure 2.1). It is this very property that allows clays to be used in nanocomposites. As will be discussed later, these counter ions can be ion exchanged with surfactants to swell the gallery space and create a more organophilic surface. Montmorillonite has an initial basal spacing of 12.4-17Å, and a cation exchange capacity (CEC) of 80-120mEq/100g.[30] The layer thickness averages 10Å and can have an aspect ratio as high as 2000. There are many studies involving sodium montmorillonite[3-10, 12, 14, 16-20, 23, 25-27, 31-46] . The same principles used to disperse MMT into a polymer matrix can be applied to my project involving layered $[Al_3P_4O_{16}]^{3-}$.

Other clays and layered materials have been used in nanocomposites. Some examples are hectrite[3, 47], Laponite[48], saponite[3, 29], synthetic mica[3, 26], vermiculite[49], fluorohectorite[13, 50], and $[Al_3P_4O_{16}]^1$. These materials have several things in common. They are all layered with relatively high aspect ratios and have negatively charged sheets that can be ion exchanged. They differ in chemical composition, aspect ratio, and charge density. As mentioned earlier the bulk of research has been performed on montmorillonite. This is because MMT is naturally occurring, commercially available, relatively inexpensive, and well documented. The other layered materials mentioned above are often used for very specific academic research. This will also be the case with the layered aluminophosphate $[Al_3P_4O_{16}]^{3-}$ which I am attempting to use for gas separations.

2.1.1 Ion Exchange and Swelling Agents

The natural forms of clays including montmorillonite are hydrophilic and not miscible at a molecular level with polymers. In order to make these layered inorganics compatible with polymer systems, a counterion, usually Na^+, inside the gallery space must be exchanged for a molecule that makes the surface of the platelet organophilic. The equilibrium Equation 2.1 below illustrates the balance of species during the exchange. The degree of exchange depends on the nature of the cations and their concentrations in solution.

$$X.clay + Y^+ \longleftrightarrow Y.clay + X^+ \qquad (2.1)$$

The exchange of this ion is said to create an “organoclay” or one more compatible with the polymer matrix. Surfactants are used in large part to accomplish this as well as other goals.

2.1.2 CEC

All clays have what is known as a cation exchange capacity (CEC). This quantity, usually expressed in meq/100g, is a measure of the amount of exchangeable cations that a clay

mineral can adsorb at a specific pH. This constant is an important quantity to know when exchanging ions in the gallery space. One usually swells a clay in water and increases the concentration of intercalate to twice the known CEC. CEC can be determined with various methods. The approach usually includes saturation of the clay with an index ion such as barium followed by an analytical technique such as TGA, ICP-AES, or titration. The CEC can also be estimated with a simple calculation using the known charge of a unit and the molecular weights of the species in the unit. For example the CEC of $[Al_3P_4O_{16}]^{3-}\cdot 3[CH_3CH_2NH_3]^+$ was estimated using Equation 2.2 below.

$$\frac{3 \ \text{eq / amu}}{599.08 \ \text{g / amu}} = 0.005008 \ \text{eq/g} = 500.8 \ \text{meq/100g} \qquad (2.2)$$

eq = equivalents

2.1.3 Swelling Agents

There are reports in the literature of many different surface modifiers being used to create organoclays. Organic molecules used as clay surface modifiers include cationic surfactants, protonated diamines, amino acids, surfactant monomers, and adducts. These surface modifiers are most often quaternary ammonium salts (surfactants) with a cationic head, and an alkyl chain tail of length C_8-C_{18}. Cationic surfactants are used instead of anionic surfactants because the surfaces of natural clays are negatively charged. Some of the surface modifiers employed in the current study are shown below in Figure 2.2. The head of the surfactant can contain methane, protons or bulky side groups and the tail may simply be a carbon chain but can contain reactive groups depending on the specific purpose. These surfactants serve two main purposes 1) to make the platelet more organophilic and, 2) to increase the d-spacing of the pristine clay. This surface modifier can also serve special purposes such as, reacting with the polymer to make a

tethered system[13, 16, 17, 51], increase dispersion of the clay in the polymer[39, 48, 51], fine tune the polarity of the gallery space[35, 36, 50], or alter the reaction kinetics of polymerization[8, 13, 32].

Making the hydrophobic surface of clay organophilic is a key to making nanocomposites. In early work Okada et al.[2] used the ammonium salt of 12-aminolauric acid to make montmorillonite more compatible with Nylon 6. With this modification they reported that the once immiscible clay dispersed at the molecular level into Nylon 6. As a result of 4 wt% addition of MMT the rate of water adsorption was lowered by 40% and the heat distortion temperature was raised by 87°C[2]. This type of surface modification has been repeated throughout the literature, and it is now rare to find a study where the clays used in nanocomposites have not been modified in some way.

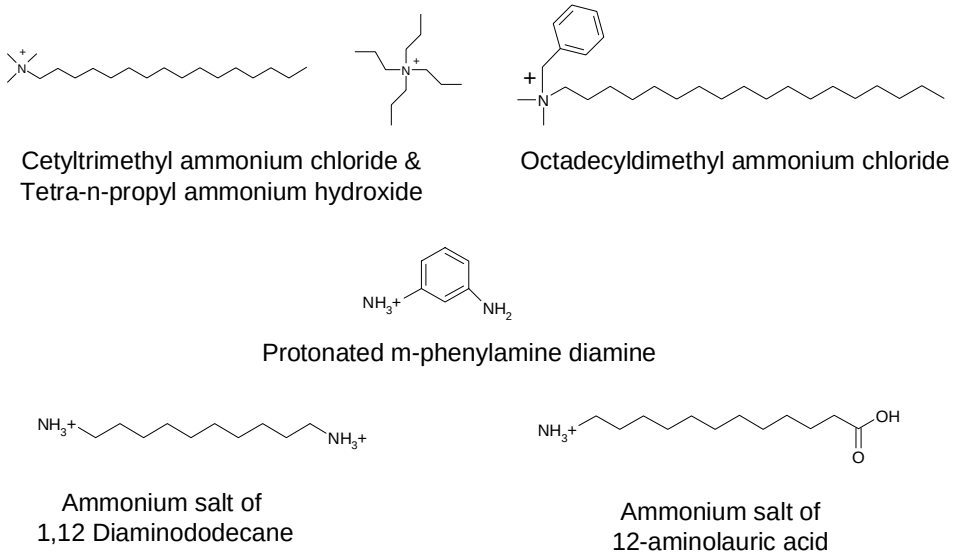

Figure 2.2. Surface modifiers used in the current study

Many studies have reported on the increase of the basal spacing in clays with the addition of a swelling agent. This includes both the pristine clay and the clay dispersed in the polymer-clay nanocomposite. X-ray diffraction (XRD) is the main tool used to measure changes in the basal spacing. When compared to the pristine clay or polymer, a shift to the left in the (001)

peak of the XRD pattern indicates an increase in d_{001}-spacing. This shift is evidence that the surfactant used has indeed intercalated and swollen the gallery space. Usuki et al. first reported on the effects of using surfactants of various alkyl chain lengths to swell MMT for nanocomposites[7]. Using amino acids containing $C_{2\text{-}18}$ in the chain, they showed that d_{001}-spacing of MMT in the final nanocomposite increased with increasing carbon chain length.

The concept of a tethered polymer-clay nanocomposite is illustrated below in Figure 2.3. A surface modifier containing a cationic head with a reactive tail is employed. The cationic head can form an ionic bond with a clay platelet and the reactive group can form a covalent bond with the polymer used. The clay platelet is therefore "tethered" to the polymer by the surfactant. Tyan et al. used montmorillonite tethered to polyimide via a surfactant containing reactive groups.[16, 17] It was shown that if the number of reactive groups was three or more, greater force was created for exfoliation when compared to the nonreactive swelling agent case. Morgan et al. used the ammonium salt of 12-aminolauric acid as a surface modifier for MMT[51]. The COOH group formed a tether with in situ synthesis of PEI. The resulting nanocomposite showed excellent exfoliation and dispersion.

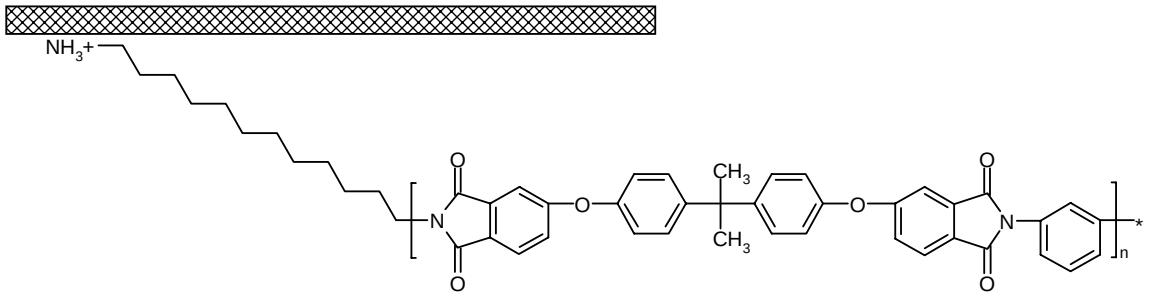

Tethered system with PEI and protonated 1,12 diaminododecane

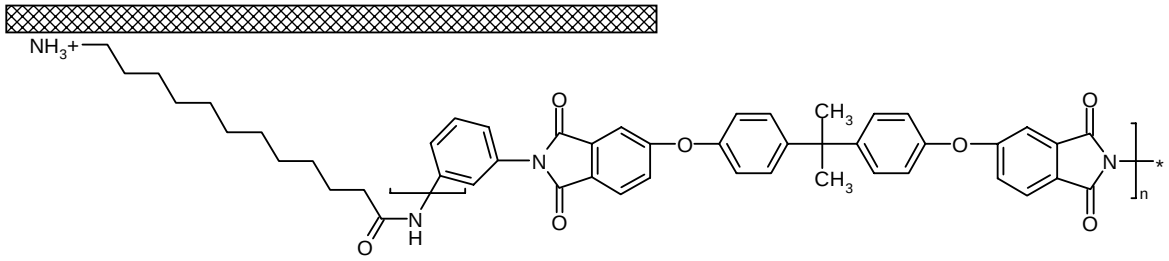

Tethered system with PEI and 12-aminolauric acid

Figure 2.3 Examples of tethered polymer clay systems

Dispersion of clay platelets in a polymer solvent or polymer melt system is often difficult to achieve. Surface modifiers can be used to aide in dispersion. In an attempt to disperse the clay Laponite in acrylamide, Muzny et al.[48] used the surfactant monomer hexadecylallyldimethyl ammonium bromide. Using dynamic light scattering, they showed that a stable solution of Laponite platelets could be formed in water if surfactant was added in excess of the CEC. This resulted in a polymer clay nanocomposite with aggregates no larger than 400 nm. Morgan chose surfactant modified montmorillonites that were shown by light scattering to disperse well in DMAc for an in situ polymer clay nanocomposite.[51] Davis et al. used the novel surfactant 1,2-dimethyl-3-N-alkyl imidazolium salt to aide in exfoliation of montmorillonite in PET at melt processing temperatures. This surfactant showed high levels of dispersion and delamination of the clay into the PET matrix[39].

Dispersion of layered materials into organic solvents is of key importance for the formation of polymer clay nanocomposites. Several groups have performed research in dispersing modified montmorillonite into different organic solvents. These groups often use commercially modified montmorillonite under the trade name of Cloisite©. Ho et al. investigated the dispersion of Cloisite 15A in seventeen different solvents to determine if the clay could be fully exfoliated in solution.[52, 53] Cloisite 15A is montmorillonite modified with a dimethyldioctadecylammonium surfactant. They found that Cloisite 15A exfoliated fully in trichloroethylene and chloroform and were able to relate the dispersion/exfoliation to the Hansen solubility parameters. Their results showed that δ_d of the solvent determined whether or not Cloisite 15A would remain in suspension, while δ_p and δ_h determined the formation of structure of the tactoids in solution. It was concluded that the solvents used to exfoliate Cloisite 15A must have weak H-bonding groups or the material would precipitate. Finally, it was determined that δ_o could be used to predict the degree of exfoliation if the other solubility parameters were satisfied. Recently, Tran et al. investigated the dispersion of Cloisite 30B ($N^+(CH_2CH_2OH)_2CH_3T$) ,where T is a C_{18} tallow group, in a large number of alcohol solvents.[54] The alcohol solvents employed were described by the alkyl chain length R_nOH where n = 2 – 8. One the authors first observations was that Cloisite 30B precipitated in alcohols with ($n < 5$) but remained in suspension when ($n \geq 5$). Their conclusion was that increased polarity and decreased hydrogen bonding forces allowed for stable suspensions of Cloisite 30B. XRD patterns of the alcohol solvents with $n \geq 5$ also showed an increased basal spacing which supported the previous conclusions.

Kornmann et al. believed strongly that the polarity of the intergallery space had a significant effect on the degree of intercalation, exfoliation, and final morphology of epoxy clay

nanocomposites[35, 36, 50]. The authors therefore, modified MMT with organic molecules of different polarities to study the effects. They used adducts, which are epoxy monomer with primary amine alkanes attached to each end, and compared them to traditional surfactants[50]. Their theory was that by closely matching the polarity of the surface modifier to the polymer, the clay would display greater miscibility. Results indicated that greater separation of the MMT platelets was achieved with the adducts. This was conformation that polarity of the surface modifier has an important effect on hybrid morphology.

Several reports have been made about surface modifiers designed to catalyze reactions in polymer clay nanocomposites. Okada et al.[8] from Toyota reported that protonated amino acids catalyzed ε-caprolactam polymerized in the gallery space of MMT. Tyan et al.[32] first used MMT modified with a surface treatment to catalyze the imidization of poly(amic acid) to polyimide. It was found that both imidization time and temperature were reduced. In another paper Kornmann et al. used a swelling agent that was shown to have a catalytic effect on the polymerization of epoxy in the gallery space of fluorohectorite.[13] Dihydro-imidazoline was found to favor the formation of nanocomposites because of its catalytic effect on polymerization.

2.1.4 Surfactant in the gallery space

The ion exchange of pristine montmorillonite with a cationic surfactant results in the gallery space being populated by the exchanged ions. The arrangement of the surfactants in the gallery and the amount exchanged will determine the increase in gallery spacing that is observed. Some of the possible arrangements of surfactants in the gallery space as reported by Vaia et al. are pictured in Figure 2.4 below. The surfactants are thought to lay either parallel to the layers or at some angle to the layers in mono- or bi-layer arrangements.[55]

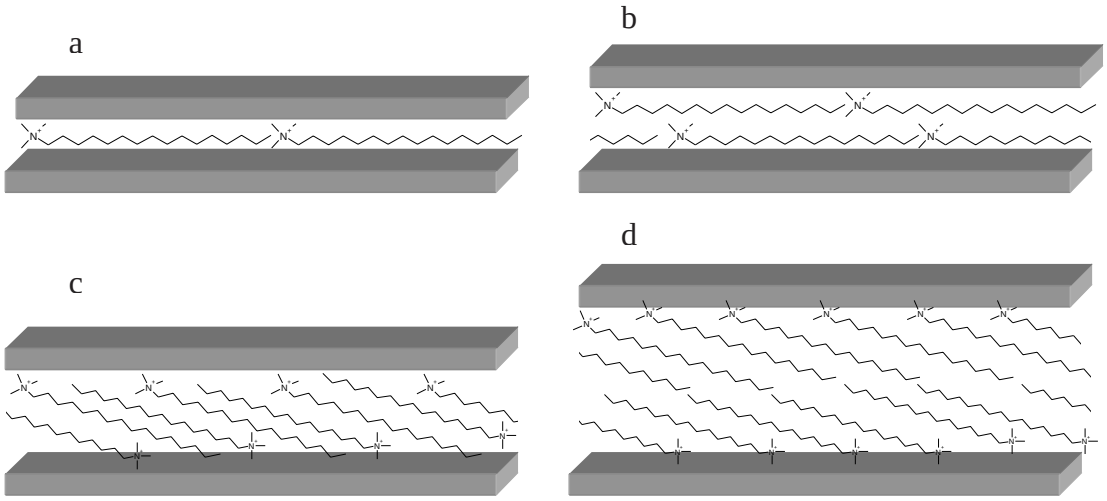

Figure 2.4 a) lateral monolayer b) lateral bilayer c) tilted bilayer d) paraffin monolayer

Figure 2.4 is a cartoon of surfactant populating the gallery space of an aluminosilicate. The figure is of a very ordered idealized system and is not meant to be a true representation of the gallery environment. The actual surfactant arrangement is more liquid like because the alkyl chains can form both trans and gauche conformations. Therefore, a certain gallery height could be the result of a tilted all trans bilayer or a mixture of gauche and trans surfactants forming a bilayer.[55] Burnside et al. used IR to probe the conformation of dodecylamine in vermiculite. Their results indicated that both gauche and trans conformers of surfactant chains coexisted in the gallery environment leading them to picture a more liquid like environment.[49] Zeng et al. studied the effect of surfactant loading on the packing of surfactants in the gallery space of montmorillonite.[56] They swelled MMT with cetyltrimethylammonium (CTA^+) at concentrations ranging from 18wt% to 30wt%. Their data indicated that the gallery height increased with increasing wt% of CTA^+ on MMT. They also concluded that as the content of CMT^+ is increased in solution that the gallery environment would progress from a lateral monolayer to a tilted bilayer (mostly trans) to a lateral bilayer. Lee et al performed similar work loading CMT^+

at a value of 1.0 and 2.5 times the CEC of a smectite clay.[57] The results of their experiments showed that swelling at 1.0 times the CEC increased the d_{001}-spacing from 15.7Å to 21.0Å and swelling with 2.5 times the CEC further increased the d-spacing to 39.4Å. They attributed these changes to the formation of a pseudotrilayer of CMT^+ followed by a paraffin complex. They also made the significant observation that a loading beyond 1.0 of the CEC causes hydrophobic bonding to occur between layers. Hydrophobic bonding is the attraction of one surfactant tail to another similar to the formation of micelles in aqueous solution.

2.1.5 Intercalated, Exfoliated or Immiscible System

There are three terms that will be used heavily in this proposal, exfoliated, intercalated and traditional composite. These terms are used to describe what type of hybrid system has been formed by the combination of clay with polymer. A cartoon depicting the difference between these terms is shown below in Figure 2.5. An exfoliated system is one in which the order of the clay platelets has been completely disrupted. This is usually defined as a composite of clay and polymer where X-ray diffraction (XRD) scans of the hybrid show no peaks. This would imply that the separation between platelets has exceeded approximately 80Å. An intercalated system is one in which polymer or other organics have entered the gallery space, however long range order is still maintained. An XRD scan of this material would show peaks with lower 2θ values indicating large spacing between clay platelets. A traditional composite or immiscible system is one in which no organic molecules have been able to enter the gallery space of the clay. The clay tactoid is therefore fully intact and polymer would simply exist on the outer surface of the particle.

X-ray diffraction and transmission electron microscopy (TEM) are the primary analytical instruments used to determine what type of system is present in a polymer-clay hybrid. Both

analyses must be performed because erroneous conclusions can be reached by simply using XRD. Potentially an XRD scan of a hybrid may show no peaks, indicating exfoliation; however this could be the result of low clay loading in the hybrid.[58] TEM must therefore be used in conjunction with XRD to confirm the existence of an exfoliated system. Another feature of a fully exfoliate hybrid is clarity. If a true nanocomposite has been formed, the resulting film should be transparent. This occurs when the molecular dispersion of the clay is smaller than the wavelength of visible light.[5]

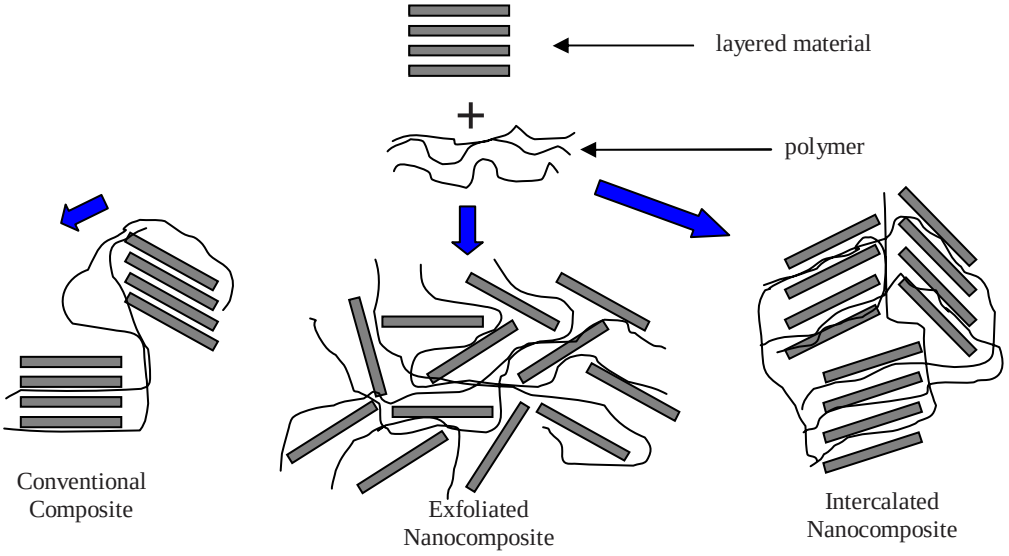

Figure 2.5 Conventional, Exfoliated, and Intercalated nanocomposites

Systems can be further characterized by comparing microscale and nanoscale dispersion. Morgan et al. employed XRD and high magnification TEM to characterize poly(etherimide) (PEI)-clay hybrids[51]. They found that one of their composites showed no change in d-spacing when measured with XRD. When the same composite was observed using TEM, it showed some degree of exfoliation. This system was characterized as *immiscible-exfoliated*. Likewise one of their hybrids showed a large increase in d-spacing with XRD. However when observed with TEM, large portions of the clay were exfoliated. These composites were termed *exfoliated-intercalated*. The authors suggest that most systems reported as exfoliated were actually

partially exfoliated and partially immiscible. They indicate that high magnification TEM is required to fully characterize a nanocomposite.

2.1.6 Exfoliation of clay in polymer

The factors affecting full exfoliation of layered clays in polymer matrices are not fully understood but some general progress has been made in understanding the process. The delamination of clay in a polymer organic solvent system is a complex problem. The idea involves making the gallery of the clay thermodynamically favorable to the intercalation of polymer chains. The first step is therefore the modification of the clay that will be intercalated. The issues associated with this problem involve such variables as the CEC of the clay, the polarity of the reaction medium, and the chemiophysical properties of the interlayer cations.[46] The trick is then to pick the surface treatment that will create the best thermodynamic environment to intercalate the polymer of interest. If one is using the solution intercalation technique the other variable is the solvent in which the modified clay will be dispersed and the polymer will be dissolved. Some insight into the thermodynamics of intercalation has been reported in studies involving melt intercalation. Vaia et al. investigated the melt intercalation of several styrene-derivative polymers and several layered clays modified with primary and quaternary ammonium salts.[59] The authors conclude that polar polymers containing hydrogen bonding groups or groups with associative interactions lead to intercalation. Burnside et al. expanded on the work of Vaia et al. using dodecylamine swollen vermiculite and a bromonated co-polymer of styrene.[49] They describe the thermodynamics of confinement of polymer chains in the gallery as a entropic penalty which is balanced by the increased conformational freedom of the surfactant. The authors conclude that this confinement penalty will be compensated only up to a certain gallery height h_c, where the surfactant chains are fully extended. Finally, in order to

expand the gallery beyond h_c, strong energetic interactions are required to overcome the entropic penalty.

Chen and Evans performed an interesting study about the size of polymer chains that are preferentially intercalated in polymer clay nanocomposites.[44] They used a solution intercalation technique to intercalate Poly(ethylene glycol) (PEG) of different molecular weights into MMT. Their experiments showed that MMT in a solution containing 35K PEG and 4K PEG preferentially absorbed the higher molecular weight species into the gallery.

2.2 Polymer Clay Nanocomposites

There are several common methods for preparing polymer-clay nanocomposites found in the literature. These methods are in-situ polymerization, solution intercalation, and melt intercalation. The type of method used to form a nanocomposite is highly dependant on the polymer-clay system in question. No one method is successful in all cases, so a variety of methods are usually employed to achieve true molecular dispersion of clay in a polymer.

In-situ polymerization refers to the intercalation of monomer into the gallery space of clay followed by polymerization. The idea behind this method is to use the energy created by polymerizing inside the interlayer to expand the gallery and exfoliate clays. For example, the first successful nanocomposites were formed by intercalation of ε-caprolactam into the gallery of montmorillonite (MMT) followed by heat induced polymerization[2]. This approach has been used successfully with both condensation reactions and chain growth reactions. Yang et al.[10] polymerized pyromellitic dianhydride and 4,4'-diamino-3,3'-dimethyldiphenylmethane in the galleries of MMT to form a polyimide clay nanocomposite. Zhu et al.[24] created polystyrene-clay nanocomposites via free radical polymerization in the galleries of MMT. The key to this method is to get the polymerization to take place inside the gallery. If the monomer used does

not intercalate into the gallery space and remain there during polymerization, a nanocomposite will not be formed.

Another common route to nanocomposite formation is simple mixing of clay and polymer in solution. This is known as solution intercalation and can be attempted with any soluble polymer. It usually involves dissolving polymer in some organic solvent, and in a separate vessel, creating a clay-solvent slurry. The two solutions are then combined and cast to produce a nanocomposite. For instance, Yano et al.[4] first mixed poly(amic acid) with MMT and then imidized the film to form a polyimide clay nanocomposite. The layered material could be mixed with the poly(amic acid) form and then imidized or simply mixed with a soluble polyimide and then cast into a film. Because this method is simple, it is attractive to our research. My research will involve simple mixing of modified $[Al_3P_4O_{16}]^{3-}$ with various polyimides to determine if a nanocomposite can be formed. The solution intercalation method is also particularly attractive because it lends itself well to the fabrication of hollow fiber membranes for gas separations.

Melt intercalation is another method employed to create polymer clay nanocomposites. This method is attractive because it could utilize existing conventional polymer processing techniques. The idea is to use the energy created during heating to drive polymer chains into the interlayer galleries of MMT. One of the main obstacles to overcome is the degradation temperature of the organic modifiers on the clay surfaces. Most of the compatiblizers used degrade below typical melt processing temperatures. One example of a successful polyimide-clay nanocomposite by melt processing was reported by Huang et al.[37] They created an exfoliated nanocomposite by melt blending poly(etherimide) and MMT at 370°C. The

nanocomposite showed homogeneous dispersion of MMT layers and improved thermal properties and solvent resistance.

2.2.1 Polymer materials used to make PCN

Because of great interest in the potential benefits of polymer clay nanocomposites a large variety of polymers have been tested with layered clays. Polyimide-clay composites represent a sizeable portion of available literature due to the favorable thermal, chemical, and mechanical properties of the pristine polymer.[3-5, 9-12, 15-18, 20, 25, 26, 32, 34, 37, 42, 43, 51]. Polyimides are the primary polymers of interest in the current work in gas separations associated with this proposal. There is data available on many other polymer clay systems including nylon-6[6-8, 23, 41, 60], epoxies[11, 13, 21, 27, 35, 36, 50, 58], acrylamide[48], ethylene vinyl acetate[19, 61], polycarbonate[62], polystyrene[22, 24, 38, 63], polyurethane[14], polyethylene, terephthalate[39], polypropylene[64], poly(methyl methacrylate)[38, 65], and poly(lactic acid)[40]. The purpose of this review is to give the reader an overview of polymer-clay systems in the literature, but to focus on polyimide clay composites.

2.2.2 Polyamide-6-Clay Nanocomposites

Any discussion of polymer clay hybrids must begin with Nylon-6 clay hybrids (NCH) discovered by a group of researchers from Toyota Central Research and Development Laboratories (TCRDL)[2]. This group was the first to obtain a fully exfoliated clay polymer nanocomposite. The NCH they developed exhibited superior mechanical properties including tensile strength, modulus, heat distortion temperature, reduced coefficient of thermal expansion and resistance to water, when compared with nylon 6. The discoveries they made set the stage for the science of polymer-clay nanocomposites as we know them today.

In 1986 TCRDL under the leadership of Dr. Kamigaito developed the first fully exfoliated polymer clay nanocomposite[66]. The successful fabrication of the NCH came after

many failed attempts. Through these failures and successes TCRDL established the basic principles that are still followed today in combining clay with polymers. The fundamental problems they faced dealt with surface modification of the clay layers, exfoliation of the nanoplatelets and dispersion of the clay into the polymer matrix.

The group first tried to melt blend nylon 6 with montmorillonite modified with alkyl ammonium. This attempt was unsuccessful and produced an inhomogeneous material. The next set of experiments focused on the intercalation of the clay. They used an amino acid to modify the surface of the MMT and intercalated ϵ-caprolactam, a monomer of nylon 6. Using XRD they found that the gallery space of MMT expanded significantly with the addition of ϵ-caprolactam to MMT swollen with 12-aminolauric acid. This led them to the conclusion that an in situ method for combining MMT with nylon 6 was the best route. They knew that several synthetic routes to nylon 6 existed and decided to try anionic polymerization. After months failing to exfoliate the clay with this method they attempted a thermal polymerization. This turned out to be a key to the formation of a nanocomposite. The thermally polymerized composite showed increased spacing with XRD and TEM confirmed formation of a truly exfoliated system. The authors theorized that the anionic polymerization occurred outside the interlayer and did not expand the gallery space. The thermal polymerization however initiated cationic ring opening of ϵ-caprolactam through the ammonium ions present in the gallery space. Because the polymerization took place in the gallery space the intergallery expanded, eventually exfoliating into a nanocomposite.

Using the information from their initial success the same group further experimented with NCH to clarify the reasons that a nanocomposite was formed[6, 7]. Usuki et al. reported on the swelling of MMT with different carbon length amino acids[7]. They cation exchanged MMT with

$NH_2(CH_2)_{n-1}COOH$ where n=2-18, then intercalated ϵ-caprolactam and characterized with XRD. Results showed the amino acid was parallel to the MMT layers when the carbon number was 8 or less and inclined when the carbon number was 11 or more. They also found that when ϵ-caprolactam was intercalated, the amino acid was stretched and arranged perpendicular to the MMT plates. In another study Usuki et al. clarified the polymerization of ϵ-caprolactam in the gallery space[6]. They found that the COOH end groups of the amino acid actually initiated the polymerization in the gallery space. They also performed end group analysis that indicated ammonium cations formed in nylon 6 and interacted with anions in montmorillonite to aid intercalation.

Others have continued to work on nylon-clay hybrids. Vaia et al. explored their use as high performance ablative material[23]. Research showed a tough char forms on the surface of nylon 6-clay nanocomposites enhancing ablative performance. Ma et al. showed the addition of MMT to nylon 6 decreased the crystallinity of the polymer and lowered the melting point[60]. Recently, Hasegawa et al. have returned to the idea of processing nylon 6-clay hybrids using melt processing[41]. They describe a process where treated MMT in a slurry and melted nylon 6 are combined in a twin screw extruder. The product is shown by TEM and XRD to be a fully exfoliated system that exhibits superior mechanical properties compared to neat nylon 6.

2.2.3 Polyimide-Clay Nanocomposites

Before discussing polyimide-clay nanocomposites a brief review of polyimide synthesis is presented. A typical polyimide synthesis begins by reacting dianhydride monomer with a diamine monomer in an organic solvent. This reaction produces a poly(amic acid) or a polyamide acid. In order to remove water and close the backbone rings, the product must undergo an additional step. This step is known as imidization and is often thermally activated.

Imidization can take place in a one step polymerization or two step polymerization. The two step method involves, polymerization, casting, drying, and heating of the polymer film. The object of heating the film is to get the temperature high enough to imidize the polymer, usually 300°C or higher. The other method, known as solution imidization, requires heating of the polyamic acid solution just after polymerization to a temperature around 180°C. There are advantages and disadvantages to both methods when making polyimide-clay nanocomposites. These advantages and disadvantages will be discussed later.

Another very important topic to mention about polyimide synthesis is the solubility of the polyimide after polymerization and casting is complete. A survey of the early literature on polyimide-clay nanocomposites will show that successful hybrids were formed by in situ polymerization of polyimides. What the reader should keep in mind as this review progresses is that most of the early work involved polyimides that were insoluble after formation. This would be unacceptable for the application of polyimide-clay nanocomposite hollow fibers. The final polymer-clay composite would have to be soluble in common solvents to allow processing into hollow fibers and use as gas separation membranes. For this reason my research will focus on soluble polyimide-clay composite systems.

1990's

Polyimide-clay composites were developed early for applications relating to microelectronics[5]. Pure polyimides are known to have excellent heat resistance, chemical stability and electric properties. Research by a group from Toyota had shown improvements in heat distortion in Nylon 6 with the addition of small amounts of montmorillonite[2, 4]. Because of this success, the same group began to develop polyimide-clay composites to reduce thermal expansion and moisture adsorption in films.

A group of researchers at Toyota led by Yano et. al were the first to claim success in fabricating polyimide-clay nanocomposites[4, 5]. They reported that with the addition of 2 wt % of montmorillonite, gas permeability of oxygen dropped to half the value measured for the pristine polymer. They also reported a lower thermal expansion coefficient for the hybrid. The improvements were attributed to increased tortuosity for the gas molecules due to the high aspect ratio of the clay platelets. Based on XRD patterns of the hybrids and TEM images they concluded that the clay platelets had been exfoliated in the polymer matrix and dispersed at a molecular level. Later work by the same group showed the effect of clay size on gas permeability. Using clays of different aspect ratio, they concluded that clays with the largest aspect ratios reduced gas permeability by the most. With the addition of 2wt % large aspect ratio synthetic mica, gas permeability coefficients were reduced to 10% of their original value and the thermal expansion coefficient was reduced by 60%[3].

Following the research of Yano, Yang and Zhu used a different approach to exfoliate montmorillonite with polyimide. Previously, Yano had used polyamic acid to intercalate the intergallery space of montmorillonite. The composite was imidized after the addition of clay and casting of the film. Yang and Zhu intercalated montmorillonite with monomer and attempted a monomer solution intercalation polymerization (or situ polymerization) followed by casting and imidization[10, 25]. Using this approach the group reported an increase in strength and toughness, improvement in thermal stability, and reduction of the thermal expansion coefficient for the composite[25]. The increases were attributed to the formation of a nanocomposite. It was determined that the surface modifier on the clay was very important to dispersion in the polyimide. They identified 1-Hexadecylamine as the best selection for the polyimide/montmorillonite system they studied[10]. Finally they concluded that the content of

montmorillonite needed to remain below 5 wt %. At clay loadings higher than 5 wt % the mechanical properties decreased due to aggregation of the clay particles.

At about the same time as Yang and Zhu, Tyan et al. began experimenting with polyimide clay nanocomposites containing reactive surfactants placed on clay surfaces[16, 17, 32, 34]. They started by exploring the effect of the modified clay on the imidization kinetics of a poly(amic acid). Tyan et al. again employed polymerization of monomers to poly(amic acid) before the addition of different loadings of montmorillonite modified with p-phenylenediamine. From this first paper they reported a decrease in both the time and temperature needed to imidize the films after the addition of 2 phrs (parts per hundred) of exfoliated clay. It was determined that addition of the clay caused a 20% drop in the activation energy for imidization and 25° increase in thermal degradation temperature.[32] In a second paper Tyan et al. attempted to fabricate a polyimide nanocomposite using a swelling agent containing one reactive group[16]. The basic idea was to mix the modified montmorillonite containing an NH_2 reactive group with anhydride terminated poly(amic acid). This would allow a tether to be formed between the polymer and the clay platelet. The surfactant and clay share an ionic bond and the surfactant and the polymer are covalently bonded. The film would then be cast and imidized into a polyimide-clay nanocomposite. They report that the tethered system makes this nanocomposite more stable thermally and stronger mechanically. There is also and added advantage of a permanent swelling of the clay layers, the polymer molecules would not slip out of the intergallery space during solvent removal reversing the formation of a true nanocomposite. In a following paper Tyan et. al. swelled montmorillonite with one of the monomers used in the synthesis of the polyimide they were studying[34]. The hope was using a swelling agent very similar to the polymer would increase polyimide/clay miscibility and therefore the mechanical properties of

the nanocomposite. The technique worked, and with a 7wt% addition of clay they reported a twofold increase in modulus, half-fold increase in maximum stress, and an increase in the elongation at break. Finally Tyan et al. experimented with polyimide-clay nanocomposites containing clays modified with multiple functional groups[17]. They employed a series of surfactants containing zero, one, two and three NH_2 groups. It was found that using swelling agents with three or more functional groups caused greater exfoliation of the clay platelets than swelling agents with no functionality. This resulted in dramatically enhanced thermal and mechanical properties.

2000-2001

A survey of the literature following the 1990's showed research from a variety of groups. Most of the work emanated from Asia and dealt with issues surrounding the process conditions of forming polyimide-clay nanocomposites.

Huang et al. explored imidizing the polyimide-clay composite in solution to avoid degradation and defects caused by post casting imidization[20]. They called their process a high temperature solution intercalation/polycondensation/imidization and referred to it as a one step approach to polyimide-clay composites. Using XRD and TEM they showed that they had produced exfoliated polyimide-clay nanocomposites in one step. They also confirmed previous work that suggested that montmorillonite content effects the properties of the hybrid significantly. At clay loadings of less than 6 wt% they report improved thermal stability, decrease in the TEC, and increases in modulus and Tg. However when the clay loading exceed 6 wt% severe particle aggregation occurred and mechanical properties of the hybrid became poor. Another advantage of the polyimide/clay system developed by Huang et al. was that after polymerization their hybrid showed solubility in common solvents such as NMP, DMA, DMF

and DMSO. This is an important processability issue that was not achieved by many of the previous groups mentioned above due to the inherent poor solubility of many polyimides. In a second paper Huang et al. attempted to melt blend poly(etherimide) (PEI) and organo-modified MMT[37]. Their goal was to improve the solvent resistance and thermal properties of PEI by making a nanocomposite. Their data showed that true nanocomposites could be formed by melt intercalating MMT in PEI. The resulting hybrid had a higher Tg, better thermal stability, and solvent resistance when compared with the virgin PEI. Using the melt intercalation technique they were able to load PEI with up to 20wt% clay and still reported good dispersion and improved thermal properties. This suggests that melt intercalation may be a better route to achieve dispersion than solution processing. Hsiao et al. followed with similar work[26]. They acknowledged the same processability issues related to non-soluble polyimides. The scheme they developed involved synthesizing a soluble polyimide SBA-6FDA that was fully imidized before mixing with the inorganic component. Using XRD and TEM they showed that it was possible to fabricate a nanocomposite using a fully formed polyimide and the resulting properties were improved.

Morgan et al. attempted a melt blending of PEI with modified MMT but according to XRD scans were unsuccessful[51]. This is curious because in the same year Huang et al. reported great success with this very technique. Morgan sited the reason for failure as no organic treatment present on the MMT; however Huang used 1-hexadecylamine as a modifier which almost certainly decomposed during melt blending. Morgan et al went on to attempt an in situ polymerization instead. They performed in situ synthesis of a poly(amic acid) containing MMT modified with a reactive (*12-aminododeconic acid ammonium salt*) and non-reactive (*n dodecylamine ammonium salt*) surfactant. The former could participate in the polymerization and

the ladder simply increased polymer/clay miscibility. The polymerization was followed by casting and imidization of the film. There was no report made about mechanical or thermal properties of the hybrids but instead the focus was on the type of nanocomposite formed. The authors employed XRD and TEM to reach several conclusions. Both modifiers produced a PEI nanocomposite. The hybrid containing non-reactive clay showed no increase in d-spacing according to XRD but showed exfoliation with TEM. This hybrid was characterized as an exfoliated-immiscible system. The hybrid containing reactive clay showed an increase in d-spacing and TEM indicated complete exfoliation. This hybrid was said to be an exfoliated-intercalated nanocomposite. The work of these authors is important. They have used high magnification TEM to further characterize the exact nature of the composites that are being formed between polyimide and MMT.

Agag et al. studied the mechanical properties of hybrids containing MMT in a rigid rod polyimide compared to a semi-flexible polyimide[18]. Their goal was to compare the mechanical changes associated with these two polyimides when 1, 2, 4, 6, and 10 wt% MMT was added. A specific aspect they wanted to study was the cold drawing of the rigid rod polyimide. It is known that cold drawing of ridged rod poly (amid acid) and subsequent imidization gives high modulus polyimide films. When MMT was added to the poly (amid acid) it was expected to enhance this feature, however it had the opposite effect. The pristine polymer showed a larger increase in modulus after cold drawing, so it was concluded that clay nanolayers hindered the mobility and reorientation of the polymer chains. In a comparison of property enhancement of the two different types of polyimides the authors conclusions did not differentiate but gave generalizations about both systems. In general a 2wt% loading of clay showed the optimal properties with increases in Tg, thermal stability and decreases in CTE.

Gu et al. experimented with adding modified MMT before and during polymerization of a poly(amic acid) and then imidizing to a polyimide[12]. Their comparison showed that optimal properties were obtained when the clay was added after the formation of the poly (amic acid).

2002

Following the above mentioned work Delozier et al. prepared polyimide-clay nanocomposites using different methods to disperse the organically modified MMT into the polymer[67]. These included simple physical mixing, mixing and sonication, high shear mixing with a homogenizer, and in-situ polymerization. The authors synthesized their own poly (amic acid) followed by one of the above mentioned treatments and imidization after casting. They began their analysis with visual inspection of the hybrids after they were cast and imidized. If a true nanocomposite is formed and particles are distributed on a nanometer scale, it is expected that a cast film would be completely transparent. This is because the particles are separated at distances greater than the wavelength of visible light. Films prepared by simple physical mixing, and sonication were observed to be cloudy indicating phase separation of the clay in the polymer. These methods were deemed unable to produce true nanocomposites. It is important to note however that these films showed large increases in modulus similar to those reported by previous authors. The film prepared by high shear mixing showed good clarity when cast. XRD and TEM confirmed that the MMT had been exfoliated however, the authors were not certain that this method had not fractured the clay. They decided to pursue the in situ route to hybrid synthesis. This method proved to give the best overall property improvement compared to pristine polyimide. TEM and XRD showed good dispersion and exfoliation with some agglomerates present. The film exhibited increased tensile modulus and lower elongations to break.

2004-present

Recently, Nah et al. studied the intercalation behavior of polyimide/clay nanocomposites containing modified MMT[42]. Using XRD on a fairly linear polyimide and one with bulky side groups, they were able to track the changes in d-spacing with temperature. Their analysis showed that two types of intercalation were occurring. In the first case, polyimide intercalated into the intergallery space and displaced the organic modifier. In the second case, the modifier remained in the gallery space along with intercalated polyimide. When temperature was increased on the linear polyimide, XRD showed that the sites containing surfactant and polyimide collapsed. The sites with just polyimide intercalate however remained intact. The same experiment repeated with the bulky polyimide showed that both sites remained intact with a broadening reported in the XRD peak for the lower angle (surfactant with polyimide) peak.

Most recently several groups have pursued new applications for polyimide-clay nanocomposites. Zhang et al. looked at the mechanical properties of polyimide clay hybrids under cryogenic conditions[15]. Using an in situ approach they fabricated nanocomposites from modified MMT and pyromellitic dianhydride with 4,4'-oxydianiline. They were successful at fabricating a polymer-clay nanocomposite that showed impressive properties under cryogenic conditions. The strength, modulus, and ductility were enhanced at both room and cryogenic temperatures. They reported that these improvements at 1-3 wt% addition of MMT. Yu et al. fabricated polyimide-clay nanocomposites for use as coatings to prevent corrosion[14]. Their research showed that films containing low clay loadings showed superior anticorrosion properties when compared to the pristine polyimide. Finally, Jeong et al. employed a polyimide synthetic layered aluminophosphate nanocomposite as a gas separation membrane.[1] Their results supported the creation of aluminophosphate polyimide nanocomposite. The XRD and TEM data

combined showed the system to be at least intercalated if not exfoliated. They were also able to show an increase in gas pair selectivities because the aluminophosphate flakes were microporous.

2.2.4 Epoxy-clay nanocomposites

Another area of polymer-clay nanocomposites that has added significantly to the literature is the area of epoxy-clay nanocomposites. The method used to fabricate these hybrids involves an epoxy resin and a curing agent, usually a diamine. The clay is modified with an organic molecule and then mixed with the epoxy resin. After some amount of time the solution is then cured or reacted to form a polymer. Because the process is similar in approach to the in situ polymerization method for polyimides, useful information can be obtained from reviewing the literature.

Kornmann et al. published a series of papers dealing with epoxy-clay nanocomposites[13, 35, 36, 50, 58]. These papers discuss the effects on composites of clays with different CEC values, effects of the reactivity of the curing agent on exfoliation, effects of the surface modification of clay on the composite, and polarity issues associated with combining modified clay with epoxies. The results presented can be directly applied to the research I am currently undertaking.

Kornmann et al. first fabricated epoxy-clay nanocomposites using clays with vastly different CEC values to determine the effects on intercalation, exfoliation and structural properties of the hybrids[35]. They found that the clay with the smaller CEC or charge density actually reached a greater degree of exfoliation than the clay with the higher CEC. The authors attribute this phenomenon to less alkylammonium ions being intercalated into the gallery space. Less surfactant creates a greater amount of space for the epoxy resin to react in the interlayer space. This result however was not only a function of the charge density. A greater degree of

exfoliation occurred because of created space but also because of homopolymerization of the epoxy resin prior to the addition of the curing agent. The authors theorize an equilibrium mechanism for the exfoliation as follows. The high surface energy of the clay attracts the polar epoxy resin into the gallery space, expanding it. If no polymerization takes places the gallery height reaches a finite value when the system comes to thermodynamic equilibrium. If however the epoxy resin homopolymerizes, the equilibrium is offset and more polar resin enters the gallery expanding the space further.

In a follow-up paper from the same work Kornmann et al. varied the curing agent used to measure the change in exfoliation of clay in the epoxy[36]. The curing agents were specifically chosen because of their particular cure kinetics. By comparing curing agents of different reactivity they discovered that a greater degree of exfoliation was reached using the curing agent with the lowest reactivity. Further they found that increasing the temperature of the cure increased exfoliation. This result was attributed to differences in diffusion rates of the curing agent into the gallery space. From their previous work the authors were aware that polarity of the diffusing organic species affected the hybrid properties. They further explained the current results by theorizing that flexibility of the organic species may play a larger role in diffusion into the gallery than does polarity. Their concluding remarks indicate that the molecular mobility and reactivity of the curing agent are important parameters for determining the final properties of the hybrid.

In another paper Kornmann et al. changed the surface modification of the clay to determine its effects on final hybrid structure[50]. In this study they employ the use of several common modifying surfactants as well as the use of adducts. The adducts were simply epoxy resin reacted on either side with primary octadecylamines. The authors designed these adducts

to increase the polarity of the clay surface and there by promote diffusion into the gallery space and exfoliation. They prepared nanocomposites of fluorohectorite modified with surfactants or adducts and epoxy. When the hybrids were examined on a nanoscale with TEM, the nanocomposites containing the adduct surface modifiers showed greater separation between nanoplatelets. Even though the adducts showed better plate separation, all the hybrids fabricated showed a similar gains in mechanical properties over conventional composites.
An important aside the authors reported was a failure of a common technique used to protonate diamines as clay surface modifiers. Typically a diamine is protonated on one side by adding a stoichometric amount of HCl to a solution. The authors of this paper report that all the amino groups of the intercalated organic ions were protonated even if the amount of HCl was adjusted during the cation exchange. They hypothesize that the unprotonated amino groups are protonated due to the acidity of the layered silicate.

A recent publication by Saber-Samandari et al. involved a variation on the typical methods used to produce epoxy-clay nanocomposites.[68] The authors employed the use of a centrifugal mixer to enhance the exfoliation of clay in an epoxy matrix. They were able to produce nanocomposites with improved mechanical properties. They determined that exfoliation of Closite clays was best when the rotor speed of the centrifugal mixer was 1500 rpm.

2.2.5 Other Polymers used in PCNs

As mentioned above many other polymer clay systems have been developed for specific purposes. In this section only a few studies adding significantly to what has been discussed above will be included.

Several groups have made a contribution in the area of nanocomposites based on cationic polymers. The advantage in using ionomers is that there is a natural affinity for positively

charged polymers to interact with negatively charged clay sheets. Layer-by-layer (LBL) deposition has been used in several cases. Ku et al.[29] used LBL assembly to combine saponite and polyelectrolytes onto the surface of PET. The membranes showed high oxygen barrier properties when compared with pristine PET. Kotov et al.[31] used self-assembly with MMT and polydiallyldimethlammonium (P) chloride. They found they could deposit layers of P followed by MMT on substrates such as glass, quartz, silica-wafers, gold, silver, and Teflon. They further discovered that the MMT platelets formed stacks on top of the polyelectrolyte layer averaging two aluminosilicate sheets. Traditional methods have also been used to combine polyelectrolytes with clay. Paczkowska et al. proved that polymer-clay nanocomposites could be fabricated by using photochemical initiated cationic polymers[69]. Song et al.[70] used the simple solution intercalation method to combine MMT and Nafion into a nanocomposite for fuel cell applications.

Some important contributions were made to the dispersion of MMT in polyurethane by Choi et al. They were able to control the dispersibility of organoclay in a polyurethane matrix using sonication[14]. They showed clear improvements in barrier properties, tensile strength and thermal stability with the use of sonication.

Yoon et al. performed a comprehensive study of different swelling agents on MMT in polycarbonate-clay composites[62]. They drew some interesting conclusions about the relationships of organoclay structure to nanocomposite properties summarized below. Comparing surfactants with one tail and two tails, surfactants with one tail gave greater overall d-spacing in the final nanocomposite. However the two tailed surfactant gave the highest modulus and elongation at break. If one compares a surfactant with a hydroxy-ethyl headgroup to one with strictly methyl head groups, the hydroxy-ethyl surfactant produces a hybrid with a

significantly higher modulus. A surfactant containing three tails gave the best mechanical improvements of any composite in the study. This particular surfactant contained one C_{18} alkyl tail and two shorter poly(ethylene oxide) tails. The authors theorize these improvements were due to good miscibility between polycarbonate and polyethylene oxide. It was found that there are some very subtle effects to nanocomposite properties when comparing unsaturated versus hydrogenated tails and when using quaternary ammonium versus tertiary amine heads groups. Finally the authors showed that when head groups containing hydrogen, methane or benzyl groups are compared that no significant effects on intercalated structures occur. The surfactant containing a benzyl group however did give a slightly higher modulus and elongation at break.

2.3 Aluminophosphates with Al/P ratio 3/4

There is a long scientific history devoted to the development of inorganic open-framework structures.[71] These structures have been used in the areas of catalysis, adsorption, and separations. They are characterized as being high surface area structures with regular microporous openings. The most well studied structures are zeolites which are made from aluminum and silica. There are however other classes of these open-framework structures which exist and are currently being studied.

In the early 1980's scientists at Union Carbide synthesized the first non-silica zeolite framework structures. The structures produced were based on aluminum and phosphorous and called aluminophosphates. These scientists synthesized 20 new aluminophosphate structures including 3-D frameworks and 2-D layered structures.[72] These aluminophosphates had chemical formulas described by $AlPO_4$-n because the structures all contained Al/P ratios of unity. Following this discovery, activity in the field increased rapidly. Today there is a large family of aluminophosphates including 1-D chain structures, 2-D layered structures and 3-D framework

structures.[73] These structures are synthesized using both hydrothermal and solvothermal methods and exhibit a variety of Al/P ratios in composition. The potential application of these structures is promising. It is hoped that unique materials will be developed that can be used in catalysis, separations, and molecular assembly.

There are many 2-D layered aluminophosphate structures reported in the literature. They include structures with Al/P ratios of 1/2, 4/5, 2/3, and 3/4.[73] Depending on the method used to synthesize these layered materials, they produce low dimensional frameworks that form net like structures. These "nets" exhibit different connectivity between the aluminum, phosphorous, and oxygen atoms. As a result they have different ring size openings and microporosities. The majority of these 2-D structures are single layered, but one example is double layered[74, 75]. The first section of this chapter will discuss this sub family of $[Al_3P_4O_{16}]^{3-}$ stoichiometry and the second section will be specific to the compound $[Al_3P_4O_{16}]^{3-} \cdot 3[CH2CH3NH3]$ which is the compound used in the current work.

2.3.1 2-D layered aluminophosphate of $[Al_3P_4O_{16}]^{3-}$ stoichiometry

A survey of literature produced 23 different structures associated with the layered $[Al_3P_4O_{16}]^{3-}$. The formulas for these structures can be seen in Table 2.1 below along with their citations, synthesis method, and some structural properties.

2.3.2 General reaction conditions

The mechanism to control the final structure of $[Al_3P_4O_{16}]^{3-}$ is not well understood. The materials used to synthesize each different $[Al_3P_4O_{16}]^{3-}$ and the reaction conditions are ,however, similar. The aluminum source is generally either pseudobohemite (Al_2O_3) or aluminum triisopropoxide ($Al(PrO^i)_3$). The source for phosphorous is generally 85% phosphoric acid. The reactions take place in a Teflon© lined autoclave at elevated temperatures (120°C-200°C). If the

reaction takes place in predominantly aqueous environment the reaction is classified as hydrothermal. If the reaction mixture is mostly organic solvent (often ethylene glycol) the reaction is said to be solvothermal. The difference in the final structure obtained is a result of the reaction conditions along with the organic template or structure directing agent (SDA) used in the synthesis. The counterion seen in the final structure (Table 2.1) is generally chemically related to this SDA. Often the counterion is a protonated form of the original SDA used in the synthesis procedure. The different counter ions seen in Table 2.1 indicate many different SDA

Table 2.1 All known $[Al_3P_4O_{16}]^{3-}$ 2D layered structures. Top ¾ table synthesized with alkylamines and ammonium salt SDA. Bottom ¼ of table synthesized with coordination complex SDA. AlPO used in the current study is highlighted.

Formula	Method	Net structure	Stacking	Citation
$[Al_3P_4O_{16}][NH_3(CH_2)_2NH_3][OH_2(CH_2)_2OH][OH(CH_2)_2OH]$	solvothermal	4 .6.8 (I)	ABAB	76
$[Al_3P_4O_{16}]^{3-}\cdot 1.5[NH_3(CH_2)_4\ NH_3]^{2+}$	hydrothermal	4.6.12	ABAB	77
$[Al_3P_4O_{16}]^{3-}\cdot(NH_3(CH_2)_5NH_3)^{2+}\cdot(C_5H_{10}NH_2)^{+}$	solvothermal	4.6.8 (I)	AAAA	78, 79
$[Al_3P_4O_{16}C_9H_{24}N_3]$	hydrothermal	4.6.12	ABAB	80
$[Al_3P_4O_{16}]^{3-}[C_4H_7NH_3^{+}]_2[C_5H_{10}NH_2^{+}]$	solvothermal	4.6.8 (I)	AAAA	81
$[Al_6P_8O_{32}]3[NH_3CHMeCH_2NH_3]\cdot H2O$	solvothermal	4.6 (I)	ABAB	82
$[Al_3P_4O_{16}]^{3-}\cdot 3[CH_3CH_2NH_3]^{+}$	solvothermal	4.6.8 (I)	AAAA	83
$[BuNH_3]_3[Al_3P_4O_{16}]$	solvothermal	4.6.12	AAAA	84
$[Al_3P_4O_{16}]\cdot 3[CH_3CH_2CH_2NH_3]^{+}$	solvothermal	4.6.8 (I)	AAAA	85
$2[N_2C_3H_5][Al_3P_4O_{16}H]$	solvothermal	2.3.6 (DL)	AAAA	74, 75
$[CH_3NH_3]_3\cdot Al_3P_4O_{16}$	solvothermal	4.8	AAAA	86
$[C_6H_{21}N_4][Al_3P_4O_{16}]$	solvothermal	4.6.8 (II)	AAAA	87
$[Al_3P_4O_{16}][C_5N_2H_9]2[NH_4]$	solvothermal	4.6 (III)	AAAA	88
$[NH_3CH_2CH(OH)CH_3]_3\cdot Al_3P_4O_{16}$	solvothermal	4.6.12	ABCABC	89
$(C_4N_2H_{12})_{4.5}[Al_3P_4O_{16}]_3\cdot 5H_2O$	hydrothermal	4.6 (IV)	AABAAB	90
$[Al_3P_4O_{16}][(CH_3)_2NHCH_2CH2NH(CH_3)_2][H_3O]$	solvothermal	4.6.8 (I)	AAAA	91
$[Al_3P_4O_{16}][C_6N_3H_{17}][H_3O]$	hydrothermal	4.6 (II)	ABAB	92
$(C_4H_{14}N_2)_{1.5}\cdot[Al_3P_4O_{16}]$	hydrothermal	4.6 (V)	ABAB	93
---	---	---	---	---
$[Co(en)_3Al_3P_4O_{16}\cdot 3H_2O]$	hydrothermal	4.6 (II)	ABAB	94
$[Al_3P_4O_{16}]^{3-}\cdot Co(tn)_3^{3+}\cdot 2H_2O$	hydrothermal	4.6.8 (I)	AAAA	95
trans-$Co(dien)_2\cdot Al_3P_4O_{16}\cdot 3H_2O$	hydrothermal	4.6 (I)		96
d-$Co(en)_3\cdot Al_3P_4O_{16}\cdot 3H_2O$	hydrothermal	4.6 (II)	ABAB	97
Δ,Λ-$Ir(en)_3[Al_3P_4O_{16}]\cdot xH_2O$	hydrothermal	4.6 (II)	ABAB	98

were used in the synthesis process. The $[Al_3P_4O_{16}]^{3-}$ formulas in Table 2.1 have been divided into two different groups according to their SDA. The top part of the table contains formulas

where the SDA was a cyclic or linear amine or alkyl ammonium salt. The bottom part of the table contains the efforts of a few groups to use transition metal coordination complexes as SDA.

2.3.3 General similarities among $[Al_3P_4O_{16}]^{3-}$

Even thought this subfamily of aluminophosphates has a lot of structural diversity it shares many properties in common. The 2-D layers of the structures in $[Al_3P_4O_{16}]^{3-}$ are made entirely from connected aluminum and phosphorous tetrahedra. This means that there are a limited number of theoretically possible net structures. This fact will be elaborated on and discussed later. In every case, the aluminum atom is in AlO_4 tetrahedra where all four oxygen atoms are connected to the main 2-D structure. The phosphorous atoms are also four coordinated to oxygen in PO_4 tetrahedra, however, only ¾ of the oxygen atoms in the tetrahedra are coordinated to oxygen in the structure. This leaves O-P bonds in each formula unit protruding away from the structure. X-ray diffraction data shows that these P-O bonds are actually double bonds in every case. It is these dangling double bonded oxygen atoms that hydrogen bond with the counter ion located in the gallery space. In every case the 2-D layered $[Al_3P_4O_{16}]^{3-}$ have these counter ions present in the gallery space. They serve to both balance the negative charge of the sheets and hold the sheets together with a series of hydrogen bonds. The dangling P=O bonds and hydrogen bonding system can be seen for an example complex $[Al_3P_4O_{16}][C_5N_2H_9]2[NH_4]$ in Figure 2.6 below. In this case the counter ions are protonated 1,2-dimethylimidazole and ammonium cations.[88]

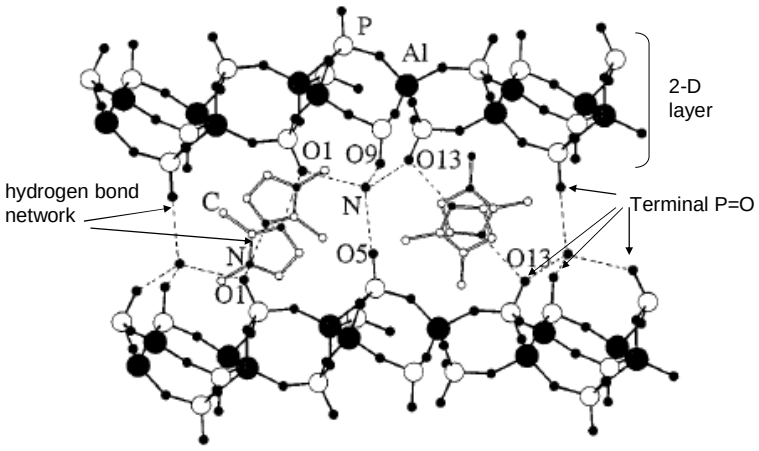

Figure 2.6 View along [010] direction of $[Al_3P_4O_{16}][C_5N_2H_9]2[NH_4]$ showing terminal P=0 and hydrogen bonding network. Adapted from Figure 3.[88]

2.3.4 General diversity among $[Al_3P_4O_{16}]^{3-}$

There is obvious diversity in the sub family of 2-D aluminophosphates with the stoichiometry $[Al_3P_4O_{16}]^{3-}$. As can be seen in Table 2.1, there are currently 23 different formulas for 2-D single sheet $[Al_3P_4O_{16}]^{3-}$ known and many more are believed to be theoretically possible. There are many different net structures produced when different reactants and reaction conditions are used. The counterion in the gallery space is different for each structure. Because of this counterion, each one of the structures produced has a very unique and complex hydrogen bonding network which holds the layered system together. As a result of this diversity structures with various microporosities and properties are produced.

2.3.5 Current net structures and stacking

The first $[Al_3P_4O_{16}]^{3-}$ layered structure synthesized by Jones et al. consisted of a 4.6.8 (I) net. Since then many other net structures have been synthesized. The $[Al_3P_4O_{16}]^{3-}$ layered structures synthesized to date contain nets with 4.6, 4.8, 4.6.8, and 4.6.12 membered rings. (see Figure 2.7). Within these net structures there are several different configurations of the 4.6 nets

and two configurations of the 4.6.8 nets. Figure 2.7 illustrates all of the known structures synthesized to date.

The 4.6 nets have the largest variety with five known structures. The latest addition to the 4.6 nets can be seen in Figure 2.7. It was synthesized very recently by Tuel et al. and was previously only known as a theoretical configuration.[93] There are two types of 4.6.8 nets known and one type of 4.6.12 nets. The type (II) 4.6.8 net has only been observed once in a synthesis by Yao et al.[87] however the 4.6.12 has been synthesized several times with different SDA. One oddity is the 4.8 net produced by Vidal et al.[86] They produced the only known example of a 4.8 net by using methylformamide as the synthesis solvent which also served as the SDA for the reaction. There is also one example of a 2.3.6 net which exists as a double layer instead of a single layer like all the other layered aluminophosphates.[74, 75] Picture of all of these net structures can be seen in Figure 2.7.

The stacking of these structures can be described most commonly as AAAA, ABAB. There are however a few exceptions which exhibit ABCABC[89] and AABAAB[90] stacking as can be seen in Table 2.1. The stacking is in general believed to be a result of the hydrogen bonding network that is formed during synthesis and recrystallization. Stacking will be discussed again in a later section.

The final net structure of these compounds is a combination of the SDA used and the reaction conditions of the synthesis. However, some general observations can be made about the nets in relation to methods and SDA. For instance, the 4.6 (II) structure (seen in Figure 2.7) is only found when the synthesis involves chiral metal coordination complexes as the SDA because they direct the formation of this chiral net. The alkyl amine compounds are produced predominately solvothermally and the metal complex compounds are produced solely using hydrothermal

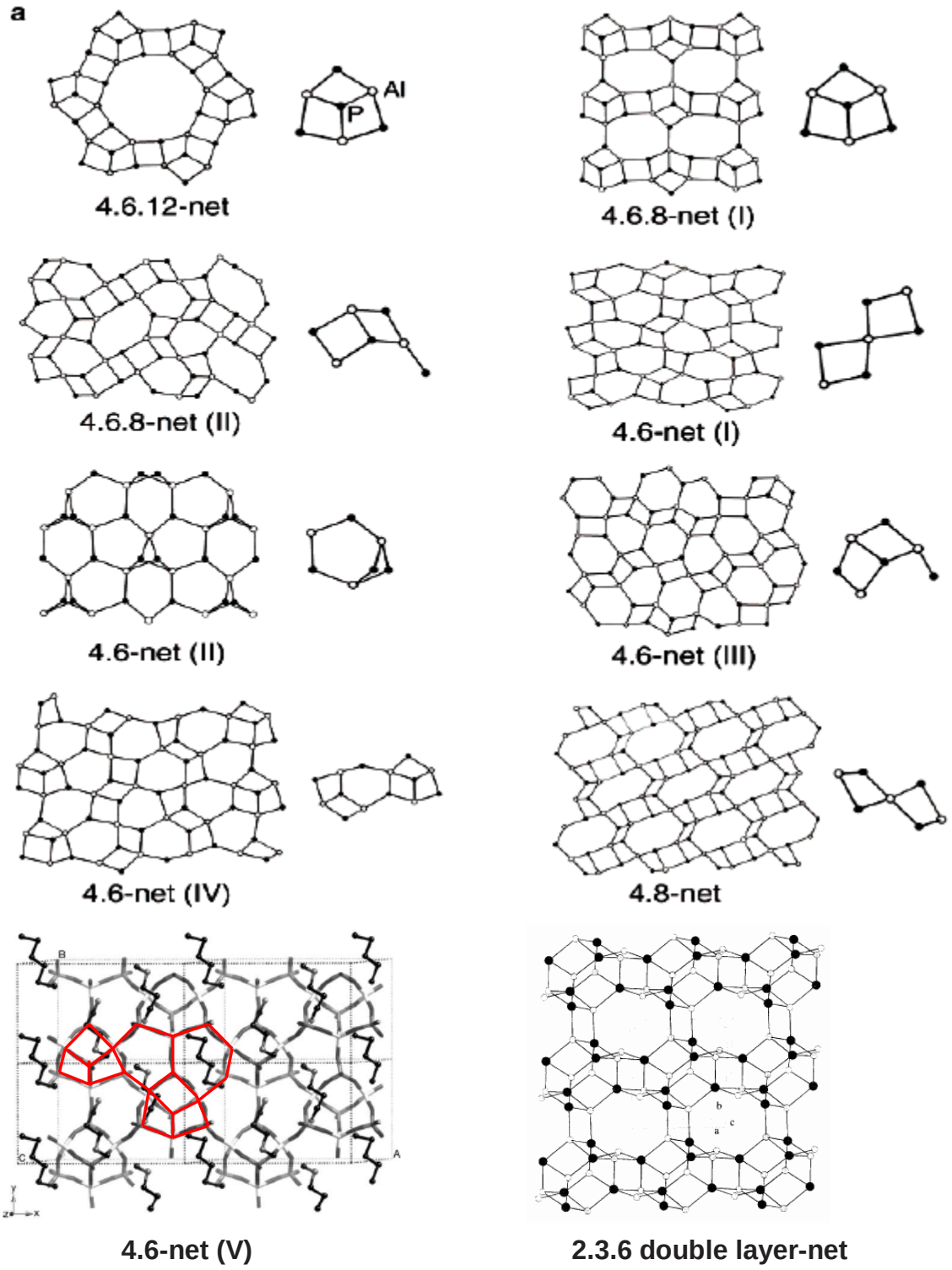

Figure 2.7 All known net structures of layered $[Al_3P_4O_{16}]^{3-}$. (top) adapted from fig 8a.[70]. (bottom) newest 4.6 structure MDAP-1 synthesized by Tuel et al. adapted from fig 2.[93] bottom right adapted from Yu et al. [75]

methods. Every net structure produced contains 4 membered rings and all but one of the net structures contains 6 membered rings.

2.3.6 Structures produced with amines and alkyl ammonium salt SDA

The majority of the $[Al_3P_4O_{16}]^{3-}$ structures have been synthesized with organo-amine SDA. The SDA used for formula in the top of Table 2.1 include various linear and cyclic, monoamines, diamines, and higher order amines. The final structures produced change with the number of amine groups as well as the position of amine groups on the organo-amine SDA. The lengths of the alkyl chains and the number of functional groups present on the SDA are known to affect such properties as the stacking and final net structure.[83]

It is not clear from the literature surveyed why every different SDA leads to a certain structure however some of the known templating effects of organo-amine SDA are summarized below. Gao et al. observed that when short chain SDA are used the formation of 4.6.8 nets dominate, however when long chain SDA are used 4.6.12 nets are synthesized.[83] The stacking is influenced by the number of amine groups on the SDA. When a monoamine is used the stacking is AAAA and when a diamines is used the stacking is ABAB.[83] The stacking phenomena was first observed by Jones et al. who synthesized the first $[Al_3P_4O_{16}]^{-3}$ net structure.[76] They used a diammonium cation and obtained a 4.6.8 net with an ABAB stacking sequence. Later they used propylamine to obtain an AAAA stacking of the same structure. The majority of the formulas listed in the top of Table 2.1 follow this general trend.

One notable exception to the above observation was found by Yao et al.[87] They used triethylenetertramine, which contains a long alkyl chain and four amine groups. The authors expected to synthesize a 4.6.12 net with ABAB stacking. However, the result was a new type of 4.6.8 net which was previously unseen and the stacking was curiously AAAA. The work of Yao

et al. represents the only example of a "triply-protonated template molecule" being used.[87] The authors explain the new type of net with the hydrogen bonding network formed under the restraints of this complex templating agent. Because of the increased number of NH_2 groups of this SDA, it arranges differently in the gallery space during crystallization. This causes the new 4.6.8 net structure to form.[87]

2.3.7 Structures produced with metal coordination complex SDA

While most $[Al_3P_4O_{16}]^{3-}$ structures have been produced using alkyl and ammonium salt structure directing agents (SDA), a few groups have utilized metal coordination complexes as SDA in the attempt to produce chiral 2D aluminophosphate sheets. Chiral forms of the 2D layered aluminophosphate $[Al_3P_4O_{16}]^{3-}$ are of interest for application in the pharmaceutical industry. They could potentially be used as "enantioselective heterogeneous catalysts"[95], or as an alternative to chiral sorbents for the separation of left and right handed molecules[96].

The names of the chiral metal complexes used are in the references for this section. The names of the complexes used are as follows $[Co(en)_3]^{3+}$ [94], $[Co(tn)_3]^{3+}$ [95], $[Co(dien)_2]^{3+}$ [96], Λ-Tris(ethylenediamine)cobalt III [97], and $[Ir(en)_3]^{3+}$ [98], where (en = ethylenediamine), (tn = 1,2 diaminopropane), and (dien = diethylenetriamine). The structures of these metal complexes and their enantiomers can be seen below in Figure 2.8.

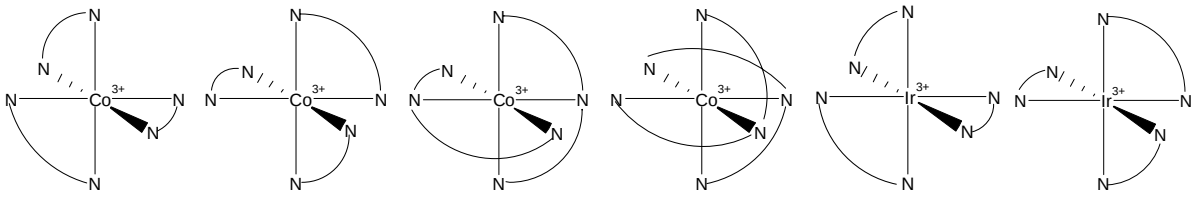

Λ-$Co(en)_3^{3+}$ or Λ-$Co(tn)_3^{3+}$ | Δ-$Co(en)_3^{3+}$ or Δ-$Co(tn)_3^{3+}$ | trans-$Co(dien)_2^{3+}$ | cis-$Co(dien)_2^{3+}$ | Λ-$Ir(en)_3^{3+}$ | Λ-$Ir(en)_3^{3+}$

Figure 2.8 Representations of the enantiomers of metal coordination complex SDA.

Several groups of researchers have attempted to use transition metal coordination complexes as structure directing agents for the formation of chiral 2D aluminophosphates with $[Al_3P_4O_{16}]^{3-}$ stoichiometry. It is known that by changing small organic directing agents along with reaction conditions that different net structure $[Al_3P_4O_{16}]^{3-}$ can be produced. It also is reasonable that metal coordination complexes containing ligands with properties similar to the small organic molecules typically used as SDA could also produce net structures in aluminophosphates.

Co(III) complexes as SDA

Morgan et al. made one of the first attempts to employ metal coordination complexes as SDA for the synthesis of chiral 2D aluminophosphates.[94] They employed the complex $[Co(en)_3]^{3+}$ which can be seen above in Figure 2.8. The most important property of this complex for use as an SDA is that it exhibits chirality. This means that there are two chemically identical SDA known as an enantiomeric pair that exist as mirror images of each other. In Figure 2.8 the two forms Δ, Λ can be clearly seen. Chirality of the SDA is important because Morgan et al. postulated that chiral SDA could produce a chiral final structure for aluminophosphate.[94]

The properties of the ligands of the $[Co(en)_3]^{3+}$ are also important for its use as an SDA. The ligands are shown in abbreviated form in Figure 2.8. The actual formula for these three bidentate ligands attached to the Co^{3+} central atom is $H_2NCH_2CH_2NH_2$. It can be seen from the formula that these ligands are very similar to other alkyl SDA that have produced aluminophosphate nets. This particular ligand, if looked at separately from the metal complex, is identical to one cited by Gao et al. for use as an alkyamine SDA.[83] It is this property of the complex that allows the final structure to have the same hydrogen bonding system necessary for this family of structures to exist. Another property of $[Co(en)_3]^{3+}$ which allows it to be used as a

chiral SDA is the slow ligand exchange kinetics of the complex. The exchange of the ligand from the main complex during a reaction is undesirable in this case. It is known that under the reaction conditions experienced in the synthesis of $[Al_3P_4O_{16}]^{3-}$ the complex $[Co(en)_3]^{3+}$ will not readily ligand exchange.[94]

In the work cited above the use of $[Co(en)_3]^{3+}$ as a SDA did produce an $[Al_3P_4O_{16}]^{3-}$ structure with chiral layers. The final formula $[Co(en)_3Al_3P_4O_{16}{\cdot}3H_2O]$ was confirmed using XRD. The structure consisted of alternating anionic $Al_3P_4O_{16}$ layers which were mirror images of each other and separated by one enantiomer of $[Co(en)_3]^{3+}$.[94] The single crystals contained both enantiomers of the metal complex and chiral AlPO layers. The theory of why the final structure was chiral is not completely understood. The explanation of Morgan et al. was that a chiral templating agent "induced chiral features in the lattice" and that the hydrogen bonding network created by a chiral SDA influenced the final topology of the net structure.[94] What ever the explanation, it is clear that chiral metal complexes can produce chiral aluminophosphate structures.

Other Co(III) metal complexes used as SDA

Several other research groups followed the success of Morgan et al. by employing different kinetically inert Co(III) coordination complexes as SDA. These included Bruce et al. $[Co(tn)_3]^{3+}$ [95], Bruce et al. $[Co(dien)_2]^{3+}$ [96], and Gray et al. Λ-Tris(ethylenediamine) cobalt III[97]. To illustrate the fact that it is difficult to predict the outcome of a particular structure by simply changing the chiral SDA, results obtained by the above authors are summarized below.

The purpose of using chiral metal coordination complexes as SDA is to create chiral aluminophosphate structures. Bruce et al. attempted to make chiral AlPO by employing $Co(tn)_3^{3+}$ as the SDA[95]. The only difference in this complex when compared to Morgan et al.

was the ligands on the Co^{3+} atom. The ligands in this case are $HN_2CH_2CH_2CH_2NH_2$ which contain one more C atom in the chain when compared to Morgan et al. The results of the synthesis were surprising. Even though a racemic mixture of $Co(tn)_3^{3+}$ was used each crystal contained only one enantiomer of $Co(tn)_3^{3+}$ and the AlPO layers were not chiral. A second attempt by Bruce et al. involve the use of $Co(dien)_2^{3+}$ as the SDA. This complex again had the same Co^{3+} center however the two tridentate ligands attached were $NH(CH_2H_4NH_2)_2$. Using a racemic mixture of $Co(dien)_2^{3+}$ resulted in single crystals with chiral AlPO layers separated by only the *trans*- form of the metal complex used. Finally, Gray et al. used a single enantiomer of the racemic mixture used by Morgan et al. They used an optically pure form of Λ-$Co(en)_3^{3+}$ as an SDA. The synthesis resulted in anionic chiral sheets of AlPO with Λ-$Co(en)_3^{3+}$ hydrogen bonded between the layers in the gallery space. The results summarized above show that sometimes chiral SDA produce chiral sheets and sometimes they do not, and that a single enantiomer can produce a chiral AlPO structure as well as a racemic mixture. The results are not consistent which is why it is difficult to predict the outcome simply from the structure of the SDA.

Ir(III) complexes for the synthesis of chiral $[Al_3P_4O_{16}]^{3-}$ layered materials

All the attempts summarized above utilized Co^{3+} based coordination complexes to make chiral AlPO structures. As mentioned above, during the synthesis of AlPO, high pressure and temperatures make it necessary to use metal complexes which are stable against ligand exchange. If the ligands are not stable, undesired products such as metal phosphates can form. It is however known that certain oxidation states of metals produce inert complexes. One of the oxidation states of Co known to inhibit ligand exchange is Co^{3+} which is why it is the subject of the research mentioned above.[94]

Recently, Williams et al. explored the use of Ir^{3+} based coordination complexes as a replacement for the Co^{3+} based complexes[98]. The authors chose Ir^{3+} because of known rate constant data. They compare the known rate constant for ligand exchange of $Ir(OH_2)_6^{3+}$ with that of the same hexaquo complexes of Cr^{3+} and Rh^{3+} at room temperature. They state that the iridium complex has a rate constant 10^4 times slower than the chromium complex and 10 times slower than the rhodium complex.[98] It is also stated that the formerly used Co^{3+} complexes would fall somewhere between these two values. One possible explanation for these kinetic differences can be seen in the periodic table. Both Co^{3+} and Ir^{3+} are group IX metal ions in high oxidation states. It can be seen however that Ir is lower on the periodic table than Cr. This indicates Ir has *5d* orbitals and Co has *3d* orbitals. It is known that bonding between metals and their ligands is improved for the "more expanded *4d* and *5d* orbitals when compared with the compact *3d* orbitals."[99] With everything else equal this improved bonding could slow the exchange of a ligand for an Ir(III) complex when compared to a Co(III) complex.

Because of the kinetic advantage Williams et al. chose a racemic mixture of $Ir(en)_3^{3+}$ for an AlPO synthesis with higher reaction temperatures to test the stability of the SDA.[98] As a result of the synthesis with this new SDA, $[Al_3P_4O_{16}]^{3-}$ layered single crystals were obtained which were identical in structure to those found by Morgan et al. (with exception of the interlayer cation). The crystals contained chiral layered AlPO and both enantiomers of $Ir(en)_3^{3+}$ were present.

2.3.8 Theoretical net structures

Several papers have been published on the theoretical structures of aluminophosphates with $[Al_3P_4O_{16}]^{3-}$ stoichiometry[100, 101]. These papers outline a method to calculate every possible geometric configuration of the aluminum and phosphorous tetrahedra. The result of these works

is a list of theoretical net structures that have not been produced experimentally along with net structures that have been seen as a result of experiments.

Although many different $[Al_3P_4O_{16}]^{3-}$ structures and net topologies have been synthesized and described, it is still not possible to predict the final structure from the reaction conditions used. For this reason, Zhou et al. used computational techniques to produce theoretical net structures of $[Al_3P_4O_{16}]^{3-}$.[100] They adapted techniques developed by other researchers for determining the structures of zeolite materials to aluminophosphates. The calculations were performed on desk top computers using both developed code and commercially available software packages.

The authors followed a simple set of rules to generate possible nets. It is known that all of the $[Al_3P_4O_{16}]^{3-}$ stoichiometry structures contain alternating 4 connected Al tetrahedra, and 3 connected P tetrahedra with the fourth O ending in a double bond. This was essentially the first rule used. The other two rules simply stated are "Rule 2 The same type of points can not directly be connected, and Rule 3 The mesh can be expanded into a periodic 2D net." [101] The authors used a hexagonal array of points so that each point could potentially be connect to six points around it. They converted the set of rules above into mathematical algorithms to generate potential nets.

The calculations produced more than 500 theoretical structures for the $[Al_3P_4O_{16}]^{3-}$ stoichiometry. After the connectivity was established the authors used a commercially available software package to minimize the energy of each structure. The structures generated were a combination of 4, 6, 8, 10 and 12 MR, and the lowest energy structures consisted of 4.6, 4.6.8, 4.6.10, 4.6.12, 4.6.8.12 and 4.8 nets.[100] The authors were able to generate some energy minimized net structures that had been previously reported in literature (see Figure 2.9 below).

These consistencies verified the validity of their models. They also generated other energy minimized nets that have yet to be seen experimentally. Some of the theoretical structures are seen below in the Figure 2.9.

Interestingly, one of the theoretical structures described by Zhou et al. has recently been experimentally verified by Tuel et al. Previously there were four known 4.6 type $[Al_3P_4O_{16}]^{3-}$ net structures. This year Tuel et al. published a new 2D layered compound which they called MDAP-1. This structure has the formula $(C_4H_{14}N_2)_{1.5}[Al_3P_4O_{16}]$.[93] They reported a previously unknown 4.6 net structure for this compound. This structure has however been previously reported as a theoretical net by Zhou et al. The structure of MDAP-1 can be seen in Figure 2.7 and matched to the theoretical net G7 in Figure 2.9.

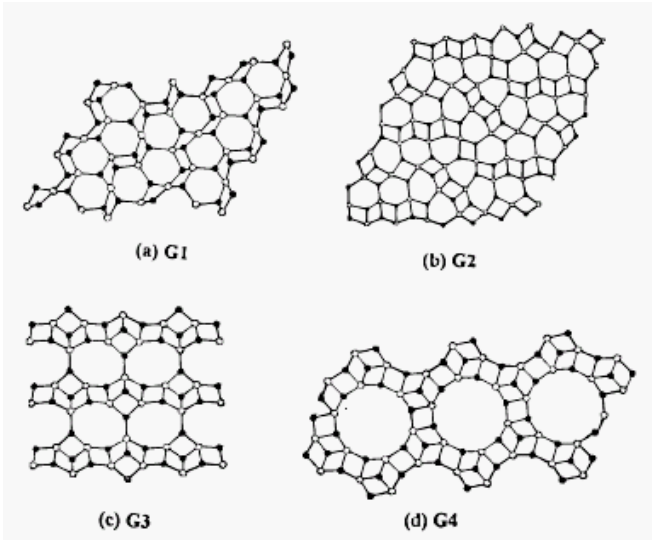

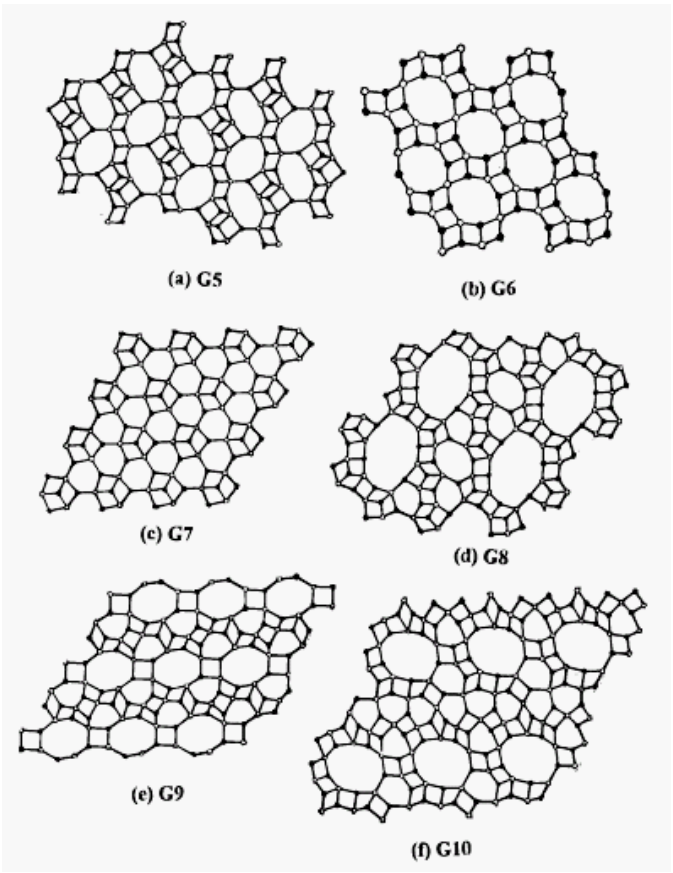

Figure 2.9 (left) Theoretical structures generated by Zhou et al. that match known $[Al_3P_4O_{16}]^{3-}$ structures. (right) Generated structures that have not yet been experimentally synthesized.[92]

2.3.9 $[Al_3P_4O_{16}]^{3-}\cdot 3[CH_3CH_2NH_3]^+$

The aluminophosphate utilized for the current work is $[Al_3P_4O_{16}]^{3-}\cdot 3[CH_3CH_2NH_3]^+$ (Table 2.1). The material is synthesized following the procedure developed by Gao et al.[83] The reaction is considered solvothermal and the main Al and P sources are $Al(OPr^i)_3$ and 85% phosphoric acid. The reaction medium is a combination of ethylene glycol / butyl alcohol and the SDA for this aluminophosphate is ethylamine. An XRD pattern for this compound is available for comparison to confirm if a synthesis is successful.

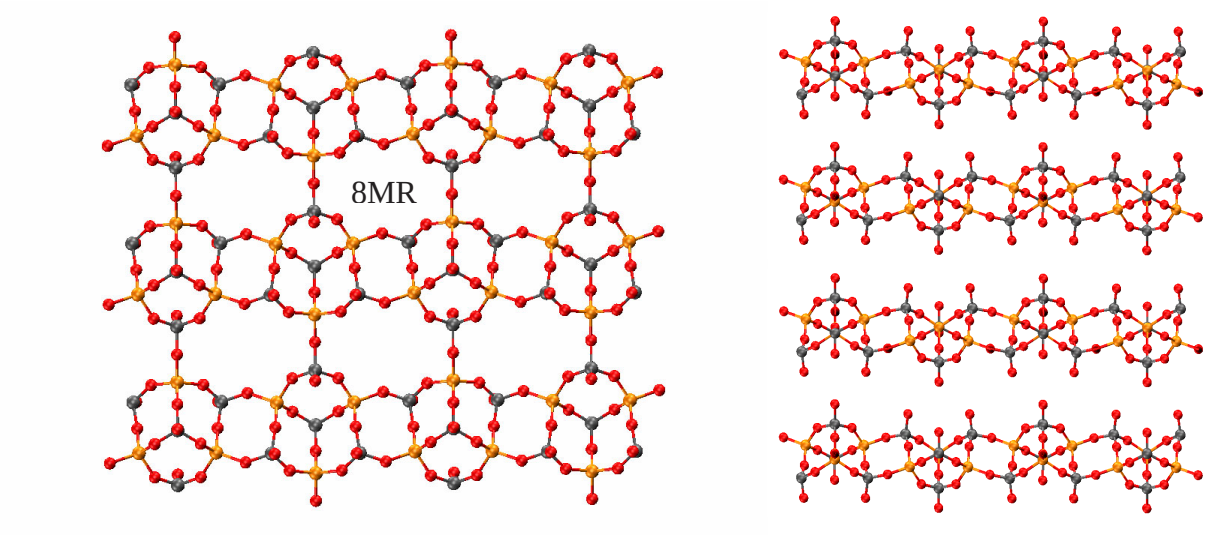

Figure 2.10 (left) view of AlPO down the (001) plane; (right) view down the (100) plane of four layers Atom positions obtained from crystallographic information Gao et al.[83] Counter ions not shown for simplicity

This aluminophosphate exhibits desirable properties for the current work. The resulting AlPO structure has a 4.6.8(I) net type seen in Figure 2.7. Figure 2.10 shows the specific net for this compound generated using single crystal X-ray data. The ring structure is known as 4.6.8 because only the heavy atoms are counted in the naming. In this case the oxygen atoms are omitted in reference to the ring structures. Thus the 4MR contains two Al and two P, the 6MR

contains three P and three Al, and the 8MR contains four P and four Al. The estimated dimensions of the oval 8MR pore are 4.44 x 3.29 x 3.17 Å. These dimensions from O to O were estimated using single crystal data reported by Gao et al.[83] and considering the ionic radius of oxygen. The stacking of this synthesized compound is AAAA (Table 2.1). Ethyl ammonium ions are present in the gallery space of the crystals to counterbalance the negative charge from the AlPO plates (Figure 2.11). There are three ethyl ammonium ions associated with each unit of AlPO. A complex hydrogen bonding network holds the 2-D layers of the structure together. As can be seen in Figure 2.11 each ethyl ammonium ion hydrogen bonds to three sites on the structure. Two of the sites are P=O protruding down from the top sheet and one site is the cap unit P=O from sheet below. It is this hydrogen bonding that must be interrupted in order to expand and eventually exfoliate the sheets of AlPO. One potential caveat of interrupting the hydrogen bonding network is collapse of the structure. If one looks closely at the structure below it is evident that the framework is made up of aluminum and phosphorous tetrahedra. Because AlPO does not contain octahedron in the structure like natural clays much of the stability derives from the hydrogen bonding network between the layers.

One way to interrupt the hydrogen bonding networks between aluminophosphate sheets is to ion exchange the smaller gallery molecules for larger ones. This serves to force the platelets apart reducing the forces between nanoplatelets. In the current work several different surfactants have been used in the attempt to achieve exfoliation. The specific surfactants used will be discussed later in the preliminary results section.

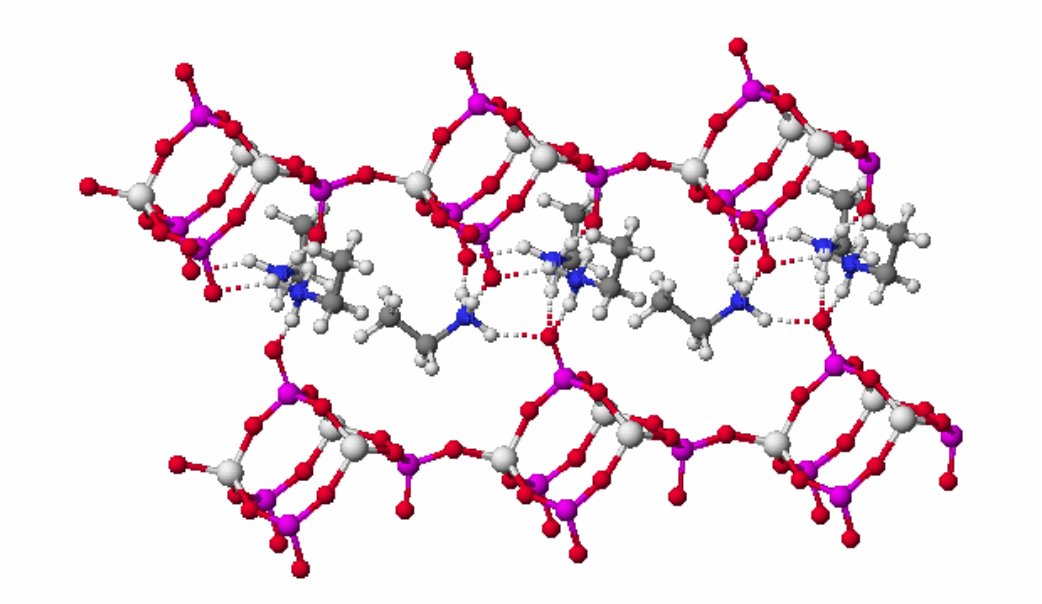

Figure 2.11 Layered structure of $[Al_3P_4O_{16}]^{3-}\cdot 3[CH_3CH_2NH_3]^+$ including the hydrogen bonding network (dotted lines) between the structure and ethyl ammonium ions in the gallery spaces. Created with data from Gao et al.[83]

2.3.10 12MR-AlPO Structures

The focus of most of the current research has been on $[Al_3P_4O_{16}]^{3-}\cdot 3[CH_3CH_2NH_3]^+$ which contains an 8MR which may sieve gases. There are however layered 12MR-AlPO structures which may be able to sieve gases as well. These structures contain larger 12MR openings which may provide a path with greater diffusion coefficients when compared to the 8MR-AlPO. Comparing transport properties of the 8MR and 12MR composites could allow us to determine if the surfactant is affecting transport. For instance, if a "well exfoliated" 12MR composite exhibits barrier behavior then pore blockage from the surfactant is likely the cause.

Two examples of 12MR-AlPO net structures can be seen below in Figures 2.12-2.13. They are both layered aluminophosphates similar in composition to the AlPO that is currently used. The first structure (Figure 2.12) is a 4.6.12 net made from a solvothermal synthesis, similar to that of the 8MR AlPO.[84] The resulting formula is $[BuNH_3]_3[Al_3P_4O_{16}]$ in which

$[Al_3P_4O_{16}]^{3-}$ layers are separated by a butyl ammonium ions. The circular 12MR ring openings have a diameter of 9.6Å from oxygen center to oxygen center. This corresponds to an opening that is approximately 6.6Å when the ionic radius of oxygen is taken into account. The second structure shown (Figure 2.13) is a 4.12 layered net structure separated by diammonium and tetrammonium cations. The solvothermal synthesis produces the formula $[Al_2P_4O_{16}][C_6H_{22}N_4][C_2H_{10}N_2]$ which has an Al/P ratio of 1/2.[102] The 12MR openings in this structure have more of an elliptical shape. The dimension along the long axis Al-Al centers is 12.4Å and the distance across the short axis Al-P centers is 7.9Å.

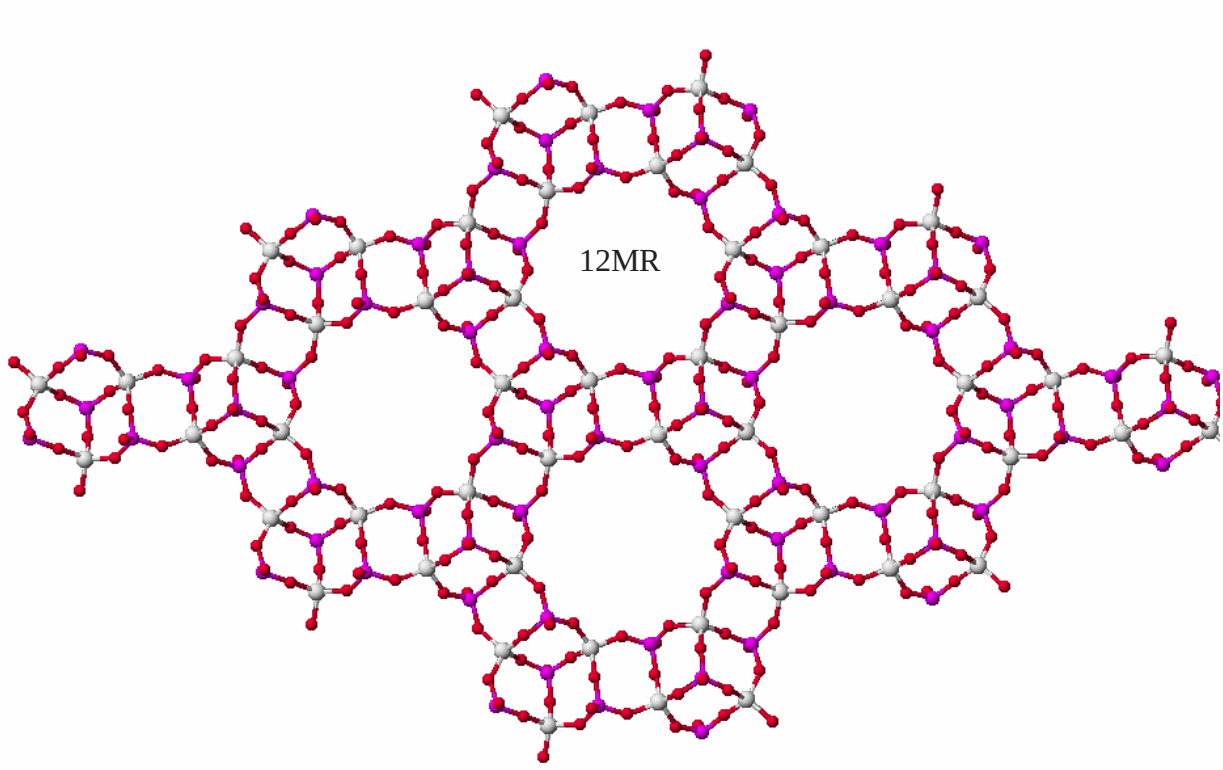

Figure 2.12 12MR $[BuNH_3]_3[Al_3P_4O_{16}]$ synthesized by Chippindale et al.[84]

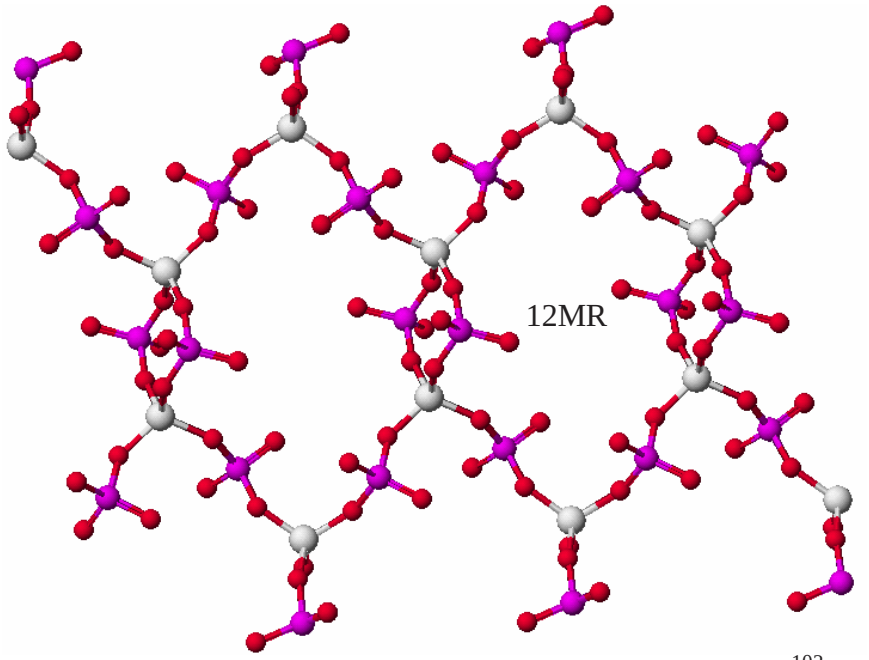

Figure 2.13 12MR $[Al_2P_4O_{16}][C_6H_{22}N_4][C_2H_{10}N_2]$ synthesized by Wei et al.[102]

2.3.11 Delamination of $[Al_3P_4O_{16}]^{3-}$

The delamination of layered aluminophosphates with $[Al_3P_4O_{16}]^{3-}$ stoichiometry has been described in the literature.[103-106] Delamination of these layered aluminophosphates is crucial to take full advantage of the benefits offered by their microporous structure. Unfortunately, the literature available on this subject only describes exfoliation in water based systems. This method is therefore difficult to apply to the current project which utilizes polymers soluble only in organic solvents.

This material is different from traditional zeolites and layered solids. The structure of $[Al_3P_4O_{16}]^{3-}\cdot 3[CH_3(CH_2)_3NH_3]^+$ is described as difficult to delaminate when compared to ordinary layered metal phosphates by Wang et al.[106] They cite the strong interactions between organic ions and the sheets along with the instability of the microporous sheets as the reason for the difference. Also, Huang et al. state that previous attempts to remove the gallery ions of $[Al_3P_4O_{16}]^{3-}$ using heating methods have caused collapse or transformation of the structure into

denser phases.[103] They cite the reason as a removal of the gallery ions. This information makes it difficult to imagine a route to combine an exfoliated $[Al_3P_4O_{16}]^{3-}$ with an engineering polymer soluble in organic solvents.

The authors of the papers cited in this section came to some conclusions about delamination of $[Al_3P_4O_{16}]^{3-}$. The conclusions are bulleted below.

- $[Al_3P_4O_{16}]^{3-}\cdot 3[CH_3CH_2NH_3]^+$ delaminates only in solutions with dielectric constants in the range of 50-70.[103]
- $[Al_3P_4O_{16}]^{3-}\cdot 3[CH_3CH_2NH_3]^+$ delaminates completely within 2hrs when 20mmol of ethylamine per gram of AlPO is added to a 3:1 water/ethanol solution.[103]
- The process of delaminating $[Al_3P_4O_{16}]^{3-}\cdot 3[CH_3(CH_2)_3NH_3]^+$ was facilitated by basic solutions.[106]
- $[Al_3P_4O_{16}]^{3-}\cdot 3[CH_3(CH_2)_3NH_3]^+$ delaminated completely in water at a pH of 10 forming a clear colloidal solution.[106]
- $[Al_3P_4O_{16}]^{3-}\cdot 3[CH_3(CH_2)_3NH_3]^+$ is easier to delaminate than $[Al_3P_4O_{16}]^{3-}\cdot 3[CH_3CH_2NH_3]^+$ due to weaker interlayer forces in the structure.[104]

2.4 Diffusion in Flake filled Barrier membranes

The molecular dispersion of small amounts of layered clay in various polymer matrices has been shown to greatly increase the barrier properties when compared to the pristine polymer. For example, the addition of only 2wt% of modified montmorillonite to a polyimide decreased the permeability of several gas species by one half.[5] These dramatic results can be attributed to an increased tortuosity encountered by a gas species as it diffuses through a polymer-clay nanocomposite. A gas species is forced to increase its path length when traveling through a polymer that contains a dispersion of impermeable flakes. If however these flakes were microporous some smaller gases may pass through the flake while other larger gases would still encounter a barrier.

Current work involves using a layered aluminophosphate as a selective barrier for gas separation. The nanoplatelets of $[Al_3P_4O_{16}]^{3-}$ (8MR-AlPO) should be permeable to smaller gases i.e. H_2, He, and CO_2 while increasing the tortuosity for larger gasses such as CH_4. Therefore, the molecular dispersion of aluminophosphate in a polymer matrix should increase the selectivity of the nanocomposite by creating a barrier for gasses with a kinetic diameter larger than the pores of 8MR-AlPO.

The modeling of diffusion behavior in barrier membranes would be useful to provide predicted values for comparison with experimental results. Over a period of fifteen years Edward Cussler and his research group published a series of papers outlining theory and mathematical models to represent diffusion in membranes containing impermeable and permeable flakes. These models are useful in analyzing the current data being collected on polyimide-aluminophosphate nanocomposites. Below is a synopsis of the progression of their work.

2.4.1 Barrier Flakes

In early studies, Cussler et al.[107] describe the development of a mathematical model for gaseous diffusion in polymer membranes containing impermeable flakes. They developed their model based on several idealized geometries including slits, pores, and random shaped flakes. Below (Figure 2.14) is a diagram of the slit model on which Cussler's theory is based. This model is also directly applicable to my current research. In developing this idealized picture several assumptions were made, first the flakes exist within regular lamella, second the flakes are rectangular and regularly spaced, and third the flakes are very long. Another assumption is that the diffusion is perpendicular to the alignment of the flakes or the flakes are aligned parallel to the surface of the membrane.

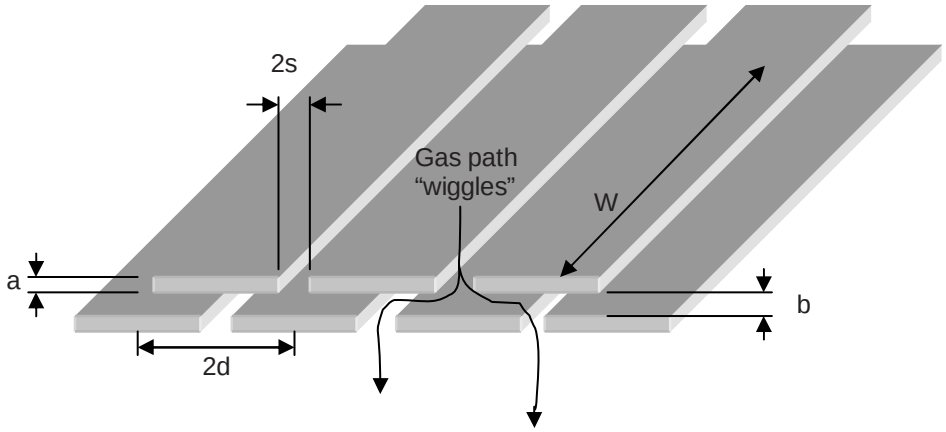

Figure 2.14 Cussler's visualization of impermeable flakes in a polymer matrix
Where a = flake thickness, b = distance between flakes, d = half flake size, s = half slit size, W = length of the flake (assumed to be infinite)

The authors began by applying Fick's first law to the representation above. Equation 2.3 describes the flux through a unit cell of area (2dW).

$$Jo = \frac{D(2dW)}{l}\Delta C \tag{2.3}$$

Where l is the thickness of the membrane and C is concentration change across l.

This equation can be rearranged to represent the resistance across the membrane which is shown in Equation 2.4.

$$\frac{D\Delta C}{Jo} = \frac{l}{2dW} \tag{2.4}$$

The right hand side of Equation 2.4 represents the resistance to diffusion of a polymer containing no barrier flakes. The authors then go on to describe flux which includes N impermeable flakes arranged in the manner shown above in Figure 2.14. This Equation 2.5 is also arranged to display the resistances to flux on the right hand side of the equation.

$$\frac{D\Delta C}{J_N} = \frac{l}{2dW} + \frac{b}{dW}\ln\left(\frac{d}{2s}\right) + \frac{Na}{2sW} + \frac{1}{2}(N-1)\frac{d}{bW} \tag{2.5}$$

The first term on the right hand side of Equation 2.5 is the resistance with no flakes present. The second term physically represents the restriction the gas encounters when entering the first layer of flakes and exiting the last layer. The third and fourth terms represent the resistance from passing through N slits, and the extra distance the gas must travel along the surface of the flakes. The extra distance traveled was termed by Cussler as "wiggles" and the factor of ½ refers to the reduced distance due to the periodicity of the flakes. A more useful equation can now be obtained by dividing Equation 2.5 by Equation 2.4 and applying several definitions. Equation 2.6 below is the reduced equation with α (= d/a) as the flake aspect ratio, σ (= s/a) as the slit aspect ratio, and ϕ = volume fraction of flakes present.

$$\frac{Jo}{J_N} = 1 + \sigma\alpha\phi + \alpha^2 \frac{\phi^2}{1-\phi} \tag{2.6}$$

Finally as the limits of this equation are explored, a useful equation emerges. The specific limit of interest is where σ/α<< 1 or when the "wiggles" dominate the resistance. Cussler believed strongly that the reduction in diffusion due to barrier flakes was due to the extra distance the gas must travel around the flakes. He termed this distance "wiggles". The final result can be seen in Equation 2.7 below.

$$\frac{Jo}{J_N} = \frac{Do}{D} = \frac{Po}{P} = 1 + \frac{\alpha^2\phi^2}{1-\phi} \tag{2.7}$$

Equation 2.7 was shown by Cussler et al. to have good correlation with data on mica flakes dispersed in a polycarbonate medium. The theory correctly predicted that the diffusion in flake filled membranes varied with $\phi^2/(1-\phi)$ however the aspect ratio α was predicted to be lower than the actual aspect ratio of the mica flakes. Subsequent publications also showed excellent agreement between Equation 2.7 and experimental data[108-111].

Several things can be noted immediately about Equation 2.7. First, it predicts that the ratio of permeabilities is independent of the polymer used and second, that the barrier properties are independent of the size of the flake as long as the aspect ratio and volume fraction are the same. Therefore, a PDMS film with 1nm thick flakes and a polyimide with 1mm thick flakes should give the same change in permeability if the volume fraction and flake shape are the same. Also Equation 2.7 is based on the theory that "wiggles" dominate the resistance to diffusion. Therefore, no terms associated with resistance due to passing through the gaps, or resistance due to necking, are included. If they were included there should be an additional resistance term proportional to φ for the gaps, and a resistance term proportional to φlnφ for necking on the right hand side of the equation.

It is important at this point to introduce several other models describing barrier flakes in a polymer medium and compare them to Equation 2.7. Several models were used early to describe barriers to diffusion in polyimide clay nanocomposites. Lan et al.[9] used Equation 2.8 derived by Nielsen[99] to describe the increased CO_2 barrier properties of a polyimide-MMT nanocomposite.

$$\frac{P_o}{P} = \frac{1+\phi(\alpha/2)}{1-\phi} \tag{2.8}$$

Similarly, Yano et al.[5] compared results of a polyimide-MMT nanocomposite to Equation 2.9 below. They found good agreement between experimental results and the model.

$$\frac{P_o}{P} = 1+(\alpha/2)\phi \tag{2.9}$$

Both Equations 2.8 and 2.9 can be traced to the same origin. Nielsen visualized a flake filled polymer system like that depicted in Figure 2.14, but only in two dimensions.[112] He defined a flake length *L* which would equate to *2d* in Figure 2.14 and a flake height *w* which corresponds to *a* in Figure 2.14. Using a "simple averaging process"[112], Nielsen derived and defined a

tortuosity term τ (the distance a molecule must travel to get through a film/ thickness of film) which is shown in Equation 2.10.

$$\tau = 1 + (L/2W)\phi_F \qquad \text{where } \phi_F \text{ is the volume fraction of filler} \tag{2.10}$$

He went on to cite previous work that defined the permeability of filled polymers with respect to pristine polymer (Equation 2.11).

$$\frac{P_o}{P} = \frac{\tau}{\phi_P} \qquad \text{where } \phi_P \text{ is the voulme fraction of polymer} \tag{2.11}$$

It can be seen that Equations 2.8 and 2.9 can be obtained by combining Equations 2.10 and 2.11 and then applying the definition of α and ϕ according to Cussler. For an unstated reason Yano et al. assumed the volume fraction of polymer to be unity.

The major difference between these early equations and those developed by Cussler is the dependence on the variable ϕ. It is clear that Equations 2.8 and 2.9 depend only on ϕ compared to $\phi^2/(1-\phi)$ in Equation 2.7. As stated above, the groups involved all reported good correlation between the model they used and the data collected. This apparent discrepancy is explained in Cussler's latest paper on flake filled membranes. This paper addresses the affect of the aspect ratio of the flake being used. Cussler defines two regimes for the loading of flakes namely, dilute and semi-dilute suspensions. The dilute system is defined where $\phi << 1$ and $\alpha\phi < 1$. For this type of system the barrier properties are best predicted by Equation 2.9. A semi-dilute system is defined where $\phi << 1$ and $\alpha\phi > 1$. For the semi-dilute case, the barrier properties are best predicted by Equation 2.7. For the current project the aspect ratios of the flakes being used are believed to be on the order of 2000. This is why we believe that Cusslers Equation 2.7 best describes our system.

Another student of Cussler's, Falla et al.[108] explored the use of more complicated models to describe diffusion in flake filled membranes. Equations (2.12-2.13) shown below contain several more terms on the right hand side when compared with Cussler's original Equation 3.5.

$$\frac{D_o}{D} = 1 + \frac{\alpha^2\phi^2}{1-\phi} + \frac{\alpha\phi}{\sigma} + \frac{4}{\pi}\frac{\alpha\phi}{1-\phi}\ln\left[\frac{\pi\alpha^2\phi}{\sigma(1-\phi)}\right] \tag{2.12}$$

$$\frac{D_o}{D} = 1 + \frac{\alpha^2\phi^2}{1-\phi} + \frac{\alpha\phi}{\sigma} + 2(1-\phi)\ln\frac{1-\phi}{2\sigma\phi} \tag{2.13}$$

As mentioned above these extra terms are associated with the resistances of solute passing through the gaps and resistance due to necking. The first two terms on the right hand side are identical to Equation 2.7, the third terms are the resistance from the gaps and the forth terms are resistance from necking of the solute. Cussler did not include these terms because he theorized that the resulting resistances were insignificant for membranes with a large number of layers of flakes[108]. Although Falla et al. showed that these terms could be significant in certain circumstances; Equation 2.7 has proven to be very accurate when compared with actual data.

There are several limitations associated with Equation 2.7. The first is that though it is very accurate in describing the ratio of P_o/P, the equation does not do a good job of predicting the aspect ratio α. This is recorded in several of Cusslers papers[107, 109, 110]. The aspect ratio is most often severely underestimated; therefore, it is important not to place too much emphasis on the predicted α. Another limitation is the assumption that all the flakes are the same size and regularly spaced like a brick wall. Several adjustments have been made to try and compensate for this problem. Equation 2.14 was developed for randomly spaced flakes by Cussler [107] and further explained by Yang [110].

$$\frac{P_o}{P} = 1 + \mu\alpha^2\left(\frac{\phi^2}{1-\phi}\right) \tag{2.14}$$

Equation 2.14 differs from Equation 2.7 by an unknown factor μ, which is a combined geometric factor. This unknown factor was then reported by Yang [110] to be μ= ½ for randomly spaced flakes. Another equation was reported by Lape et al.[111] for a mono-disperse random array of flakes. This formula is shown below in Equation 2.15.

$$\frac{P_o}{P} = \frac{[1+(2/3)\alpha\phi]^2}{1-\phi} \tag{2.15}$$

Yet another limitation of the model that has been improved upon is the alignment of the flakes. The original model described by Equation 2.7 assumes that the flakes are perfectly parallel to the surface of the membrane. Any deviation of the angle of these flakes can change the barrier properties of a nanocomposite severely. Eitzman et al.[109] report that a change in orientation of the flake from 0°-10° reduces the effect of the flakes by 40%, and a flake with a 20° orientation reduces the effect by 50%. They theorize that this reduction has a cosine dependence and provide Equation 2.16 below to compensate for the effect of a tipped flake.

$$\frac{P_o}{P} = \frac{\alpha^2\phi^2\cos^2\theta}{1-\phi} \tag{2.16}$$

It can be seen that Equations 2.14-2.16 are very similar to Equation 2.7 with some slight adjustments. These equations can be compared to determine what type of system is present in a nanocomposite or for known flake sizes and orientations the equations can be used to fit the data.

In a follow-up paper Perry et al.[113] utilized Cussler's idealized picture to develop an equation describing unsteady state diffusion across a flake filled membrane. They developed Equation 2.17 was based on the lag time method. The lag time method is used to determine the time required for a gas diffusing across a membrane to reach steady state. The well known Equation 2.18 for lag time can be seen below.

$$\frac{t_o(\text{with flakes})}{t_o(\text{without flakes})} = \alpha^2\phi^2 \tag{2.17}$$

$$t_o = \frac{l^2}{6D} \tag{2.18}$$

where t_o is the lag time and l is the membrane thickness.

The authors tested Equation 2.17 experimentally and found good agreement with lag time data however the predicted aspect ratio of the barrier material was not accurate.

2.4.2 Selective Flakes

The primary goal of the current research is to use a layered microporous aluminophosphate as the inorganic portion of a polymer-clay nanocomposite for gas separations. This aluminophosphate has a microporous structure that may allow some small kinetic diameter gases to pass through while acting as a barrier for larger kinetic diameter gases. The section above addressed several models for impermeable flakes in a polymer medium. Here we follow Cussler's model describing diffusion in a membrane containing selective flakes,[114] which should be directly applicable to our current work.

The semi-permeable flake model begins with the same idealized lamellae structure seen in Figure 2.14 and the same assumptions as stated in the previous section. The idealized lamella as seen in Figure 2.15 consists of a layer of pure polymer and a layer of polymer and flakes. The diffusion is described as encountering three resistances as it passes through this lamella. The first resistance is from the pure polymer and is in series with the parallel resistances of the flakes and the wiggles around the flakes. The progression of the derivation precedes much the same as the barrier model described in the previous section. The final Equation 2.19 also contains the same reduced variables as Equation 2.7 with the exception of δ. This new variable δ is defined

as the ratio of the diffusion coefficient in the pure polymer to the diffusion coefficient in the pure flake, D_P/D_F.

$$\frac{P_o}{P} = 1 - \phi + \left[\frac{1}{\frac{1}{\delta\phi} + \frac{1-\phi}{\alpha^2\phi^2}} \right] \tag{2.19}$$

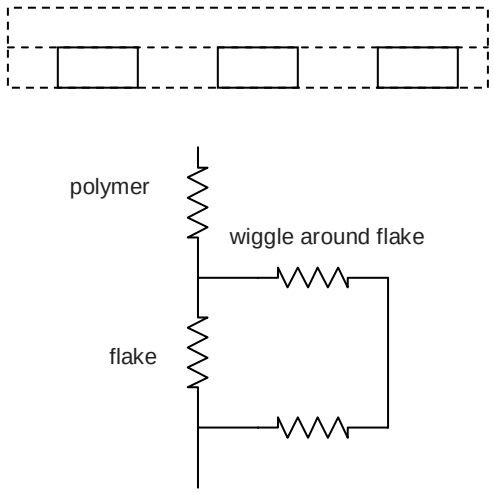

Figure 2.15 Description of resistances encountered by a gas molecule passing through a polymer matrix containing selective flakes

Cussler did not collect any experimental data to verify this model and to our knowledge no data has currently been produced to compare with the model. Equation 2.19 could be used to predict the permeability or diffusion coefficient of an aluminophosphate nanocomposite based on the permeability of the pure polymer and flake. Permeability data is not currently available for the pure aluminophosphate. It is possible to estimate permeabilities using adsorption from the pure aluminophosphate. It is also possible to predict D_F using Equation 2.19 and then compare this value to other polymer aluminophosphate systems.

2.4.3 Example Calculation of analysis using Cussler's barrier model

A simple analysis of the permeability data collected for various polymer-aluminophosphate systems was performed. Experimental permeability data was compared to permeabilities estimated by Equation 2.7 above. The assumptions made for the use of this equation are stated above. However, additional assumptions were made to apply this equation to the current work. Because Equation 2.7 is known to give inaccurate estimates of aspect ratio, an effective aspect ratio was calculated. The procedure used involves the assumption that CH_4 cannot pass through the 8MR of AlPO. The kinetic diameter of this gas is much larger than the 8MR opening therefore this is a reasonable assumption. If CH_4 cannot penetrate the pores of AlPO then the inorganic material should always (assuming good polymer 8MR-AlPO contact) act as a barrier material to methane. Experimental permeability data for methane in the pure polymer and polymer containing 8MR-AlPO are plugged into Equation 2.7. The volume fraction in Equation 2.7 is replaced by the wt% and an effective aspect ratio is calculated. The wt% is used instead of the volume fraction because it is simply a scaling factor. We are not attempting to predict aspect ratios but simply trying to ascertain if any of the gas species are deviating from barrier behavior. After an effective aspect ratio is obtained the other parameters including inorganic wt%, and pure polymer permeability are used with Equation 2.7 to predict the permeability values for He, O_2, N_2, CO_2. The predicted and measured permeabilities can then be compared to see how closely they match. A measured permeability value close to the value predicted would indicate 8MR-AlPO was acting as a barrier to the gas species used. If the experimental permeability for a gas species is higher than predicted it may indicate that gas is passing through the microporous openings known to exist in 8MR-AlPO. Below is an example calculation for a 5wt% PDMS-AlPO composite.

Experimental permeability(Barrers)		
Gas	Pure PDMS	5wt% AlPO
He	480	452
CO_2	3190	2926
O_2	699	629
N_2	336	303
CH_4	987	921

Therefore: $Po_{CH_4} = 987, P_{CH_4} = 921, \phi = 0.05$

$$\alpha_{CH_4} = \left[\frac{\left[\frac{Po_{CH_4}}{P_{CH_4}} - 1 \right] * (1-\phi)}{\phi^2} \right]^{\frac{1}{2}} = 5.22$$

Using the value of $\alpha_{effective} = 5.22$

$$P_{He} = \frac{Po_{He}}{\left[1 + \frac{\alpha^2 \phi^2}{1-\phi} \right]} = 448$$

The predicted value for the permeability of He if 8MR-AlPO is acting as a barrier is 448 Barrer. Since the experimental value is 452 Barrer, it appears that in this case the 8MR-AlPO is acting as a barrier.

2.4.4 Polymer matching: Interfaces, and Cussler's Selective Flake Model

Preliminary experiments with 8MR-AlPO indicated that it may be impossible to reproduce the same desired effect obtained by Jeong et al.[1] It is possible that the pores of the

8MR-AlPO which has been used exclusively are not accessible to the gases being tested. The pore size may be blocked by surfactant or simply too small to allow the passage of even the smallest gases. In other words the diffusion coefficients of the inorganic component may not match well with the polymer diffusion coefficients. The interface region between inorganic and polymer may also reduce the likelihood of a gas species diffusing through AlPO.

Recent discussions with Sankar Nair's research group at Gerogia Tech indicate that the size of the interface region between AlPO and polymer is a key issue.[115] Their simulations show that if the gap between polymer and inorganic reaches a certain distance, gas will tend to diffuse around the microporous structure instead of through it. The size of the gap may still be on an angstrom level when this takes place. Figure 5.3 shows a snapshot of a simulation Nair's group performed on a PDMS - layered 8MR microporous silicate (AMH-3) nanocomposite. Simulations for PDMS-AlPO composites should be available soon. We hope to be able to establish if this phenomenon extends to our systems. If so it will be an issue in what polymers are chosen for our future studies. For instance very glassy polymers may have large inherent interface gaps while rubbery polymers may have smaller ones. We will also consider potential interactions between the surfactant on the surface of AlPO and the groups of the polymer being used as a matrix material. Good interaction between surfactant and polymer should result in a smaller interface gap promoting diffusion of a gas species into AlPO.

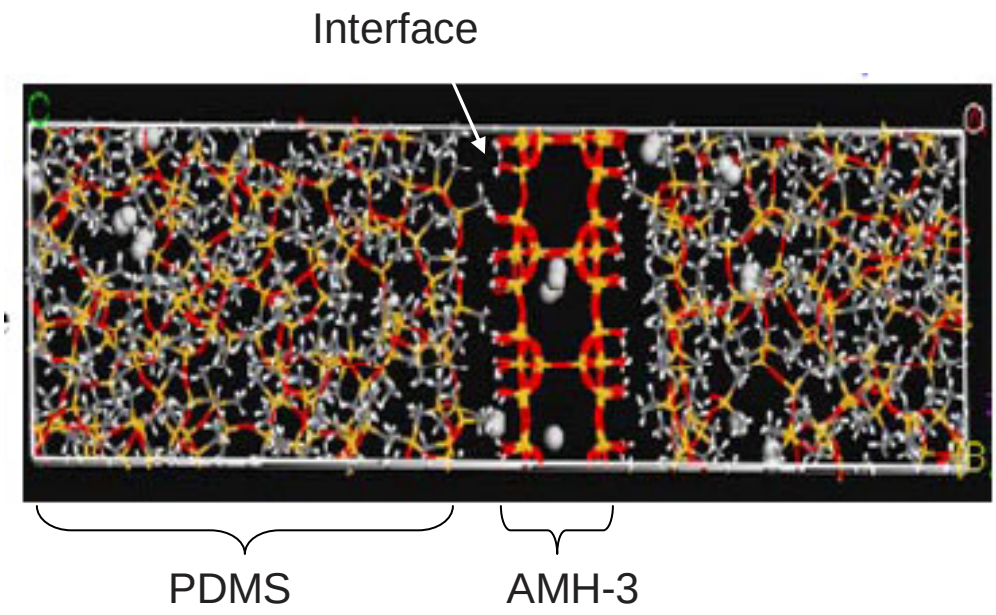

Figure 2.16 Snapshot of simulated gas species passing through layered AMH-3-PDMS nanocomposite performed by Nair's group at Georgia Tech.[115]

A model for predicting the effects of porous flakes in a polymer matrix was proposed by Cussler (Equation 2.19).[114] A graphical representation of that equation can be seen below in Figure 2.17. Reasonable values of aspect ratio $\alpha = 20$, permeability P = 35, and volume % 2-20, were chosen and substituted into the equation to obtain some qualitative trends. The predicted permeability was plotted against the ratio of diffusion in the pure polymer (D_P) / diffusion in the pure flake (D_F) ($D_P/D_F = \delta$). The limits of the equation are visible on the ends of the curves. When $D_F << D_P$ the permeability drops and flakes act as a barrier and when $D_F >> D_P$ the diffusion is limited only by the polymer. This curve was generated for a fictional polymer with a permeability of 35 Barrer for some gas species. The equation predicts that increasing the loading does allow for increasing permeability well beyond that of the matrix material when high volume fractions are used (Figure 2.17). Another useful bit of information from the graph is that even if D_F is 10^2-10^3 times less than the D_P there is still gas permeating through the membrane. Figure 2.17 also shows that if the D_P/D_F is unity, the permeability of a gas species in the composite is

equal to the permeability through the pure polymer. Cussler's model also indicates that permeability will be affected by the aspect ratio of the selective flake. Figure 2.18 shows the effect of changing the aspect ratio for a fixed set of conditions. For the case when alpha reaches around 200, a gas species that cannot pass through the flake would have a flux of almost zero.

For our applications it is interesting to look at selectivity of a composite containing selective flakes using Cussler's model. For this reason we used actual data for pure Matrimid© along with Equation 2.19 to predict the selectivity between He and CH_4. The flake aspect ratio was fixed at 25 and the loading at 2vol%. Our assumption for 8MR-AlPO is that CH_4 is too large to pass through the microstructure and will be rejected while He will diffuse through at some rate. Selectivity can be determined by dividing Equation 2.19 for He by Equation 2.19 for CH_4. The result can be seen in Figure 2.19. If the flake is a true barrier to CH_4 then the equation predicts an increase in selectivity even if diffusion in the flake (D_{He-F}) is less than the diffusion in the polymer (D_{He-P}) by 10^2-10^3.

Some of the information predicted by the graphs is not entirely practical. It would appear from Figure 2.17 that the benefits in terms of selectivity would be greatest for a composite with a very large vol% of selective flakes. However, a survey of polymer-clay nanocomposite literature indicates that molecular dispersion is overcome by particle re-aggregation at around 6wt% nanoplatelets.[18, 20] Aggregation leads to an undesirable reduction in properties, therefore, lower vol% loadings are believed to be optimal. Aspect ratio is also shown to affect permeability significantly as illustrated by Figure 2.18. For reasons mentioned previously, not too much emphasis should be placed on this parameter.[107, 109, 110] However, an increase in the aspect ratio of the particle certainly increases its barrier properties. For our purposes an effective aspect ratio of 20-200 should work very well because it would create a good barrier to the larger gases.

While aspect ratio for AlPO cannot be increased after synthesis it can be reduced by mechanical mixing or sonication.

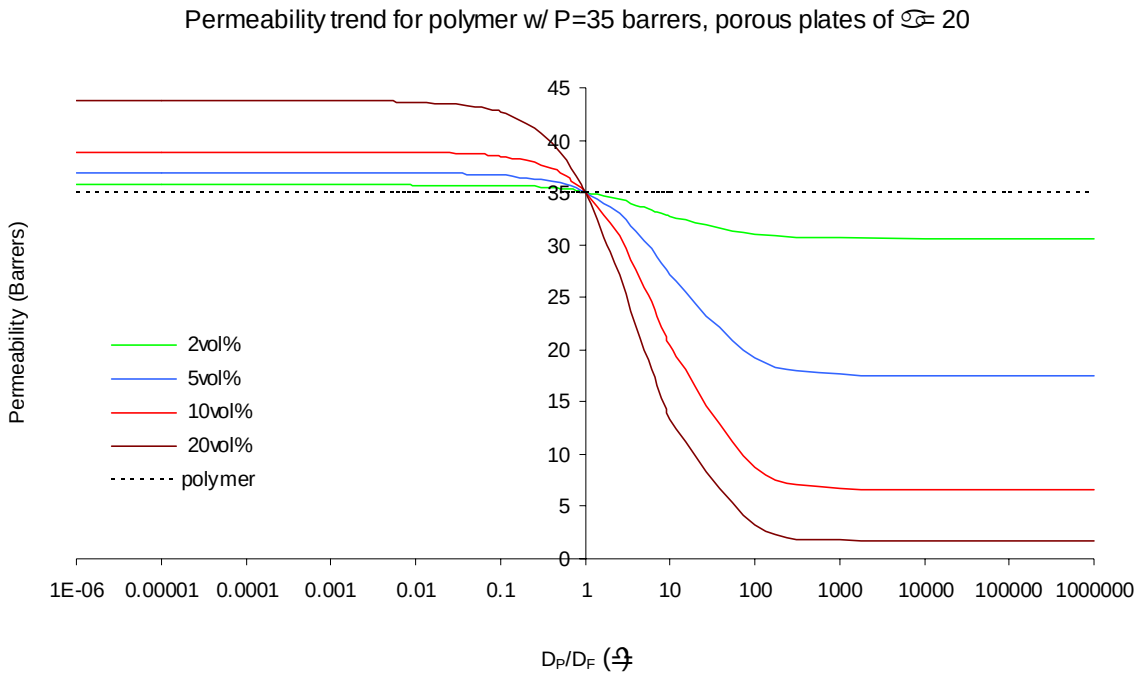

Figure 2.17 Graphical representation of Cussler's equation describing the flux through a polymer membrane containing different volume % of selective flakes

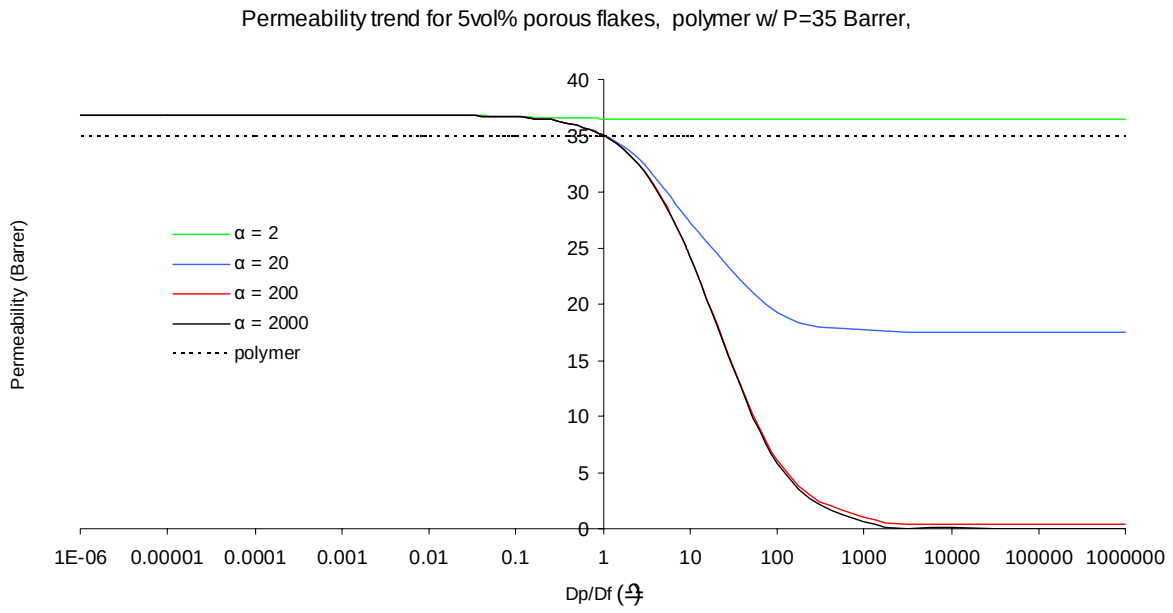

Figure 2.18 Graph of the permeability through a fictional polymer containing selective flakes using Cussler's equation and varying aspect ratio.

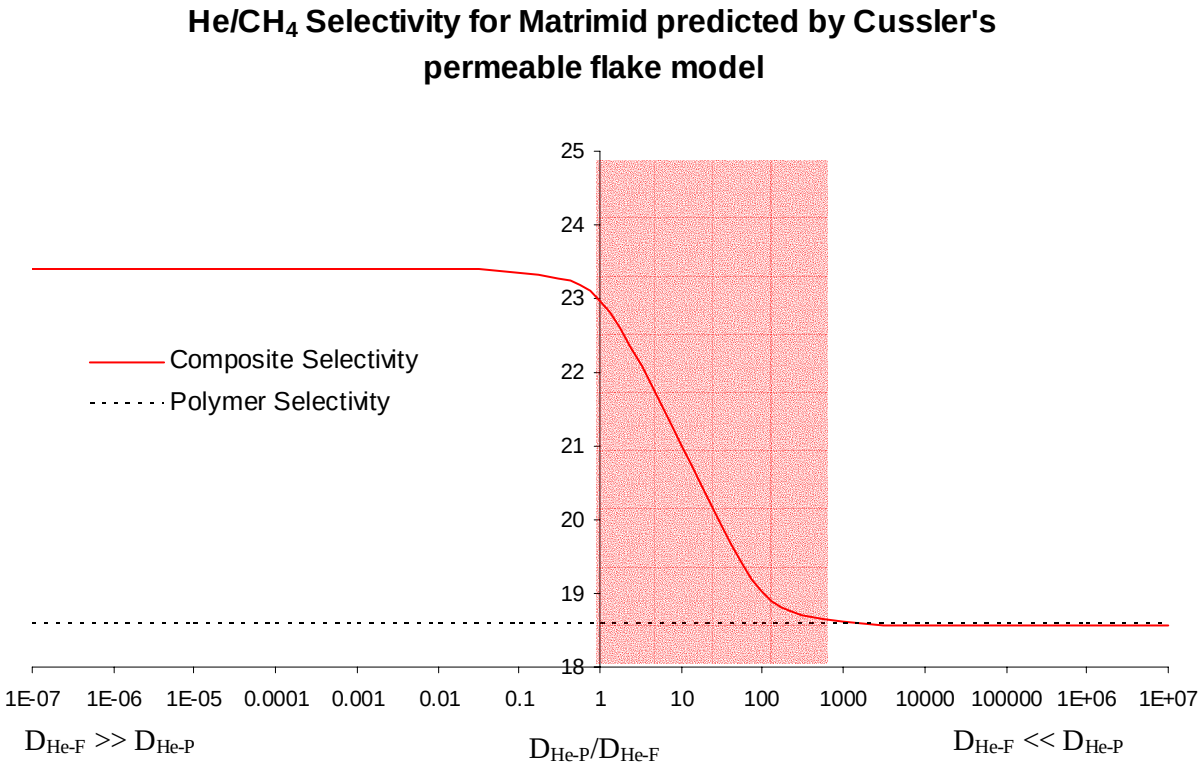

Figure 2.19 The Selectivity of He/CH_4 calculated using Cussler's equation for permeable flakes and permeability, diffusion data from Matrimid.

(1) Jeong, H.-K.; Krych, W.; Ramanan, H.; Nair, S.; Marand, E.; Tsapatsis, M., Fabrication of Polymer/Selective-Flake Nanocomposite Membranes and Their Use in Gas Separation. *Chemistry of Materials* **2004,** 16, (20), 3838 -3845.

(2) Okada, A.; Kawasumi, M.; Usuki, A.; Kojima, Y.; Kurauchi, T.; Kamigaito, O., Nyoln 6-clay hybrid. *Materials Research Society Symposium Proceedings* **1990,** 171, 45-50.

(3) Yano, K.; Usuki, A.; Okada, A., Synthesis and properties of polyimide-clay hybrid films. *Journal of Polymer Science, Part A: Polymer Chemistry* **1997,** 35, (11), 2289-2294.

(4) Yano, K.; Usuki, A.; Okada, A.; Kurauchi, T.; Kamigaito, O., Synthesis and properties of polyimide-clay hybrid. *Polymer Preprints (American Chemical Society, Division of Polymer Chemistry)* **1991**, (32), 65-66.

(5) Yano, K.; Usuki, A.; Okada, A.; Kurauchi, T.; Kamigaito, O., Synthesis and properties of polyimide-clay hybrid. *Journal of Polymer Science, Part A: Polymer Chemistry* **1993,** 31, (10), 2493-8.

(6) Usuki, A.; Kojima, Y.; Kawasumi, M.; Okada, A.; Fukushima, Y.; Kurauchi, T.; Kamigaito, O., Synthesis of nylon 6-clay hybrid. *Journal of Materials Research* **1993,** 8, (5), 1179-84.

(7) Usuki, A.; Kawasumi, M.; Kojima, Y.; Okada, A.; Kurauchi, T.; Kamigaito, O., Swelling behavior of montmorillonite cation exchanged for w-amino acids by e-caprolactam. *Journal of Materials Research* **1993,** 8, (5), 1174-8.

(8) Okada, A.; Usuki, A., The chemistry of polymer-clay hybrids. *Materials Science and Engineering:C* **1995,** 3, (2), 109-115.

(9) Lan, T.; Kaviratna, P. D.; Pinnavaia, T. J., On the Nature of Polyimide-Clay Hybrid Composites. *Chemistry of Materials* **1994,** 6, (5), 573-5.

(10) Yang, Y.; Zhua, Z.-k.; Yina, J.; Wang, X.-y.; Qi, Z.-e., Preparation and properties of hybrids of organo-soluble polyimide and montmorillonite with various chemical surface modification methods. *Polymer* **1999,** 40, (15), 4407-4414.

(11) LeBaron, P. C.; Wang, Z.; Pinnavaia, T. J., Polymer-layered silicate nanocomposites: an overview. *Applied Clay Science* **1999,** 15, (1-2), 11-29.

(12) Gu, A.; Kuo, S.-W.; Chang, F.-C., Syntheses and properties of PI/clay hybrids. *Journal of Applied Polymer Science* **2001,** 79, (10), 1902-1910.

(13) Kornmann, X.; Berglund, L. A.; Thomann, R.; Mulhaupt, R.; Finter, J., High performance epoxy-layered silicate nanocomposites. *Polymer Engineering and Science* **2002,** 42, (9), 1815 - 1826.

(14) Choi, W. J.; Kim, S. H.; Kim, Y. J.; Kim, S. C., Synthesis of chain-extended organifier and properties of polyurethane/clay nanocomposites. *Polymer* **2004,** 45, (17), 6045-6057.

(15) Zhang, Y.-H.; Wu, J.-T.; Fu, S.-Y.; Yang, S.-Y.; Li, Y.; Fan, L.; Li, R. K.-Y.; Li, L.-F.; Yan, Q., Studies on characterization and cryogenic mechanical properties of polyimide-layered silicate nanocomposite films. *Polymer* **2004,** 45, (22), 7579-7587.

(16) Tyan, H.-L.; Liu, Y.-C.; Wei, K.-H., Thermally and Mechanically Enhanced Clay/Polyimide Nanocomposite via Reactive Organoclay. *Chemistry of Materials* **1999,** 11, (7), 1942-1947.

(17) Tyan, H.-L.; Leu, C.-M.; Wei, K.-H., Effect of Reactivity of Organics-Modified Montmorillonite on the Thermal and Mechanical Properties of Montmorillonite/Polyimide Nanocomposites. *Chemistry of Materials* **2001,** 13, (1), 222-226.

(18) Agag, T.; Koga, T.; Takeichi, T., Studies on thermal and mechanical properties of polyimide–clay nanocomposites. *Polymer* **2001,** 42, (8), 3399-3408.

(19) Alexandre, M.; Beyer, G.; Henrist, C.; Cloots, R.; Rulmont, A.; Jérôme, R.; Dubois, P., Preparation and Properties of Layered Silicate Nanocomposites Based on Ethylene Vinyl Acetate Copolymers. *Macromolecular Rapid Communications* **2001,** 22, (8), 643-646.

(20) Huang, J.-C.; Zhu, Z.-K.; Ma, X.-D.; Qian, X.-F.; Yin, J., Preparation and properties of montmorillonite/organo-soluble polyimide hybrid materials prepared by a one-step approach. *Journal of Materials Science* **2001,** 36, (4), 871 - 877.

(21) Velmurugan, R.; Mohan1, T. P., Room temperature processing of epoxy-clay nanocomposites. *Journal of Materials Science* **2004,** 39, (24), 7333 - 7339.

(22) Ryu, J. G.; Kim, H.; Lee, J. W., Characteristics of polystyrene/polyethylene/clay nanocomposites prepared by ultrasound-assisted mixing process. *Polymer engineering and science* **2004,** 44, (7), 1198 - 1204.

(23) Vaia, R. A.; Price, G.; Ruth, P. N.; Nguyend, H. T.; Lichtenhan, J., Polymer/layered silicate nanocomposites as high performance ablative materials. *Applied Clay Science* **1999,** 15, (1-2), 67-92.

(24) Zhu, J.; Morgan, A. B.; Lamelas, F. J.; Wilkie, C. A., Fire Properties of Polystyrene-Clay Nanocomposites. *Chemistry of Materials* **2001,** 13, (10), 3774-3780.

(25) ZHU, Z.-K.; YANG, Y.; YIN, J.; WANG, X.-Y.; KE, Y.-C.; ZONG-NENG, Preparation and Properties of Organosoluble Montmorillonite/Polyimide Hybrid Materials. *Journal of Applied Polymer Science* **1999,** 73, (11), 2063-2068.

(26) Hsiao, S.-H.; Liou, G.-S.; Chang, L.-M., Synthesis and properties of organosoluble polyimide/clay hybrids. *Journal of Applied Polymer Science* **2001,** 80, (11), 2067-2072.

(27) Kornmann, X.; Berglund, L. A.; Sterte, J.; Giannelis, E. P., Nanocomposites based on montmorillonite and unsaturated polyester. *Polymer Engineering and Science* **1998,** 38, (8), 1351-1358.

(28) Alexandre, M.; Dubois, P., Polymer-layered silicate nanocomposites: preparation, properties and uses of a new class of materials. *Materials Science and Engineering. R Reports: A Review Journal* **2000,** 28, (1-2), 1-63.

(29) Ku, B.-C.; Froio, D.; Steeves, D.; Kim, D. W.; Ahn, H.; Ratto, J. A.; Blumstein, A.; Kumar, J.; Samuelson, L. A., Cross-linked Multilayer Polymer-Clay Nanocomposites and Permeability Properties. *Journal of macromolecular science. Part A, Pure and applied chemistry* **2004,** 41, (12), 1401-1410.

(30) Auerbach, S. M.; Carrado, K. A.; Dutta, P. K., *Handbook of layered materials*. ed.; M. Dekker: New York, 2004; 'Vol.' p.

(31) Kotov, N. A.; Haraszti, T.; Turi, L.; Zavala, G.; Geer, R. E.; Dékány, I.; Fendler, J. H., Mechanism of and Defect Formation in the Self-Assembly of Polymeric Polycation-Montmorillonite Ultrathin Films. *Journal of the American Chemical Society* **1997,** 119, (29), 6821-6832.

(32) Tyan, H.-L.; Yau-Cheng, L.; Kung-Hwa, W., Enhancement of imidization of poly(amic acid) through forming poly(amic acid)/organoclay nanocomposites. *Polymer* **1999,** 40, (17), 4877-4886.

(33) Mamedov, A.; Ostrander, J.; Aliev, F.; Kotov, N. A., Stratified Assemblies of Magnetite Nanoparticles and Montmorillonite Prepared by the Layer-by-Layer Assembly. *Langmuir* **2000,** 16, (8), 3941-3949.

(34) Tyan, H.-L.; Wei, K.-H.; Hsieh, T.-E., Mechanical properties of clay-polyimide (BTDA-ODA) nanocomposites via ODA-modified organoclay. *Journal of Polymer Science: Part B: Polymer Physics* **2000,** 38, (22), 2873-2878.

(35) Kornmann, X.; Lindberg, H.; Berglund, L. A., Synthesis of epoxy–clay nanocomposites: influence of the nature of the clay on structure. *Polymer* **2001,** 42, (4), 1303-1310.

(36) Kornmann, X.; Lindberg, H.; Berglund, L. A., Synthesis of epoxy–clay nanocomposites. Influence of the nature of the curing agent on structure. *Polymer* **2001,** 42, (10), 4493-4499.

(37) Huang, J.-C.; Zhu, Z.-k.; Yin, J.; Qian, X.-f.; Sun, Y.-Y., Poly(etherimide)/montmorillonite nanocomposites prepared by melt intercalation:

morphology, solvent resistance properties and thermal properties. *Polymer* **2001,** 42, (3), 873-877.

(38) Wang, D.; Zhu, J.; Yao, Q.; Wilkie, C. A., A Comparison of Various Methods for the Preparation of Polystyrene and Poly(methyl methacrylate) Clay Nanocomposites. *Chemistry of Materials* **2002,** 14, (9), 3837 -3843.

(39) Davis, C. H.; Mathias, L. J.; Gilman, J. W.; Schiraldi, D. A.; Shields, J. R.; Trulove, P.; Sutto, T. E.; Delong, H. C., Effects of melt-processing conditions on the quality of poly(ethylene terephthalate) montmorillonite clay nanocomposites. *Journal of polymer science. Part B, Polymer physics* **2002,** 40, (23), 2661 - 2666.

(40) Chang, J.-H.; An, Y. U.; Sur, G. S., Poly(lactic acid) nanocomposites with various organoclays. I. Thermomechanical properties, morphology, and gas permeability. *Journal of Polymer Science, Part B Polymer Chemistry* **2002,** 41, (1), 94 - 103.

(41) Hasegawa, N.; Okamoto, H.; Kato, M.; Usuki, A.; Sato, N., Nylon 6/Na–montmorillonite nanocomposites prepared by compounding Nylon 6 with Na–montmorillonite slurry. *Polymer* **2003,** 44, (10), 2933-2937.

(42) Nah, C.; Han, S. H.; Lee, J.-H.; Lee, M.-H.; Lim, S. D.; Rhee, J. M., Intercalation behavior of polyimide/organoclay nanocomposites during thermal imidization. *Composites Part B: Engineering* **2004,** 35, (2), 125-131.

(43) Yu, Y.-H.; Yeh, J.-M.; Liou, S.-J.; Chen, C.-L.; Liaw, D.-J.; 3, H.-Y. L., Preparation and properties of polyimide-clay nanocomposite materials for anticorrosion application. *Journal of Applied Polymer Science* **2004,** 92, (6), 3573 - 3582.

(44) Chen, B.; Evans, J. R. G., Preferential Intercalation in Polymer-Clay Nanocomposites. *The journal of physical chemistry. B, Condensed matter, materials, surfaces, interfaces & biophysical* **2004,** 108, (30), 14986 -14990.

(45) Pospíil, M.; Kalendová, A.; apková, P.; imoník, J.; Valáková, M., Structure analysis of intercalated layer silicates: combination of molecular simulations and experiment. *Journal of colloid and interface science* **2004,** 277, (1), 154-161.

(46) Toth, R.; Coslanich, A.; Ferrone, M.; Fermeglia, M.; Pricl, S.; Miertus, S.; Chiellini, E., Computer simulation of polypropylene/organoclay nanocomposites: characterization of atomic scale structure and prediction of binding energy. *Polymer* **2004,** 45, (23), 8075-8083.

(47) Carrado, K. A., Synthetic organo- and polymer–clays: preparation, characterization, and materials applications. *Applied Clay Science* **2000,** 17, (1-2), 1-23.

(48) Muzny, C. D.; Butler, B. D.; Hanley, H. J. M.; Tsvetkov, F.; Peiffer, D. G., Clay platelet dispersion in a polymer matrix. *Materials Letters* **1996,** 28, (4-6), 379-384.

(49) Burnside, S. D.; Wang, H.-C.; Giannelis, E. P., Direct Polymer Intercalation in Single Crystal Vermiculite. *Chemistry of Materials* **1999,** 11, (4), 1055-1060.

(50) Kornmann, X.; Thomann, R.; Mülhaupt, R.; Finter, J.; Berglund, L., Synthesis of amine-cured, epoxy-layered silicate nanocomposites: The influence of the silicate surface modification on the properties. *Journal of Applied Polymer Science* **2002,** 86, (10), 2643-2652.

(51) Morgan, A. B.; Gilman, J. W.; Jackson, C. L., Characterization of the Dispersion of Clay in a Polyetherimide Nanocomposite. *Macromolecules* **2001,** 34, (8), 2735-2738.

(52) Ho, D. L.; Briber, R. M.; Glinka, C. J., Characterization of Organically Modified Clays Using Scattering and Microscopy Techniques. *Chemistry of materials* **2001,** 13, (5), 1923 -1931.

(53) Ho, D. L.; Glinka, C. J., Effects of Solvent Solubility Parameters on Organoclay Dispersions. *Chemistry of materials* **2003,** 15, (6), 1309 -1312.

(54) Tran, N. H.; Dennis, G. R.; Milev, A. S.; Kannangara, G. S. K.; Williams, P.; Wilson, M. A.; Lamb, R. N., Dispersion of organically modified clays within n-alcohols. *Journal of Colloid and Interface Science* **2006,** 297, (2), 541-545.

(55) Vaia, R. A.; Teukolsky, R. K.; Giannelis, E. P., Interlayer Structure and Molecular Environment of Alkylammonium Layered Silicates. *Chemistry of Materials* **1994,** 6, (7), 1017-1022.

(56) Zheng, Q.; Xu, B.; Song, Y.; Yang, H.; Pan, Y., Interlayer structure of organically modified montmorillonites: Effect of surfactant loading. *Journal of Materials Research: JMR* **2005,** 20, (2), 357-363.

(57) Lee, S. Y.; Kim, S. J., Expansion characteristics of organoclay as a precursor to nanocomposites. *Colloids and Surfaces. A, Physicochemical and Engineering Aspects* **2002,** 211, (1), 19-26.

(58) Kornmann, X. Synthesis and Characterization of Thermoset-Layered Silicate Nanocomposites. Lulea Tekniska Universitet, Luleå, Sweden, 2001.

(59) Vaia, R. A.; Giannelis, E. P., Polymer Melt Intercalation in Organically-Modified Layered Silicates: Model Predictions and Experiment. *Macromolecules* **1997,** 30, 8000-8009.

(60) Ma, C.-C. M.; Kuo, C.-T.; Kuan, H.-C.; Chiang, C.-L., Effects of swelling agents on the crystallization behavior and mechanical properties of polyamide 6/clay nanocomposites. *Journal of Applied Polymer Science* **2003,** 88, (7), 1686-1693.

(61) Gelfer, M.; Avila-orta, C.; Liu, L.; Yang, L.; Chu, B.; Hsiao, B. S.; Song, H. H.; Si, M.; Rafailovich, M.; Tsou, A. H., Manipulating the microstructure and rheology in polymer-organoclay composites. *Polymer Engineering and Science* **2002,** 42, (9), 1841 - 1851.

(62) Yoon, P. J.; Hunter, D. L.; Paul, D. R., Polycarbonate nanocomposites. Part 1. Effect of organoclay structure on morphology and properties. *Polymer* **2003,** 44, 5323–5339.

(63) Xu, Z.-K.; Xiao, L.; Wang, J.; Xu, Y.-Y. In *Novel PMDA-ODA Polyimide/Polystyrene Nanocomposite Membranes for Carbon Dioxide Separation*, First National Conference on Carbon Sequestration, 2001; 'Ed.'^'Eds.' 2001; p^pp.

(64) MA, J.; QI, Z.; HU, Y., Synthesis and Characterization of Polypropylene/Clay Nanocomposites. *Journal of Applied Polymer Science*, **2001,** 82, 3611–3617.

(65) Hwu, J. M.; Jiang, G. J.; Gao, Z. M.; Xie, W.; Pan, W. P., The characterization of organic modified clay and clay-filled PMMA nanocomposite. *Journal of Applied Polymer Science* **2001,** 83, (8), 1702-1710.

(66) Kawasumi, M., The Discovery of Polymer-Clay Hybrids. *Journal of polymer science. Part A, Polymer chemistry* **2004,** 42, (4), 819 - 824.

(67) Delozier, D. M.; Orwoll, R. A.; Cahoon, J. F.; Johnston, N. J.; J. G. Smith, J.; Connell, J. W., Preparation and characterization of polyimide/organoclay nanocomposites. *Polymer* **2002,** 43, (3), 813-822.

(68) Saber-Samandari, S.; Khatibi, A. A.; Basic, D., An experimental study on clay/epoxy nanocomposites produced in a centrifuge. *Composites Part B, Engineering* **2007,** 38, (1), 102-107.

(69) Pczkowska, B.; Strzelec, S.; Jdrzejewska, B.; Linden, L.-Å.; Pczkowski, J., Photochemical preparation of polymer-clay composites. *Applied Clay Science* **2004,** 25, (3-4), 221-227.

(70) Song, M.-K.; Park, S.-B.; Kim, Y.-T.; Rhee, H.-W.; Kim, J., NANOCOMPOSITE POLYMER MEMBRANE BASED ON CATION EXCHANGE POLYMER AND NANO-DISPERSED CLAY SHEETS. *Molecular Crystals and Liquid Crystals* **2003,** 407, 15-23.

(71) Yu, J.; Xu, R., Rich Structrue Chemistry in the Aluminophosphate Family. *Accounts of Chemical Research* **2003,** 36, 481-490.

(72) Wilson, S. T.; Lok, B. M.; Celeste A. Messina; Cannan, T. R.; Flanigen, E. M., Aluminophosphate Molecular Sieves: A New Class of Microporous Crystalline Inorganic Solids. *Journal of the American Chemical Society* **1982,** 104, 1146-1147.

(73) Yu, J.; Xu, R.; Li, J., Structural diversity of a family of aluminophosphates with Al/P ratio of non-unity. *Solid state sciences* **2000,** 2, (2), 181-192.

(74) Yu, J.; Williams, I. D., Two Unusual Layer Aluminophosphates Templated by Imidazolium Ions; [N2C3H5][AlP2O8H2 á 2H2O] and 2[N2C3H5][Al3P4O16H]. *Journal of Solid State Chemistry* **1998,** 136, 141-144.

(75) Yu, J.; Terasaki, O.; Williams, I. D.; Quiv, S.; Xu, R., Solvothermal synthesis and characterization of new aluminophosphate layers templated by imidzolium ions. *Supramolecuolar Scinece* **1998,** 5, 297-302.

(76) Jones, R. H.; Thomas, J. M.; U, R. X.; Huo, Q. i. h.; Cheetham, A. K.; Powellc, A. V., Synthesis and Structure of a Novel Aluminium Phosphate Anion: (AI3P4Ol6)3-. *Journal of the Chemical Society. Chemical communications* **1991**, (18), 1266 - 1268.

(77) Thomas, J. M.; Jones, R. H.; Xu, R.; Chen, J.; Chippindale, A. M.; Natarajan, S.; Cheetham, A. K., A Novel Porous Sheet Aluminophosphate: AI3P40,& 1 .5[NH3(CH2)4NH3]+. *Journal of the Chemical Society. Chemical communications* **1992**, (13), 929-931.

(78) Chippindale, A. M.; Natarajan, S.; Thomas, J. M.; Jones, R. H., An Example of a Reactive Template in the Synthesis of a Novel Layered Aluminum Phosphate, (Al3P4O16)3-(NH3(CH2)5NH3)2+(C5H10NH2)+. *Journal of solid state chemistry* **1994,** 111, (1), 18-25.

(79) Ghosal, K.; Freeman, B. D., Gas separation using polymer membranes: an overview. *Polymers for advanced technologies* **1994,** 5, (11), 673-697.

(80) Barrett, P. A.; Jones, R. H., The Pore Size Modification of a Layered Aluminophosphate [A13P401&9H24N3] by Rational Selection of the Intercalated Template Cation. *Journal of the Chemical Society. Chemical communications* **1995**, (19), 1979-1981.

(81) Oliver, S.; Kuperman, A.; Lough, A.; Ozin, G. A., Synthesis and Crystal Structures of Two Novel Anionic Aluminophosphates: A One-Dimensional Chain, UT-7 ([Al3P5O20H]5-[C7H13NH3+]5), and a Layer Containing Two Cyclic Amines, UT-8 ([Al3P4O16]3-[C4H7NH3+]2[C5H10NH2+]). *Inorganic chemistry* **1996,** 35, (22), 6373 -6380.

(82) Williams, I. D.; Gao, Q.; Chen, J.; Ngai, L.-Y.; Lin, Z.; Xu, R., Organo-template control of inorganic structures: a low-symmetry two-dimensional sheet aluminophosphate3[NH3CHMeCH2NH3][Al6P8O32]·H2O. *Chemical Communications* **1996**, (15), 1781 - 1782.

(83) Gao, Q.; Li, B.; Chen, J.; Li, S.; Xu, R.; Williams, I.; Zheng, J.; Barber, D., Nonaqueous Synthesis and Characterization of a New 2-Dimensional Layered Aluminophosphate [Al3P4O16]3-· 3[CH3CH2NH3]+. *Journal of solid state chemistry* **1997,** 129, (1), 37-44.

(84) Chippindale, A. M.; Cowley, A. R.; Huo, Q.; Jones, R. H.; Law, A. D.; Thomas, J. M.; Xu, R., Synthesis and structure of a new layered aluminium phosphate: [BuNH3]3[Al3P4O16]. *Journal of the Chemical Society Dalton Transactions* **1997**, (15), 2639-2643.

(85) Togashi, N.; Yu, J.; Zheng, S.; Sugiyama, K.; Hiraga, K.; Yan, W.; Qiu, S.; Xu, R., Synthesis and structure of a 2-D aluminophosphate Al3P4O16·3CH3CH2CH2NH3. *Journal of materials chemistry* **1998,** 8, (12), 2827-2830.

(86) Vidal, L.; Marichal, C.; Gramlich, V.; Patarin, J.; Gabelica, Z., Mu-7, a New Layered Aluminophosphate [CH3NH3]3[Al3P4O16] with a 4 × 8 Network: Characterization, Structure, and Possible Crystallization Mechanism. *Chemistry of materials* **1999,** 11, (10), 2728 -2736.

(87) Yao, Y.-W.; Natarajan, S.; Chen, J.-S.; Pang, W.-Q., Synthesis and Structural Characterization of a New Layered Aluminophosphate Intercalated with Triply-Protonated Triethylenetetramine [C6H21N4][Al3P4O16]. *Journal of solid state chemistry* **1999,** 146, (2), 458-463.

(88) Yu, J.; Li, J.; Sugiyama, K.; Togashi, N.; Terasaki, O.; Hiraga, K.; Zhou, B.; Qiu, S.; Xu, R., Formation of a New Layered Aluminophosphate [Al3P4O16][C5N2H9]2[NH4]. *Chemistry of materials* **1999,** 11, (7), 1727 -1732.

(89) Yuan, H.-M.; Zhu, G.-S.; Chen, J.-S.; Chen, W.; Yang, G.-D.; Xu, R.-R., Dual Function of Racemic Isopropanolamine as Solvent and as Template for the Synthesis of a New Layered Aluminophosphate: [NH3CH2CH(OH)CH3]3·Al3P4O16. *Journal of solid state chemistry* **2000,** 151, (1), 145-149.

(90) Tuel, A.; Gramlich, V.; Baerlocher, C., Synthesis, structure determination and characterization of a new layered aluminophosphate templated by piperazinium ions. *Microporous and Mesoporous Materials* **2001,** 46, (1), 57-66.

(91) Yan, W.; Yu, J.; Li, Y.; Shi, Z.; Xu, R., Synthesis and Characterization of a New Layered Aluminophosphate [Al3P4O16][(CH3)2NHCH2CH2NH(CH3)2][H3O]. *Journal of solid state chemistry* **2002,** 167, (2), 282-288.

(92) Tuel, A.; Jorda, J.-L.; Gramlich, V.; Baerlocher, C., Synthesis and crystal structure of a new layered aluminophosphate [Al3P4O16][C6N3H17][H3O]. *Journal of solid state chemistry* **2004,** 177, (7), 2484-2493.

(93) Tuel, A.; Jorda, J.-L.; Gramlich, V.; Baerlocher, C., Synthesis and characterization of two aluminophosphates templated by N-methyl-1,3-diaminopropane. *Journal of Solid State Chemistry* **2005,** 178, (3), 782-791.

(94) Morgan, K.; Gainsford, G.; Milestone, N., A novel layered aluminium phosphate [Co(en)3Al3P4O16·3H2O] assembled about a chiral metal complex. *Journal of the Chemical Society. Chemical communications* **1995**, (4), 425-426.

(95) Bruce, D. A.; Wilkinson, A. P.; White, M. G.; Bertrand, J. A., The synthesis and structure of a chiral layered aluminophosphate containing the template Co(tn)33+. *Journal of the Chemical Society. Chemical Communications* **1995**, (20), 2059 - 2060.

(96) Bruce, D. A.; Wilkinson, A. P.; White, M. G.; Bertrand, J. A., The Synthesis and Characterization of an Aluminophosphate with Chiral Layers;trans-Co(dien)2·Al3P4O16·3H2O. *Journal of solid state chemistry* **1996,** 125, (2), 228-233.

(97) Gray, M. J.; Jasper, J. D.; Wilkinson, A. P.; Hanson, J. C., Synthesis and Synchrotron Microcrystal Structure of an Aluminophosphate with Chiral Layers Containing Tris(ethylenediamine)cobalt(III). *Chemistry of materials* **1997,** 9, (4), 976 -980.

(98) Williams, D. J.; Kruger, J. S.; McLeroy, A. F.; Wilkinson, A. P.; Hanson, J. C., Iridium(III) Amine Complexes as High-Stability Structure-Directing Agents for the Synthesis of Metal Phosphates. *Chemistry of materials* **1999,** 11, (8), 2241 -2249.

(99) Shriver, D.; Atkins, P., *Inorganic Chemistry*. ed.; W.H. Freeman and Company: New York, 2003; 'Vol.' p.

(100) Zhou, B.; Yu, J.; Li, J.; Xu, Y.; Xu, W.; Qiu, S.; Xu, R., Rational Design of Two-Dimensional Layered Aluminophosphates with [Al3P4O16]3- Stoichiometry. *Chemistry of materials* **1999,** 11, (4), 1094 -1099.

(101) Zhou, B.; Li, J.-Y.; Yu, J.-H.; Xu, Y.-H.; Xu, W.-G.; Shi, N.; Qiu, S.-L.; Xu, R.-R., Systematic enumeration of two-dimensional layered aluminophosphates with [Al3P4O16]3- stoichiometry. *Computers & chemistry* **1999,** 23, (6), 555-563.

(102) Wei, B.; Yu, J.; Shi, Z.; Qui, S.; Li, J., A new layered aluminphosphate $[Al_2P_4O16][C_6H_{22}N_4][C_2H_{10}N_2]$ with 4.12-net porous sheets. *Journal of the Chemical Society Dalton Transactions Communication* **2000**, (13), 1979-1980.

(103) Huang, Q.; Wang, W.; Yue, Y.; Hua, W.; Gao, Z., Delamination and intercalation of layered aluminophosphate with $[Al_3P_4O_{16}]^{3-}$ stoichiometry in water/alcohol/amine solutions. *Journal of colloid and interface science* **2003,** 257, 268-275.

(104) Huang, Q.; Wang, W.; Yue, Y.; Hua, W.; Gao, Z., Delamination and alkylamine intercalation of a layered microporous aluminophosphate [Al3P4O16][CH3(CH2)3NH3]3. *Microporous and Mesoporous Materials* **2004,** 67, (2-3), 189-194.

(105) Wang, C.; Hua, W.; Yue, Y.; Gao, Z., Delamination and aromatic amine intercalation of layered aluminophosphate with [Al3P4O16]3- stoichiometry. *Journal of Colloid and Interface Science* **2005,** 285, (2), 731-736.

(106) Wang, C.; Hua, W.; Yue, Y.; Gao, Z., Controlled delamination and intercalation of layered microporous aluminophosphate by a novel two-step method. *Microporous and Mesoporous Materials* **2005,** 84, (1-3), 297-301.

(107) Cussler, E. L.; Hughes, S. E.; William J. Ward, I.; Aris, R., Barrier membranes. *Journal of Membrane Science* **1988,** 38, (2), 161-174.

(108) Falla, W. R.; Mulski, M.; Cussler, E. L., Estimating diffusion through flake-filled membranes. *Journal of Membrane Science* **1996,** 119, (1), 129-138.

(109) Eitzman, D. M.; Melkote, R. R.; Cussler, E. L., Barrier membranes with tipped impermeable flakes. *AIChE Journal* **1996,** 42, (1), 2-9.

(110) Yang, C.; Smyrl, W. H.; Cussler, E. L., Flake alignment in composite coatings. *Journal of Membrane Science* **2004,** 231, (1-2), 1-12.

(111) Lape, N. K.; Nuxoll, E. E.; Cussler, E. L., Polydisperse flakes in barrier films. *Journal of Membrane Science* **2004,** 236, (1-2), 29-37.

(112) Nielsen, L. E., Models for the Permeability of Filled Polymer Systems. *The Journal of Macromolecular Sciences: Part A Chemistry* **1967,** A1, (5), 929-942.

(113) Perry, D.; Ward, W. J.; Cussler, E. L., Unsteady diffusion in barrier membranes. *Journal of Membrane Science* **1989,** 44, (2-3), 305-311.

(114) Cussler, E. L., Membranes containing selective flakes. *Journal of Membrane Science* **1990,** 52, (3), 275-288.

(115) Nair, S., Simulation of gas transport in PDMS AMH-3 nanocomposites. *Simulation of gas transport in PDMS AMH-3 nanocomposites* **2006**.

Chapter 3

Study of the properties of swollen 8MR-AlPO

3.1 Introduction

Layered clays dispersed in various polymer matrices have been used to produce a class of materials known as polymer-clay nanocomposites. Polymer-clay nanocomposites containing small amounts of layered clays have been shown to dramatically improve gas barrier properties when compared to the neat polymer[1-8]. Other clay-like microporous layered materials are available that may act as semi-barriers. These materials if dispersed in a polymer matrix may selectively allow a smaller gas species to pass through, while obstructing a larger gas species. The compound of interest in this paper is a layered aluminophosphate known as $[Al_3P_4O_{16}]^{3-} \cdot 3[NH_3CH_2CH_3]^+$ or AlPO[9]. Jeong et al. showed that dispersing 5-10 wt% of this material into a hexa-fluorinated polyimide improved the gas separation properties significantly when compared

to the pure polymer[10]. Our ultimate goal is to determine whether similar improvements can be achieved by dispersing AlPO in other polymer matrix materials. However, the dispersion of AlPO is a key factor in achieving viable membranes. The interaction between the surface of AlPO and the polymer determines the structure and morphology of the nanocomposite and consequently the final transport properties. It is therefore necessary to modify the surface of AlPO with different chemical species that promote molecular interaction, before combining it with the polymer.

The first step in the fabrication of a polymer-aluminophosphate nanocomposite is the intercalation or swelling of the aluminophosphate with a small organic molecule. This serves to both increase the gallery spacing of AlPO, and to act a compatiblizer between the polymer and inorganic component. Several swelling agents were chosen including cetyltrimethylammonium chloride, octadecyldimethylbenzyl ammonium chloride, and protonated 1,12 diaminodocecane. These swelling agents have different molecular lengths and cationic head groups which can interact with the anionic AlPO sheets. This paper discusses the results of characterization studies of these modified aluminophosphates using SEM, XRD and ^{31}P NMR.

3.2 Experimental

3.2.1 Materials

The aluminophosphate used in our experiments $[Al_3P_4O_{16}]^{3-}\cdot 3[NH_3CH_2CH_3]^+$ was synthesized in our lab according to the procedure reported by Gao et al.[9] Typically 66g of ethylene Glycol (EM Science), 80g of N-butyl alcohol (EMD), and 8g of aluminum isopropoxide (Aldrich) were allowed to mix thoroughly. This was followed by the addition of 34.72g of ethylamine 70 wt % in water (Aldrich), and 13.44 g of phosphoric acid drop wise. The resulting mixture was sealed in Teflon© lined autoclaves at autogeneous pressure and allowed to heat at

180°C for 13 days. The aluminophosphate was then collected by filtration and washed with deionized water. The resulting material consisted of monoclinic crystals with an average size similar to those reported by Gao et al. $(40-60)\times(45-75)\times(80-120)\mu m$.[9] The cetyltrimethyl ammonium chloride 25 wt% (Aldrich) in water, octadecyldimethyl benzyl ammonium chloride (Pfaltz & Bauer), and 1,12 diaminododecane (Aldrich) were used as received.

3.2.2 Modification of Aluminophosphate

The first swelling procedure involved cetyltrimethyl ammonium chloride as the swelling agent ($CTMA^+$). The procedure reported by Jeong et al. was followed[10]. The ratio of cetyltrimethyl ammonium chloride: Tetrapropyl ammonium hydroxide : AlPO used was 37:1.2: 1 by weight.. Typically 1g of aluminophosphate was refluxed for 16 hrs at 80°C in a round bottom flask fitted with a condenser. After swelling the material was recovered with vacuum filtration and washed thoroughly with deionized water.

In order to estimate the required quantities of the other two swelling agents, a rough calculation of the cation exchange capacity (CEC) for AlPO was made. The ratio of the charge of one AlPO unit to its molecular weight gives an AlPO CEC of 500meq/100g. Layered clays are typically swollen with an amount of surfactant equal to twice the CEC of the material. The amount of swelling agent used for the protonated 1,12 diamminododecane ($112DADD^{2+}$), and octadecyldimethyl benzyl ammonium ($ODDMBA^+$) AlPOs were determined using the equation $CEC_{ALPO}\times 1g_{AlPO}\times 2 = (X / Mw\,\text{of intercalating agent})\times 1\times 1000$ reported by Yu et al.[11] where the CEC is in units of meq/100g, X is the amount of intercalating agent needed in grams, and 2 represents the excess of surfactant used.

As-synthesized AlPO was ion exchanged in the presence of ocatadecyldimethyl benzyl ammonium chloride. Typically 4.25g of octadecyldimethyl benzyl ammonium chloride was

added to 50mL of water and allowed to dissolve. Subsequently 1g of AlPO was added and the mixture was allowed to reflux at 80°C for 16hrs. The swollen AlPO was then collected by filtration and washed thoroughly with deionized water.

Similarly, as-synthesized AlPO was also ion exchanged with protonated 1,12 diamminododecane. Typically 1.65 mL of concentrated HCl was added to 50 mL of deionized water. Then 2.0 g of 1,12 diamminododecane ($112DADD^{+2}$) was added and allowed to fully dissolve. Finally 1 g of as-synthesized AlPO was added to the mixture and allowed to reflux for 16hrs at 80°C.

3.2.3 Characterization

XRD measurements were taken on a Scintag XDS 2000 powder x-ray diffractometer with Cu Kα radiation at a sample rate of 0.5°/min. CAChe software from Fujitsu Limited was used to analyze and visualize molecular structures. Solid–state ^{31}P NMR was performed on a Brooker MSL 300 with an operating frequency of 121.5 MHz, and the reference standerd used was 85% H_3P0_4. Scanning Electron Micrographs were taken on a LEO 1550 FESEM. The sonicator used was a VWR model 50HT operating at a frequency of 38.5-40.5 kHz.

3.3 Results and Discussion

3.3.1 As-synthesized AlPO

As-synthesized AlPO crystals shown in Figure 3.1a are monoclinic rectangular blocks, with an average long dimension in the range of 80-120μm. The microstructure consists of layers of $[Al_3P_4O_{16}]^{3-}$ anionic sheets with a 4.6.8 MR net structure[9]. Using crystallographic coordinates and the van der Waals radius of oxygen, the thickness of one sheet was calculated to be 7.5 Å. The anionic sheets are separated by ethylammonium ions which counterbalance the sheets' negative charge and hydrogen bond the upper and lower platelets together. This structure is

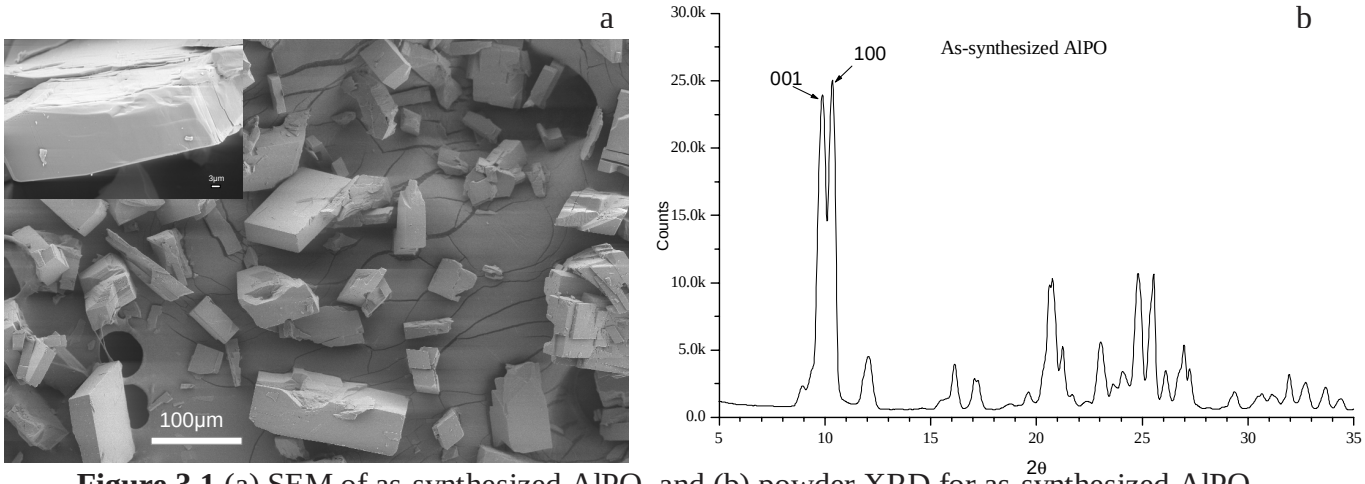

Figure 3.1 (a) SEM of as-synthesized AlPO, and (b) powder XRD for as-synthesized AlPO

shown schematically in Figure 3.2. There are three $[NH_3CH_2CH_3]^+$ ions for every one AlPO unit. The counterions hydrogen bond to the P=O which protrude from the top and bottom of each sheet. These counterions almost certainly provide some structural support for the 4.6.8 net framework of the layers. It is our intent to exchange the ethylammonium ions for larger surfactant molecules. This should expand the gallery spacing and render the surfaces more hydrophobic. Swelling is necessary to increase the likelihood of intercalation and exfoliation of the particles into a polymer matrix. Our eventual goal is to disperse this material into a polymer to form a successful nanocomposite.

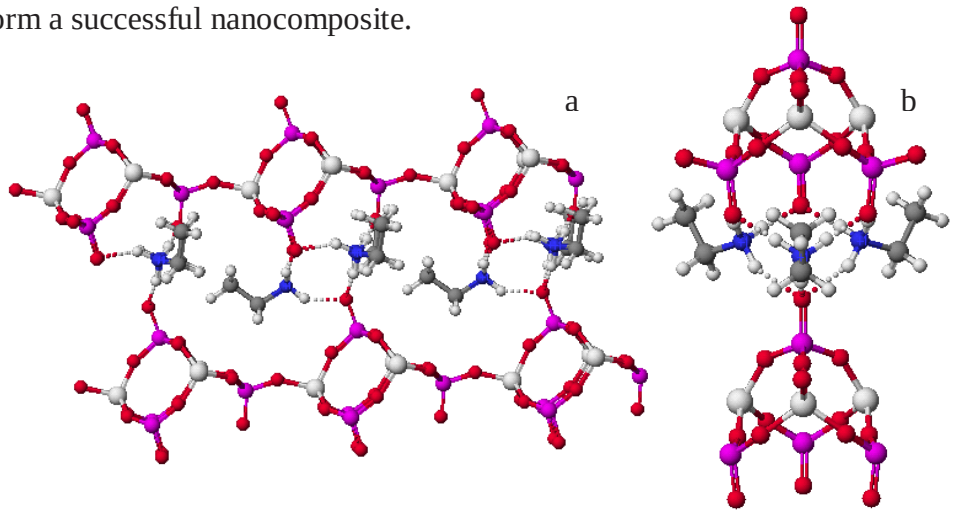

Figure 3.2 Partial views along 010(a), and 100(b) of as-synthesized AlPO showing hydrogen bonding network of gallery ethylammonium ions

The XRD pattern of as-synthesized AlPO can be seen in Figure 3.1b. The pattern was compared with single crystal data from Gao et al.[9] to confirm that the correct structure was obtained. The peak which represents the 001 plane is marked in the XRD pattern. A shift of this peak to the left in a subsequent XRD pattern of AlPO swollen with a surfactant would indicate an expansion of the basal spacing for the material. Using Bragg's law the position of the 001 peak indicates that the basal spacing for as-synthesized AlPO is 8.97 Å. This corresponds closely to the basal spacing determined from plotting atom coordinates reported by Gao et al.[9] When the structure is plotted using CAChe, and atom distances are measured, a basal spacing of 8.96 Å was determined. The spacing consists of 7.50 Å for plate thickness and 1.46 Å for the gallery height.

The magnitude of basal expansion can be assed by determining the d-spacing of the material using powder XRD. Although most of the original XRD pattern is lost after the swelling process due to fragmentation of the particles and loss of crystallinity, the [001] peak remains visible. Using Bragg's law and the 2θ value of the 001 peak the expanded basal spacing can be calculated. The resulting basal and gallery spacing along with the estimated length of the surfactants are shown in the Table 3.1.

Table 3.1 Basal, gallery and surfactant lengths for swollen AlPO

Swelling agent	basal spacing (nm)	gallery height (nm)	Surfactant length (nm)
As-synthesized	0.90	0.15	-
$112DADD^{+2}$	2.10	1.35	2.04
$CTMA^{+}$	3.20	2.45	2.53
$ODDMBA^{+}$	3.30	2.55	3.06

Figure 3.3 compares the ^{31}P NMR spectrum of as-synthesized AlPO with the ^{31}P NMR spectra of $CTMA^{+}$, $ODDMBA^{+}$, and $112DADD^{2+}$ AlPO. In particular the ^{31}P NMR spectrum of

as-synthesized AlPO shows three separate peaks at chemical shift values of -14.6, -19.5, and -21.6. The peak at -21.7 is consistent with the Q^3 peak reported for this material by Zhou et al.[12] It is known from Gao et al. that all of the phosphate tetrahedra in the as-synthesized AlPO material are of the same type Q^3 (PO_3=O). The tetrahedra contain three bridging oxygens which connect to aluminum in the framework and one terminal =O. It has been reported that phosphorus tetrahedra of the same type can produce multiple peaks in ^{31}P NMR spectra depending on the geometry around the P atom.[13] The presence of three peaks is therefore attributed to the three crystallographically unique P reported by Gao et al.[9]

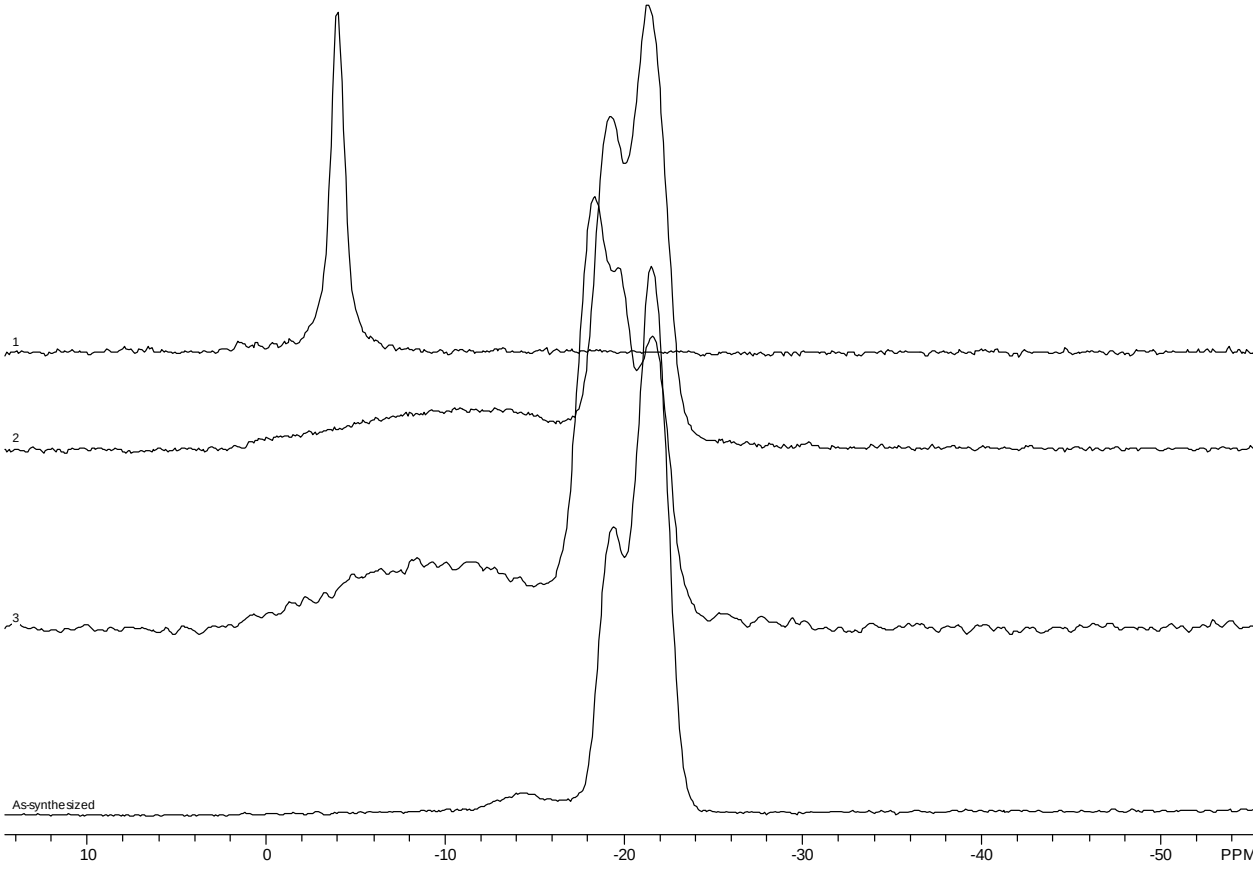

Figure 3.3 ^{31}P NMR of AlPO swollen with (1) 112DADD^{2+}, (2) ODDMBA^{+}, (3) CTMA^{+}, and As-synthesized AlPO

3.3.2 Cetyltrimethyl ammonium swollen AlPO

The cetyltrimethyl ammonia swelling treatment was chosen for comparison reasons. Jeong et al. have already reported a successful nanocomposite made with $CTMA^+$ swollen AlPO[10]. The alternative swelling treatments presented here were tested in order to evaluate whether these agents can tune the surface properties of AlPO. A detailed assessment of the $CTMA^+$ AlPO system was not reported in the earlier work.[10] A more rigorous evaluation of the swollen material is reported below.

When the AlPO was treated with $CTMA^+$, changes were observed in the SEM of the AlPO crystals consistent with an increase in the basal spacing. The crystals were further characterized with XRD, and NMR to confirm that the AlPO had been swollen.

The crystal sizes of $CTMA^+$ swollen AlPO (not pictured) and as-synthesized AlPO were compared using SEM and found to be comparable. However, an SEM image of the side of one of the swollen AlPO crystals shown in Figure 3.4b shows a change in the appearance of layers in the material. In comparison, Figure 3.4a shows the as-synthesized AlPO. The layers are only faintly apparent in this micrograph. The side of the as-synthesized crystal is very smooth with only some visible heat cracking caused by the electron beam. The SEM of the $CTMA^+$ swollen AlPO, however, shows a clearly layered material. The scale of theses images are much too large to see individual layers, however, a definitive increase in the layer spacing has taken place.

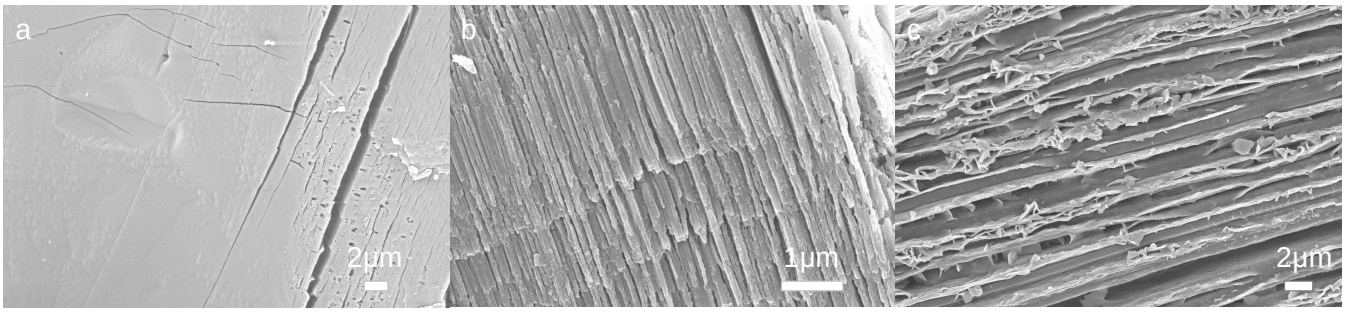

Figure 3.4 SEM views along the sides of AlPO crystals (a) as-synthesized, and swollen with (b) $CTMA^+$, (c) $ODDMBA^+$

The XRD pattern of $CTMA^+$ swollen AlPO in Figure 3.5 shows three prominent peaks at regular intervals and several small peaks at a 2θ values around 10°. This indicates that the swollen AlPO is a mix of both expanded crystals and some starting material with the original basal spacing intact. The 001 peak of as-synthesized AlPO can be seen at a 2θ value of 9.8° in Figure 3.1. In contrast, the XRD pattern of AlPO swollen with $CTMA^+$ in Figure 3.5 shows a shift of the 001 peak to a 2θ value of 2.76°. This shift corresponds to an expansion of the basal spacing to a value 32.0 Å. Figure 3.6 shows the dimensions of idealized perfectly straight molecules of the swelling agents used in this study made using CAChe. For the case of cetyltrimethly ammonium, the length of the molecule is based on van der Waals radius, bond lengths and angles. Comparing the calculated length of this molecule with the gallery height can give some clues about the orientation of the gallery ions.[14] The difference in the molecule length and gallery height is a mere 0.8 Å, indicating the molecules are likely in a monolayer arrangement and nearly perpendicular to the layer surfaces.

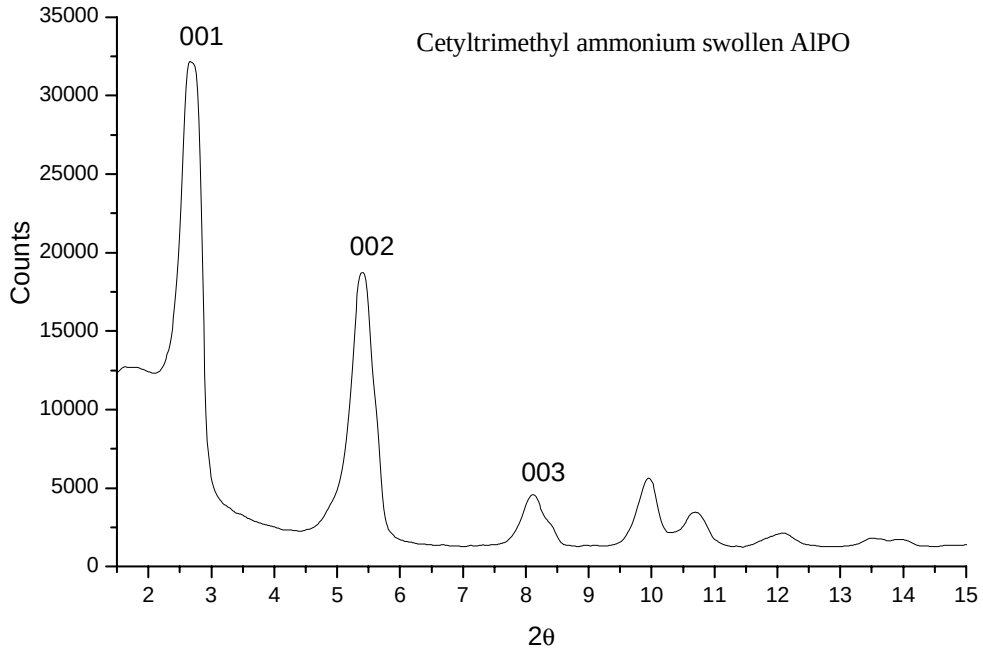

Figure 3.5 XRD powder pattern of $CTMA^+$ AlPO

Further it was found that adding a sonication step before the swelling process reduced the final particle sizes of the crystals significantly. Figure 3.7 shows an SEM of $CTMA^+$ swollen AlPO with and without a sonication step just before swelling. The image to the left was the result of no sonication or stirring during swelling. The particle sizes are comparable to as-synthesized AlPO. It can be seen in the image to the right that the particle size is reduced significantly by simply sonicating the material for 30 minutes in the swelling medium.

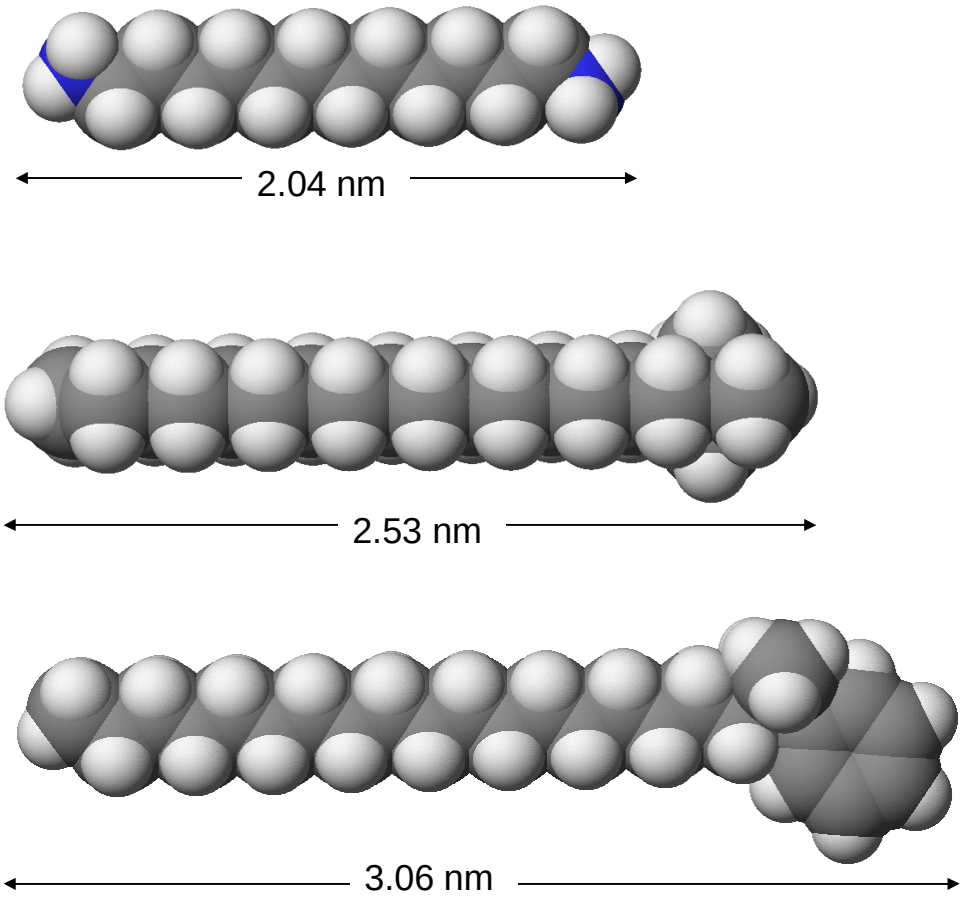

Figure 3.6 Idealized pictures and lengths of (top) protonated 1,12 diamminododecane, (middle) cetyltrimethyl ammonium, (bottom) octadecyldimethyl benzyl ammonium

It appears that the overall phosphorus coordination environment of swollen AlPO is the same as that of as-synthesized AlPO. The ^{31}P NMR of $CTMA^+$ swollen AlPO shown in Figure 3.3 on line 3 is similar to that of as-synthesized AlPO. The peak at -14.6 has broadened some, and now has a maximum at -11. The peaks at -19.7 and -21.6 are still present indicating that these two crystalographically unique phosphate tetrahedra are still intact after swelling. However, the relative magnitudes of these two peaks have switched when compared with the as-synthesized AlPO. A fourth peak has appeared at -18.4 which indicates a new tetrahedral coordination environment is present. This is not surprising, considering a very large molecule has replaced the smaller ethylammonium ion in the gallery. This would certainly change the hydrogen bonding environment in the gallery space. The ^{31}P results are consistent with an intact framework even after swelling.

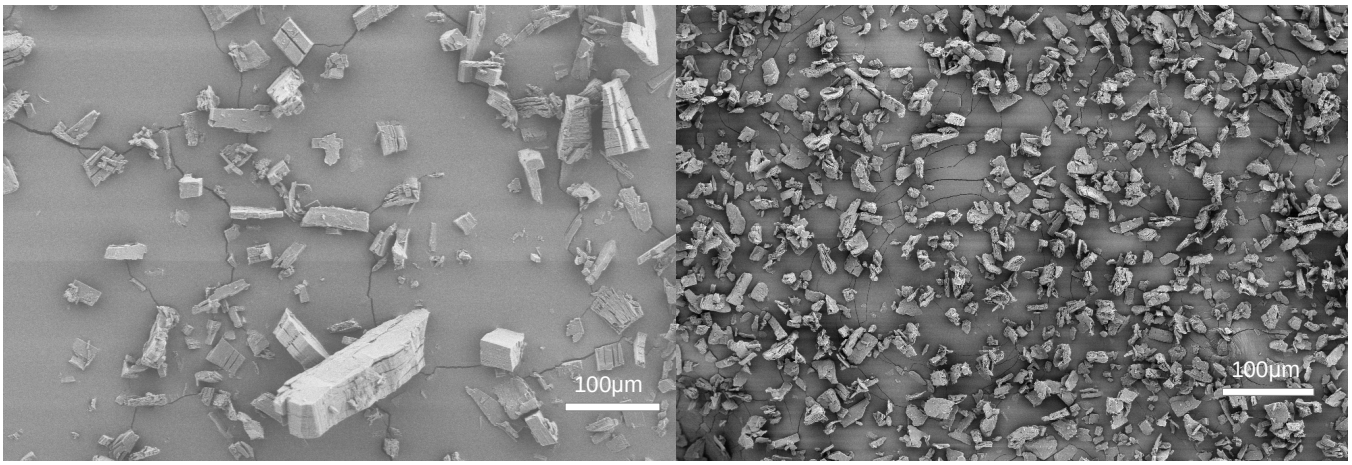

Figure 3.7 $CTMA^+$ AlPO with (right) and without (left) a sonication step

3.3.3 Octadecyldimethyl benzyl ammonium swollen AlPO

The swelling of AlPO with octadecyldimethyl benzyl ammonium was done in preparation for mixing with the polymer Matrimid©. Chung et al. modified the fullerene C_{60} with benzylamine and successfully combined it with Matrimid©.[15] Our intention is to reproduce a similar interaction by modifying AlPO with a surfactant containing a benzene ring.

The treatment of AlPO with $ODDMBA^+$ produced a swollen structure similar to that seen previously in the $CTMA^+$ swollen AlPO. The XRD, SEM, and NMR results are consistent with an increased basal spacing and intact framework layered material.

The XRD pattern for $ODDMBA^+$ swollen AlPO shown in Figure 3.8 has the 001 peak at a 2θ value of 2.6°. Using Bragg's Law the d-spacing is calculated to be 33.0 Å. The length of the intercalating molecule as seen in the bottom of Figure 3.6 in this case is 30.6 Å. Comparing the gallery height to a perfectly straight $ODDMBA^+$ molecule gives a difference of 5.1 Å. The gallery space is several angstroms smaller than the surfactant, suggesting that the molecules are lying in a monolayer arrangement at some angle to the surface of AlPO or in a disordered folded conformation. Remnants of the as-synthesized pattern can clearly be seen in the swollen AlPO pattern in Figure 3.8. This demonstrates that the exchange during the swelling process is not complete. Therefore, the sample consists of two phases, the original material, and some material swollen with the surfactant.

Much like the $CTMA^+$ swollen AlPO, SEM of the $ODDMBA^+$ swollen crystals (not pictured) suggested that the crystals were similar in size to the as-synthesized AlPO crystals. The SEM image of the side of an $ODDMBA^+$ swollen AlPO crystal shown in Figure 3.4c indicates shows a change from the smooth surface of the as-synthesized material. The layered

structure is now clearly visible and gaps between stacks of layers can be seen. The morphology is different

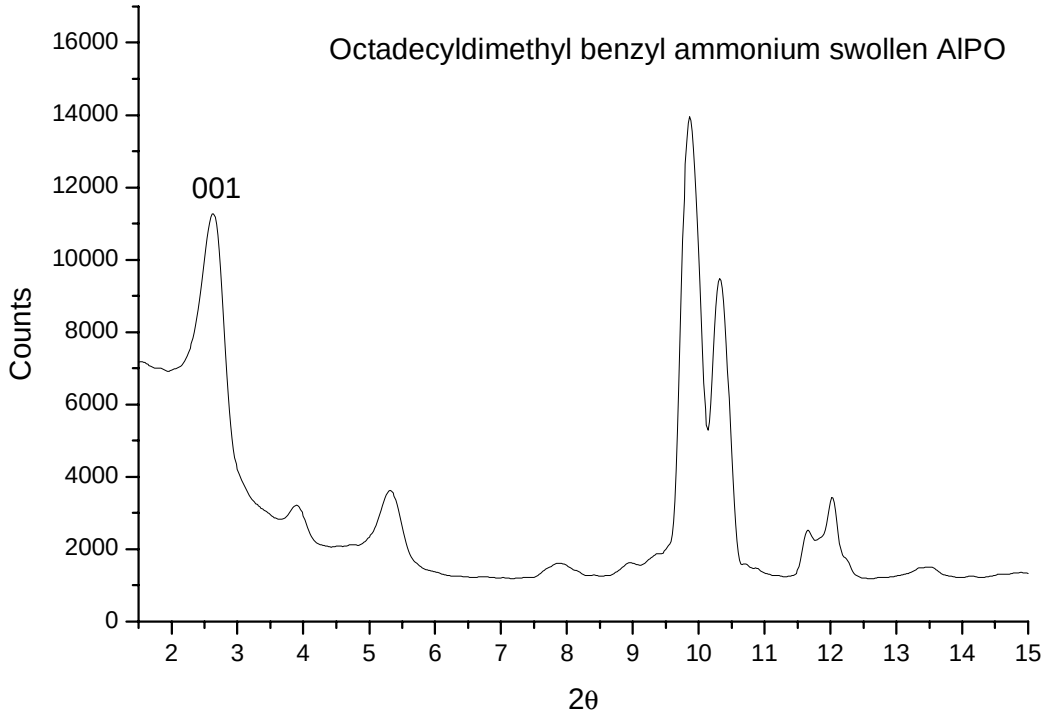

Figure 3.8 Powder XRD pattern for ODDMBA$^+$ AlPO

from the same view of the CTMA$^+$ swollen crystals. Larger gaps in the layers are visible and the layers do not look as linear as those of CTMA$^+$ AlPO seen in Figure 3.4b.

From ^{31}P NMR results, it appears that the framework of AlPO is intact after swelling. Figure 3.3 compares ^{31}P NMR spectra for as-synthesized AlPO with that of ODDMBA$^+$ swollen AlPO on line 2. The patterns are almost identical with the exception of the broadening of the chemical shift peak at -14.6 seen in as-synthesized AlPO. This same broadening was observed in the CTMA$^+$ AlPO. The peaks at -19.5 and -21.6 are present indicating the phosphorus tetrahedra have remained the same after swelling.

3.3.4 Protonated 1,12 Diamminododecane swollen AlPO

The final swelling agent used was the protonated form of 1,12 diamminododecane. This molecule was chosen because once protonated, both ends of the molecule would possess potential hydrogen bonding sites. The molecule could then span the gallery space of AlPO attached at both ends to a platelet. Therefore, using this molecule may gently exfoliate AlPO by providing support for the top of one layer and the bottom of another while intercalation of the molecule takes place.

The swelling of AlPO with protonated 1,12 diamminododecane produced unexpected changes in the morphology and structure of AlPO. These changes were probed using SEM, powder XRD, and NMR.

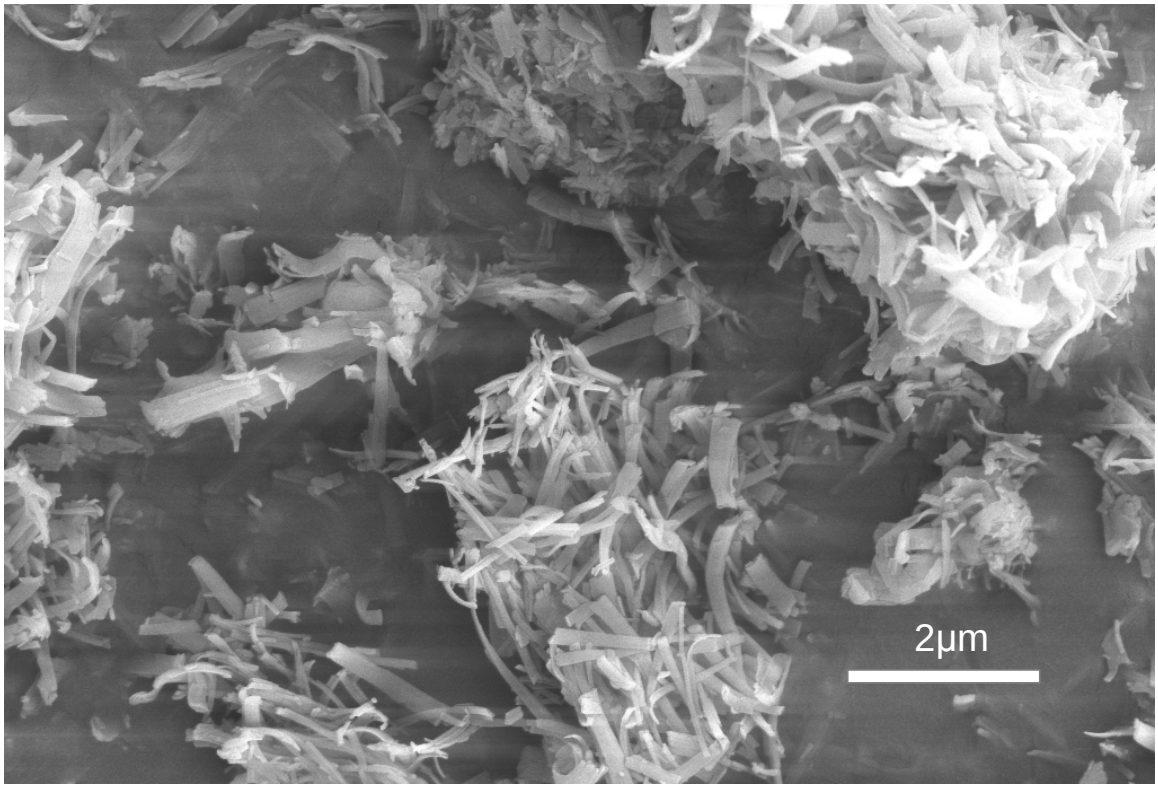

Figure 3.9 SEM of 112DADD^{2+} AlPO

An SEM photo of 112DADD^{+2} AlPO can be seen in Figure 3.9. The particle size of the swollen material has been reduced significantly when compared with as-synthesized AlPO shown in Figure 3.1a. The crystals of as-synthesized AlPO have a long dimension of 80-100μm, whereas the largest 112DADD^{+2} AlPO particles are smaller than 10μm. The particles look more like small ribbons and the large particles appear to consist of agglomerates of these ribbons. It can be seen from the scale bar on the SEM image that the width of 112DADD^{+2} AlPO is certainly in the nanometer range. This swelling procedure clearly produces the most dramatic effect on exfoliation of the layers.

The XRD pattern of 112DADD^{+2} AlPO is shown in Figure 3.10. It appears that very little if any of the original pattern from as-synthesized AlPO is present in the swollen pattern. This indicates that the material is one phase and that the original as-synthesized phase is no longer present. A peak at the 2θ value of 4.24° can be seen. If it is assumed that this is the $_d$001, a basal spacing of 21.0 Å can be calculated. The idealized 112DADD^{+2} molecule pictured in Figure 3.6 is 20.4 Å in length. The gallery height is therefore 6.9 Å shorter than the molecule, indicating it is lying at an angle in the gallery space. If the 112DADD^{+2} was bonded to the top of one sheet and the bottom of another via hydrogen bonding on both sides the gallery height should match more closely with the molecule length. It does not appear from XRD pattern, however, that this is the case.

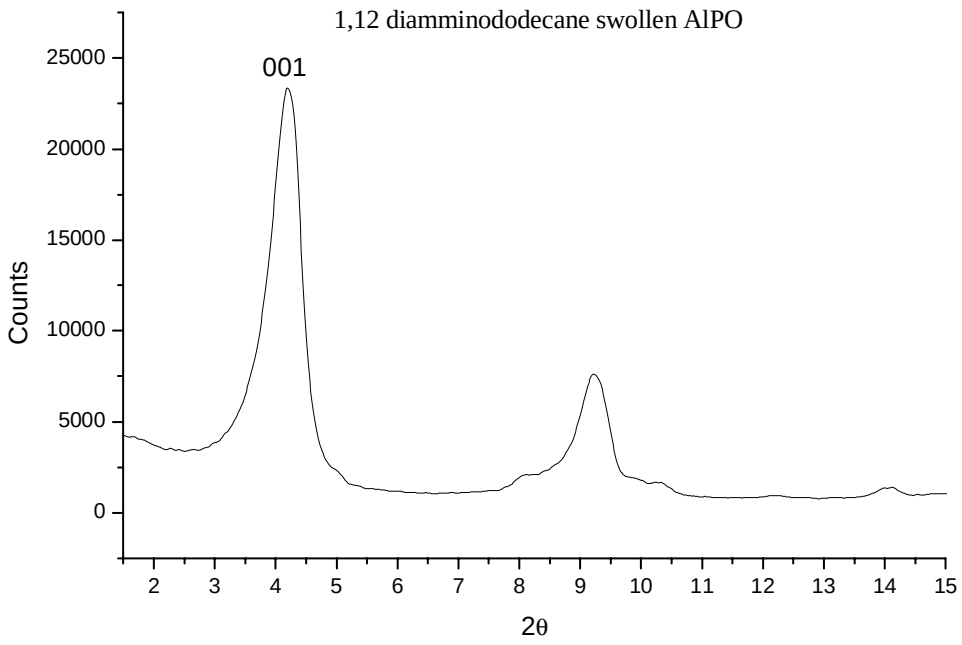

Figure 3.10 Powder XRD of 112DADD^{2+} AlPO

The ^{31}P NMR spectra for 112DADD^{+2} AlPO is considerably different than the as-synthesized spectra seen in Figure 3.3 line 1. Instead of the three peaks seen in the previous swollen AlPO spectra around -21 shift, there is a solitary peak located at a chemical shift value of -4.1. This indicates that the previously seen phosphorus tetrahedral environments have consolidated into a single form. The shift value seen, however, is still consistent with other Q^3 type tetrahedra reported on other aluminophosphates in the literature.[16, 17] Therefore, it is likely that the phosphorus atoms are still in a tetrahedral environment, yet the original framework may be distorted in some way.

3.4 Conclusions

The layered aluminophosphate $[Al3P4O16]^{3-}\cdot 3[NH_3CH_2CH_3]^+$ was swollen for the first time with octadecyldimethyl benzyl ammonium and protonated 1,12 diamminododecane. SEM images were presented that showed physically expanded structures, and altered morphology for the swollen AlPO. Results of ^{31}P NMR studies suggested that after AlPO was swollen,

phosphorus remained in a tetrahedral coordination, and the layered frameworks were, therefore, likely intact. The swollen AlPO was compared to AlPO obtained by previous swelling procedures developed by Jeong et al. and shown to be comparable in gallery expansion. Because intercalation was achieved it is possible that these alternative swelling agents could be used to create successful aluminophosphate-polymer nanocomposites.

(1) Okada, A.; Kawasumi, M.; Usuki, A.; Kojima, Y.; Kurauchi, T.; Kamigaito, O., Nyoln 6-clay hybrid. *Materials Research Society Symposium Proceedings* **1990,** 171, 45-50.

(2) Yano, K.; Usuki, A.; Okada, A.; Kurauchi, T.; Kamigaito, O., Synthesis and properties of polyimide-clay hybrid. *Polymer Preprints (American Chemical Society, Division of Polymer Chemistry)* **1991**, (32), 65-66.

(3) Usuki, A.; Kojima, Y.; Kawasumi, M.; Okada, A.; Fukushima, Y.; Kurauchi, T.; Kamigaito, O., Synthesis of nylon 6-clay hybrid. *Journal of Materials Research* **1993,** 8, (5), 1179-84.

(4) Usuki, A.; Kawasumi, M.; Kojima, Y.; Okada, A.; Kurauchi, T.; Kamigaito, O., Swelling behavior of montmorillonite cation exchanged for w-amino acids by e-caprolactam. *Journal of Materials Research* **1993,** 8, (5), 1174-8.

(5) Yano, K.; Usuki, A.; Okada, A.; Kurauchi, T.; Kamigaito, O., Synthesis and properties of polyimide-clay hybrid. *Journal of Polymer Science, Part A: Polymer Chemistry* **1993,** 31, (10), 2493-8.

(6) Lan, T.; Kaviratna, P. D.; Pinnavaia, T. J., On the Nature of Polyimide-Clay Hybrid Composites. *Chemistry of Materials* **1994,** 6, (5), 573-5.

(7) Okada, A.; Usuki, A., The chemistry of polymer-clay hybrids. *Materials Science and Engineering:C* **1995,** 3, (2), 109-115.

(8) Yano, K.; Usuki, A.; Okada, A., Synthesis and properties of polyimide-clay hybrid films. *Journal of Polymer Science, Part A: Polymer Chemistry* **1997,** 35, (11), 2289-2294.

(9) Gao, Q.; Li, B.; Chen, J.; Li, S.; Xu, R.; Williams, I.; Zheng, J.; Barber, D., Nonaqueous Synthesis and Characterization of a New 2-Dimensional Layered Aluminophosphate [Al3P4O16]3-· 3[CH3CH2NH3]+. *Journal of solid state chemistry* **1997,** 129, (1), 37-44.

(10) Jeong, H.-K.; Krych, W.; Ramanan, H.; Nair, S.; Marand, E.; Tsapatsis, M., Fabrication of Polymer/Selective-Flake Nanocomposite Membranes and Their Use in Gas Separation. *Chemistry of Materials* **2004,** 16, (20), 3838 -3845.

(11) Yu, Y.-H.; Yeh, J.-M.; Liou, S.-J.; Chen, C.-L.; Liaw, D.-J.; 3, H.-Y. L., Preparation and properties of polyimide-clay nanocomposite materials for anticorrosion application. *Journal of Applied Polymer Science* **2004,** 92, (6), 3573 - 3582.

(12) Zhou, D.; Xu, J.; Yu, J.; Chen, L.; Deng, F.; Xu, R., Solid-State NMR Spectroscopy of Anionic Framework Aluminophosphates: A New Method to Determine the Al/P Ratio. *The journal of physical chemistry. B, Condensed matter, materials, surfaces, interfaces & biophysical* **2006,** 110, (5), 2131-2137.

(13) Tuel, A.; Gramlich, V.; Baerlocher, C., Synthesis, crystal structure and characterization of AP2DAO, a new layered aluminophosphate templated by 1,8-diaminooctane molecules. *Microporous and Mesoporous Materials* **2001,** 47, 217-229.

(14) He, H.; Frost, R. L.; Bostrom, T.; Yuan, P.; Duong, L.; Yang, D.; Xi, Y.; Kloprogge, J. T., Changes in the morphology of organoclays with HDTMA+ surfactant loading. *Applied Clay Science* **2006,** 31, (3-4), 262-271.

(15) Chung, T.-S.; Chan, S. S.; Wang, R.; Lu, Z.; He, C., Characterization of permeability and sorption in Matrimid/C60 mixed matrix membranes. *Journal of membrane science* **2003,** 211, (1), 91-99.

(16) Cheng, S.; Tzeng, J.-N.; Hsu, B.-Y., Synthesis and Characterization of A Novel Layered Aluminophosphate of Kanemite-like Structure. *Chemistry of Materials* **1997,** 9, (8), 1788-1796.

(17) Gao, Q.; Chen, J.; Xu, R.; Yue, Y., Synthesis and Characterization of a Family of Amine-Intercatalated Lamellar Aluminophosphates from Alcoholic System. *Chemistry of Materials* **1997,** 9, (2), 457-462.

Chapter 4

A sorption study including, XRD, and TGA of $CMTA^+$ 8MR-AlPO treated with several template removal methods and several other basic properties

4.1 Introduction

One of the main problems to overcome in making polymer-aluminophosphate nanocomposites is the treatment of the inorganic to best exfoliate and disperse it in organic solvent. We have been unsuccessful in fabricating gas-selective membranes in part because 8MR-AlPO has proven very difficult to swell, exfoliate and maintain the the useful properties of the sheets. We have been following techniques used in polymer clay nanocomposite (PCN) literature to modify 8MR-AlPO.[1-3] This involves ion exchanging 8MR-AlPO with a surfactant and then washing away the excess surfactant in preparation

for combining it with a polymer matrix. This step is performed to expand the gallery space, reduce hydrogen bonding between layers, and make the surface more organophilic. One possible problem with this method for our purposes is that the surfactant could block the 8MR opening through which we believe small gas species may pass. It may be possible to remove the surfactant used to swell 8MR-AlPO leaving only the framework structure. In this experiment we will use several different methods in the attempt to gently remove the surfactant used to swell 8MR-AlPO leaving only the inorganic structure. We have used XRD, TGA, and sorption measurements to characterize the samples.

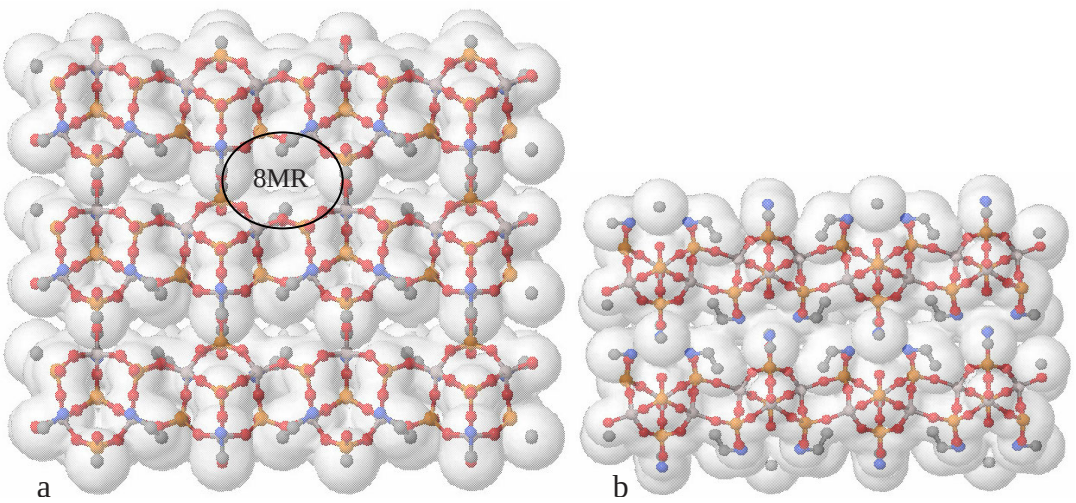

Figure 4.1 a) view of as-synthesized 8MR-AlPO looking down the top of a layer (001) with Van der Waals surface included. b) view of as-synthesized 8MR-AlPO looking down the plane of the layer (010) with Van der Waals surface included.

A representation of as-synthesized $[Al_3P_4O_{16}]^{3-} \cdot 3[CH_3CH_2NH_3]^+$ is shown in Figure 4.1. The framework structure can be seen along with the ethylammonium ions present in the gallery. The representation includes a Van der Waals surface created with Jmol.[4] This figure illustrates the potential problem of having organic molecules present in the structure. The oval shaped 8MR that we believe small gas species may pass

through can be seen in Figure 4.1a. The dimensions given by Gao et al. for this opening are 6.0 x 3.8Å.[5] This distance, however, represents a measurement from atom center to atom center. If the Van der Waals radii are added for each atom the 8MR opening becomes much smaller and the opening appears obstructed when the gallery ions are represented in the picture. We believe that the ethylammonium ions in the as-synthesized structure or even the $CMTA^+$ molecules in the swollen structure may be obstructing the diffusion of small gas species. One caveat of removing these ions however is collapse of the structure. The gallery ions play an important role by hydrogen bonding the layers together and forming the shape of the 8MR openings. It is unfortunately very difficult to remove the gallery ions without destroying the structure. Wang et al. report the difficulty lies in the instability of the microporous sheets and Huang et al. cite removal of the cations by calcination collapsed the structure or transformed the material into other dense phases.[6, 7] Gao et al. reported as-synthesized 8MR-AlPO became amorphous after 300°C when the ethylammonium ions were completely removed. For this reason we propose some gentler methods to remove some of the gallery surfactant.

4.2 Experimental Setup

First 8MR-AlPO was synthesized and then swollen with cetyltrimethyl ammonium ($CMTA^+$) to swell the gallery space. The method used to swell 8MR-AlPO was consistent with the procedure outlined by Jeong et al.[8] Three methods were chosen to test for effectiveness in template removal. The methods were heat with ozone, ozone and ultraviolet radiation, and Soxhlet extraction with a solvent.

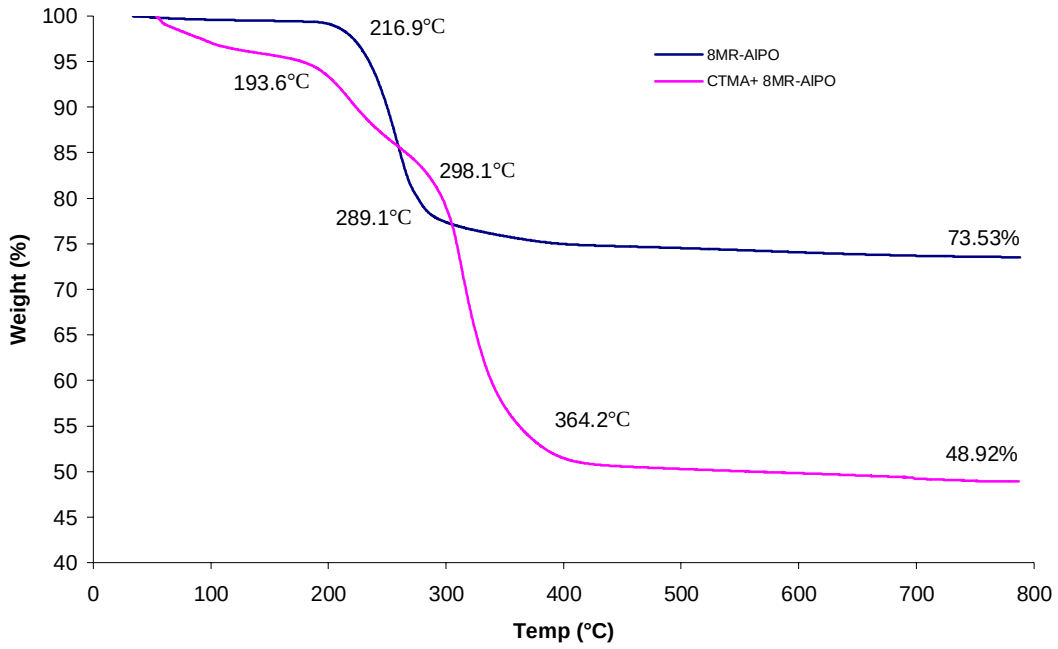

Figure 4.2. TGA of as-synthesized 8MR-AlPO

4.2.1 200°C and Ozone treatment of 8MR-AlPO

The experimental setup for removal of $CMTA^+$ from 8MR-AlPO using heat and ozone is displayed in Figure 4.3. Oxygen was passed in to an ozone generator at a flow rate of 200ml/min. At this flow rate and a setting of 4 on the generator the output was known to be 10,000ppm by manufacturer's standards. The flowing stream of ozone was piped into a quartz cell that contained 0.2 g of $CMTA^+$ swollen 8MR-AlPO. The quartz cell was suspended inside an insulated oven at 200°C and the ozone exited out of the oven and into a bubbler unit. Ozone was chosen as an oxidizer because it is known from literature that zeolites can be calcined effectively at low temperatures using ozone.[9] The temperature of 200°C was determined from the TGA of as-synthesized 8MR-AlPO (Figure 4.2). At 217°C a large loss of weight is recorded. The weight loss may be attributed to ethylammonium ions beginning to degrade. Gao et al. performed an XRD

study varying temperatures of 8MR-AlPO and report that it becomes amorphous at 300°C.[5] In our TGA results (Figure 4.2) the weight loss levels off at about 300°C. The amorphous state likely corresponds to a collapse of the structure after all of the gallery ions are removed. To avoid a complete collapse of the structure a safe temperature of 200°C was chosen. The heat and ozone system was run for 10 hours at a time and 2 batches of AlPO were recovered for analysis.

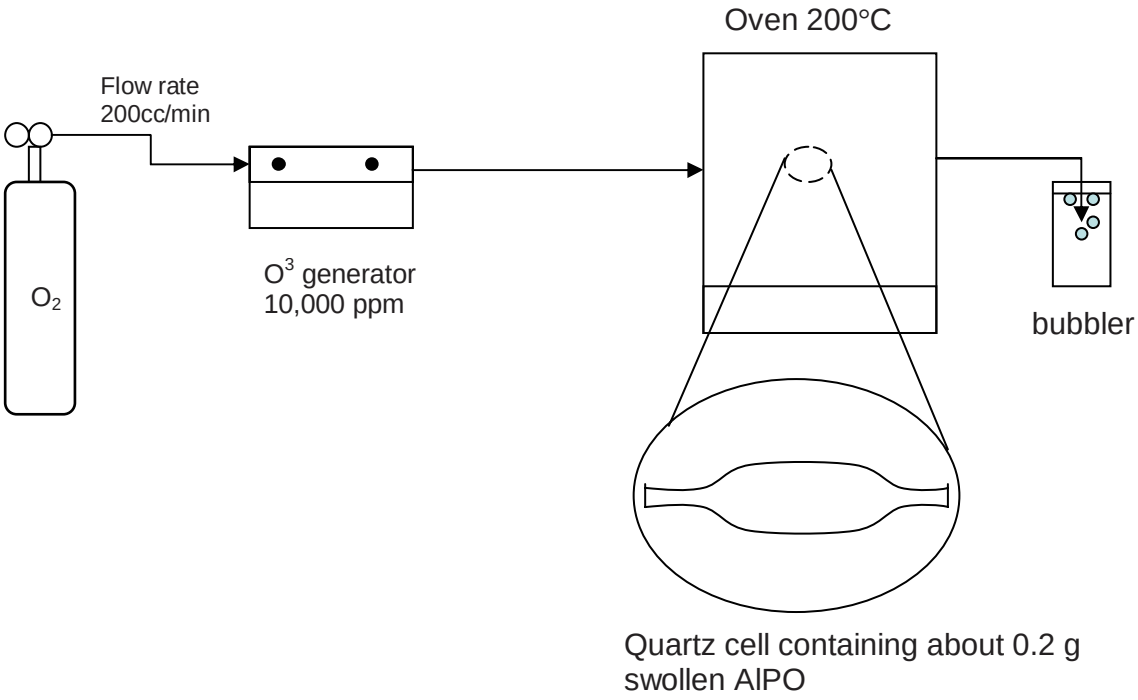

Figure 4.3. Experimental setup using UV/200°C to remove template form 8MR-AlPO

4.2.2 Ozone and Ultraviolet Radiation treatment of 8MR-AlPO

For the second treatment of 8MR-AlPO we wanted to try a non-thermal method that should be gentler than the thermal method used above. The experimental setup for this method is displayed in Figure 4.4 below. Oxygen was flowed into an ozone generator at a flow rate of 200ml/min. At this flow rate and a setting of 4 on the generator the output was known to be 10,000ppm by manufacturer's standards. The

flowing stream of ozone was piped into a quartz cell that contained 0.2 g of $CMTA^+$ swollen 8MR-AlPO. The quartz cell was suspended inside a box with a UV lamp at a wavelength of 254nm. The temperature inside the box equilibrated at 30°C. The use of ozone and short wavelength UV radiation as a non-thermal calcination method for aluminophosphates and other zeolites is consistent with examples found in the literature.[10, 11] This system was run for 6 hours at a time and 2 batches of AlPO were recovered for analysis.

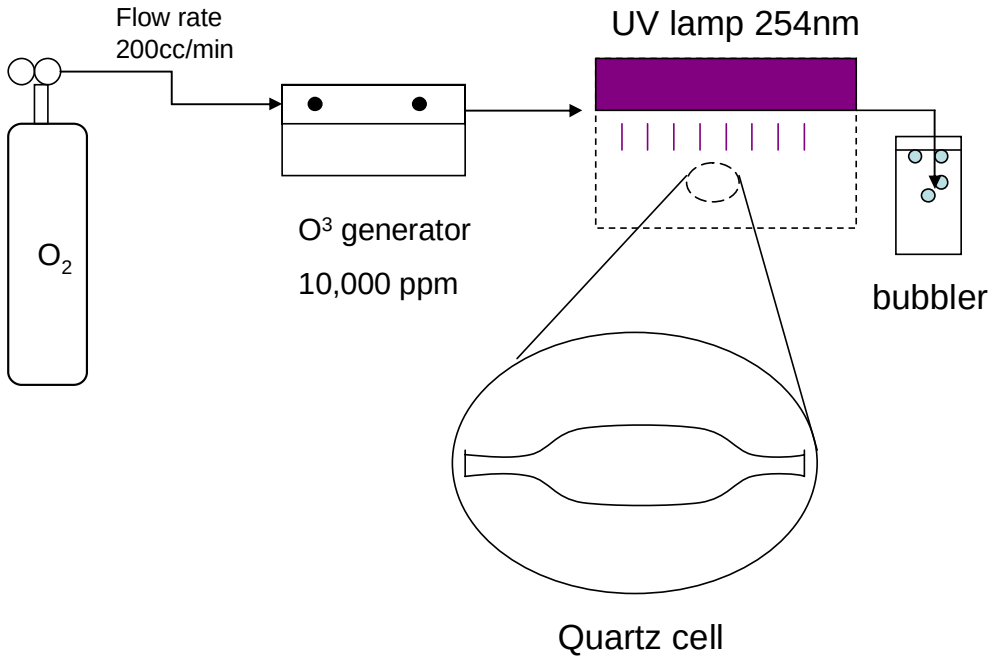

Figure 4.4 Experimental setup for 0_3/UV treatment of 8MR-AlPO

4.2.3 Soxhlet Extraction of 8MR-AlPO

Another attempt at template removal using a gentler method was made using solvent extraction. Tuel et al. reported that a mesoporous silica zeolite collapsed when calcined at high temperatures, however, remained intact when the template removal was performed gently with solvent extraction.[12] A diagram of the Soxhlet extractor used for

our experiment can be seen in Figure 4.5 below. A small amount of $CMTA^+$ 8MR-AlPO (0.4g) was charged in a cellulose thimble and placed into the Soxhlet extractor. The washing solvent is placed in the flask at the bottom of the extractor and washes the inorganic by evaporation and condensation. The solvent we used contained 200mL of ethanol and 1.0mL of N-butylamine (pH = 11.52). The choice of extracting solvent was consistent with one used for an aluminophosphate in literature.[13] The solvent was stirred and a temperature of 90° was sufficient to keep a constant stream of solvent dripping onto 8MR-AlPO.

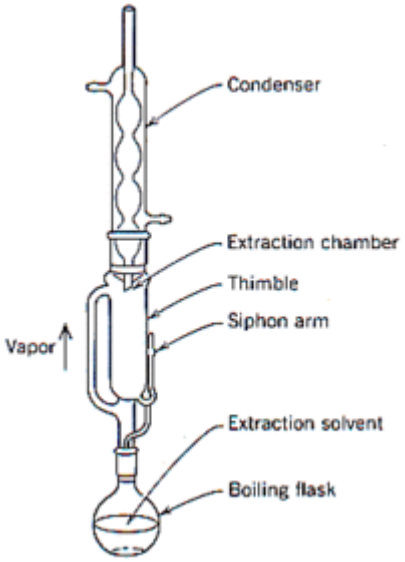

Figure 4.5 Soxhlet extractor

4.3 Results and Discussion

4.3.1 TGA and XRD data

Thermogravimetric analysis (TGA) scans were performed on as-synthesized, swollen 8MR-AlPO and the samples treated to remove the $CMTA^+$ ions. All TGA scans were carried out at ramp rate of 10°C/min. The samples were ramped at this rate to

100°C and held there for 1hr to ensure the removal of water. After that the run was continued at the same rate until it reached 800°C.

The TGA of as-synthesized 8MR-AlPO and $CMTA^+$ 8MR-AlPO are compared in Figure 4.2. The as-synthesized 8MR-AlPO shows a large weight loss beginning at 217°C and ending at around 300°C. As mentioned above this is likely the loss of the ethylammonium ions in the gallery space of the material. This is corroborated by the mass loss at this temperature (23%) which corresponds to the weight of the gallery ions in the molecular formula $[Al_3P_4O_{16}]$ $[NH_3CH_2CH_3]_3$. The TGA scan of $CMTA^+$ 8MR-AlPO confirms that there was not complete ion exchange of $CMTA^+$ for ethylammonium. If all of the ethylammonium ions had been replaced a weight loss of 65% was expected. The actual weight loss recorded after all the organics were removed was around 45%. This means that some combination of ethylammonium and $CMTA^+$ populated the surface of 8MR-AlPO. In order to determine the exact exchange a much more extensive series of TGA experiments would have to be performed. A quick estimate can be obtained from observation. First, the initial weight loss below 100°C is attributed to water loss. The next large loss is about 14% of the mass and the final drop results in another 31% mass loss. The first drop seems to correspond to temperatures associated with the removal of ethylammonium and the second drop would then correspond to the removal of $CMTA^+$. If this assumption is accurate it can be estimated that about 31% of the mass loss is due ethylammonium and 69% is due to $CMTA^+$. When these numbers are reconciled with the molecular formula it is estimated that only about 1/3 of the ethylammonium ions were replaced with $CMTA^+$ ions.

A comparison of TGA for the different methods used to remove CMTA+ is shown in Figure 4.6. The immediate observation is that the O_3/200°C method removed the most organic molecules prior to TGA being run. Comparing the scan of $CMTA^+$ 8MR-AlPO with the O_3/200°C treated sample 25% of the organics were removed as a result of the heat treatment. This is in contrast to the O_3/UV and Soxhlet extraction methods which resulted in only 6% removal of the organics when compared to untreated sample. The shapes of all the treated samples showed a similar slow drop in weight between 400°C and 650°C. This drop was not recorded in the as-synthesized or $CMTA^+$ swollen 8MR-AlPO samples which were nearly stable in this range. The shape of the O_3/200°C was flat when compared to the other scans. There is a large initial drop which is attributed to low molecular weight molecules degraded by the treatment followed by a small weight loss between 300-350°C which is likely the larger inorganic molecules coming off. The O_3/UV and Soxhlet extraction methods performed similarly but the curves were different in shape. It appears that the Soxhlet method removed a little more of the low molecular weight organics because only two major drops in weight were seen when compared to the O_3/UV method which showed a weight loss before 300°C.

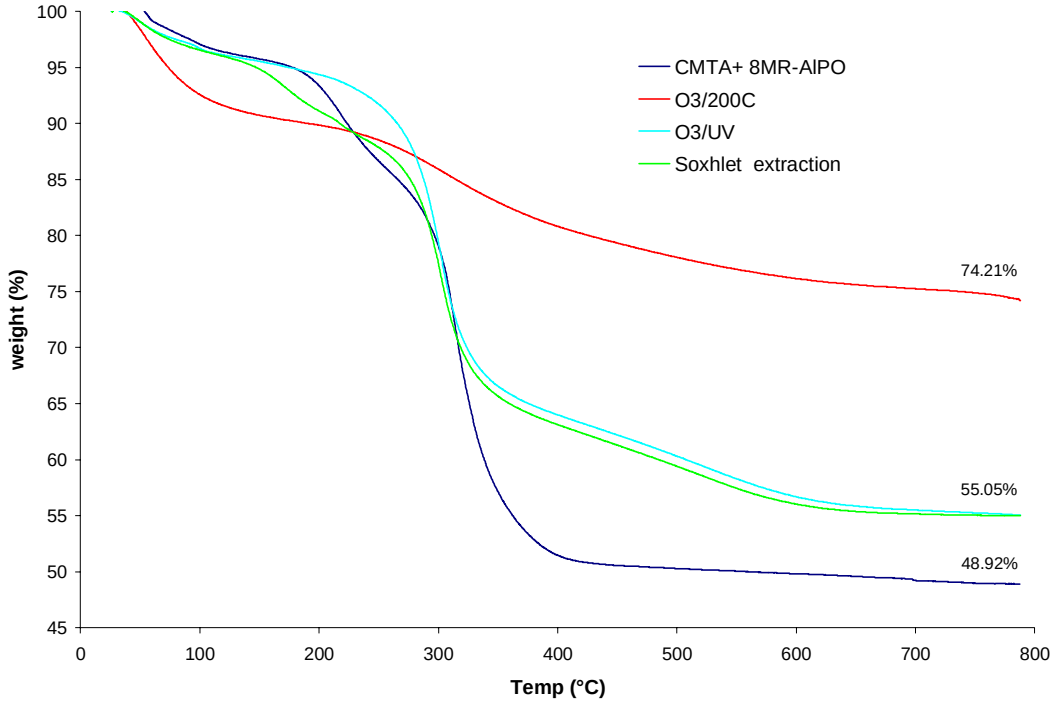

Figure 4.6 TGA of CTMA+8MR-AlPO and the samples treated to remove the surfactant used to swell the material

X-ray diffraction data of each of the samples was taken to probe any changes in crystallinity as a result of the treatments used. The as-synthesized pattern (not pictured) of 8MR-AlPO was checked to confirm that the correct structure was obtained. This pattern showed the characteristic 001 peak at $2\theta = 9.8°$ which corresponds to a d_{001}-spacing of 9Å. The XRD pattern of $CMTA^+$ 8MR-AlPO is shown below in Figure 4.7. It can be seen that the 001 peak has shifted to a lower angle $2\theta = 2.74$ which corresponds to a d_{001}-spacing of 32 Å. A change or shift in this 001 peak for the treated samples would indicate a change in the d_{001}-spacing of 8MR-AlPO. The O_3/200°C treatment resulted in the greatest change in the XRD pattern when compared to CMTA+ 8MR-AlPO. The 001 peak has shifted to the left to a position of $2\theta = 1.74$. This position indicates an increase in the gallery spacing with a d_{001}-spacing of 51Å. This increase in

d_{001}-spacing was unexpected because surfactant was being removed. The 001 peak is also much broader when compared to the other peaks, which indicates a range of d_{001}-spacings. The O_3/UV treatment resulted in an XRD pattern which was almost identical to the untreated sample. The Soxhlet extracted sample showed some unusual split peaks. The first peaks overlapped the untreated sample while the twin peak was shifted to the right. This indicates two very distinct phases one with a d_{001}-spacing equal to the untreated sample and one with smaller gallery spacing. The 001 peak shift results in a reduction of 4Å for the gallery space. This is small and may be due to some exchange of butyl amine for $CMTA^+$ ions from the washing process.

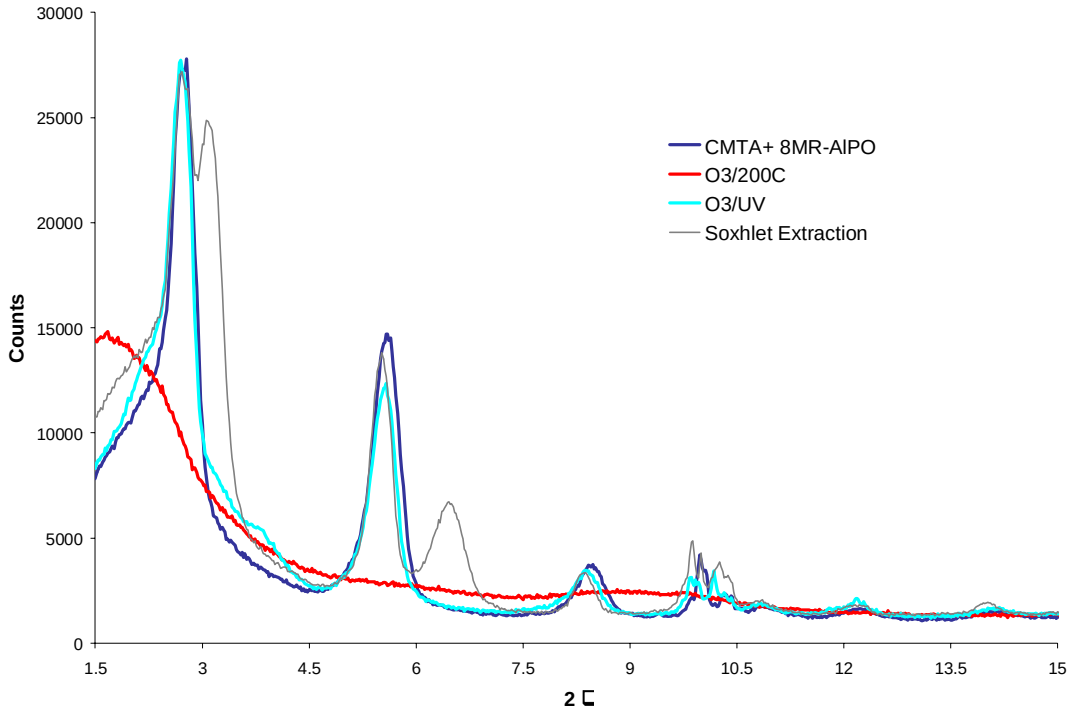

Figure 4.7 XRD powder patterns of 8MR-AlPO samples with different treatments

4.3.2 Sorption Data

Five small gas species were tested on the 8MR-AlPO treated with the different methods mentioned above. The gas species tested were H_2, O_2, N_2, CH_4 and CO_2.

Approximately 100mg of sample was placed in an Isochema IGA sorption apparatus and isotherms were run at 35°C and from a pressure of 100mbar to 18,000mbar. The objective was to see if the template became more accessible to gas species once they were treated to remove some amount of the surfactant used to modify the surface of 8MR-AlPO. We expect to see a large increase in sorption if this is the case. The graphs below report the same data in two different forms. The first five graphs contain adsorption isotherms for each gas species with the sample as a constant. The second five graphs have adsorption isotherms for one gas species and the sample is varied. The former illustrates which gas species have the greatest adsorption and the ladder gives information on which treatment was most effective.

Isotherms separated by samples

The isotherms collected for the 8MR-AlPO samples showed adsorption differences between the samples. The as-synthesized sample showed (Figure 4.8a) the largest adsorption for H_2 followed by CO_2, O_2, N_2, and CH_4. This order is consistent with the kinetic diameters of the gas species. In the untreated 8MR-AlPO swollen with $CMTA^+$ the sorption of CO_2 was increased while the H_2 sorption decreased. The O_2 and N_2 sorption dropped slightly below CH_4 sorption which stayed the same. The increased sorption of CO_2 can be accounted for by specific interactions with the $CMTA^+$ and the drop in the other gas species may be due to the gallery and pores being clogged by the surfactant. Removal of the excess surfactant was expected to increase the sorption of smaller gases if the gallery and pore spaces were more accessible. This did not appear to be true for any of the treated samples. The H_2 adsorption remained largely the same as the untreated sample except for the Soxhlet treated sample where H_2 adsorption dropped.

The adsorption of CO_2 exceeded the adsorption of H_2 in the O_3/200°C and Soxhlet treated samples. The isotherms show that none of the treatments caused H_2 to increase significantly over the larger gas species like CH_4.

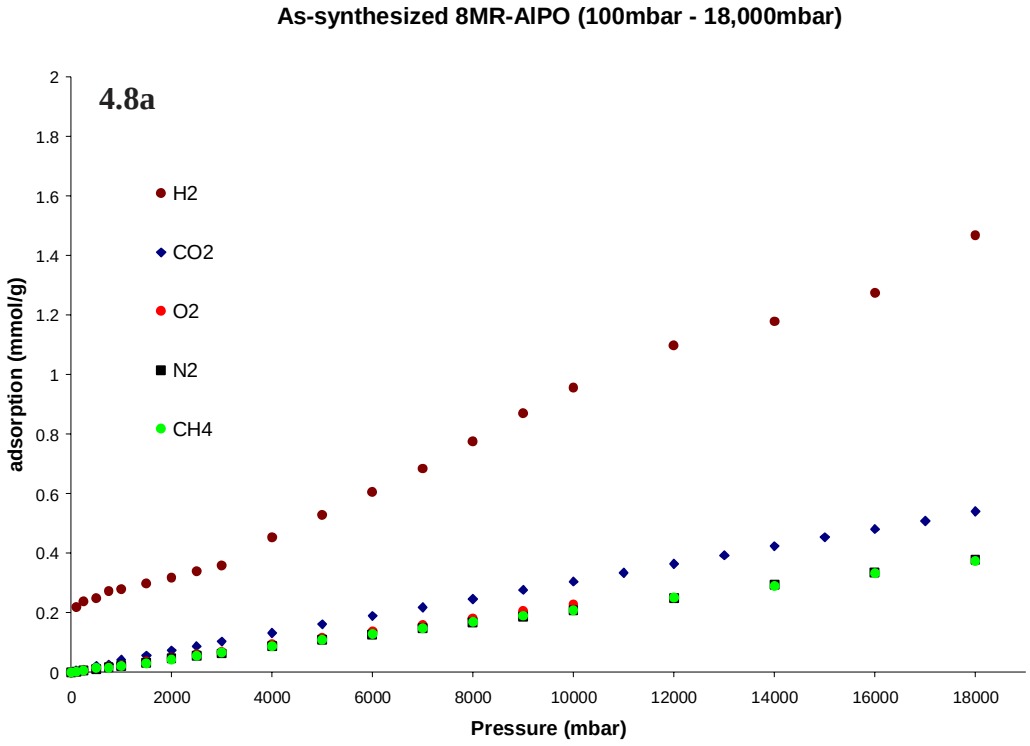

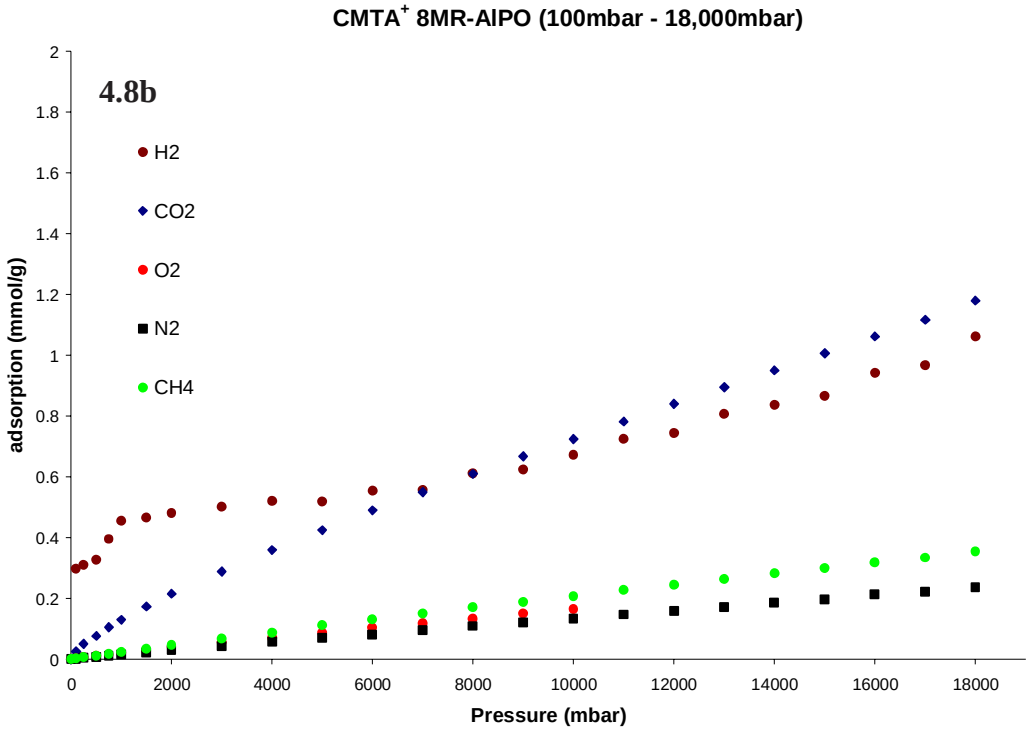
CMTA+ 8MR-AlPO (100mbar - 18,000mbar)
4.8b
H2
CO2
O2
N2
CH4
adsorption (mmol/g)
Pressure (mbar)
0
0.2
0.4
0.6
0.8
1
1.2
1.4
1.6
1.8
2
0
2000
4000
6000
8000
10000
12000
14000
16000
18000

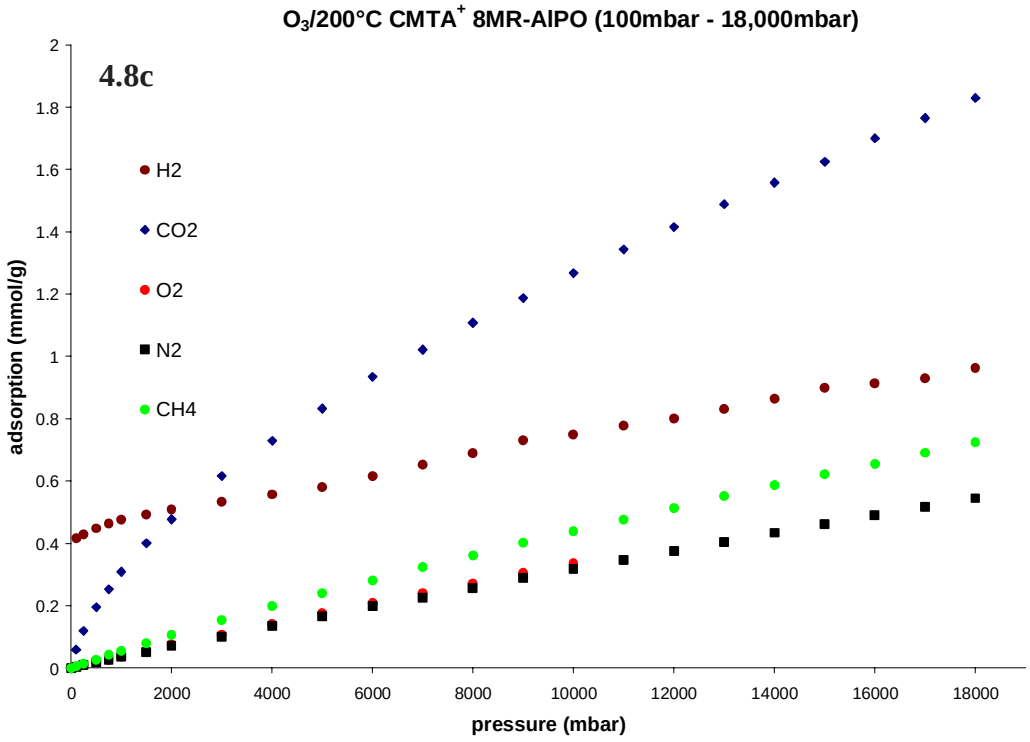
O3/200°C CMTA+ 8MR-AlPO (100mbar - 18,000mbar)
4.8c
H2
CO2
O2
N2
CH4
adsorption (mmol/g)
pressure (mbar)
0
0.2
0.4
0.6
0.8
1
1.2
1.4
1.6
1.8
2
0
2000
4000
6000
8000
10000
12000
14000
16000
18000

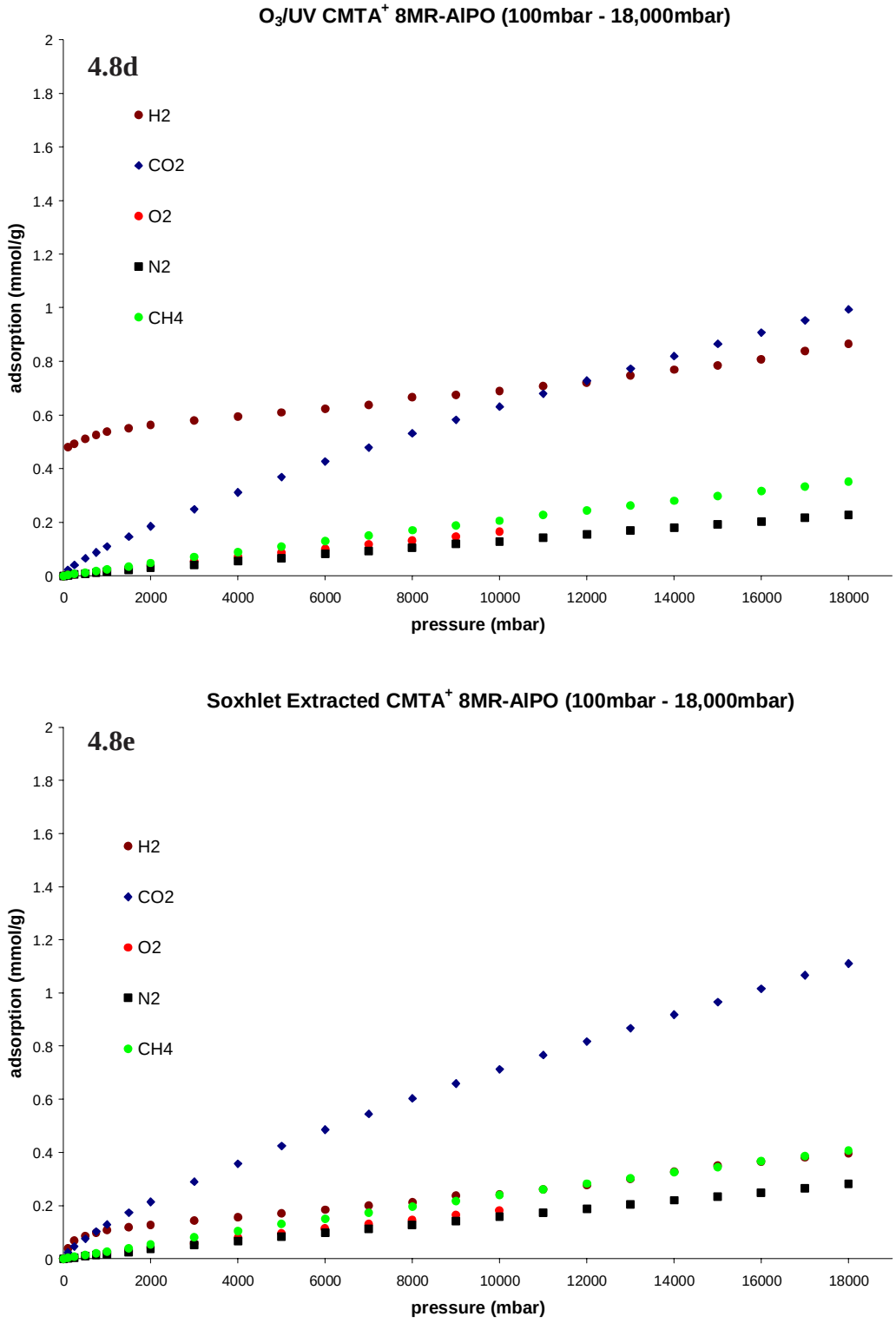

Figure 4.8 a) isotherms of as-synthesized 8MR-AlPO b) isotherms of $CMTA^+$ 8MR-AlPO c) isotherms of O_3/200°C treated 8MR-AlPO d) isotherms of O_3/UV treated 8MR-AlPO e) isotherms of Soxhlet extracted treated 8MR-AlPO

Isotherms separated by gas species

Observation of the data displayed in Figure 4.9(a-e) reveals that the O_3/200°C treatment increased the adsorption of all the gas species except for H_2 when compared to the other 8MR-AlPO samples. The adsorption of CO_2 increased the most followed by O_2, N_2, and CH_4 (Figure 4.9b-e).

The adsorption of H_2 (Figure 4.9a) was not increased by the O_3/200°C treatment but remained similar to the $CMTA^+$ 8MR-AlPO. For this gas species the highest adsorption was seen on the as-synthesized sample. Hydrogen is the smallest of the species tested and may be able to access the gallery space before 8MR-AlPO is swollen with surfactant. The adsorption of H_2 drops when surfactant is added to 8MR-AlPO suggesting that the surfactant is actually restricting the sorption of H_2. Even when some of the surfactant is removed with the O_3/200°C treatment and the gallery space is increased as shown by XRD, the adsorption of H_2 did not return to the levels seen in as-synthesized 8MR-AlPO.

The other gases tested showed an increase in adsorption with the O_3/200°C treatment. However, the O_3/UV and Soxhlet treatments resulted in isotherms that were very similar to the untreated $CMTA^+$ 8MR-AlPO. The CO_2 adsorption increased more than any of the other gas species potentially due to some specific interaction with the surfactant used to swell 8MR-AlPO. There could also be some specific interaction with CH_4 due to the surfactant being added. As a result of surfactant being removed by the O_3/200°C treatment the adsorption of the gas species mentioned above went up. We believe this happened because the gallery space expanded and was more accessible to the

larger gas molecules. It does not appear, however, that the pore spaces were completely opened because the adsorption did not increase to a large degree.

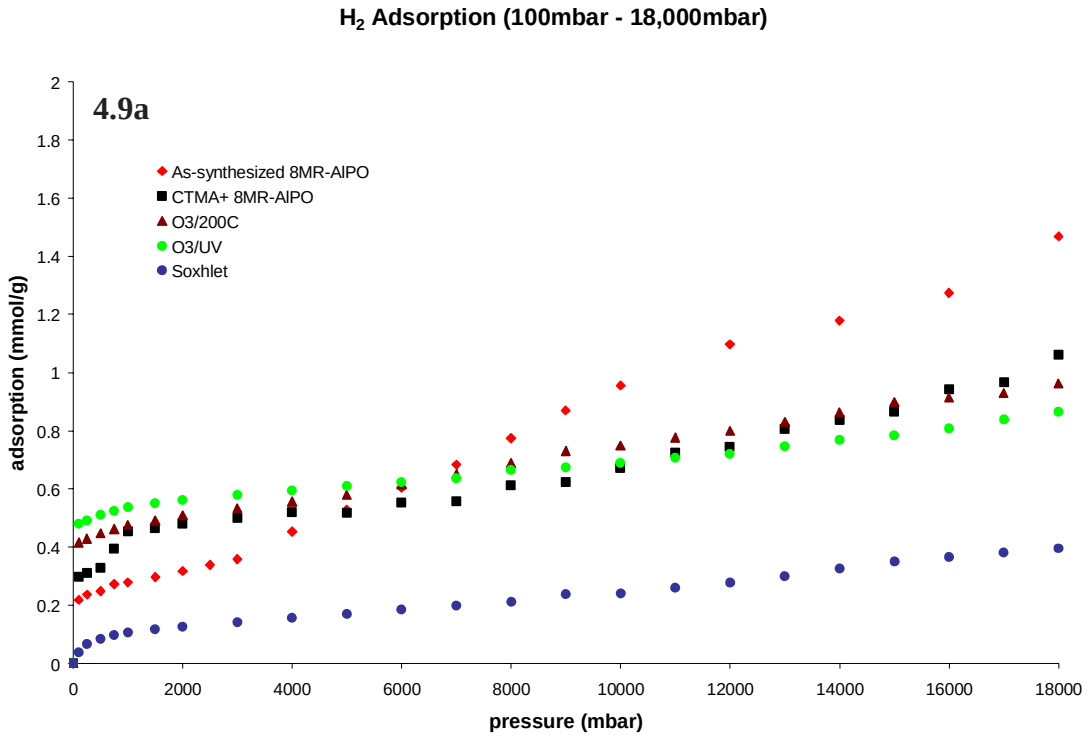

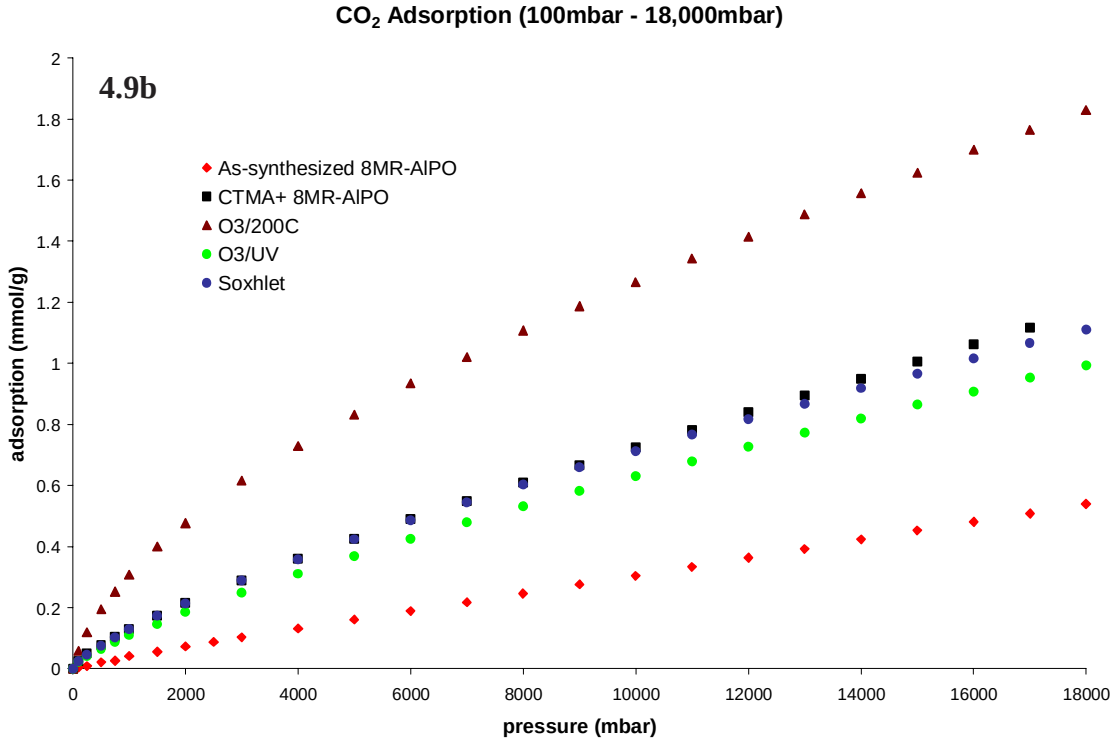

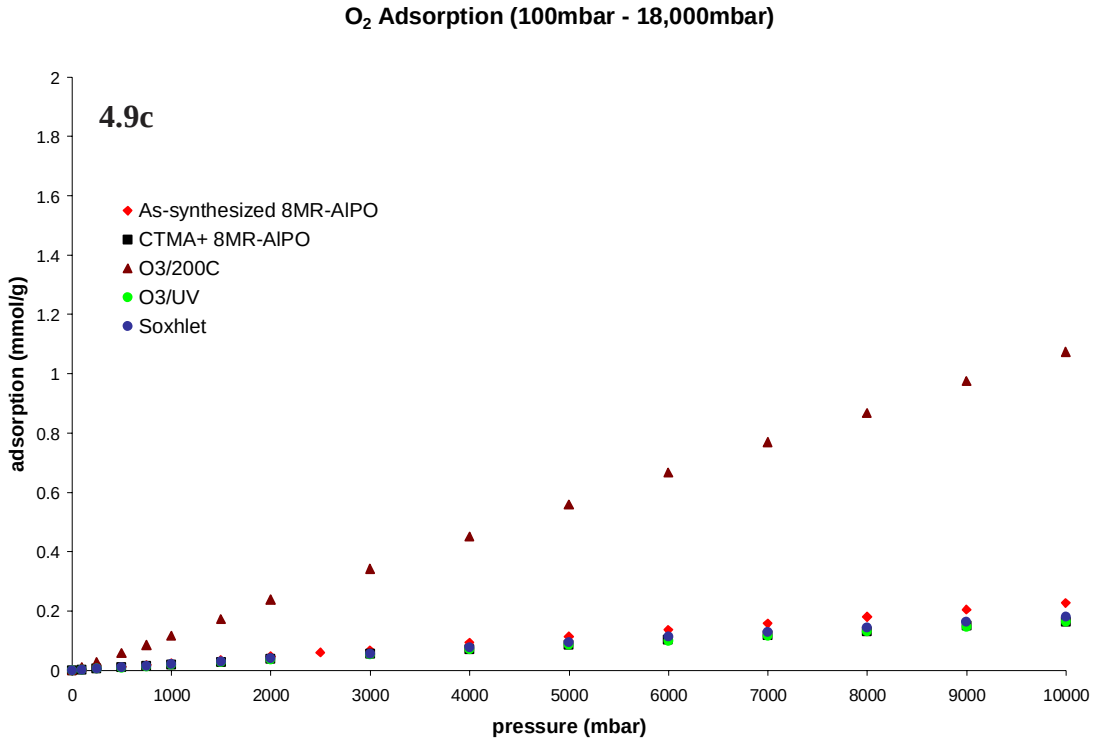
O_2 Adsorption (100mbar - 18,000mbar)
4.9c
As-synthesized 8MR-AlPO
CTMA+ 8MR-AlPO
O3/200C
O3/UV
Soxhlet
adsorption (mmol/g)
pressure (mbar)
0
0.2
0.4
0.6
0.8
1
1.2
1.4
1.6
1.8
2
0
1000
2000
3000
4000
5000
6000
7000
8000
9000
10000

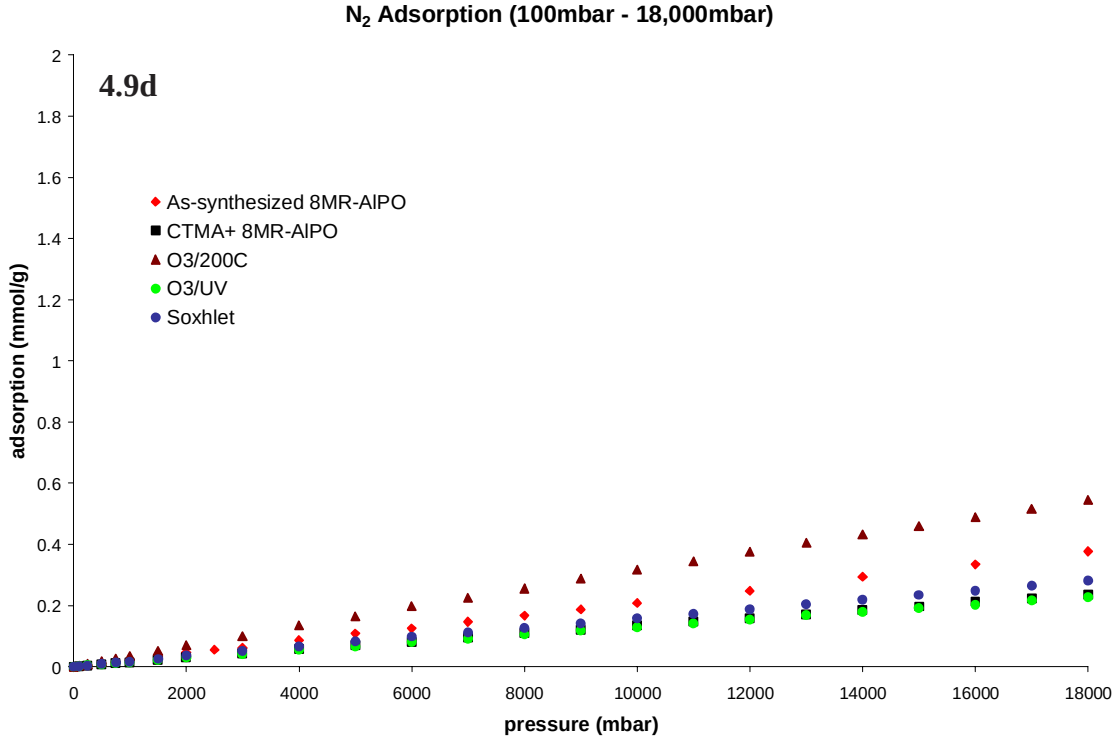
N_2 Adsorption (100mbar - 18,000mbar)
4.9d
As-synthesized 8MR-AlPO
CTMA+ 8MR-AlPO
O3/200C
O3/UV
Soxhlet
adsorption (mmol/g)
pressure (mbar)
0
0.2
0.4
0.6
0.8
1
1.2
1.4
1.6
1.8
2
0
2000
4000
6000
8000
10000
12000
14000
16000
18000

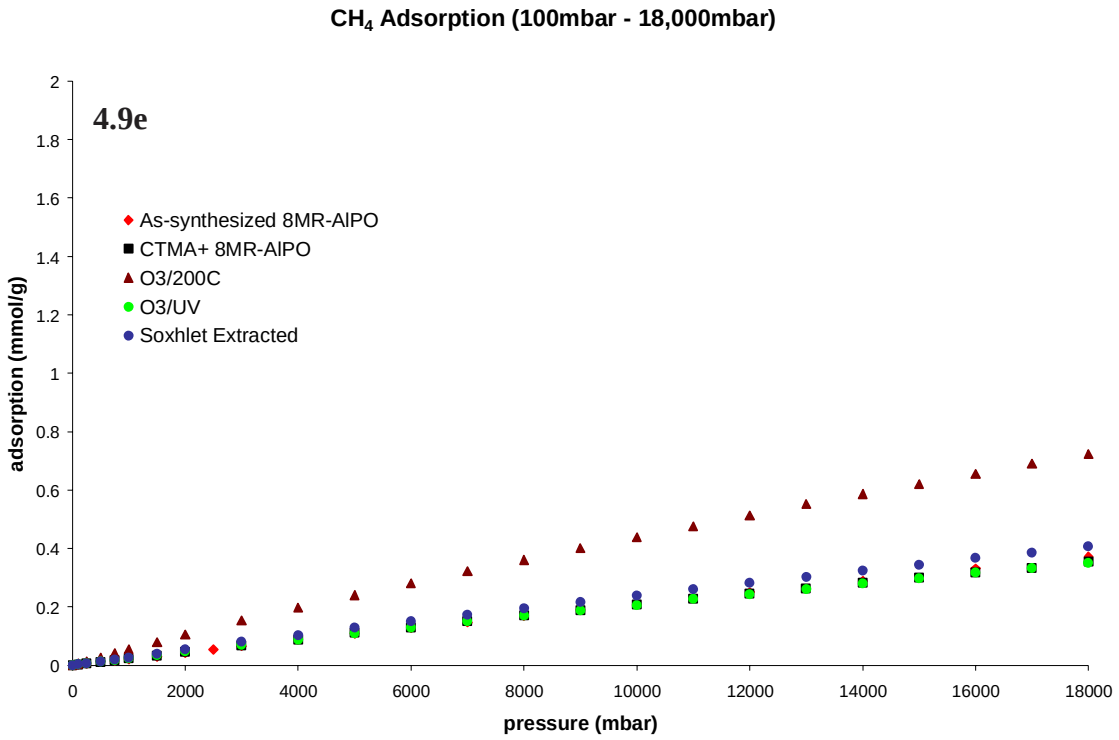

Figure 4.9 a) isotherms of H_2 for all samples b) isotherms of CO_2 for all samples c) isotherms of O_2 for all samples d) isotherms of N_2 for all samples e) isotherms of CH_4 for all samples

4.4 BET, Estimation of diffusion coefficients, elemental analysis

Some other basic information on the surface area, transport properties, and composition of as-synthesized 8MR-AlPO and an 8MR-AlPO exfoliated in an aqueous system was collected. The as-synthesized 8MR-AlPO was synthesized as described previously in this dissertation. In the attempt to obtain data on an exfoliated form of 8MR-AlPO a new technique described in the literature was employed. Huang et al. describe the complete exfoliation of 8MR-AlPO in water/ethanol/amine solutions.[7] They reported that solutions of water/ethanol with a ratio of 3:1 and an ethylamine concentration of 20 mmol / gram 8MR-AlPO exfoliated completely in solution. We can confirm that 8MR-AlPO dispersed in this solution does form a clear colloidal solution

within 2hrs. We attempted to recover the solid dispersed in this solution by simply drying the solution at 70°C. An XRD pattern of the recovered material showed no peaks indicating that the material was exfoliated. SEM images collected of some of the dried material on the surface of a polymer revealed a morphology that looked like dried mud. A continuous layer of the material with cracks in it was observed. No individual layers were visible in the SEM image.

The as-synthesized 8MR-AlPO and exfoliated 8MR-AlPO was measured on an ASAP 2020 pore size analyzer. The measurements were carried out at the University of Cincinnati by the research group of Dr. Vadim Guliants. The surface area and pore sizes of the samples were determined by collecting nitrogen isotherms at 77K. The software utilized the following methods to arrive at the values: surface area was determined using the Brunauer-Emmett-Teller (BET) method, and pore volume and average pore size were determined using the Barret-Joyner-Halenda (BJH) and Horvath-Kawazoe (H-K) methods. Table 4.1 contains a summary of the results. Dr. Guliants comments after seeing the data were that 8MR-AlPO and the 8MR-AlPO that we thought was exfoliated were not microporous. It can be seen that both samples have very small specific surface areas, very small total pore volume, and that the pore sizes determined are not representative of the 4 Å openings that we believe are present. This is not entirely surprising since 8MR-AlPO does not contain actual pores but simply openings in the delaminated sheets. This does however confirm that exfoliation of 8MR-AlPO in the above mentioned solution and recovery is not a viable method to prepare it for polymer aluminophosphates nanocomposites.

Table 4.1 Pore structure data for 8MR-AlPO after degassing 4 h at 150 ^{o}C:

Sample	Surface area (m^2/g)	Pore volume (cm^3/g)	Average pore size (nm)
As-synthesized	1.8	0.002	4.0
Ethylamine exfoliated	0.6	0.0002	1.0

Attempts were also made to determine diffusion coefficients for some gas species through the as-synthesized 8MR-AlPO and water/ethanol/ethylamine exfoliated 8MR-AlPO. The kinetic data from sorption isotherms of H_2, O_2, N_2, CH_4, and CO_2 was analyzed. Only a couple of the pressure points collected for H_2, and CO_2 yielded data good enough to fit to the Fickian Diffusion Equation 4.1 for slabs seen below.[14] The sorption of the other gases on 8MR-AlPO was negligible and produced very erratic kinetic data.

$$\frac{M_t}{M_\infty} = 1 - \frac{8}{\pi^2}\sum_{n=0}^{\infty}\frac{1}{(2n+1)^2}\exp\left[\frac{-D(2n+1)^2\pi^2 t}{l^2}\right] \qquad (4.1)$$

Where M_t is the mass of the sample at time t, D is the diffusion coefficient in cm^2/s, M_∞ is the equilibrium mass at infinite time, and l is the average full thickness of an 8MR-AlPO particle. An l = 25 μm was estimated from FESEM used for the calculations. Kinetic data was collected at pressures between 1.0 and 2.0 bar. The kinetics with the smoothest curves were chosen for analysis. The data was sometimes fit with a sigmoidal curve with a Boltzmann function using Origin 6.0 before comparison with Equation 4.1. For as-synthesized 8MR-AlPO the hydrogen and carbon dioxide diffusion coefficients were calculated to be 1.5 x 10^{-9} cm^2/s, and 3.0 x 10^{-10} cm^2/s respectively. For the 8MR-AlPO exfoliated with water/ethanol/ethylamine and recollected the hydrogen and carbon dioxide diffusion coefficients were found to be 2.6 x 10^{-10} cm^2/s and 1.0 x 10^{-9} cm^2/s.

The drop in the hydrogen diffusion coefficient is consistent with the pore size analysis which showed decreased surface area. The carbon dioxide diffusion coefficient increased which could be due to ethylamine groups on the surface that are adsorbing carbon dioxide. The important point to notice is that the diffusion coefficients for these small gases are on the order of 10^{-9} and 10^{-10} cm^2/s which is similar to the diffusion coefficients of the polymers that are used as matrix materials. The diffusion coefficients were not as high as would be expected if the material was actually exfoliated. It is probably wise not to place too much emphasis on the calculated diffusion coefficients since the thickness of AlPO flakes was estimated and a distribution of sizes actually exists. It would be interesting to obtain sorption kinetic data and calculate diffusion coefficients for exfoliated 8MR-AlPO.

An elemental analysis of as-synthesized 8MR-AlPO was run by the group of Dr. Mirosalav Bleha of Institute for Macromolecular Chemistry in Prague, Czech Republic. The C, H, and O percentages determined for 8MR-AlPO are shown in Table 4.2 below along with the percentages expected from the molecular formula $[Al_3P_4O_{16}]^{3-} \cdot 3[NH_3CH_2CH_3]^+$.

Table 4.2 Elemental Analysis of 8MR-AlPO

	Elemental Analysis	Formula
C	9.97 %	12.03 %
H	4.03 %	4.04 %
N	5.68 %	7.03 %

In the literature review section of this dissertation we used a calculation to estimate the cation exchange capacity of 8MR-AlPO to be 5 meq/g. We were interested in the CHN

analysis to see if the number of ethylammonium ions matched the formula. The C/N ratio from the formula and elemental analysis are 1.71 and 1.76 respectively. The difference in ratio suggests that there may actually be fewer ethylammonium molecules in the gallery space than indicated by the formula. This would result in a lower maximum CEC than was calculated from the formula, but only by a small amount.

4.5 Conclusions

Samples of 8MR-AlPO were swollen with $CMTA^+$ and then treated with three separate methods to remove the surfactant. The methods included O_3/200°C, O_3/UV, and Soxhlet extraction with a solvent. The TGA data showed that the greatest amount of surfactant was removed by the O_3/200°C method while the other methods resulted in only nominal removal of surfactant. The XRD data revealed that the O_3/200°C treatment increased the gallery spacing by 19Å over the $CMTA^+$ 8MR-AlPO while the other treatments resulted in no change in the d_{001}-spacing. The sorption data collected for five gas species also confirmed that the 0_3/200°C treatment was the most effective in adding surface area for adsorption to take place. In the case of CO_2, O_2, N_2, and CH_4 the adsorption was increased by treatment by O_3/200°C. For H_2 the best adsorption was recorded for the as-synthesized material. This suggests data suggests that the gallery space became more accessible for larger gas species once it was expanded, but H_2 had the best access before surfactant was added to the 8MR-AlPO. This data calls into question the feasibility of accomplishing our overall goal. It was expected that the smaller gas species (H_2) would increase in adsorption significantly while the other gas species would remain similar with treatment. Unfortunately the H_2 adsorption was not increased with any of the treatments tried.

The overall sorption of gases on 8MR-AlPO was very low compared with what is expected for a microporous solid. The BET analysis confirmed that 8MR-AlPO had a very small surface area and that the pores were not accessible to gas molecules. This did not change even after a treatment reported to exfoliate the individual sheets. Kinetic data revealed that even small molecules like hydrogen had a diffusion coefficient in the range of 10^{-9}-10^{-10} cm^2/s similar to the polymers used for matrix materials. This data reflects the fact that when 8MR-AlPO is not fully exfoliated it will likely act as a barrier because the 8MR openings are not accessible.

Cellulose Acetate Butyrate treated AlPO membranes

To determine if the treatments were successful from a composite membrane standpoint 2wt% of the Soxhlet extracted 8MR-AlPO and 2wt% of the O_3/200°C treated 8MR-AlPO were combined with cellulose acetate butyrate (CAB). Films were cast on glass, annealed and tested for gas permeability. The permeability of the composite films changed very little when compared to the pure CAB and the selectivities were not improved.

(1) Yano, K.; Usuki, A.; Okada, A.; Kurauchi, T.; Kamigaito, O., Synthesis and properties of polyimide-clay hybrid. *Journal of Polymer Science, Part A: Polymer Chemistry* **1993,** 31, (10), 2493-8.

(2) Tyan, H.-L.; Liu, Y.-C.; Wei, K.-H., Thermally and Mechanically Enhanced Clay/Polyimide Nanocomposite via Reactive Organoclay. *Chemistry of Materials* **1999,** 11, (7), 1942-1947.

(3) Morgan, A. B.; Gilman, J. W.; Jackson, C. L., Characterization of the Dispersion of Clay in a Polyetherimide Nanocomposite. *Macromolecules* **2001,** 34, (8), 2735-2738.

(4) *www.jmol.org*, 2007.

(5) Gao, Q.; Li, B.; Chen, J.; Li, S.; Xu, R.; Williams, I.; Zheng, J.; Barber, D., Nonaqueous Synthesis and Characterization of a New 2-Dimensional Layered Aluminophosphate [Al3P4O16]3-· 3[CH3CH2NH3]+. *Journal of solid state chemistry* **1997,** 129, (1), 37-44.

(6) Wang, C.; Hua, W.; Yue, Y.; Gao, Z., Controlled delamination and intercalation of layered microporous aluminophosphate by a novel two-step method. *Microporous and Mesoporous Materials* **2005,** 84, (1-3), 297-301.

(7) Huang, Q.; Wang, W.; Yue, Y.; Hua, W.; Gao, Z., Delamination and intercalation of layered aluminophosphate with $[Al_3P_4O_{16}]^{3-}$ stoichiometry in water/alcohol/amine solutions. *Journal of Colloid and Interface Science* **2003,** 257, 268-275.

(8) Jeong, H.-K.; Krych, W.; Ramanan, H.; Nair, S.; Marand, E.; Tsapatsis, M., Fabrication of Polymer/Selective-Flake Nanocomposite Membranes and Their Use in Gas Separation. *Chemistry of Materials* **2004,** 16, (20), 3838 -3845.

(9) Heng, S.; Lau, P. P. S.; Yeung, K. L.; Djafer, M.; Schrotter, J.-C., Low-temperature ozone treatment for organic template removal from zeolite membrane. *Journal of Membrane Science* **2004,** 243, 69-78.

(10) Parikh, A. N.; Navrotsky, A.; LI, Q.; Yee, C. K.; Amweg, M. L.; Corma, A., Non-thermal calcination by ultraviolet irradiation in the synthesis of microporous materials. *Microporous and Mesoporous Materials* **2004,** 76, 17-22.

(11) Li, Q.; Amweg, M. L.; Yee, C. K.; Navrotsky, A.; Parikh, A. N., Photochemical template removal and spatial patterning of zeolite MFI thin films using UV/ozone treatment. *Microporous and Mesoporous Materials* **2005,** 87, 45-51.

(12) Tuel, A.; Gontier, S., Synthesis and Characterization of Trivalent Metal Containing Mesoporous Silicas Obtained by a Neutral Templating Route. *Chemistry of Materials* **1996,** 8, 114-122.

(13) Masson, N. C.; Pastore, H. O., Synthesis and characterization of tubular aluminophosphate mesoporous materials containing framework magnesium. *Microporous and Mesoporous Materials* **2001,** 44-45, 173-183.

(14) Crank, J., *The Mathematics of Diffusion Second Edition*. ed.; Oxford University Press: New York, 1975; 'Vol.' p 414.

Chapter 5

Study of Polymer $[Al_3P_4O_{16}]^{3-}$ composites for gas separations utilizing simple mixing in organic solvent systems

5.1 Introduction

It is known that the addition of small amounts of clay to some polymer matrices can reduce permeability of gas species when compared to the neat polymer. Yano et al. reported the reduction of He, and O_2 permeability by one half with the addition of just 2wt% of montmorillonite clay to a polyimide.[1] This class of materials is known as polymer clay nanocomposites (PCN). There is considerable number of review papers available on this topic covering many different polymer clay systems.[2-6] A PCN can be formed using several different methods including melt intercalation[7, 8], in-situ polymerization[9, 10], and simple mixing[11, 12]. The objective of all of these techniques is to fully exfoliate the clay into the polymer matrix on a molecular level. Once the clay is

dispersed at a molecular level, the high aspect ratio of the particles creates a barrier to gas transport through the matrix. The clay platelets create a more tortuous path for a gas molecule traveling through the film slowing diffusion for all gas species that permeate through the membrane. The current work will focus on the transport properties that result from dispersing a layered microporous clay-like aluminophosphate into several different polymer matrices using simple mixing in organic solvents.

The layered microporous aluminophosphate used for this work was $[Al_3P_4O_{16}]^{3-} \cdot 3[NH_3CH_2CH_3]^+$ (8MR-AlPO) was first reported by Gao et al.[13] The crystals of this material contain sheet like layers composed of aluminum and phosphorous tetrahedra separated by ethyl ammonium ions. The sheets are of comparable thickness and aspect ratio to montmorillonite clay. The difference is that the bonding in the framework structure of the 8MR-AlPO sheets forms a microporous net consisting of 4 x 6 x 8 rings. The largest 8MR has a diameter on the order of 4-5Å which may be large enough for small kinetic diameter gases such as H_2, He, or CO_2 to pass through. The possibility that some of the smaller gases may pass through this structure unobstructed is the basis for this research. Our hypothesis is that, if this material is exfoliated into a polymer matrix, a small penetrant should pass through the platelets while a larger gas molecule would take a tortuous path around the platelets resulting in a change in selectivity for the composite material when compared to a pure polymer.

It was reported by Jeong et al. that the addition of 5-10wt% of the aluminophosphate $[Al_3P_4O_{16}]^{3-} \cdot 3[NH_3CH_2CH_3]^+$ to a hexafluorinated polyimide improved the selectivity of small gases over large gases significantly.[14] The aluminophosphate and hexafluorinated polyimide were combined with simple mixing and

yet resulted in dramatic changes in selectivity for some gas pairs. The selectivity of the gas pair He/CH_4 increased by 240% and the selectivity improvement for CO_2/CH_4 was 203% when compared with the neat polymer. It is the intent of the current research to repeat these experiments using other polymer matrix materials and to measure the resulting transport properties. Using other matrix materials with different properties should give insight into how to optimize the transport properties of a composite which contains microporous aluminophosphate.

A series of chemically different polymer matrix materials were chosen for comparison. The polymers used in this study were Polydimethyl Siloxane (PDMS), 20%PDMS-2,2'-Bis(3,4-dicarboxyphenyl)hexafluoroporpane dianhydride-4, 4' – hexaflouroisopropylidene dianiline (20%PDMS-6FDA-6FpDA), UDEL P-3500, Matrimid 5218, and Cellulose Acetate (CA). A brief description of why these polymers were chosen is presented in the results/discussion section of this paper.

5.2 Experimental

5.2.1 Materials

The layered aluminophosphate used in this study was $[Al_3P_4O_{16}]^{3-} \cdot [NH_3CH_2CH_3]^+$. The synthesis of this layered inorganic and details of the modification of this compound are discussed in detail in chapter 3 of this dissertation.[15] The small molecules used to modify 8MR-AlPO were cetyltrimethyl ammonium chloride 25 wt% (Aldrich) in water, octadecyldimethyl benzyl ammonium chloride (Pfaltz & Bauer), and 1,12 diaminododecane (Aldrich) and were used as received. The polymer materials used include PDMS RTV615 (GE plastics), Matrimid 5218 (Ciba-Geigy), UDEL P3500 (Solvay Advanced Polymers), Cellulose Acetate (Eastman Chemicals), and 20% PDMS-

6FDA-6FpDA co-polymer synthesized in our laboratory. The reagents for the synthesis of the co-polymer included 2,2'-Bis(3,4-dicarboxyphenyl)hexafluoroporpane dianhydride (Clariant Corp.), 4, 4' – hexaflouroisopropylidene dianiline (SynQuest Labs Inc.), and aminopropyl terminated PDMS (Gelest Inc.). The synthesis of this copolymer was described by Todd Pechar in his dissertation and will not be repeated in this paper.[16] The structures of the polymers listed can be seen in Figure 5.1 below. The solvents used to dissolve the polymers listed above were anhydrous Tetrahydrofuran and Chlorofrom.

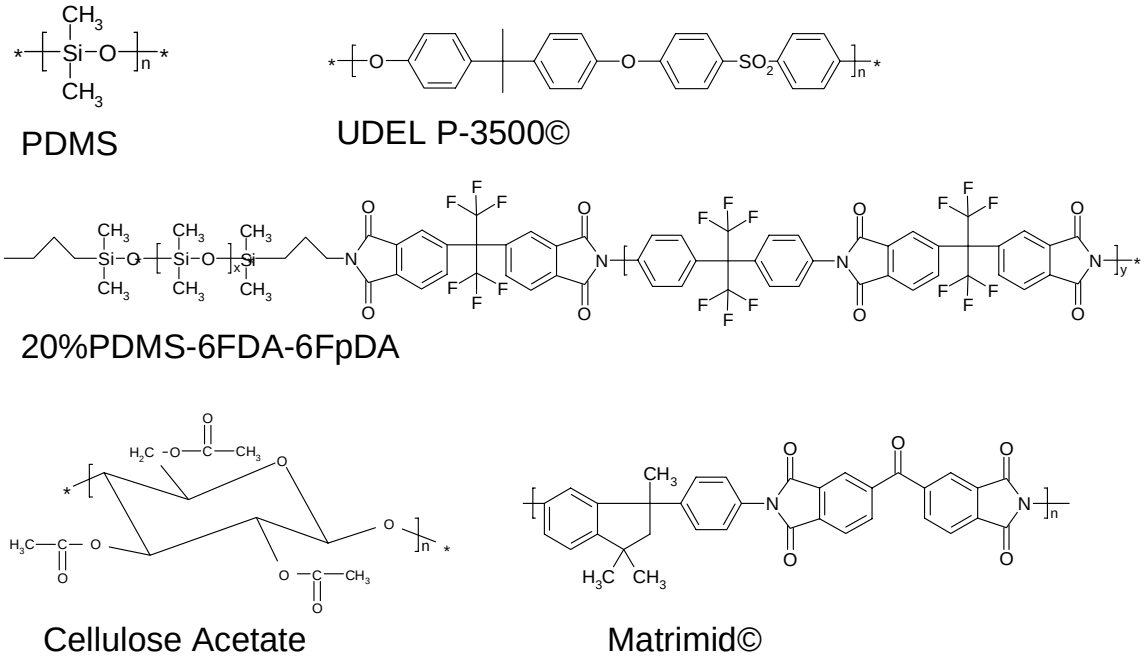

Figure 5.1 Structure of polymers used for matrix composites

5.2.2 Fabrication of polymer aluminophosphate composites

The technique employed to fabricate polymer aluminophosphate composites for this paper was solution intercalation by simple mixing. The concept involves dissolving a polymer in organic solvent followed by the addition of inorganic aluminophosphate to the solution. It is hoped that the polymer chains will intercalate into the gallery spaces of

the aluminophosphate and exfoliate them into the polymer matrix. The procedures used to fabricate the composites were similar but each polymer matrix required slightly different procedures to form a film that could be measured for gas separation.

The basic procedure used to make the polymer 8MR-AlPO solution was as follows. An amount of polymer that was equal to 10-15wt% solids was dissolved in the THF or Chloroform (polysulfone only). The required amount of swollen 8MR-AlPO was mixed in a small amount of the same solvent, stirred then sonicated in a bath (VWR 50HT) for 30 minutes. The solutions were combined and allowed to mix together at room temperature for at least 24 hours. PDMS is a thermoset and therefore not soluble in its crosslinked form. Uncrosslinked PDMS was therefore diluted in THF before the addition of 8MR-AlPO. The THF was driven off before the crosslinking agent was added. The solutions were then cast onto either glass or a Teflon coated pan. The solutions cast on glass were spread using a casting blade and the solutions cast in Teflon pans were simply poured.

5.2.3 Membrane Characterization

For measurement by TEM the composite membranes were embedded in epoxy and microtomed into thin slices. The membrane cross-sections were placed on 300 mesh copper grids and observed using a Jeol 100 CX-II at 100kV. Scanning Electron Micrographs were taken on a LEO 1550 FESEM.

X-ray diffraction (XRD) was used to characterize many of the samples. Each batch of as-synthesized AlPO and modified AlPO as well as the polymer-8MR-AlPO composites was tested using a Scintag XDS-2000. The samples were run using CuKα (λ = 1.5418 Å) radiation at 40mA and -45kV. Powder XRD was used to confirm the

synthesized structure of 8MR-AlPO and the degree to which it was swollen. The composite membranes were scanned on both sides to determine the degree of exfoliation present in the composite.

The permeability of five small gases was measured using a constant volume apparatus. Permeability of He, O_2, N_2, CH_4, and CO_2 was measured for each pure and composite membrane utilizing the lag time method. The membranes were placed in a stainless steel cell with volumetric chambers one each side. One side of the membrane was evacuated to vacuum and the other side was pressurized with 4 atm at 35°C of the gas species of interest. The pressure change on the permeate side was allowed to reach steady state and then the data was analyzed to calculate permeability.

5.3 Results and Discussion

5.3.1 Barrier Theory

Edward Cussler introduced a simple equation to describe the change in permeability as a result of adding impermeable flakes to a polymer matrix. He described diffusion through an idealized exfoliated and oriented system of flakes using equation 1 below.[17]

$$\frac{P_o}{P_c} = 1 + \frac{\alpha^2 \phi^2}{1 - \phi} \qquad (1)$$

Where P_o is the permeability of the pure polymer, P_c is the permeability of the composite, α is the aspect ratio of the flakes, and ϕ is the volume fraction of flakes.

This equation can be used to test our theory that smaller gases should pass through a composite membrane faster than larger gases as the result of a molecular sieving effect. In a given membrane the volume fraction of filler and the aspect ratio of the flakes is a

constant. The fraction of filler is known, and permeabilities of the composite and pure polymer can be easily measured. An effective aspect ratio can therefore be calculated and compared for each gas species in a membrane using available data. If a large aspect ratio is calculated for a gas species its diffusion has been retarded by the addition of 8MR-AlPO, but if the calculated aspect ratio is small the flakes have not created a barrier to diffusion. The magnitude of the aspect ratio can therefore be used as a direct measure of how effective a barrier 8MR-AlPO is for a given gas species.

For example if the addition of 2wt% (1.5 vol%) clay reduces the permeability of a gas species by 50% (as reported for clays), the resulting effective aspect ratio α can be calculated to be 132. This value is for α defined as the smallest flake width divided by the thickness of the flake. The Cussler model of course is an idealized case where all of the flakes are perfectly exfoliated, regularly spaced, and aligned parallel to the surface of the membrane. Any negative deviation from the predicted aspect ratio could be due to incomplete exfoliation or flakes not parallel to the membrane surface which would drive the aspect ratio to much smaller values. This value of 132 is for a modest wt%. As the wt% is increased even larger aspect ratios should be seen.

5.3.2 PDMS, 6FDA-6FpDA-PDMS, Polysulfone with varied wt% of 8MR-AlPO

Early attempts at making polymer-aluminophosphate composites in our laboratory involved the addition of relatively large amounts of 8MR-AlPO consistent with the work of Jeong et al. The literature on PCNs indicates that composites made from 2-5wt% clay yield the best mechanical and gas permeation properties due to re-aggregation of the exfoliated clay platelets beyond this loading.[18, 19] However, Jeong et al. obtained selectivity increases up to a loading of 10wt% in 6FDA-6FpDA-8%DABA. For this

reason PDMS and 20% PDMS 6FDA-6FpDA were loaded with 5wt%, and 10wt% of $CMTA^+$ 8MR-AlPO. The membranes were tested for transport using single gas permeation of He, O_2, N_2, CH_4, and CO_2.

PDMS is a transparent rubbery polymer at room temperature. This material has found limited use as a gas separation polymer because although the permeability of PDMS is very high, the selectivity of most non-hydrocarbon simple gas pairs is low. The addition of microporous aluminophosphate could enhance the selectivity of PDMS by reducing the permeability of large gas molecules like methane while allowing small gas molecules to permeate unobstructed. This polymer was therefore chosen to test the transport properties of a rubbery low T_g polymer with 8MR-AlPO.

The PDMS composites were loaded with 5wt%, 10wt%, and 15wt% for transport and XRD measurement. The 8MR-AlPO used was modified with swollen with $CMTA^+$. Powder XRD performed on the treated 8MR-AlPO (not pictured) showed that it was swollen prior to mixing with the PDMS. A characteristic 001 peak could be seen that corresponds to a d_{001}-spacing of 35Å.

The XRD of the composite membranes can be seen in Figure 5.2 below. In all of the composites two peaks are visible one at a two theta value of 5.5° and one at a value of 9.8°. The peak at 9.8° is sharper and represents some of the left over as-synthesized phase that is still present. This phase has a d_{001}-spacing of 9Å and was not intercalated by any organic molecules. The other peak seen at $2\theta = 5.5°$ shows that some of the 8MR-AlPO in the composite remained intercalated with $CMTA^+$. The spacing however has been reduced from the pure swollen material. The new peak corresponds to a phase with a d_{001}-spacing of 16Å. This indicates that the gallery spacing of 8MR-AlPO is reduced at

some point during the mixing, casting, or annealing steps used to form a membrane. These composites are therefore not fully exfoliated but contain some domains intercalated with $CMTA^{+}$.

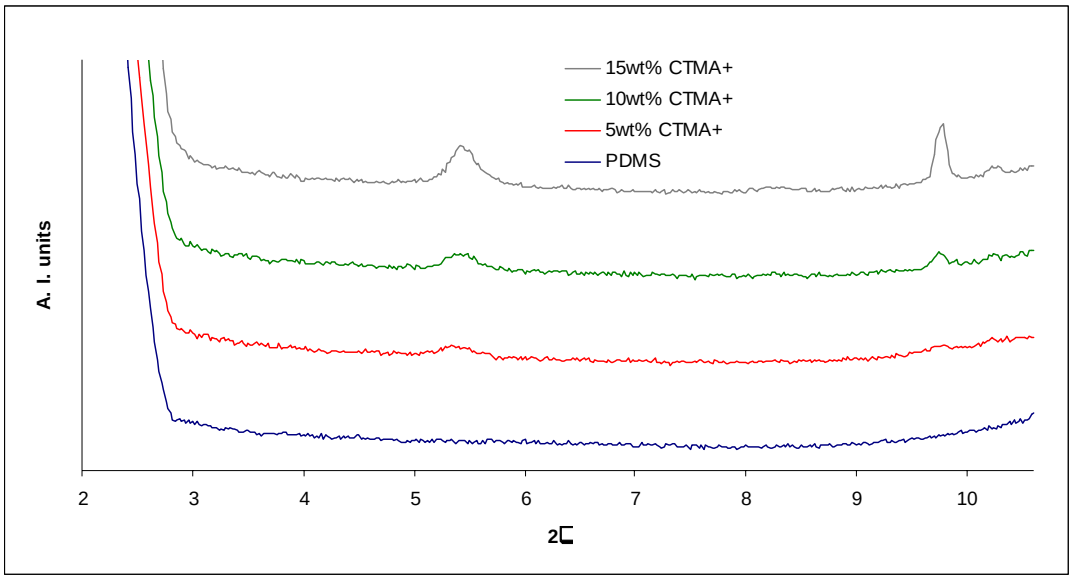

Figure 5.2 XRD of PDMS-AlPO composites

The permeability results for PDMS are summarized in Table 5.1 below. These membranes were solution cast on glass with no casting blade so the particles are randomly oriented within the matrix. It can be seen that the addition of 8MR-AlPO reduces the permeability of PDMS at both the 5wt% and 10wt% loading. The drop in permeability at 5wt% loading of PDMS was between 6% - 10% for all of the five gases tested and between 24% - 26% at a loading of 10wt%. The permeability values for the 15wt% loaded composites showed a drop of between 32%-34%. The effective aspect ratio reported in the same table shows a small drop in calculated α as more 8MR-AlPO is added . This result indicates that the flakes are less effective as a barrier when the wt% of loading increases. All gas species are being obstructed slightly as evidenced by reduced permeability but the predicted α values are much smaller than expected at such

high loadings. The small α values can at least be partially explained by unoriented flakes, incomplete exfoliation, and particle aggregation. This is not entirely unexpected as literature indicates that PCN at high wt% loading exhibit particle aggregation. This result could also be due to the high intrinsic permeability of PDMS. Diffusion through PDMS may be greater than diffusion through the 8MR-AlPO framework for even small gases. The % drop in permeability for each gas species at a particular loading was similar. This is reflected in the ideal selectivity numbers reported in Table 5.2 and the α values in Table 5.1. The gas pair selectivities for He/CH_4 and CO_2/CH_4 do not change from pure PDMS, to 15wt% loading of 8MR-AlPO. They are flat across the table indicating that none of the gases are preferentially permeating through the 8MR of AlPO. The α values are consistent along the column with a small exception for 5wt% loaded PDMS which shows a smaller calculated α for He and CH_4.

Table 5.1 Permeability and α for PDMS 8MR-AlPO composites

	Permeability of PDMS & $CTMA^+$ AlPO (Barrers)				Effective α		
	Pure PDMS	5 wt%	10 wt%	15 wt%	α-5wt%	α-10wt%	α-15wt%
He	479.9	452.3	357.3	320.0	16	18	14
CO_2	3190.4	2926.0	2390.2	2104.2	19	17	14
O_2	699.3	629.3	518.5	463.4	21	18	14
N_2	336.5	303.2	249.3	221.7	21	18	14
CH_4	986.9	921.1	747.2	670.3	17	17	13

Table 5.2 Ideal Selectivity of 8MR-$CMTA^+$ AlPO composites

	PDMS				20%PDMS-6FPI			Polysulfone			
	Pure	5wt%	10wt%	15wt%	Pure	5wt%	10wt%	Pure	2wt%	5wt%	30wt%
He/CH_4	0.5	0.5	0.5	0.5	8.7	11.9	11.2	42.8	45.6	43.9	17.3
CO_2/CH_4	3.2	3.2	3.2	3.1	1.2	1.3	1.2	22.8	22.8	22.0	12.7

A co-polymer containing chemical groups of the polymer reported by Jeong et al. and PDMS was also used as a matrix material. Jeong et al. fabricated aluminophosphate nanocomposites using 6FDA-6FpDA-8%DABA as the matrix material.[14] They obtained excellent increases in separation of certain gas species. It should be useful to compare the results of a glassy polyimide with that of rubbery PDMS. Therefore, a co-polymer composed of 20% PDMS 6FDA-6FpDA was synthesized for use as matrix material. This material should display transport properties between the hexafluorinated polymer matrix reported in by Jeong et al. in the literature and the PDMS transport properties reported in this paper.

The XRD patterns for 5wt% and 10wt% composites of 20%PDMS-6FDA-6FpDA and $CMTA^+$ treated 8MR-AlPO are reported in Figure 5.3. A sharper peak can be seen at $2\theta = 9.8°$ in both composite membranes. This peak represents some left over amount of as-synthesized phase in the composite which contains the as-synthesized d_{001}-spacing. For the 5wt% composites a small broad shoulder can be seen in the pattern at $2\theta = 3.0°$-3.6°. This corresponds to a d_{001}-spacing of 27Å. In the 10wt% composite a distinct peak can be seen at $2\theta = 4.3°$ (d_{001}-spacing = 21 Å). The broad peaks seen in the composite membranes suggest that some of the 8MR-AlPO is still intercalated with $CMTA^+$, but that the co-polymer has not intercalated this phase. The broader peaks also indicate that some distribution of gallery spacing is present as opposed a very homogenous spacing.

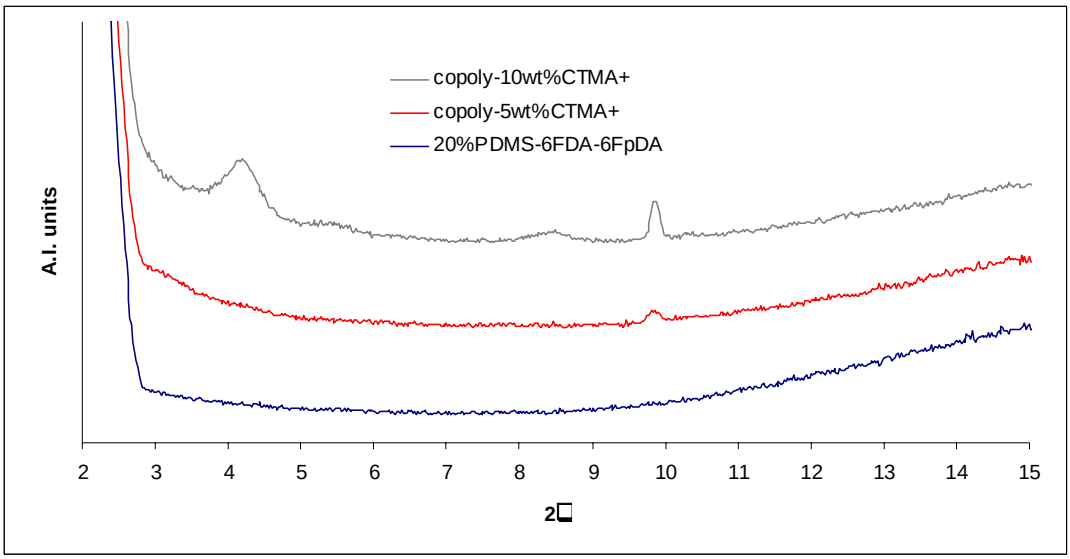

Figure 5.3 XRD of 20%PDMS-6FDA-6FpDA-AlPO composites

The permeability values of the pure co-polymer and composites containing 5wt% and 10wt% are reported in Table 5.3 along with the calculated values for α. An immediate observation is that the permeability is reduced by the addition of 8MR-AlPO, however, the addition of 10wt% 8MR-AlPO did not decrease the permeability significantly when compared to the 5wt% addition. The % drop in helium did increase slightly but the other gases maintained about the same % drop in permeability when compared to the pure polymer. This may be attributed to particle reaggregation from increasing the loading but it is not certain. This phenomenon is reflected in the calculated values of α which takes into account the loading of flakes. The α calculated for the 10wt% loading has an average of 22 while the average α for the 5wt% was 43. Both composites should predict similar aspect ratios if everything else is equal but the effective aspect ratio for the 10wt% composite has been reduced. The ideal selectivity values for the gas pairs that should be affected most if size sieving is taking place are shown in Table 5.2. The He/CH_4 ideal selectivity shows a very small increase with the addition of 8MR-AlPO, but the CO_2/CH_4 selectivity is unaffected by the addition of 8MR-AlPO.

Table 5.3 20%PDMS-6FDA-6FpDA Permeability

	20%PDMS-6F-CTMA$^+$ AlPO permeability (Barrers)			Effective α	
	Pure Co-polymer	5 wt%	10 wt%	α-5wt%	α-10wt%
He	78.88	51.49	40.54	38	24
CO_2	71.89	49.76	48.21	34	17
O_2	17.21	10.59	9.4	41	23
N_2	6.64	3.21	3.46	53	24
CH_4	8.24	4.17	4.3	51	24

UDEL P-3500 is a trade name for Polysulfone. Polysulfone under the trade name Permea of Air Products was the first engineering polymer used in large scale industrial gas separations.[20] Neat polysulfone exhibits good separation of hydrogen and methane. Microporous aluminophosphate was dispersed in this matrix to determine if the selectivity of this pair can be improved.

The composites made with polysulfone represent a fundamental change in thinking from the previous two composite systems. Instead of using a high loading we tested a 2wt% composite and then made a medium loading 5wt% composite, and a very high 30wt% composite to determine if aggregation was lowering selectivity advancement. The literature available on PCN has suggested that low loadings (2wt% - 5wt%) produce optimal properties.[18, 19] Beyond this loading re-aggregation of flakes takes place. This is assuming that most of the inorganic can be exfoliated in the polymer matrix.

XRD was performed on the polysulfone composite membranes and can be seen in Figure 5.4. For the 2wt% and 5wt% composites a peak at $2\theta = 4°$ is evident. The d_{001} spacing for this peak is 22 Å indicating that this phase is still intercalated by some of the $CMTA^+$ used in the swelling procedure. The 30wt% composite shows two peaks. We believe these peaks correspond to a d_{001}-spacing of 29 Å and a d_{002}-spacing of 14 Å. The

magnitude of the peaks is more evident in the 30wt% composite because there is more inorganic material present. The peaks are broader than those for the lower loading composites indicating a wide distribution of gallery spacings around the values calculated. The pattern for the 30wt% composite is similar to what is seen for the pure $CMTA^+$ swollen 8MR-AlPO which appears to be the dominant phase in the highest loaded composite.

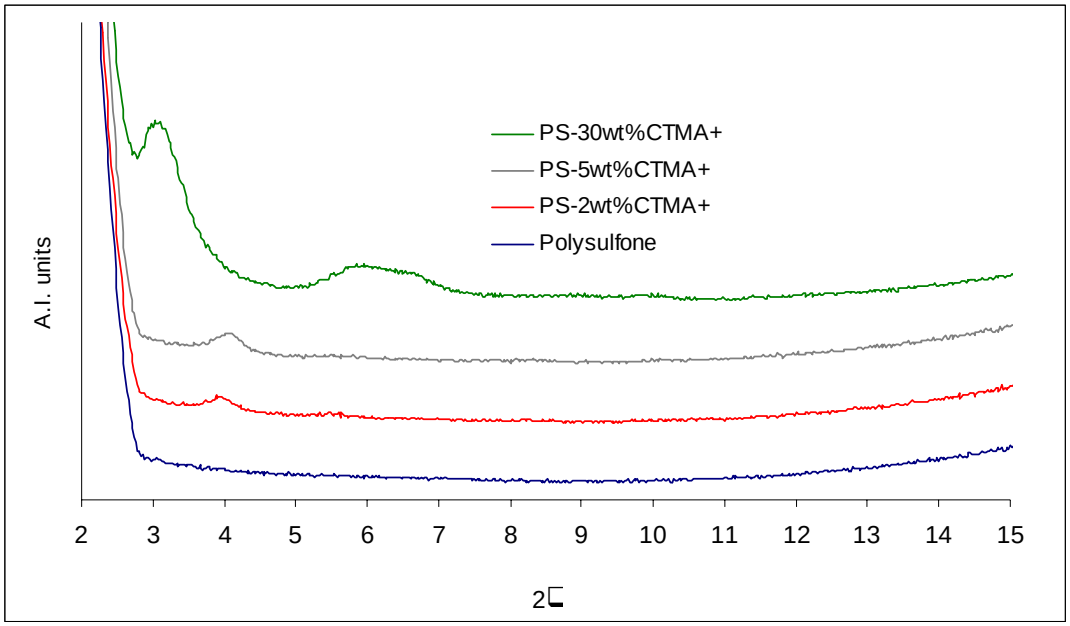

Figure 5.4 XRD of Polysulfone-AlPO composites

TEM images of the 5wt% polysulfone composite were taken to compare to the XRD data of the same membrane. Images of the bulk material showed particles less than 1µm to particles 3µm in length. The particles appeared fairly well dispersed but were aggregated in some areas. A close up of one of the particles can be seen below in Figure 5.5. When a corner of the image is zoomed in, the platelets and spacing between them becomes visible. An attempt to measure the spacing between plates indicates that the distance is close to 2.5nm. This tactoid corresponds to one intercalated by $CMTA^+$ and is

consistent with the distances of 2.2nm calculated from the XRD data shown in Figure 5.4.

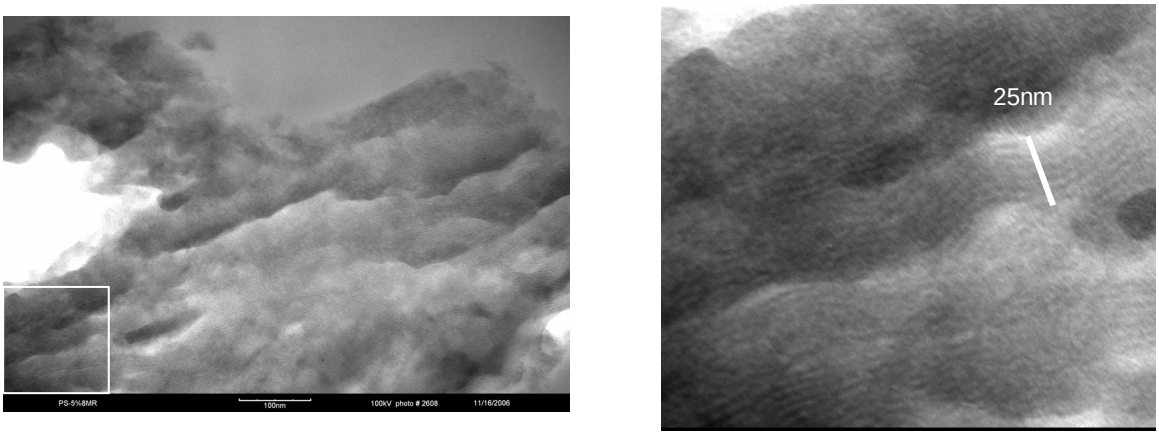

Figure 5.5 TEM of particle from Polysulfone 5wt% AlPO composite membrane

The results of the permeability measurements made on the polysulfone-composite membranes are shown in Table 5.4. In all but one case the permeability of each gas species decreased with the addition of increasing amounts of 8MR-AlPO. This indicates that there was good adhesion between 8MR-AlPO and the polysulfone matrix. At 30wt% loading of 8MR-AlPO the CH_4 permeability increased over that of the pristine polysulfone. We believe this is due to increased solubility of methane in the surfactant ($CMTA^+$) used to modify the surface of 8MR-AlPO. The addition of 2wt% 8MR-AlPO resulted in a modest drop in permeability. The drop in permeability was less for He than for the other gasses. This is reflected in the calculated values of α and the He/CH_4 ideal selectivity. The calculated α is a measure of how efficient the flakes are at acting like a barrier to gas diffusion. In the case of both the 2wt% and 5wt% composites it can be seen that the predicted α for He is lower than the other gases. The disparity is more dramatic in the 2wt% composite perhaps because the platelets have fewer tendencies to

aggregate in lower loading systems. The ideal selectivity values in Table 5.2 show that there was a slight increase in the He/CH_4 selectivity for the 2wt% composite and an even smaller increase for the 5wt% composite. We believe the 2wt% composite is closer to an ideal system for 8MR-AlPO. The He/CH_4 selectivity increase of 6.5% is insignificant, however, when compared to the increase seen for the same pair by Jeong et al. Also the CO_2/CH_4 was unchanged while Jeong et al. saw a large selectivity increase for this gas pair. Finally the 30wt% is shown to be too high of a loading for $CMTA^+$8MR-AlPO. The He/CH_4 selectivity actually dropped by 60%. This is reflected in the calculated α values which also drop dramatically for the 30wt% composite. The ability of the flakes to act as a barrier has dropped possibly due to defects from particle aggregation in the composite. Selectivity for all of the gas pairs dropped for this composite.

Table 5.4 Permeability and effective aspect ratio of polysulfone composite membranes

Polysulfone-$CTMA^+$ AlPO permeability (Barrers)					Effective α		
	Pure PS	2 wt%	5 wt%	30 wt%	α-2wt%	α-5wt%	α-30wt%
He	13.44	13.00	12.12	6.72	24	18	7
CO_2	7.16	6.50	6.07	4.94	42	22	5
O_2	1.56	1.42	1.34	1.13	41	21	5
N_2	0.28	0.26	0.25	0.26	38	20	2
CH_4	0.31	0.29	0.28	0.39	42	20	0

5.3.3 Matrimid, Cellulose Acetate with 2wt% 8MR-AlPO and varied swelling agents

The permeability data and predicted α values from the composites reported above indicate that 8MR-AlPO –polymer composites with low loading (2wt%) are more likely to produce the desired effect than the highly loaded composites. For the next set of experiments we decided to fix the loading at 2wt% and vary the surface treatment on 8MR-AlPO to determine if the surface modification might produce a better result. Changing the surface treatment might improve interaction between 8MR-AlPO and the

polymer matrix, increase exfoliation, or stabilize the structure of AlPO so the 8MR's are accessible to small gas species.

Three small organic molecules were chosen to ion exchange with the ethyl ammonium ions present in as-synthesized 8MR-AlPO and are pictured in Figure 5.6. Cetyltrimethyl ammonium ($CMTA^+$), Octadecyldimethylbenzyl ammonium ($ODDMBA^+$), and protonated 1,12 Diamminododecane ($112DADD^{2+}$) were used to treat the 8MR-AlPO. The $CMTA^+$ was chosen to keep continuity with previous work in our lab and the swelling procedure reported by Jeong et al.[14] Swelling procedures were developed for the other two molecules. The $ODDMBA^+$ treatment was chosen because of the work of Chung et al.[21] They reported that good adhesion was achieved between Matrimid and C_{60} when it was modified with a molecule similar to $ODDMBA^+$. Finally, the $112DADD^{2+}$ treatment was chosen initially because it was believed that this treatment would stabilize the 8MR-AlPO structure while swelling it. Details about the swelling procedures and data collected on these modifications were reported in an earlier paper.[15]

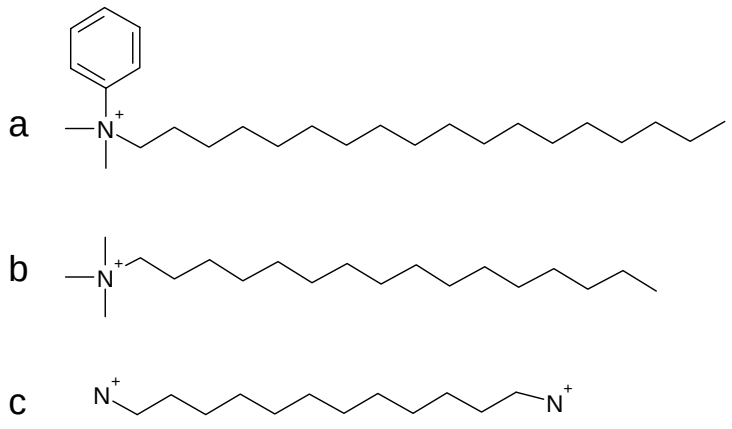

Figure 5.6 (a) $ODDMBA^+$, (b) $CTMA^+$, (c) $112DADD^{2+}$
All of the modified 8MR-AlPO's showed promising properties for introduction into a polymer matrix.

Matrimid-AlPO composites

Matrimid 5218 is a high T_g, glassy polyimide with good thermal and mechanical properties. Matrimid has been reported in the literature as a good membrane material and is known to have good separation properties for certain gas pairs.[22] Further, it has been used by several groups as the matrix for mixed matrix gas separation membranes. For example, Matrimid was used by Chung et al. to make C_{60} mixed matrix membranes which were shown to improve the separation of He/N_2.[21] Mahajan et al. discussed the transport properties of mixed matrix membranes fabricated from Matrimid and zeolites.[23] Finally, Vu et al. used pyrolized Matrimid and Matrimid polymer to make a mixed matrix membrane with enhanced gas separation properties.[24] Matrimid is a polyimide which is in the same class of polymer reported by Jeong et al. It is therefore expected that the selectivity will be enhanced with the addition of 8MR-AlPO. For this reason Matrimid was chosen as one of the polymer materials used to fabricate polymer aluminophosphate composite membranes.

Composite membranes were fabricated and XRD was run on both sides of the film to determine what inorganic phases were present in the matrix. The XRD patterns of pure Matrimid and the composites can be seen in Figure 5.7. The XRD patterns for all of the composite membranes show some features which indicates that the 8MR-AlPO is not fully exfoliated in any of the composites. The $ODDMBA^+$ composite shows the most prominent peak at $2\theta = 9.8°$. As mentioned previously this indicates that some of the as-synthesized phase is still present in the composite. There is also a very slight shoulder between $2\theta = 3°$-$4°$ which means there are some tactoids with a spacing in the 22 Å - 29 Å range. The pure inorganic phase showed a peak at $2\theta = 2.7$ which could correlate with

this shoulder. The 112DADD^{2+} composite shows a solitary broad peak from 2θ = 3.4°-4.8° which means there is a distribution of gallery spaces around 22 Å. This peak corresponds to a peak seen in the pure inorganic 112DADD^{2+} 8MR-AlPO at 2θ = 4.2°. The CTMA^{+} composite shows a broad shoulder between 3.0°-3.6°, a broad peak from 4.3°-6.8°, and a small sharp peak at 9.8°.

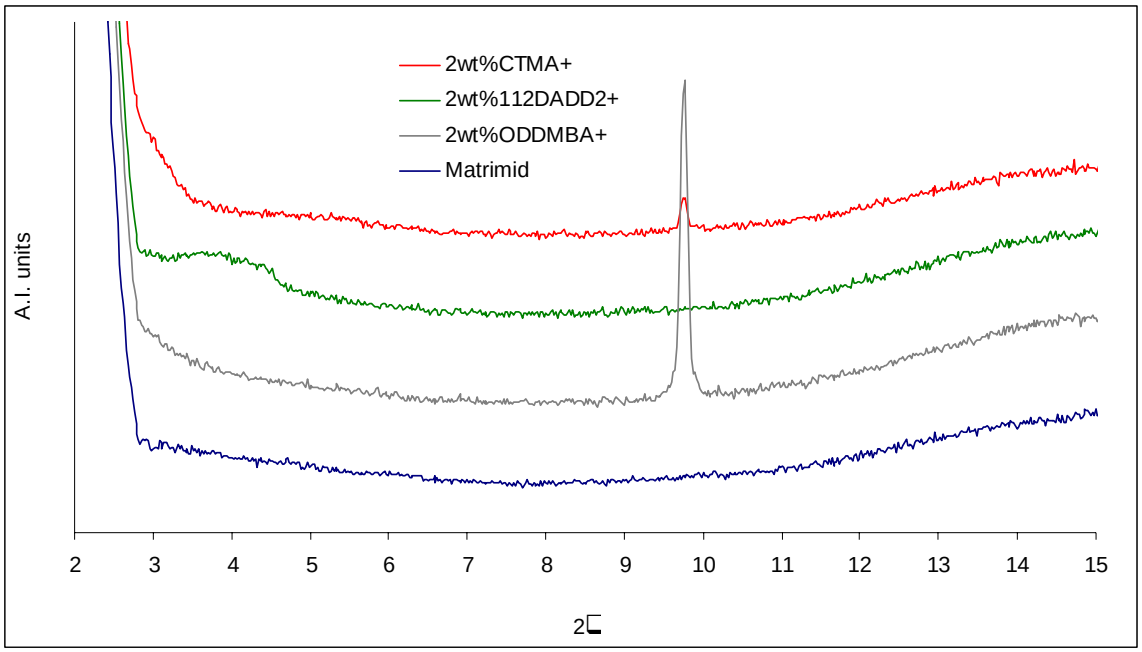

Figure 5.7 XRD of Matrimid-AlPO composites

The TEM images revealed that the bulk properties of the three composites made with Matrimid were very similar. In general the composites showed well dispersed particles. Some of the particles were on the order of 1-2μ but most were much smaller in the 100-500nm range. Two TEM images are shown below in Figure 5.8, one of 2wt% CMTA^{+}8MR-AlPO in Matrimid (a) and the other of 2wt% ODDMBA^{+}8MR-AlPO in Matrimid (b). These images show that some of the original 8MR-AlPO is dispersed at the molecular level. Several very thin tactoids can be seen in the left top corner of Figure 5.8(a). The width of these tactoids is on the order of a couple of nanometers. In the as-synthesized material the thickness of one layer of 8MR-AlPO is on the order of 8Å.

Tactoids of this thickness are very close to exfoliated consisting of only a few sheets of 8MR-AlPO. These are the types of particle we would ideally like to see over the entire bulk of the material in order to achieve the desires sieving effect. The larger tactoid in Figure 5.8(a) consists of a stack of 15-20 8MR-AlPO layers. Figure 5.8(b) shows another very thin particle in the $ODDMBA^+$ composite. It is estimated that the aspect ratio of this particle is over 100. We know particles like these exist in the bulk but the numbers do not appear to be sufficient to give the desired sieving effect.

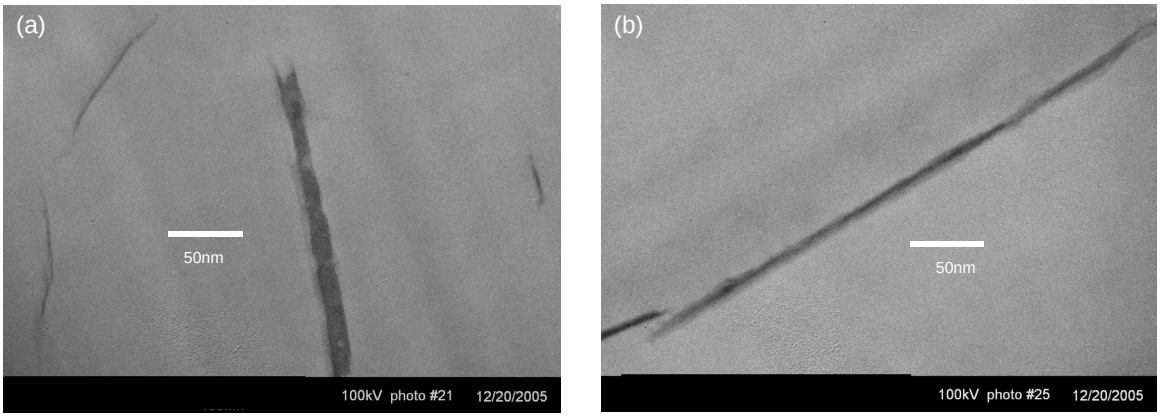

Figure 5.8 TEM of Matrimid-8MR-AlPO (a) 2wt% $CTMA^+$ composite, (b) 2 wt% $ODDMBA^+$ composite.

The permeability data along with the calculated aspect ratios for pure Matrimid and the 2wt% composites are reported in Table 5.5. Making a quick glance at the effective α columns it can be seen that the most effective surface treatment for Matrimid was the $CMTA^+$. The α values are largest for this composite indicating good barrier properties and therefore good adhesion between the 8MR-AlPO particles and Matrimid. The permeability values for each gas species in the $CMTA^+$ composite dropped between 18%-24%. The permeability of the smaller gas species (He, CO2) experienced the same ratio drop as the larger ones leading to the ideal selectivities reported in Table 5.6

remaining the same as pure Matrimid. Looking at the last two columns in Table 5.5 it is can be seen the 8MR-AlPO did not act as a barrier to O_2, N_2, or CH_4 for the other composites. The permeability increased for these gas species in the $112DADD^{2+}$ and $ODDMBA^{+}$ composites when compared to pure Matrimid. The permeability values for theses two composite display the opposite of the desired result. The permeability of the small gases is reduced while the permeability of the larger gases has increased. As a result the ideal selectivity of He/CH_4 and CO_2/CH_4 in Table 5.8 shows a 70% drop for the $112DADD^{2+}$ and $ODDMBA^{+}$ when compared to pure Matrimid. This is indicative of problems at the interface between 8MR-AlPO and the Matrimid. A defect at the interface could cause an increase in the permeability of the larger gas species.

Table 5.5 Permeability and effective α for Matrimid 8MR-AlPO composites

	Matrimid-2wt% AlPO permeability (Barrers)				Effective α		
	Matrimid	$CTMA^{+}$	$112DADD^{2+}$	$ODDMB^{+}$	α-$CTMA^{+}$	α-$112DADD^{2+}$	α-$ODDMB^{+}$
He	24.51	18.77	22.42	19.92	73	40	64
CO_2	7.57	6.22	7.22	6.44	61	29	55
O_2	1.93	1.56	2.09	1.94	65	0	0
N_2	0.31	0.24	0.72	0.72	73	0	0
CH_4	0.24	0.19	0.80	0.66	64	0	0

Table 5.6 Ideal Selectivity for 2wt% 8MR-AlPO composites

	Matrimid				Cellulose Acetate			
	Pure	$CTMA^{+}$	$112DADD^{2+}$	$ODDMB^{+}$	Pure	$CTMA^{+}$	$112DADD^{2+}$	$ODDMB^{+}$
He/CH_4	103.3	97.6	27.9	30.3	61.8	66.4	57.9	32.2
CO_2/CH_4	31.9	32.4	9.0	9.8	24.1	25.3	22.2	12.0

Cellulose acetate-AlPO composites

Cellulose acetate (CA) has been used commercially to remove carbon dioxide from methane since the mid 1980's. Despite a modest separation factor of 12-15 for CO_2/CH_4 it remains today the dominant material used for methane purification with membrane unit operations.[20] The material is a tough film forming thermoplastic with a moderate T_g in the range of 190°C. Its chemical makeup is different than that of a polyimide. It is a tough glassy polymer that contains hydroxyl and acetyl groups on the backbone. There would be immediate benefits then if the CO_2/CH_4 selectivity of this material could be improved by the addition of a microporous inorganic. Cellulose acetate was therefore chosen as another test matrix for microporous aluminophosphate. If the permeability of methane could be decreased while maintaining the permeability of carbon dioxide, the selectivity of the composite material would be better than pristine cellulose acetate.

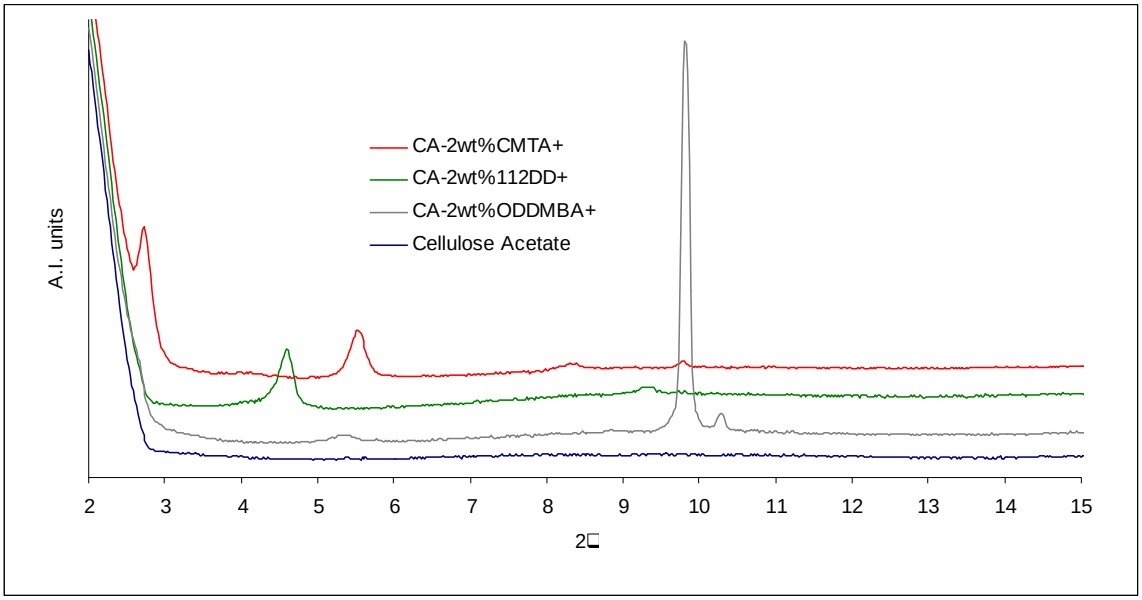

Figure 5.9 XRD patterns of cellulose acetate 2wt% 8MR-AlPO composite membranes

The results of XRD on a pure cellulose acetate membrane and the 2wt% composite membranes made with swollen 8MR-AlPO are shown in Figure 5.9. The peaks in these composites are much sharper than seen in other composites indicating a high degree of crystallinity still remains in the 8MR-AlPO. It is important to note that the inorganic material used in the cellulose acetate membranes was the exact same material used in the Matrimid membranes. In comparison to the XRD patterns of the Matrimid membranes, these patterns shows much sharper peaks compared to the very broad peaks in Matrimid. In the $CMTA^+$ composite there are three clear peaks visible corresponding to d_{001}, d_{002}, and d_{003} along with a very small peak at $2\theta = 9.8°$. These d-spacings correspond almost exactly with those seen in the pure swollen material. From the data it can be concluded that there is still a large amount of the $CMTA^+$ intercalated phase present in the composite and that further exfoliation has been limited. The $112DADD^{2+}$ composite shows a prominent peak corresponding to $d_{001} = 19Å$. The gallery space determined for the pure inorganic was 21Å which means it decreased some as a result of incorporation in to a polymer. There was, therefore, no further intercalation of cellulose acetate into the gallery space using the $112DADD^{2+}$ treatment and the intercalated phase still exists. Finally, the composite containing $ODDMBA^+$ treated 8MR-ALPO showed two very sharp characteristic peaks for the as-synthesized material and one more broad peak at $2\theta = 5.4°$. Clearly a large amount of the as-synthesized phase is still present in this composite along with some material that is intercalated with ODDMBA+. The gallery-spacing of the intercalated phase is 16Å which is less than the 33Å spacing seen in the pure inorganic material.

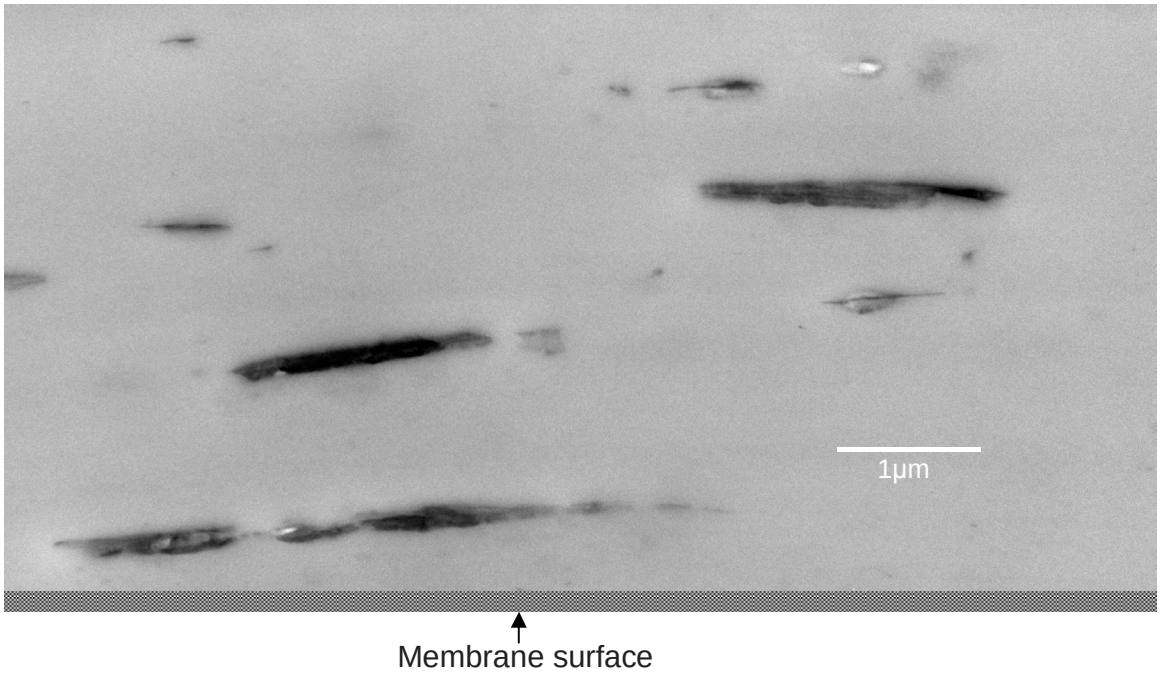

Figure 5.10 Showing edge of CA-2wt% $CMTA^+$ membrane and partial orientation due to casting solution with a blade

TEM images of the CA-AlPO composite membranes were taken and compared. All of these membranes were cast on glass with a casting blade. The particle sizes were different in each membrane. The CA-112DADD^{2+} membrane contained the smallest particles. All of the particles were in the nanometer range for both thickness and length which leads to a small aspect ratio. The CA-$CMTA^+$ membrane contained a few large particles with thickness in the micron range but also a large number of particles with lengths in the micron range and thickness in the nanometer range (100nm). This results in some particles with large aspect ratios. The CA-$ODDMBA^+$ membrane contained the largest particles. Some of the particles were similar to the thin long particles seen the CA-$CMTA^+$ membrane but there were also a fair number of particles with thicknesses close to 1-2 µm. One question we wanted to answer was could particles be oriented parallel to the surface of the membrane by casting with a blade. Figure 5.10 shows the

surface of the membrane in relation to the particle orientation. It can be seen from the TEM that there is preferential orientation of the particles parallel to the surface of the membrane when the solution is cast with a casting knife and shear is applied to the surface. All of the CA-AlPO composite membranes showed orientation of particles parallel to the surface of the membrane as a result of casting the solution with a blade.

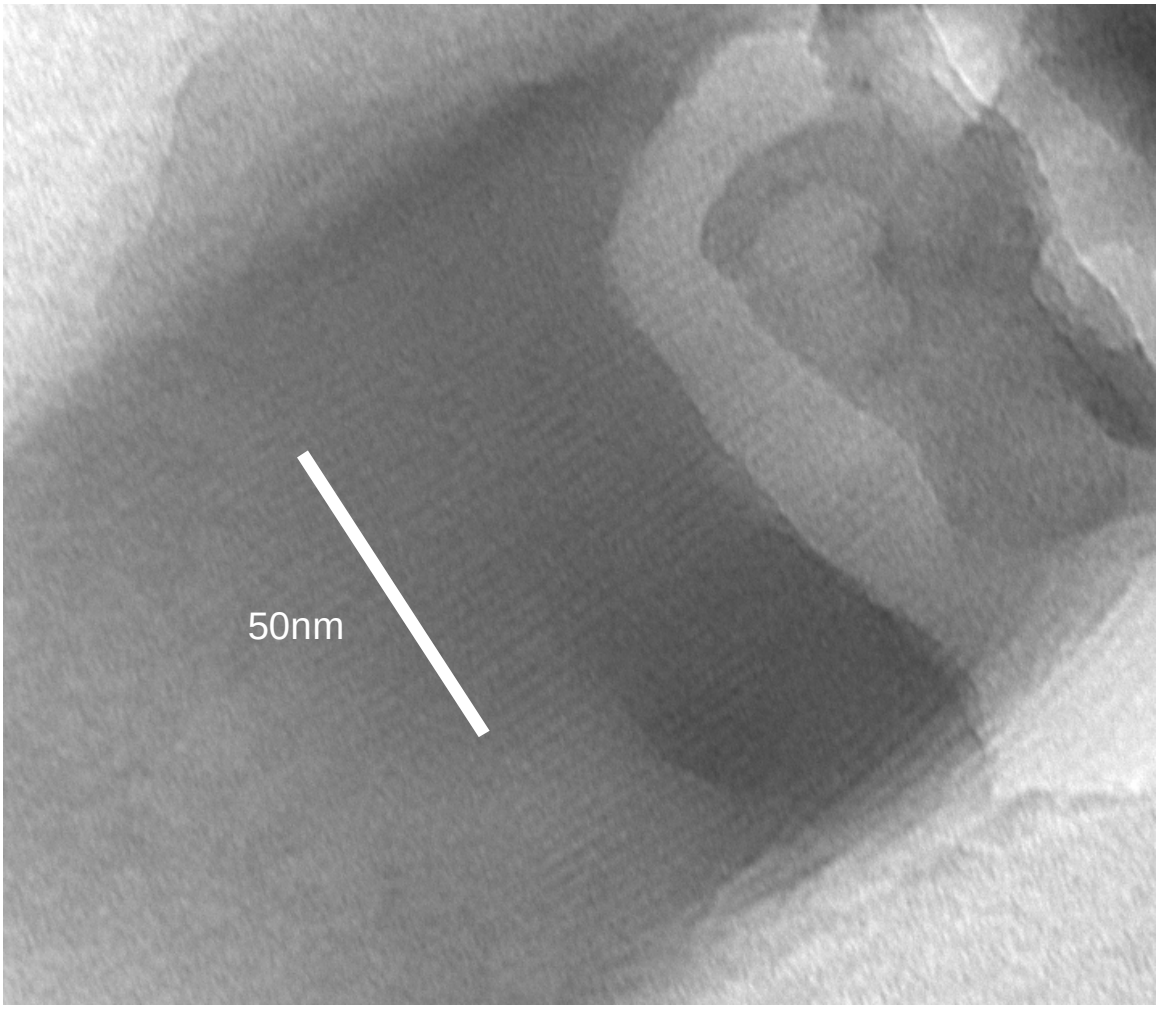

Figure 5.11 TEM showing layers in one of the particles from Figure (CA-112DADD) above

Figure 5.11 is a TEM image of one of the particles in the 2wt% CA-112DADD^{2+} membrane showing the spacing between layers. The gallery spacing measured in the

TEM image is consistent with the value of 19Å measured with XRD. This also confirms that AlPO is swollen with surfactant but not intercalated with polymer.

The ideal selectivity of the composites made with 8MR-AlPO and cellulose showed only a modest improvement for the $CMTA^+$ membrane while other two had decreased selectivity when compared to neat cellulose acetate. The selectivities for He/CH_4 and CO_2/CH_4 can be seen in Table 5.6. The permeability values along with the calculated α values are reported in Table 5.7. A quick look at the effective α values calculated for the composite membranes shows that the $ODDMBA^+$ 8MR-AlPO did not produce a barrier effect in CA. Further, the permeability of all of the gas species increased when compared to the neat polymer. An increase in permeability can be an indication that there were non-selective voids at the inorganic polymer interface. This could be due to a mismatch in hydrophobicity between polymer and surface treatment. The other two composites ($CMTA^+$ and $112DADD^{2+}$) showed reduced permeability in some cases and some barrier effect as a result of adding 8MR-AlPO. As already mentioned the $CMTA^+$ composite showed a slight improvement in selectivity but much smaller than would be expected if microsieving was actually dominating the transport. The permeability of the small gas species He, CO_2 dropped as well as the CH_4 permeability. This is similar to what we would like to see. The CH_4 permeability dropped more than the small species so there was a modest increase in selectivity seen. The O_2 and N_2 permeabilities were unchanged when compared to the neat polymer. Because there was a barrier effect with this polymer it is believed there was good interaction between polymer and inorganic but the exfoliation was not great enough to give the desired effect. The $112DADD^{2+}$ showed the opposite of the effect we would like

to see. The smallest gas species were obstructed by 8MR-AlPO while the permeability of the large gas species increased slightly. There was only a slight increase in N_2 and CH_4 permeability, therefore, we believe that while good interaction between 8MR-AlPO and CA was achieved, the desired sieving effects were minimal.

Table 5.7 Permeability and effective α for Cellulose Acetate 8MR-AlPO composites

Cellulose Acetate-2wt% AlPO permeability (Barrers)					Effective α		
	Pure CA	$CTMA^+$	$112DADD^{2+}$	$ODDMB^+$	α-$CTMA^+$	α-$112DADD^{2+}$	α-$ODDMBA^+$
He	18.66	17.68	17.94	19.81	29	25	0
CO_2	7.28	6.74	6.88	7.40	35	30	0
O_2	1.32	1.35	1.26	1.54	0	26	0
N_2	0.28	0.28	0.29	0.51	0	0	0
CH_4	0.30	0.27	0.31	0.62	45	0	0

5.4 Conclusions

Aluminophosphate-polymer composites were fabricated using the solution intercalation method with five different polymers as the matrix material. Composites containing relatively high loadings of 8MR-AlPO compared with traditional PCN were fabricated. The polymer matrix materials used for this part of the study were PDMS, 20%PDMS-6FDA-6FpDA, and polysulfone. In some cases a barrier effect was seen as result of incorporating 8MR-AlPO but significant selectivity enhancements were not seen. It was found that better barrier properties were achieved when loadings of < 5wt% 8MR-AlPO were used. The surface treatment of 8MR-AlPO was varied to attempt to encourage interaction between the inorganic and Matrimid or Cellulose Acetate. Incorporation of 8MR-AlPO produced a barrier effect in several cases but molecular sieving of large gas species was not seen. None of the composites achieved selectivity enhancements that compared to the results reported by Jeong et al. for simple mixing of 8MR-AlPO with a hexa-fluorinated polyimide.

(1) Yano, K.; Usuki, A.; Okada, A.; Kurauchi, T.; Kamigaito, O., Synthesis and properties of polyimide-clay hybrid. *Polymer Preprints (American Chemical Society, Division of Polymer Chemistry)* **1991**, (32), 65-66.

(2) Alexandre, M.; Dubois, P., Polymer-layered silicate nanocomposites: preparation, properties and uses of a new class of materials. *Materials Science and Engineering. R Reports: A Review Journal* **2000,** 28, (1-2), 1-63.

(3) Giannelis, E. P., Polymer Layered Silicate Nanocomposites. *Advanced Materials* **1996,** 8, (1), 29 - 35.

(4) LeBaron, P. C.; Wang, Z.; Pinnavaia, T. J., Polymer-layered silicate nanocomposites: an overview. *Applied Clay Science* **1999,** 15, (1-2), 11-29.

(5) Tjong, S. C., Structural and mechanical properties of polymer nanocomposites. *Materials science & engineering. R, Reports : a review journal* **2006,** 53, (3-4), 73-197.

(6) Zanetti, M.; Lomakin, S.; Camino, G., Polymer layered silicate nanocomposites. *Macromolecular materials and engineering* **2000,** 279, (1), 1 - 9.

(7) Huang, J.-C.; Zhu, Z.-k.; Yin, J.; Qian, X.-f.; Sun, Y.-Y., Poly(etherimide)/montmorillonite nanocomposites prepared by melt intercalation: morphology, solvent resistance properties and thermal properties. *Polymer* **2001,** 42, (3), 873-877.

(8) Davis, C. H.; Mathias, L. J.; Gilman, J. W.; Schiraldi, D. A.; Shields, J. R.; Trulove, P.; Sutto, T. E.; Delong, H. C., Effects of melt-processing conditions on the quality of poly(ethylene terephthalate) montmorillonite clay nanocomposites. *Journal of polymer science. Part B, Polymer physics* **2002,** 40, (23), 2661 - 2666.

(9) Yang, Y.; Zhua, Z.-k.; Yina, J.; Wang, X.-y.; Qi, Z.-e., Preparation and properties of hybrids of organo-soluble polyimide and montmorillonite with various chemical surface modification methods. *Polymer* **1999,** 40, (15), 4407-4414.

(10) Gu, A.; Kuo, S.-W.; Chang, F.-C., Syntheses and properties of PI/clay hybrids. *Journal of Applied Polymer Science* **2001,** 79, (10), 1902-1910.

(11) Delozier, D. M.; Orwoll, R. A.; Cahoon, J. F.; Johnston, N. J.; J. G. Smith, J.; Connell, J. W., Preparation and characterization of polyimide/organoclay nanocomposites. *Polymer* **2002,** 43, (3), 813-822.

(12) Yano, K.; Usuki, A.; Okada, A.; Kurauchi, T.; Kamigaito, O., Synthesis and properties of polyimide-clay hybrid. *Journal of Polymer Science, Part A: Polymer Chemistry* **1993,** 31, (10), 2493-8.

(13) Gao, Q.; Li, B.; Chen, J.; Li, S.; Xu, R.; Williams, I.; Zheng, J.; Barber, D., Nonaqueous Synthesis and Characterization of a New 2-Dimensional Layered Aluminophosphate [Al3P4O16]3-· 3[CH3CH2NH3]+. *Journal of solid state chemistry* **1997,** 129, (1), 37-44.

(14) Jeong, H.-K.; Krych, W.; Ramanan, H.; Nair, S.; Marand, E.; Tsapatsis, M., Fabrication of Polymer/Selective-Flake Nanocomposite Membranes and Their Use in Gas Separation. *Chemistry of Materials* **2004,** 16, (20), 3838 -3845.

(15) Vaughan, B. Polymer-aluminophosphate membranes for gas separations. Virginia Tech, Blacksburg, 2007.

(16) Pechar, T. Zeolite Polymer Composites for Gas separations. Virginia Tech, Blacksburg, 2005.

(17) Cussler, E. L.; Hughes, S. E.; William J. Ward, I.; Aris, R., Barrier membranes. *Journal of Membrane Science* **1988,** 38, (2), 161-174.

(18) Agag, T.; Koga, T.; Takeichi, T., Studies on thermal and mechanical properties of polyimide–clay nanocomposites. *Polymer* **2001,** 42, (8), 3399-3408.

(19) Huang, J.-C.; Zhu, Z.-K.; Ma, X.-D.; Qian, X.-F.; Yin, J., Preparation and properties of montmorillonite/organo-soluble polyimide hybrid materials prepared by a one-step approach. *Journal of Materials Science* **2001,** 36, (4), 871 - 877.

(20) Baker, R. W., Future Directions of Membrane Gas Separation Technology. *Industrial & engineering chemistry research* **2002,** 41, (6), 1393 -1411.

(21) Chung, T.-S.; Chan, S. S.; Wang, R.; Lu, Z.; He, C., Characterization of permeability and sorption in Matrimid/C60 mixed matrix membranes. *Journal of membrane science* **2003,** 211, (1), 91-99.

(22) Barsema, J. N.; Klijnstra, S. D.; Balster, J. H.; Vegt, N. F. A. v. d.; Koops, G. H.; Wessling, M., Intermediate polymer to carbon gas separation membranes based on Matrimid PI. *Journal of membrane science* **2004,** 238, (1-2), 93-102.

(23) Mahajan, R.; Burns, R.; Schaeffer, M.; Koros, W. J., Challenges in Forming Sucessful Mixed Matrix Membranes with Rigid Polymeric Materials. *Journal of Applied Polymer Science* **2002,** 86, 881-890.

(24) Vu, D. Q.; Koros, W. J.; Miller, S. J., Mixed matrix membranes using carbon molecular sieves I. Preparation and experimental results. *Journal of membrane science* **2003,** 211, (2), 311-334.

Chapter 6

Study of a gas separation composite membrane using in-situ polymerization of polyetherimide in the presence of $[Al_3P_4O_{16}]^{3-}$

6.1 Introduction

The molecular level incorporation of clay into polymers to make polymer clay nanocomposites (PCN) is a well known technique. Layered clays have been exfoliated in a variety of polymer materials and shown to improve mechanical properties[1], thermal stability[2], and gas barrier properties[3]. Lan et al. reported a dramatic drop in the permeability (50%) of CO_2 in a polyimide membrane after modest amounts of clay (< 2 vol%) were added.[4] This drop was seen despite the fact that a large fraction of the clay was not exfoliated and unoriented. While a sizeable amount of work has been performed on the incorporation of layered clays as barrier materials in polymers, relatively no work has been done on microporous layered materials.

These materials are similar to clays but contain micropores which may allow for gas selectivity enhancements once dispersed at a molecular level into a polymer matrix.

The incorporation of microporous layered aluminophosphates like $[Al_3P_4O_{16}]^{3-}$ into polymer matrices may improve the gas selectivity of some polymers if the inorganic can be dispersed at a molecular level. Our earlier work has shown it is difficult to disperse, intercalate, and exfoliate the layered aluminophosphate $[Al_3P_4O_{16}]^{3-}$ into polymers using simple mixing in organic solvents.[5] In this previous study polymer composites containing 8MR-AlPO were fabricated, however, the desired molecular sieving effect was not observed in the transport data. Several polymers were employed in previous studies including PDMS, 20%PDMS-6FDA-6FpDA, Matrimid, Cellulose Acetate, and Polysulfone. The surface treatment of 8MR-AlPO was also varied to improve interaction with the polymer. None of the attempted pathways improved the final result. Microscopy and XRD suggested the reasons were poor exfoliation and incomplete dispersion of the 8MR-AlPO into the polymer matrices. If a significant level of exfoliation could be achieved, it is hypothesized that this microporous inorganic framework could enhance the separation factor of small gasses over large gases (ex. CO_2/CH_4) when compared with neat polymer. In-situ polymerization or monomer solution intercalation of polyimides has proven a useful technique to exfoliate clays in PCN.[6-8] The current study will therefore focus on this method to make a polymer-aluminophosphate composite membrane.

A study performed by Jeong et al. showed selectivity enhancements of over 200% for some gas pairs when 8MR-AlPO was incorporated in a hexafluorinated polyimide.[9] Polyetherimide is in the same family of polymers, it displays similar mechanical properties, it can be spun into hollow fibers, and is more cost effective to synthesize. For this reason in-situ polymerization of polyetherimide (PEI) in the presence of 8MR-AlPO treated with different

surface modifiers was chosen as a test polymer. The hypothesis is that the monomers used to make PEI could enter the gallery space of 8MR-AlPO, polymerize in gallery space, and exfoliate the platelets by a physical mechanism. The expanding polymer chains in the gallery space would force the layers apart to a point where they may completely exfoliate. A similar experiment using sodium montmorillonite (MMT) was reported by Morgan et al.[10] They performed an in-situ polymerization of polyetherimide with modified MMT. Using this technique they were able to successfully synthesize PEI-MMT nanocomposites.

6.2 Experimental

6.2.1 Materials

The layered aluminophosphate used in this study was $[Al_3P_4O_{16}]^{3-}\cdot 3[NH_3CH_2CH_3]^+$. The synthesis of this layered aluminophosphate was performed according to the original work on the compound by Gao et al.[11] Some of the specifics of the synthesis and swelling of this compound are can be found in detail in an earlier paper.[12] The agents used to modify 8MR-AlPO were cetyltrimethyl ammonium chloride 25 wt% ($CMTA^+$) (Aldrich) in water, M_W = 10K g/mol PEI oligomer (Hydrosize Inc.), and 12 Aminododecanonic Acid (Aldrich) and were used as received. The monomers used to synthesize PEI were 4,4'-(4,4'-Isopropylidene-diphenoxy)-bis(phthalic anhydride) or (BPADA) (Aldrich), and 1,3 Phenylenediamine (m-PD) (Aldrich) were used as received. Anhydrous N,N Dimethylacetamide (DMAc) from Aldrich was used as the solvent for polymerization.

6.2.2 Treatment of 8MR-AlPO

As-synthesized 8MR-AlPO was swollen with $CMTA^+$ according to the procedure reported by Jeong et al.[9] 8MR-AlPO was also treated with a low Mw PEI. Some of the $CMTA^+$ 8MR-AlPO (0.76g) was mixed at 80°C in NMP in a 1wt% solution of 10K PEI oligomer for 16hrs to coat or

intercalate the particle with low molecular polymer. The treated 8MR-AlPO was precipitated with water, recovered and washed with NMP using a centrifuge. Finally it was dried under vacuum in preparation for use. The final treatment of 8MR-AlPO involved swelling it with 12 aminododecanoic acid. To swell 1g of 8MR-AlPO, a solution of 2.157g of 12 aminododecanoic acid and 0.83 mL of HCl were dissolved in 50mL of water at 80°C. After the solution cleared, 1g of as-synthesized 8MR-AlPO was added to the mixture and allowed to stir for 16hrs. The solid was then recovered with filtration and allowed to dry. After drying the solid was washed with several liters of 80°C-90°C water and filtered to ensure excess surfactant was removed.

6.2.3 Membrane Fabrication

The PEI was synthesized at a concentration of 20 wt% in DMAc in a three neck flask with argon as the purge gas at 40°C. Approximately 3g of PEI was synthesized in each batch using a 1:1 ratio of BPPADA to m-PD. A stoichiometric amount of BPADA was added to DMAc and allowed to fully dissolve. Following the complete dissolution of BPADA, 5wt% of treated 8MR-AlPO was added to the solution. The solution was stirred for 24 hrs and at the 12 hour mark sonicated in a bath (VWR 50HT) for 2 hrs to ensure the particle were separating in solution. After 24hrs a stoichiometric amount of m-PD was added to the solution and allowed to react for 24hrs. The solution was placed in a test tube and centrifuged at 1000 rpm for about 10 seconds to settle any very large particle still left in the solution. The supernatant was then pipetted onto a large glass plate and allowed to evaporate in a small oven at 75°C overnight. The dry film was placed in a vacuum oven and imidized at 130°C 12hrs, ramped slowly to 250°C over a 4 hour period, and then left at 250°C for 1 hour to complete imidization. The membrane was then allowed to cool to room temperature under vacuum removed from the oven and peeled off the glass for measurements.

6.2.4 Membrane Characterization

For measurement by TEM the composite membranes were embedded in epoxy and microtomed into thin slices. The membrane cross-sections were placed on 300 mesh copper grids and observed using a Jeol 100 CX-II at 100kV.X-ray diffraction (XRD) was used to characterize many of the samples. Each batch of as-synthesized AlPO and modified AlPO as well as the polymer-8MR-AlPO composites was tested using a Scintag XDS-2000. The samples were run using CuKα (λ = 1.5418 Å) radiation at 40mA and -45kV. Powder XRD was used to confirm the synthesized structure of 8MR-AlPO and the degree to which it was swollen. The composite membranes were scanned on both sides to determine the degree of exfoliation present in the composite. A LEO 1550 FESEM was used to take Scanning Electron Micrographs (SEM) of the modified 8MR-AlPO. Dynamic Mechanical Thermal Analysis (DMTA) was performed on a Rheometric Scientific DMTA IV with a ramp rate of 2°/min and a frequency of 1 Hz. The permeability of five small gases was measured using a constant volume apparatus. Permeability of He, O_2, N_2, CH_4, and CO_2 was measured for each pure and composite membrane utilizing the lag time method. The membranes were placed in a stainless steel cell with volumetric chambers one each side. One side of the membrane was evacuated to vacuum and the other side was pressurized with 4 atm at 35°C of the gas species of interest. The pressure change on the permeate side was allowed to reach steady state and then the data was analyzed to calculate permeability.

6.3 Results and Discussion

A summary of the mechanism for in-situ polymerization of PEI with 8MR-AlPO can be seen in Figure 6.1. The 8MR-AlPO was mixed into DMAc after the BPADA was fully dissolved. The BPADA monomer is approximately 18Å in length. All of the swollen samples of

8MR-AlPO showed d_{001}-spacings in this range when measured with XRD. The BPADA monomer should therefore be able to intercalate into the gallery space of 8MR-AlPO. It is also hoped that the partial positive charge on the carbonyl groups at the ends of the BPADA monomer will encourage it to interact with the negatively charged 8MR-AlPO platelets. The monomers were reacted in the presence of 8MR-AlPO to form a polyamic acid. The polyamic acid was then cast onto glass and thermally imidized into a polyimide.

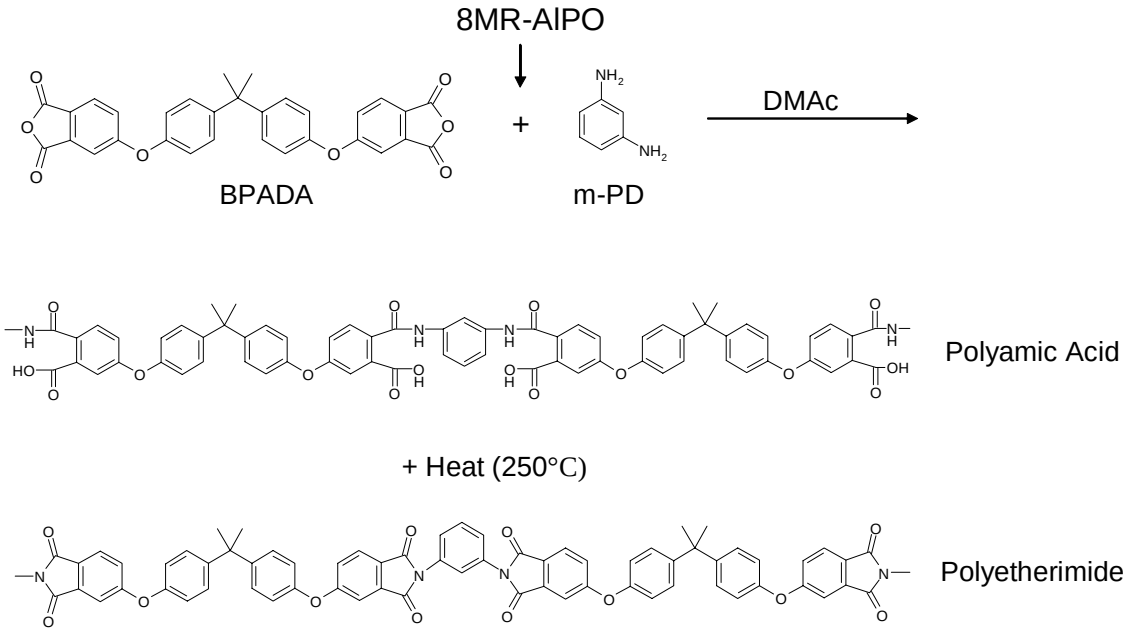

Figure 6.1 Reaction scheme for PEI

6.3.1 XRD, SEM of treated 8MR-AlPO

The 8MR-AlPO used in the study was modified with three separate surface treatments in the attempt to maximize the interaction of the inorganic with the polyetherimide. A treatment using $CMTA^+$ was used successfully by Jeong et al. to make a polyimide-aluminophosphate composite with increased selectivity.[9] Therefore, this same treatment of 8MR-AlPO was reproduced for this study. The membrane made using this 8MR-AlPO was called PEI-$CMTA^+$. Another treatment involved "priming" the $CMTA^+$ -AlPO with a small amount of low molecular

weight PEI. This technique had been used successfully by Koros et al. to make zeolite polymer composites that eliminated nonselective voids between zeolite and polymer.[13] A PEI oligomer with a M_W of 10K g/mol was chosen for this purpose. The 8MR-AlPO was coated with this oligomer and the composite made from this material was called PEI-10K. The final treatment of 8MR-AlPO involved the use of a swelling agent with a reactive group at one end. In the literature on PCNs, this type of surface modifier is known as a tether.[10, 14, 15] The concept of a molecular tether is illustrated in Figure 6.2. The platelets of 8MR-AlPO carry a negative charge on the surface. The idea is, therefore, to use a surface treatment that can form an ionic bond with the surface of the 8MR-AlPO as well as a covalent bond with the polymer that is being synthesized in-situ. The ammonium salt of 12 aminododecanoic acid should work well with the PEI. As seen in Figure 6.2 one end of the molecule can form an ionic bond with 8MR-AlPO and the other end can form an amide linkage with the m-PD and therefore the PEI. This composite was called PEI-12COOH$^+$. Even if the 12COOH$^+$ treatment does not result in a covalent attachment between 8MR-AlPO and the PEI there should be added benefits. The carboxyl group on the surfactant should hydrogen bond with the poly(amic acid) form of the polymer promoting interaction and dispersion of the inorganic with the polymer.[16]

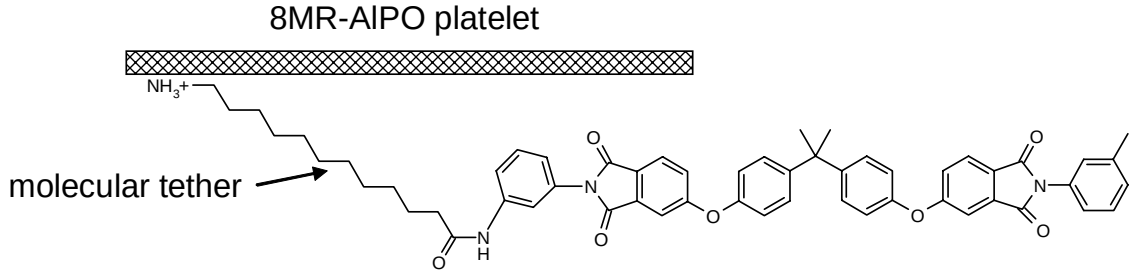

Figure 6.2 Illustration of 8MR-AlPO tethered to PEI

The pure inorganic samples as well as the films were analyzed with XRD. The XRD patterns for the pure treated 8MR-AlPO samples are shown in Figure 6.3. The as-synthesized peak is shown at the bottom of Figure 6.3 and the 001 peak ($2\theta = 9.8°$) indicating the layer spacing of the pure 8MR-AlPO can be seen. The layer spacing can be calculated to be $d_{001} = 9Å$ using Bragg's Law. Any shift of this characteristic 001 peak to the left therefore would show an increase in the gallery spacing of 8MR-AlPO. All of the XRD patterns of the treated 8MR-AlPO samples show increase gallery spacing. The $CMTA^+$ and 10K treated 8MR-AlPO's both show the 001 peak at a value of $2\theta = 2.7$ indicating that the spacing of the layers has increased to 32Å. This spacing should be large enough to allow the BPADA monomer to intercalate once it is mixed in solution. The next strong peak in both of those samples corresponds to the d_{002} spacing which is half that of d_{001}. The XRD pattern of the pure inorganic 8MR-AlPO swollen with $12COOH^+$ shows a substantial peak at $2\theta = 3.8°$. This peak is the shifted 001 peak indicating a new gallery height of 23Å.

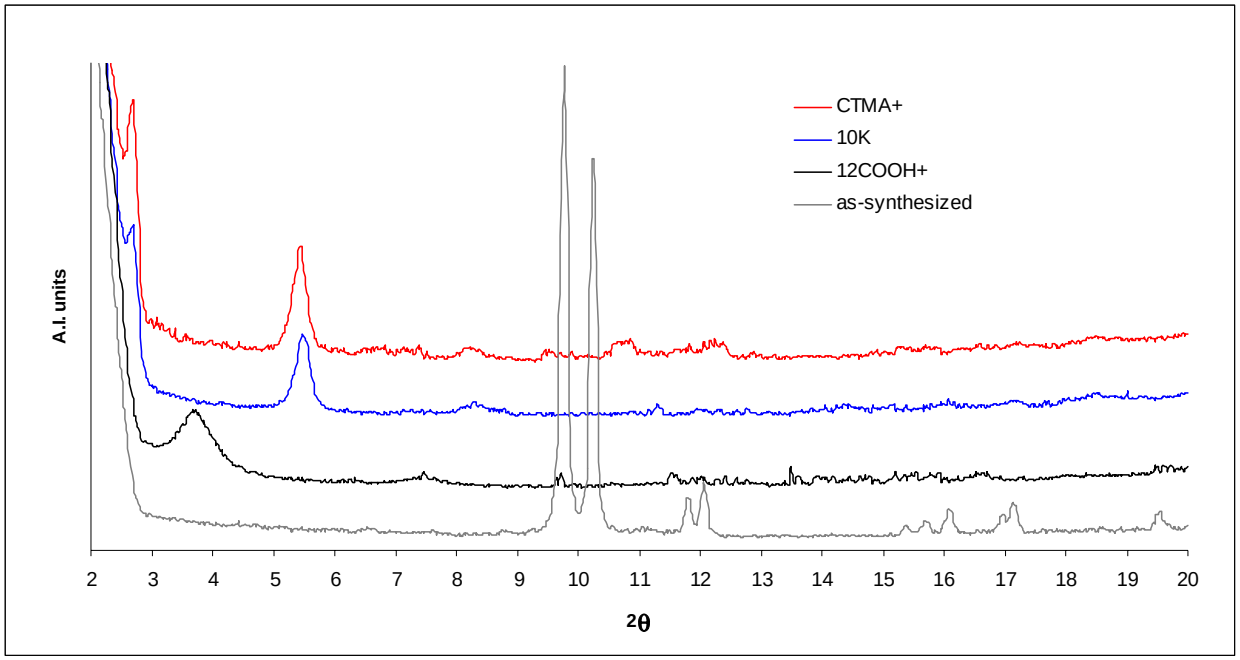

Figure 6.3 XRD patterns of 8MR-AlPO modified with various surface treatments

The treated 8MR-AlPO samples were also characterized using Scanning Electron Microscopy (SEM). The images of the four samples are pictured in Figure 6.4. The as-synthesized material is pictured in Figure 6.4a. As-synthesized 8MR-AlPO consists of rectangular crystals with smooth sides. In general, after the addition of swelling agents the crystals appear more fractured and layers become visible. The crystals break into smaller pieces and thinner tactoids can usually be seen.[12] The $CMTA^+$ 8MR-AlPO in Figure 6.4b can be seen to be broken up and flaky compared with the as-synthesized material. The particles were smaller than the as-synthesized material and the layered nature of the material is now clearly visible. The 10K 8MR-AlPO in Figure 6.4c is the same material covered by a thin layer of low molecular weight PEI. When compared with Figure 6.4b the material appears covered with a layer of polymer. This material is the 10K PEI and its visibility on the surface indicates a fairly thick layer in the hundreds of nanometers range. Energy dispersion spectroscopy (EDS) of these particles (not pictured) showed the presence of Al, and P which means that the covering of PEI is less than 1μm thick. Because the XRD of this sample showed the same layer spacing as the $CMTA^+$ 8MR-AlPO the oligomer is likely just covering the outside of the particles and did not intercalate into the gallery space. Finally, the SEM image of the $12COOH^+$ swollen 8MR-AlPO is pictured in Figure 6.4d. The particles are smaller and more fractured when compared with as-synthesized 8MR-AlPO. There also appears to be some residual surfactant present on the surface of the material, but the layered nature can still be seen clearly.

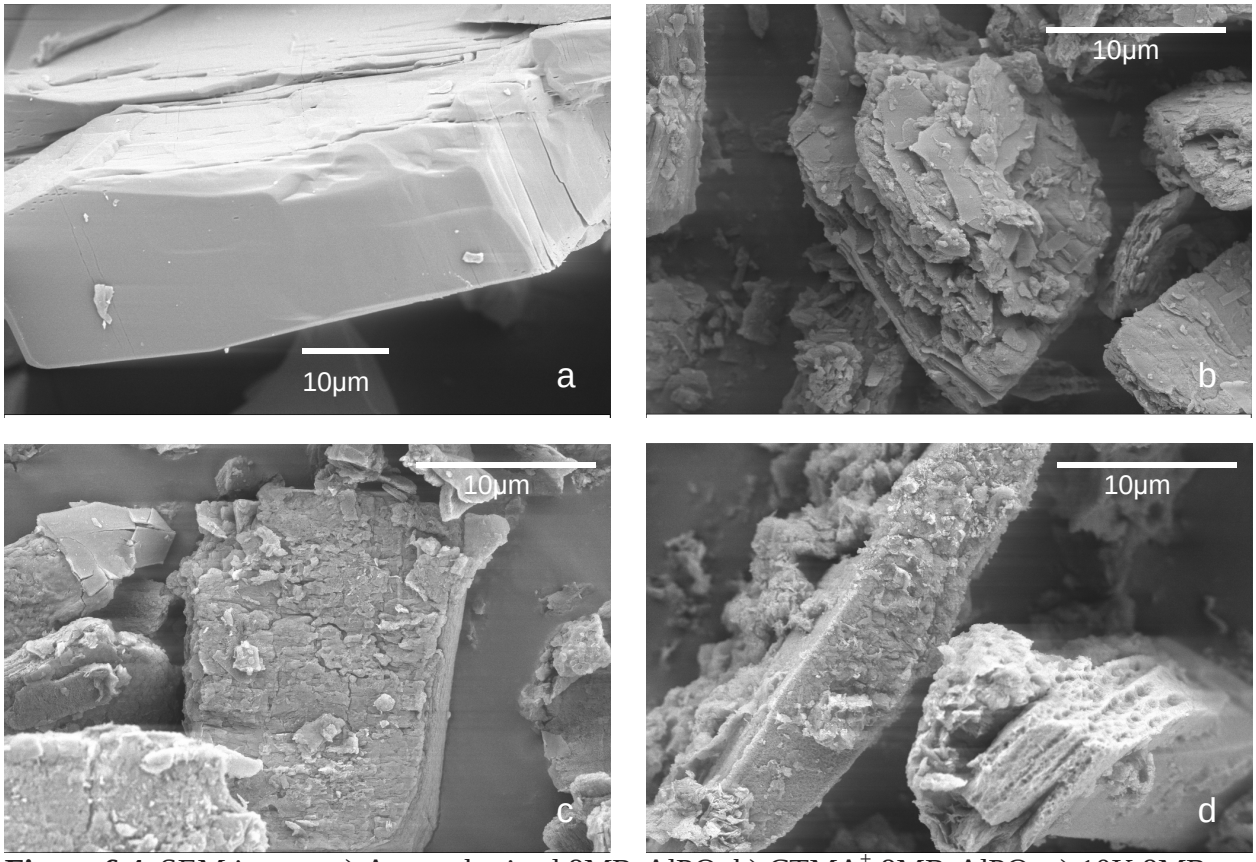

Figure 6.4 SEM images a) As-synthesized 8MR-AlPO, b) $CTMA^+$ 8MR-AlPO, c) 10K 8MR-AlPO, and d) $12COOH^+$ 8MR-AlPO.

6.3.2 XRD, TEM, DMTA, and permeability of PEI-8MR-AlPO composites

Four separate polymerizations were therefore carried out. The first polymerization produced a pure PEI film. The molecular weigh of this film was tested with gel permeation chromatography using a polystyrene standard and NMP as the solvent. The molecular weight of the sample was measured by gel permeation chromatography and found to be M_W = 61,000. The molecular weigh of the three other composites could not be determined because they contained 8MR-AlPO. The same procedure was replicated for each batch so the molecular weights of the polymer in the composites should be similar. The other thee polymerizations including the treated 8MR-AlPO's resulted in composites of PEI and 5wt% $CTMA^+$ 8MR-AlPO, 10K 8MR-AlPO, and $12COOH^+$ 8MR-AlPO. The composite films were yellow in tint. The pure PEI was

completely transparent and the composite films were transparent with some degree of translucence. The membranes were characterized using XRD, TEM, DMTA, and a permeability apparatus.

XRD was performed on both sides of the 5wt% composites to observe the ordered domains present in the matrix. These patterns are reported in Figure 6.5. An immediate observation is that all of the scans are featureless. This may be the first indication that the particles have completely exfoliated. It has been reported in literature however that Transmission Electron Microscopy (TEM) must also be used to verify the results obtained by XRD. Kornmann et al. used XRD and TEM to show that PCN systems with low clay content may show no pattern on an XRD even though there are still intact tactoids present in the matrix.[17]

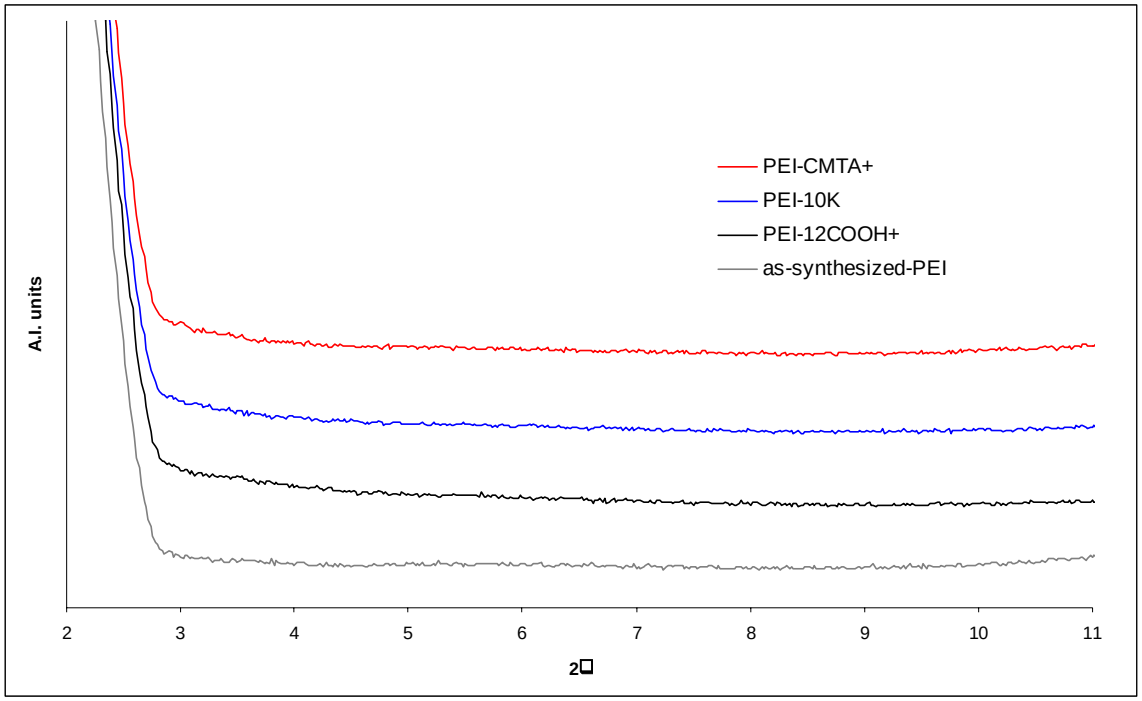

Figure 6.5 XRD pattern of PEI-8MR AlPO composite membranes

The films were also observed using TEM to further investigate the dispersion and exfoliation of the inorganic particles. Some of the TEM pictures are shown below in Figure 6.6.

The first observation to make is that particles are present in the pictures indicating that full exfoliation has not taken place. This is opposite to what was observed when XRD was performed on the films. The $CMTA^+$ and 10K composites showed very similar images so only one set are pictured. A cross section of the $CMTA^+$ composite membrane (Figure 6.6a) shows that there were still large particles present in the matrix and that they settled to the bottom of the membrane as the solvent evaporated. In the top ½ of the membrane small white circles can be seen. They are lighter in color than the surrounding polymer and likely represent some other phase. We suggest that these circles could be excess surfactant which phase separated and collected into small spheres in the membrane. Although large particles (1-5μm) can be seen in Figure 6.6a, smaller particles were also present in the matrix. Figure 6.6b shows a picture of such a particle which is in the range of a couple hundred nanometers. When the picture was magnified and examined, layering was seen with gallery spacing on the order of 25Å. This is smaller spacing than observed for XRD but in the same range. A very similar result was obtained for the 10K composite (not pictured) with some small differences. The cross section of the 10K membrane showed settling of large particles but there were less (80% less) small white circles in the top ½ of the membrane. This could be a result of some surfactant removal during the coating process and washing with NMP. The 10K composite also showed small tactoids in the same range (100-200nm) as the $CMTA^+$ composite. The average particle size seen in the 12COOH+ composite (Figure 6.6c) is much smaller than in the other two composites. There is that occasional micron sized particle but most are in the nanometer range. The particles also appear well dispersed and there appears to be no settling of particles to the bottom of the membrane. A close up of several particles in the 100nm range can be seen in Figure 6.6d. When the image was magnified layer spacing between platelets was found to be 25Å-30Å. This is

consistent with XRD of the pure inorganic but contrary to the XRD of the film which showed complete exfoliation. Perhaps the concentration of 8MR-AlPO particles is not sufficient to lead to scattering in the composite films.

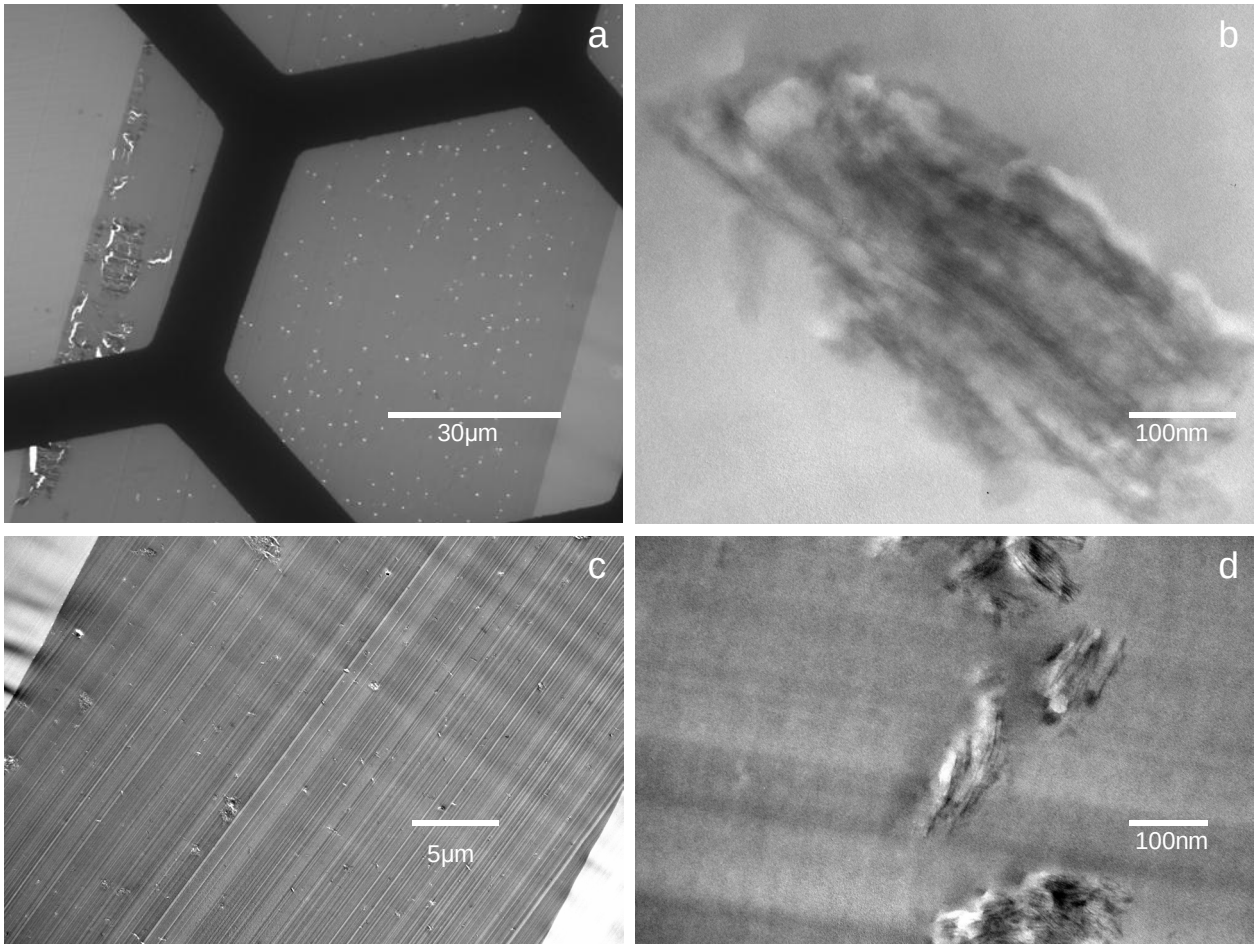

Figure 6.6 TEM images of PEI-8MR-AlPO composites. a) PEI-$CMTA^+$ film cross section b)PEI-$CMTA^+$ particle close up c)PEI-$12COOH^+$ film cross section d) PEI-$12COOH^+$ particle close up.

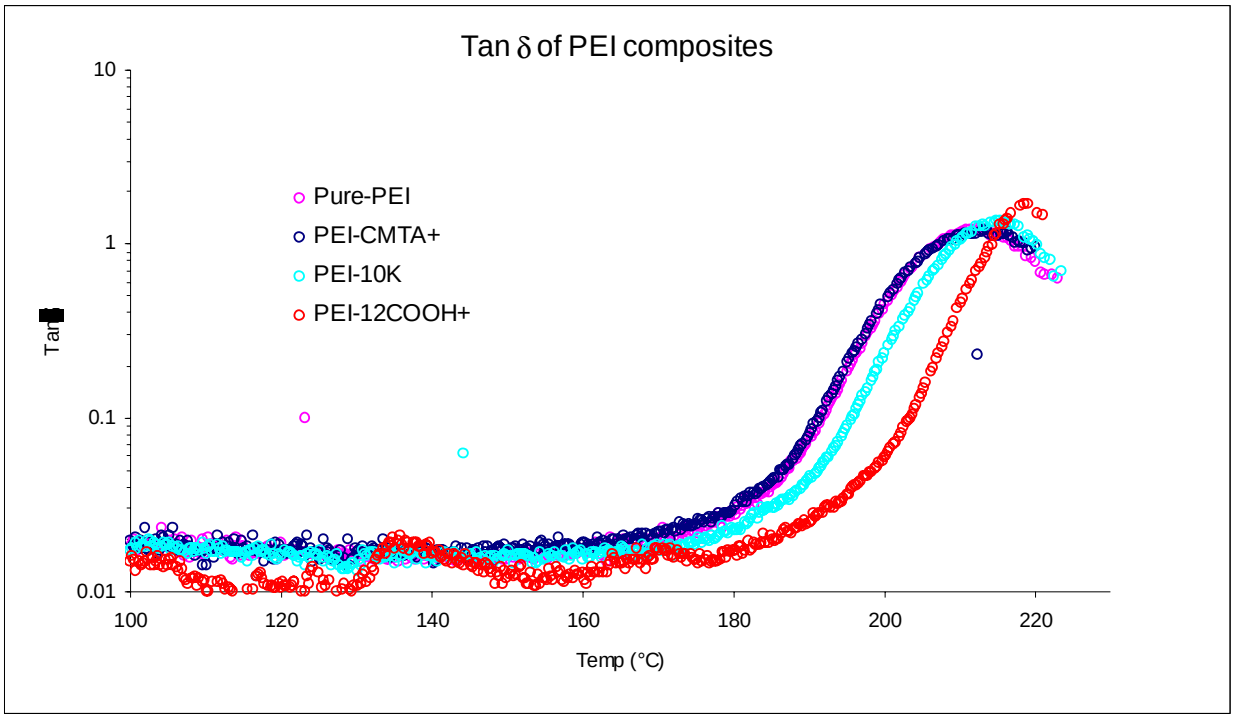

Figure 6.7 DMTA of PEI composites

The mechanical properties of the synthesized PEI and PEI-8MR AlPO composites were tested using a DMTA. The tan delta lines can be seen in Figure 6.7. The starting storage modulus values were similar for all of the films. The pure PEI was 1.8 x 10^9 Pa (not pictured) and all the composite values were around 1.7 x 10^9 Pa. The tan delta line is the ratio of the storage and loss modulus. The peak of this line can be used to determine the glass transition temperature (T_g) of a polymer. It can be seen in Figure 6.7 that the glass transition temperatures of pure PEI and the PEI-8MR AlPO composites fall in a fairly tight range. The glass transition of the membranes from the data is 212°C for pure PEI, 214°C for PEI-CMTA$^+$, 215°C for PEI-10K, and 219°C for PEI-12COOH$^+$. The consistency of the glass transition temperatures indicates that each synthesized batch has similar mechanical properties. Though M_W could not be measured for the composites the mechanical data indicates the polymer properties are comparable. The composites show very modest mechanical enhancement as a result of the

incorporation of 8MR-AlPO. The greatest increase in T_g was seen in the PEI-12COOH$^+$ composite. This is consistent with the TEM images, which showed that this composite had the best dispersion and the smallest tactoids when compared with the other membranes. Mechanical enhancement is one way to support an argument for molecular dispersion of PCN particles. The increase in T_g seen here is small but may indicate some of the platelets are dispersed at a molecular level. The T_g's of the other two composites PEI-10K and PEI-CMTA$^+$ were similar as expected because they both contain cetyltrimethyl ammonium swollen 8MR-AlPO. The only difference is that the inorganic in PEI-10K was primed with a low molecular weight PEI. Finally, the tan delta line for PEI-10K is shifted slightly to the right suggesting there may be better interaction between 8MR-AlPO and the polymer matrix as a result of priming the particle with low molecular weight polymer.

The permeability values for pure PEI and the three PEI composites are reported in Table 6.1. A scan from left to right across Table 6.1 for each gas species indicates that the permeability is affected very little by the addition of 5wt% of 8MR-AlPO. It was expected that there may be some preferential permeation of small gas species such as He and a barrier effect for large gases like CH_4. Different surface treatments were used on 8MR-AlPO in hopes that the monomers of PEI would intercalate and exfoliate individual microporous sheets into the matrix. The desired selectivity effect, however, was not seen in any of the in-situ composites. The permeability values for pure PEI are shown in the far left column of Table 6.1 and the ideal selectivity values are shown in Table 6.2. The values of the pure synthesized PEI are close to permeabilities and ideal selectivity for commercial PEI reported in literature.[18] With the other data collected on the pure polymer including the molecular weight of 66K and the T_g from DMTA, it appears that the synthesis was successful and that high quality polymer was fabricated.

The permeability values for the composites containing 5wt% 8MR-AlPO were similar to those of pure PEI. The PEI-$COOH^+$ composite matched closely the permeability properties of pure PEI. The permeabilities of the individual gas species are slightly higher when compared to the pure PEI. This can be seen by looking at the calculated aspect ratio values recorded in Table 6.1. These values were calculated using Equation 1 below developed by Cussler.[19]

$$\frac{P_o}{P_c} = 1 + \frac{\alpha^2 \phi^2}{1 - \phi} \qquad (1)$$

Where P_o is the permeability of the pure polymer, P_c is the permeability of the composite, α is the aspect ratio of the flakes, and ϕ is the volume fraction of flakes.

The aspect ratio is calculated using a ratio of permeabilities and is an indication of how well the inorganic is acting as a barrier to gas diffusion. It is an easy way to evaluate an experiment of this type. The larger the value, the better a barrier the inorganic material is to diffusion. In this case the aspect ratio is zero for all gas species except N_2 which means there is no barrier effect from the addition of 8MR-AlPO for the other gases. The similarity to pure PEI is also reflected in the ideal selectivity data in Table 6.2. Many of the gas pairs have the same or slightly higher selectivities when compared with neat PEI. The TEM data showed this composite had the best dispersion with the smallest tactoids when compared to the other composites. Even though the tactoids appeared dispersed and DMTA indicated a mechanical enhancement, this did not result in a definitive selectivity increase for large gases over small gases. The PEI-10K and PEI-$CMTA^+$ composites performed in a similar manner with respect to selectivity changes. There was an overall drop in selectivity when these composites were compared with the pure PEI. The permeability did drop in the composites for He when compared to pure PEI. The other gas species were largely unaffected by 8MR-AlPO as reflected in the α values reported in Table 6.1.

Table 6.1 Permeability and calculated aspect ratio values for PEI 8MR-AlPOcomposites

	Permeability of In-situ PEI & 5wt% AlPO				Calculated Effective α		
	Pure PEI	PEI-CTMA$^+$	PEI-12COOH$^+$	PEI-10K Oligomer	α-CTMA$^+$	α-12COOH$^+$	α-10K
He	8.17	6.91	8.18	7.35	21	0	17
CO_2	0.99	1.03	1.12	1.11	0	0	0
O_2	0.32	0.30	0.33	0.33	13	0	0
N_2	0.05	0.05	0.05	0.05	2	18	0
CH_4	0.03	0.03	0.03	0.04	0	0	0

Table 6.2 Ideal selectivity values for PEI 8MR-AlPO composites

	Ideal Selectivity of In-situ PEI & 5wt% AlPO			
Gas pairs	Pure PEI	PEI-CTMA$^+$	PEI-12COOH$^+$	PEI-10K Oligomer
He/O_2	25.4	22.1	24.9	22.9
He/N_2	156.9	137.8	176.3	132.8
He/CH_4	266.4	204.6	260.9	205.0
He/CO_2	8.2	6.6	7.3	6.7
O_2/N_2	6.2	6.2	7.1	5.8
O_2/CH_4	10.5	9.3	10.5	9.0
N_2/CH_4	1.7	1.5	1.5	1.5
CO_2/O_2	3.1	3.3	3.4	3.4
CO_2/N_2	19.0	20.8	24.1	19.8
CO_2/CH_4	32.3	30.9	35.7	30.5

6.4 Conclusions

The 8MR-AlPO was successfully intercalated with two surfactants and coated with low molecular weight PEI in one case. In-situ PEI-8MR AlPO composites with good mechanical properties were fabricated. Although XRD patterns showed no peaks for the PEI-composites TEM revealed that there was a significant amount of aluminophosphate not exfoliated in each composite. The 8MR-AlPO modified by $COOH^+$ showed the best dispersion from TEM and the highest Tg of all the films however only slight selectivity enhancements were seen for small gases over large gases. The other two composites based on $CMTA^+$ modified 8MR-AlPO showed a reduction in selectivity when compared to the pristine polymer.

(1) Kornmann, X.; Berglund, L. A.; Thomann, R.; Mulhaupt, R.; Finter, J., High performance epoxy-layered silicate nanocomposites. *Polymer Engineering and Science* **2002,** 42, (9), 1815 - 1826.

(2) Ryu, J. G.; Kim, H.; Lee, J. W., Characteristics of polystyrene/polyethylene/clay nanocomposites prepared by ultrasound-assisted mixing process. *Polymer engineering and science* **2004,** 44, (7), 1198 - 1204.

(3) Yano, K.; Usuki, A.; Okada, A., Synthesis and properties of polyimide-clay hybrid films. *Journal of Polymer Science, Part A: Polymer Chemistry* **1997,** 35, (11), 2289-2294.

(4) Lan, T.; Kaviratna, P. D.; Pinnavaia, T. J., On the Nature of Polyimide-Clay Hybrid Composites. *Chemistry of Materials* **1994,** 6, (5), 573-5.

(5) Vaughan, B.; Eva, M., Polymer [Al3P4O16]3- composites for gas separations utilizing simple mixing in organic solvent systems. **2007**.

(6) Yang, Y.; Zhua, Z.-k.; Yina, J.; Wang, X.-y.; Qi, Z.-e., Preparation and properties of hybrids of organo-soluble polyimide and montmorillonite with various chemical surface modification methods. *Polymer* **1999,** 40, (15), 4407-4414.

(7) Zhu, Z.-K.; Yang, Y.; Yin, J.; Wang, X.-Y.; Ke, Y.-C.; Zong-Neng, Preparation and Properties of Organosoluble Montmorillonite/Polyimide Hybrid Materials. *Journal of Applied Polymer Science* **1999,** 73, (11), 2063-2068.

(8) Gu, A.; Kuo, S.-W.; Chang, F.-C., Syntheses and properties of PI/clay hybrids. *Journal of Applied Polymer Science* **2001,** 79, (10), 1902-1910.

(9) Jeong, H.-K.; Krych, W.; Ramanan, H.; Nair, S.; Marand, E.; Tsapatsis, M., Fabrication of Polymer/Selective-Flake Nanocomposite Membranes and Their Use in Gas Separation. *Chemistry of Materials* **2004,** 16, (20), 3838 -3845.

(10) Morgan, A. B.; Gilman, J. W.; Jackson, C. L., Characterization of the Dispersion of Clay in a Polyetherimide Nanocomposite. *Macromolecules* **2001,** 34, (8), 2735-2738.

(11) Gao, Q.; Li, B.; Chen, J.; Li, S.; Xu, R.; Williams, I.; Zheng, J.; Barber, D., Nonaqueous Synthesis and Characterization of a New 2-Dimensional Layered Aluminophosphate [Al3P4O16]3-· 3[CH3CH2NH3]+. *Journal of solid state chemistry* **1997,** 129, (1), 37-44.

(12) Vaughan, B.; Marand, E., Characterization of swollen $[Al_3P_4O_{16}]^{3-}$ $3[NH_3CH_2CH_3]^{3+}$ in preparation for polymer-aluminophosphate nanocomposite fabrication. *Chemistry of Materials* **2007,** Submitted.

(13) Mahajan, R.; Koros, W. J., Factors Controlling Successful Formation of Mixed-Matrix Gas Separation Materials. *INDUSTRIAL & ENGINEERING CHEMISTRY RESEARCH* **2000,** 39, (8), 2692-2696.

(14) Tyan, H.-L.; Liu, Y.-C.; Wei, K.-H., Thermally and Mechanically Enhanced Clay/Polyimide Nanocomposite via Reactive Organoclay. *Chemistry of Materials* **1999,** 11, (7), 1942-1947.

(15) Tyan, H.-L.; Leu, C.-M.; Wei, K.-H., Effect of Reactivity of Organics-Modified Montmorillonite on the Thermal and Mechanical Properties of Montmorillonite/Polyimide Nanocomposites. *Chemistry of Materials* **2001,** 13, (1), 222-226.

(16) Agag, T.; Koga, T.; Takeichi, T., Studies on thermal and mechanical properties of polyimide–clay nanocomposites. *Polymer* **2001,** 42, (8), 3399-3408.

(17) Kornmann, X. Synthesis and Characterization of Thermoset-Layered Silicate Nanocomposites. Lulea Tekniska Universitet, Luleå, Sweden, 2001.

(18) Vu, D. Q.; Koros, W. J.; Miller, S. J., Mixed matrix membranes using carbon molecular sieves I. Preparation and experimental results. *Journal of membrane science* **2003,** 211, (2), 311-334.

(19) Cussler, E. L.; Hughes, S. E.; William J. Ward, I.; Aris, R., Barrier membranes. *Journal of Membrane Science* **1988,** 38, (2), 161-174.

Chapter 7

Study of 8MR-AlPO vs 12MR-AlPO for enhancing the separation properties of polysulfone

7.1 Introduction

Several studies have been conducted in our laboratory on the gas transport properties of polymer-layered aluminophosphate $[Al_3P_4O_{16}]^{3-} \cdot 3[NH_3CH_2CH_3]^+$ (8MR-AlPO) composites. The first such study by Jeong et al. showed a large increase in selectivity for small gas species over large gas species when 8MR-AlPO was added to a hexa-fluorinated polyimide using solution intercalation.[1] The results showed an increase in selectivity of 240% for He/CH_4 and 200% for CO_2/CH_4 when compared to the neat polymer. Recent studies in our lab designed to obtain the same results using different polymers and 8MR-AlPO have not produced such promising increases in selectivity. The results of these experiments can be found in Ch 5-6 in this dissertation. The current work

will compare the transport properties of 8MR-AlPO-polysulfone composite and a polysulfone composite made with a layered aluminophosphate of the same type with 12MR openings that are much larger.

The theory behind the enhanced selectivity seen by Jeong et al. in their mixed matrix membranes was that small gas species could pass through the microporous sheets of 8MR-AlPO while large gas species had to take a tortuous path around the platelets. The diffusion of large gas species was, therefore, slowed to a greater extent producing an increase in selectivity when compared to the neat polymer. We have attempted several times to reproduce this work using solution intercalation with other polyimides. We have seen a reduction in permeability for all gases in some cases but not a substantial increase in selectivity. One possible explanation for our failure is that the ring openings of 8MR-AlPO (3.8-6.0 Å) are too small for even the smallest gas species to pass through. Jeong el al. tested five small gases with known kinetic diameters. The kinetic diameter of a gas is defined as the smallest zeolite window through which a particular species is known to pass. The five gases tested along with their kinetic diameters were He (2.6Å), CO_2 (3.3Å), O_2 (3.46Å), N_2 (3.64Å), and CH_4 (3.8Å). The size of 8MR-AlPO opening given above was determined by Gao et al. using single crystal XRD who solved the structure. The ring opening was measured from oxygen center to oxygen center.[2] The actual opening through which a gas species might pass is in reality much smaller. Therefore, we propose using a different aluminophosphate with a larger ring opening. We would like to determine if a selectivity increase can be obtained by dispersing a layered aluminophosphate with larger microporous openings (9.0 Å) in polysulfone.

The microporous layered aluminophosphate $[Al_3P_4O_{16}]^{3-}$ $\cdot 3[NH_3CH_2CH(OH)CH_3]^+$ (12MR-AlPO) has a very similar structure to 8MR-AlPO.[3] They are both in the layered aluminophosphate family with Al/P ratios of 3/4. The main difference between the two is in the net structure of the layers. The 12MR-AlPO has a 4 x 6 x 12 net as opposed to the 4 x 6 x 8 net of 8MR-AlPO. A picture of the microstructure of the two types of AlPO can be seen in Figure 7.1. The shape of the largest ring openings is another difference between the two AlPO's. 12MR-AlPO contains a twelve membered ring with a circular shape while 8MR-AlPO has an oval shaped eight membered ring opening. Estimating the size of the openings with the CAChe program showed that the 12MR is around 6.5Å in diameter while the 8MR-AlPO opening has a size of 3.3 x 4.5Å. Another difference between the AlPO's is the gallery ion. In this class of materials the structure directing agent (SDA) used in the synthesis often becomes the counterion in the gallery space of the layered aluminophosphate. For example the SDA in the 8MR-AlPO is ethylamine which becomes the counterion ethylammonium located in the gallery space of the final structure. The SDA isopropanolamine in the 12MR-AlPO becomes isopropanolammonium in the gallery space of the final structure. These counterions balance the negative charge on the AlPO platelets and hold the sheets together through a complex hydrogen bonding network. We believe that the counterions are similar enough that they can both be ion exchanged using the same procedure.

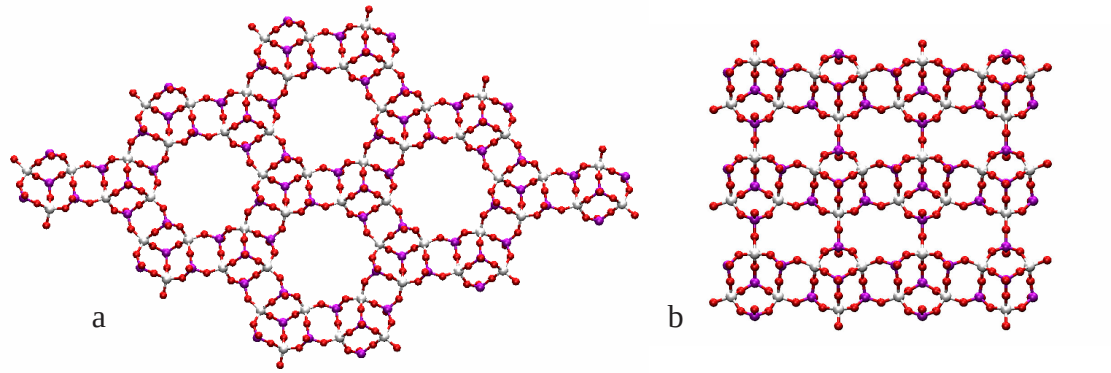

Figure 7.1 a) microstructure of single platelet 12MR-AlPO b) microstructure of single platelet 8MR-AlPO

7.2 Experimental

UDEL-P3500 (polysulfone) from Solvay Advanced Polymers was used as the polymer matrix. The 8MR-AlPO $[Al_3P_4O_{16}]^{3-} \cdot 3[NH_3CH_2CH_3]^+$ was synthesized according to the procedure published by Gao et al.[2] Details of this synthesis can be found in chapter 3 of this dissertation. The 12MR-AlPO $[Al_3P_4O_{16}]^{3-} \cdot 3[NH_3CH_2CH(OH)CH_3]^+$ was provided by the research group of Dr. Michael Tsapatsis from the University of Minnesota. Both layered aluminophosphates were ion exchanged with cetyltrimethyl ammonium cations to prepare them for mixing with polysulfone. The specific ion exchange procedure for AlPO can be found in chapter 3 of this dissertation. The solvent used to disperse AlPO and dissolve polysulfone was 99+% anhydrous chloroform from Sigma-Aldrich.

All polysulfone AlPO composite membranes were fabricated in the same manner. The desired wt% of dry $CMTA^+$ AlPO was added to 2.8mL of chloroform and stirred at room temperature until dispersed. Then 0.5g of dried UDEL-P3500 was added to the mixture and stirred for 24 hours. The solution was then cast onto a level glass plate with a blade and covered with a glass dish to slow the evaporation of chloroform. After at

least 12 hours the film was pealed from the glass and placed in a vacuum oven for annealing. The membranes were annealed under full vacuum for 12 hours at 75°C, 2 hours at 125°C, two hours at 150°C, two hours at 175°C and finally 1 hour at 190°C. The membranes were then removed for transport measurement.

Single gas permeability measurements were carried out on a constant volume gas permeation apparatus utilizing the lag time method. Five small gases including He, O_2, N_2, CH_4, and CO_2 were measured. For measurement by TEM the composite membranes were embedded in epoxy and microtomed into thin slices. The membrane cross-sections were placed on 300 mesh copper grids and observed using a Jeol 100 CX-II at 100kV. Scanning Electron Micrographs (SEM) were taken with a LEO 1550 FESEM. X-ray diffraction (XRD) was used to characterize many of the samples. The 8MR-AlPO and 12MR-AlPO samples were tested on a Scintag XDS-2000. The samples were run using CuKα (λ = 1.5418 Å) radiation at 40mA and -45kV. Powder XRD was used to confirm structure of the AlPO's and the degree to which it was swollen. The composite membranes were scanned on both sides to determine the degree of exfoliation present in the composite.

7.3 Results and Discussion

Polysulfone is a well know industrially used gas separation polymer.[4] We determined polysulfone would be a good polymer to test the effects of AlPO. The permeability values for small gas species are available in the literature.[5, 6] Polysulfone has also been shown in the literature to be a good material for mixed matrix membranes.[7-9] We believe that the addition of microporous AlPO may enhance the gas selectivity of the polymer. For this reason 8MR-AlPO and 12MR-AlPO were dispersed in a UDEL P3500

matrix to determine if any changes in the gas selectivity could be measured. Composite membranes containing 2wt% and 5wt% of both aluminophosphates were fabricated using the solution intercalation method. Transport properties of the composites were measured along with TEM, XRD, and SEM to further characterize the membrane materials.

Both of the as-synthesized AlPO materials were ion exchanged with cetyltrimethyl ammonium to prepare the surface for mixing with polysulfone. The method successfully used by Jeong et al. was followed.[1] The replacement of the gallery ions serves to expand the gallery space, aide in exfoliation of the material, and make the surface more organophilic. Scanning Electron Micrograms and X-ray diffraction were performed on the as-synthesize and treated aluminophosphates. The results are shown in Figure 7.2 and Figure 7.3.

To observe any physical changes in the aluminophosphate after ion exchange SEM were taken of the as-synthesized and swollen materials. In our past experiments with 8MR-AlPO we were able to observe a physical change in the crystals when the material was swollen with a surfactant. The bulk materials of both 8MR-AlPO and 12MR-AlPO showed a reduction in overall particle size after treatment with $CMTA^+$. Gao et al. reported that as-synthesized 8MR-AlPO crystals are rectangular in shape with dimensions of (40-60) x (45-75) x (80-120) μm. The SEM images of our material revealed the largest particles of as-synthesized 8MR-AlPO were 80 - 100μm in length while the largest particles after swelling with $CMTA^+$ were 10 - 20μm in length. A close up of an as-synthesized 8MR-AlPO is pictured in Figure 7.2a. The sides of the crystal are very smooth with very few features except some cracking caused by the electron beam of the SEM. In contrast, Figure 7.2b shows the layered nature of the material as a

result of swelling with $CMTA^+$. The basic shape of the crystal has remained intact but layers can now clearly be seen because the smaller ethylammonium ion was exchanged with the much larger cetyltrimethyl ammonium ion which expanded the gallery spaces. In a similar way the particle size of 12MR-AlPO was also reduced as a result of swelling with $CMTA^+$. The as-synthesized rhombohedral crystals of 12MR-AlPO had a diameter of 150μm on average. After swelling with $CMTA^+$ the original crystal shapes were no longer visible and the resulting plate like particle sizes were reduced to 10 - 20μm in length. An as-synthesized rhombohedral crystal of 12MR-AlPO with smooth sides can be seen in Figure 7.2c. The side of one of the particles resulting from swelling 12MR-AlPO with $CMTA^+$ is shown in Figure 7.2d. The layered nature of the material can be observed after swelling due to the expansion of the gallery space.

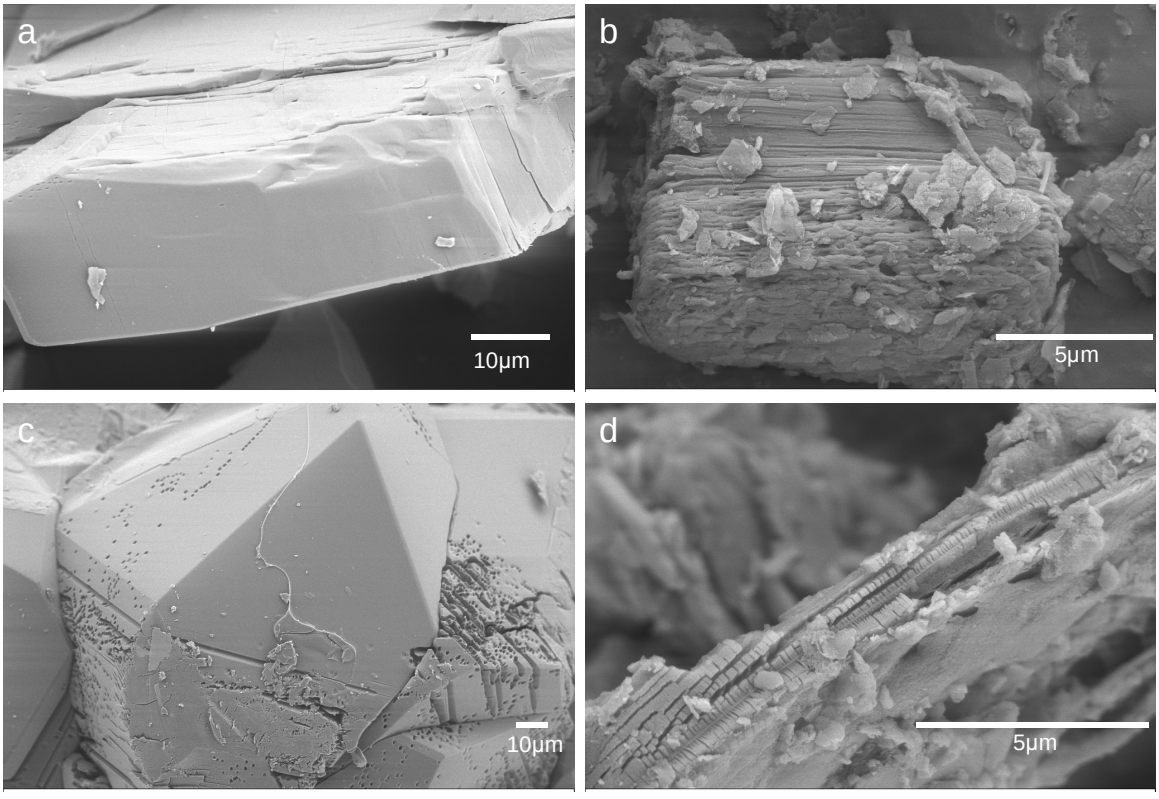

Figure 7.2 SEM of a) as-synthesized 8MR-AlPO crystal, b)8MR-AlPO swollen with $CMTA^+$, c) as-synthesized 12MR-AlPO, d) 12MR-AlPO swollen with $CMTA^+$

The XRD results of as-synthesized and treated layered aluminophosphate can be seen in Figure 7.3a – b. The XRD results confirm what was seen in the SEM images. Figure 7.3a shows the characteristic peaks of as-synthesized 8MR-AlPO with the d_{001} peak located around $2\theta = 9.8°$. In the same figure the 8MR-AlPO swollen with $CMTA^+$ is plotted. The 001 peak has shifted to the left and is located at a value of $2\theta = 2.7°$. Using Bragg's equation the d_{001} spacing can be found to be 33 Å. The gallery space has therefore been expanded which indicates $CMTA^+$ molecules are now present in the gallery of 8MR-AlPO. The XRD pattern for as-synthesized 12MR-AlPO can be seen in Figure 7.3b and the characteristic 003 peak can be seen at $2\theta = 9.9°$. The unit cell of 12MR-AlPO contains three layers therefore the d_{003} spacing is of interest. Using Bragg's law the d_{003} spacing is calculated to be 8.9 Å. A movement of this peak to the left would indicate an increase in the gallery spacing. As can be seen in Figure 7.3b the XRD pattern of 12MR-AlPO treated with $CMTA^+$ showed no peaks indicating that the layers of the material have lost all periodicity. The SEM pictures of this material showed plate-like structures with layers visible in the sides. The data taken, while not conclusive, suggests that the material is exfoliated after swelling with $CMTA^+$.

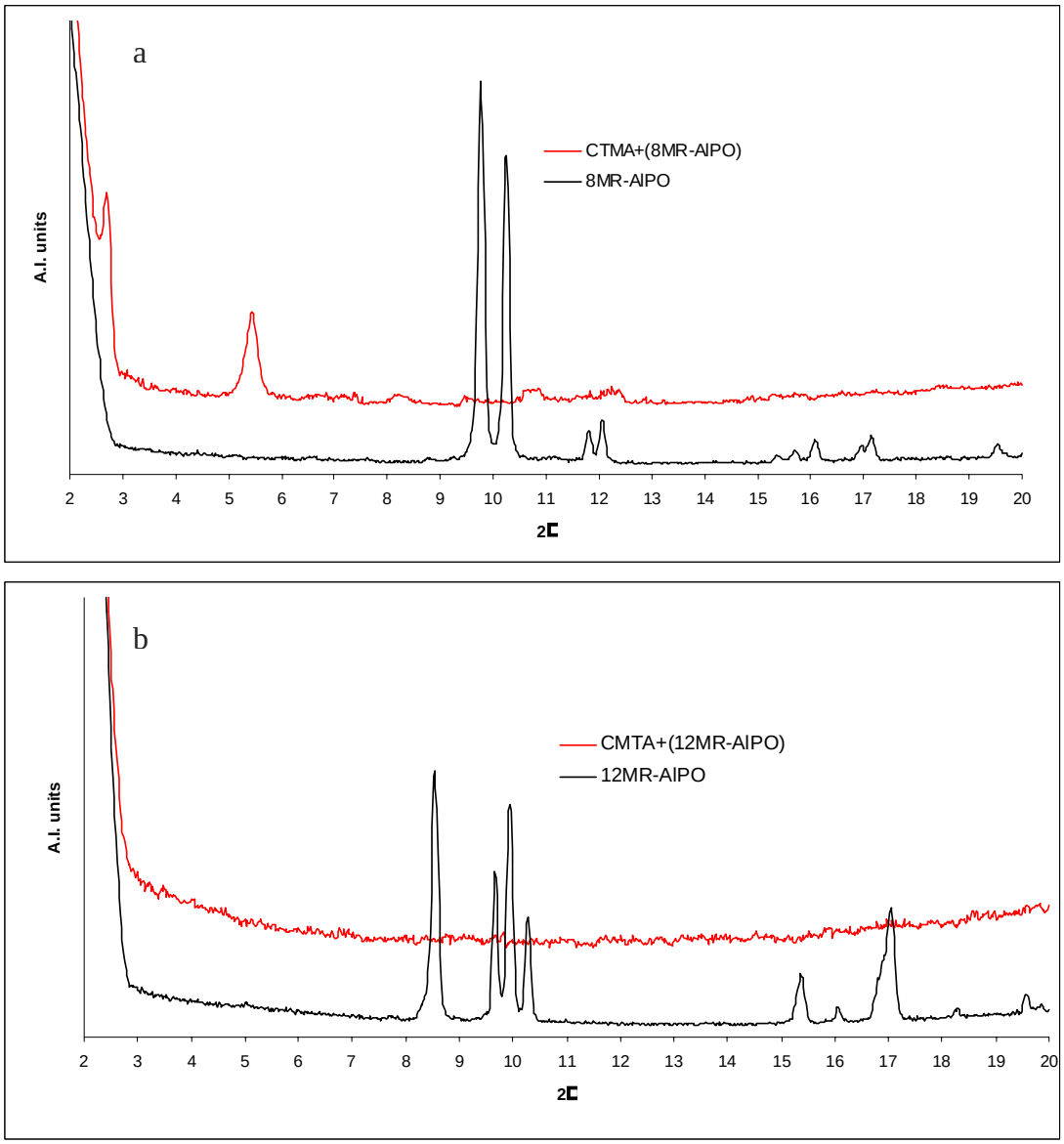

Figure 7.3 a) XRD pattern of as-synthesized 8MR-AlPO and $CMTA^+$ swollen 8MR-AlPO b) XRD pattern of as-synthesized 12MR-AlPO and $CMTA^+$ swollen 12MR-AlPO

The XRD patterns for the polysulfone AlPO composites reflected the XRD results of the powder patterns. The pattern of pure polysulfone can be seen in Figure 7.4 to be featureless except for the amorphous hump around a two theta value of 18°. The patterns of 2wt% and 5wt% 12MR-AlPO also showed featureless XRD patterns. This is an indication that the material is exfoliated in polysulfone, however, we know the XRD

powder pattern of $CMTA^+$ 12MR-AlPO was also featureless. For this reason TEM images are needed to confirm the actual dispersion of 12MR-AlPO in the bulk. The 8MR-AlPO composite membranes showed a small peak at $2\theta = 4.1°$. This peak is broader than that seen in the powder pattern and the peak height increases with wt%. The two theta value corresponds to a d_{001} spacing of 21.5 Å. The d_{001} spacing in the composite is smaller than the spacing measured for swollen 8MR-AlPO but larger than the spacing measure for as-synthesized 8MR-AlPO. This is evidence that 8MR-AlPO remained intercalated with $CMTA^+$, however, the polysulfone does not seem to have intercalated into the gallery space.

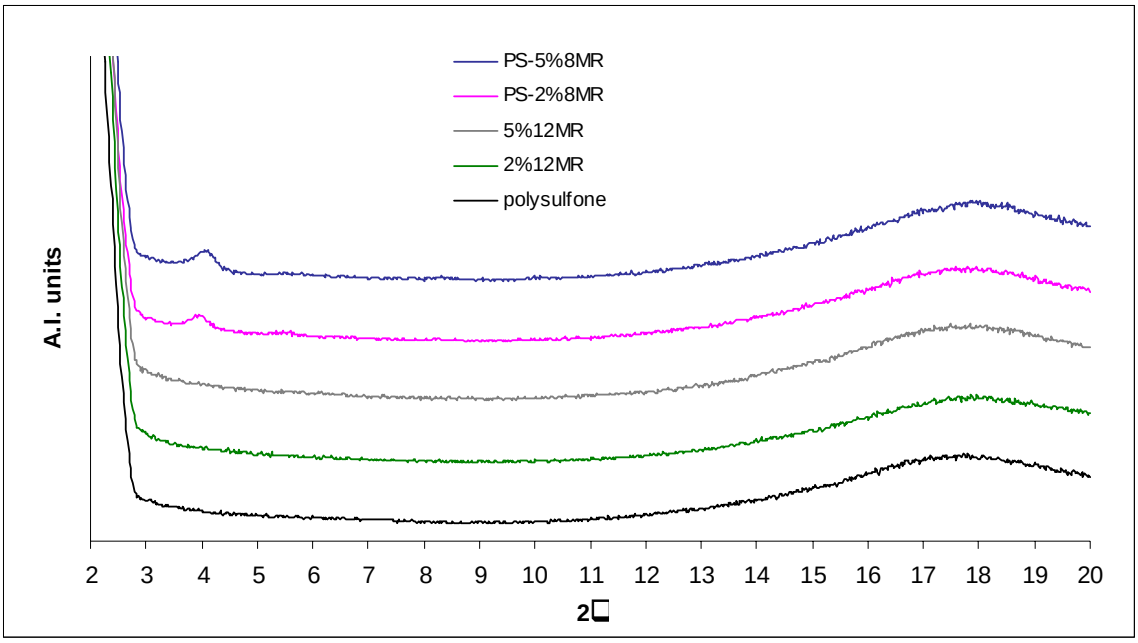

Figure 7.4 XRD patterns of polysulfone membranes and the composite membranes containing 8MR-AlPO and 12MR-AlPO.

Some selected pictures from TEM images of the 5wt% 12MR-AlPO and 5wt% 8MR-AlPO polysulfone composites are shown in Figure 7.5 a-d. The 12MR-AlPO composite TEM cross section showed large particles suspended in the matrix with smaller particles in between. The largest particles were in the range of 3 – 5 μm and the

smaller particles were in the nanometer range. Some examples of these particles can be seen in Figure 7.5 c – d. The particles were dispersed; however, the large particles dominated the field of view in the pictures. We made a lot of effort to find particles where layering could be seen but were unable to find any. We were hoping to confirm that the platelet like particles placed in the matrix were exfoliated but the TEM did not confirm the XRD results. The cross-section of the 8MR-AlPO composites showed a similar distribution with a slightly smaller particle sizes. The largest particles were in the 1 -3 μm range and the smaller particles were in the nanometer range. Figure 7.5a shows some of the bulk material with the larger particles visible. Figure 7.5b is a close up of one of the particles found in the matrix. Some layers of 8MR-AlPO can be identified by dark lines with light lines indicating the gallery spaces in between. The spacing between the layers is consistent with a value of 2 nm which was seen in the XRD pattern of this composite. This particle is an example of a largely intact tactoid intercalated with $CMTA^{+}$.

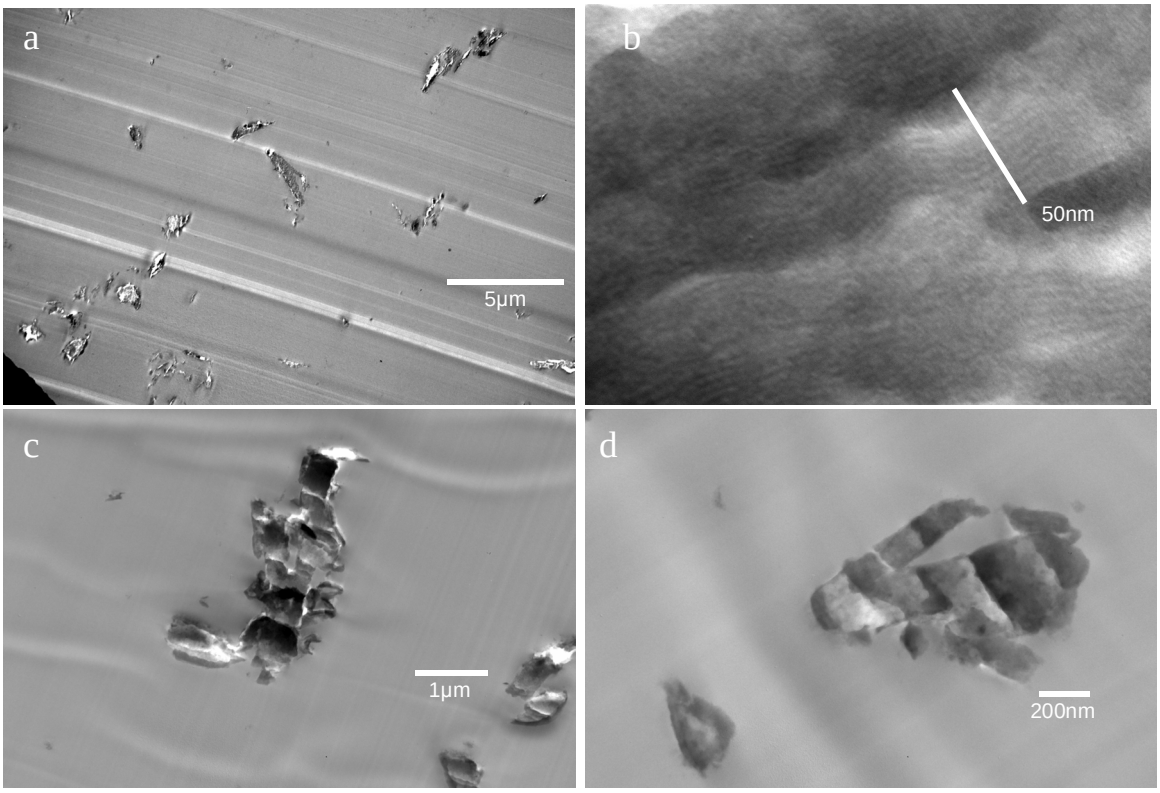

Figure 7.5 TEM images of a) bulk view of 5wt% 8MR-AlPO polysulfone composite b) close up particle in 5wt% 8MR-AlPO polysulfone composite c) large particle in 5wt% 12MR-AlPO polysulfone composite d) close up of a particle in 5wt% 12MR-AlPO polysulfone composite

The main goal of this work is to measure changes in the permeability of the polymer aluminophosphate composite membranes. The results of the transport data for all of the composites are summarized in Table 7.1 and Table 7.2. Five small gas species including He, O_2, N_2, CH_4, and CO_2 were tested on a constant volume permeability apparatus. Table 7.1 also contains the aspect ratios calculated using an equation developed by Edward Cussler and mentioned in previous chapters. The permeability values for pure UDEL are similar to values found in literature. As expected the permeability decreased with the addition of 2wt% and 5wt% 8MR-AlPO and the permeability was lowest when 5wt% 8MR-AlPO was used. The calculated aspect ratios shown on the right side of Table 7.1 indicate how efficient AlPO acted as a barrier to gas

transport. The higher aspect ratio values for the 2wt% composite show that AlPO was more effective as a barrier than in the 5wt% composite. This same trend can be seen in the 12MR-AlPO composite membranes. The aspect ratio numbers for the 2wt% composite are around 60 for most gas species and 0 for the 5wt% composite. This could be a result of better dispersion of AlPO at the 2wt% loading and some particle aggregation at the 5wt% loading. The drop in permeability for the 2wt% 12MR-AlPO composite was the greatest of all the composites fabricated. The XRD data indicated that this sample was exfoliated which could have lead to the increased decrease in permeability.

The ideal selectivity was calculated and recorded in Table 7.2. It was hoped that the addition of one of the AlPO's would increase selectivity for small gas species over large gas species. The 2wt%, 5wt% 8MR-AlPO and 2wt% 12MR-AlPO composites showed modest selectivity increases for the He/O_2, He/N_2, He/CH_4, and He/CO_2 gas pairs. While this is the effect we were looking for, the improvements were much smaller than those seen by Jeong et al. The other gas pair selectivities were for the most part unaffected by the addition of AlPO to the matrix.

Table 7.1 Permeability and effective aspect ratio for the 8MR and 12MR AlPO polysulfone composite membranes

	Polysulfone & $CTMA^+$ 8MR and 12MR AlPO					Calculated aspect ratio α			
	Pure PS	2%-8MR	5%-8MR	2%-12MR	5%-12MR	α-2%-8MR	α-5%-8MR	α-2%-12MR	α-5%-12MR
He	13.44	13.00	12.12	12.07	13.52	24	18	48	0
CO_2	7.16	6.50	6.07	6.05	7.17	42	22	61	0
O_2	1.56	1.42	1.34	1.32	1.57	41	21	61	0
N_2	0.28	0.26	0.25	0.24	0.29	38	20	60	0
CH_4	0.31	0.29	0.28	0.26	0.31	42	20	63	5

Table 7.2 Ideal selectivity for the 8MR and 12MR AlPO polysulfone composite membranes

Ideal Selectivity for 8MR & 12MR $CTMA^+$ AlPO					
Gas pairs	Pure PS	2%-8MR	5%-8MR	2%-12MR	5%-12MR
He/O_2	8.60	9.13	9.01	9.18	8.64
He/N_2	47.33	49.63	48.84	50.10	47.09
He/CH_4	42.76	45.59	43.88	46.11	43.40
He/CO_2	1.88	2.00	2.00	2.00	1.89
O_2/N_2	5.50	5.43	5.42	5.46	5.45
O_2/CH_4	4.97	4.99	4.87	5.02	5.03
N_2/CH_4	0.90	0.92	0.90	0.92	0.92
CO_2/O_2	4.59	4.57	4.52	4.60	4.58
CO_2/N_2	25.22	24.80	24.48	25.10	24.98
CO_2/CH_4	22.79	22.79	21.99	23.10	23.03

7.4 Conclusions

Composites of polysulfone with 12MR-AlPO and 8MR-AlPO were successfully fabricated. XRD results indicated that the 12MR-AlPO may have been fully exfoliated in the polysulfone but TEM showed that large particles were still present in the matrix. XRD and TEM of the 8MR-AlPO polysulfone composites indicated that the polysulfone did not intercalate the gallery spaces of AlPO. Finally, the permeability measurements showed that both 8MR and 12MR AlPO acted as a barrer to gas transport. The selectivities of some gas pairs showed a modest improvement but the gains were less than what should have been seen if the desired effect was achieved.

(1) Jeong, H.-K.; Krych, W.; Ramanan, H.; Nair, S.; Marand, E.; Tsapatsis, M., Fabrication of Polymer/Selective-Flake Nanocomposite Membranes and Their Use in Gas Separation. *Chemistry of Materials* **2004,** 16, (20), 3838 -3845.

(2) Gao, Q.; Li, B.; Chen, J.; Li, S.; Xu, R.; Williams, I.; Zheng, J.; Barber, D., Nonaqueous Synthesis and Characterization of a New 2-Dimensional Layered Aluminophosphate [Al3P4O16]3-· 3[CH3CH2NH3]+. *Journal of solid state chemistry* **1997,** 129, (1), 37-44.

(3) Yuan, H.-M.; Zhu, G.-S.; Chen, J.-S.; Chen, W.; Yang, G.-D.; Xu, R.-R., Dual Function of Racemic Isopropanolamine as Solvent and as Template for the Synthesis of a New Layered Aluminophosphate: [NH3CH2CH(OH)CH3]3·Al3P4O16. *Journal of solid state chemistry* **2000,** 151, (1), 145-149.

(4) Baker, R. W., Future Directions of Membrane Gas Separation Technology. *Industrial & engineering chemistry research* **2002,** 41, (6), 1393 -1411.

(5) Kim, I.-W.; Lee, K. J.; Jho, J. Y.; Park, H. C.; Won, J.; Kang, Y. S.; Guiver, M. D.; Robertson, G. P.; Dai, Y., Correlation between Structure and Gas Transport Properties of
Silyl-Modified Polysulfones and Poly(phenyl sulfone)s. *Macromolecules* **2001,** 34, 2908-2913.

(6) Dai, Y.; Guiver, M. D.; Robertson, G. P.; Kang, Y. S.; Lee, K. J., Enhancement in the Gas Permeabilities of Novel Polysulfones with
Pendant 4-Trimethylsilyl-R-hydroxylbenzyl Substituents. *Macromolecules* **2003,** 36, 6807-6816.

(7) Reid, B. D.; Ruiz-Trevino, F. A.; Musselman, I. H.; Jr., K. J. B.; Ferraris, J. P., Gas Permeability Properties of Polysulfone Membranes Containing the Mesoporous Molecular Sieve MCM-41. *Chemistry of Materials* **2001,** 13, 2366-2373.

(8) Wang, H.; Holmberg, B. A.; Yan, Y., Homogeneous polymer–zeolite nanocomposite membranes by incorporating dispersible template-removed zeolite nanocrystals. *Journal of Materials Chemistry* **2002,** 12, 3640 - 3643.

(9) Jiang, L. Y.; Chung, T. S.; Kulprathipanja, S., An investigation to revitalize the separation performance of hollow fibers with a thin mixed matrix composite skin for gas separation. *Journal of membrane science* **2006,** 276, 113–125.

Chapter 8

Final Conclusions and Future Work

As stated in the introduction to this dissertation, the objective of the current work was to fabricate polymer aluminophosphate mixed matrix membranes with improved selectively when compared with neat membranes of the same polymer. We attempted to follow the success of Jeong et al. by combining 8MR-AlPO with a variety of polymer materials using a simple solvent intercalation method. Our initial experiments included 8MR-AlPO modified with cetyltrimethyl ammonium. Composite membranes containing 8MR-AlPO and PDMS, 6FDA-6FpDA-20%PDMS, PSF, and CAB were successfully fabricated. These initial attempts did not produce the desired effect which was an increase in selectivity for small/large gas pairs such as He/CH_4. After the initial

experiments were unsuccessful a procedure was developed to swell 8MR-AlPO with several other surfactants. The purpose was to try and increase exfoliation and dispersion of 8MR-AlPO in the polyimide Matrimid or Cellulose Acetate. Mixed matrix membranes were fabricated but surface treatments chosen did not result in the desired increase in selectivity for the polymers used. We then tried an in-situ polymerization of PEI and 8MR-AlPO treated with a reactive surfactant. It was anticipated that the monomers would intercalate the gallery spaces of 8MR-AlPO and exfoliate the layers as the polymer polymerized. Microscopy, XRD and transport data confirmed that the in-situ method was no more effective at achieving the desired selectivity increase than the simple solvent intercalation. In general the permeability of the membranes containing 8MR-AlPO did show reduced permeability when compared to the neat polymers. This means that the 8MR-AlPO was acting as a barrier much like clay in polymer clay nanocomposites. The barrier phenomenon could be due to several things including blocking of the framework from the surfactant used to swell 8MR-AlPO. We made some attempts to remove the surfactant and recover the template using heat, ozone, and Soxhlet extraction. The 8MR-AlPO treated in this manner was dispersed in CAB and transport was measured. Even though TGA, and sorption measurements showed that at least some of the surfactant was removed from 8MR-AlPO the resulting mixed membranes did not show the desired selectivity increase. An attempt was also made to incorporate a 12MR-AlPO with larger framework openings into PSF but no sieving effect was observed.

Our inability to reproduce the selectivity improvements reported by Jeong et al. left an unanswered question; how were Jeong et al. able to produce such a dramatic effect using a very simple method on the first attempt? It is difficult to be certain exactly why

the results obtained were so different from the current work. However, some independent transport data for the polymer used in the study may provide a partial explanation. The polymer used in the Jeong et al. study was from the same batch of 56K 6FDA-6FpDA-8%DABA (P6F) synthesized by a former lab member Chris Cornelius. Some previously unchecked permeability data collected by Cornelius for this polymer was recorded on one of our laboratory computers. Tables 8.1 and 8.2 below contain the permeability and selectivity data reported by Jeong et al. and also includes the data for the pure polymer recorded by Cornelius. The data in table 8.1 shows that the permeability of P6F did decrease as 8MR-AlPO was added. The concern with the Jeong et al. data is that the pure polymer permeabilities are very different than those recorded by Cornelius. These two lines of interest are highlighted in red. The pure polymer permeabilities reported by Jeong et al. were much higher than those recorded by Cornelius. Keep in mind these polymer membranes are made from the same batch of polymer and measured on the same permeability apparatus. The selectivities reported by Jeong et al. are shown in Figure 8.2. The pure P6F selectivities reported by Jeong et al. are much lower than those recorded by Cornelius. The best selectivities reported by Jeong et al. and the pure P6F selectivities recorded by Cornelius are highlighted in yellow. A comparison of these two lines reveals that the best nanocomposite selectivities reported by Jeong et al. are very similar to the pure P6F permeabilities recorded by Cornelius. This new data is an indication that 8MR-AlPO reduced the permeability of P6F but resulted in little to no change in the selectivity. After examining the data reported by Jeong et al. we believe that they did not observe the desired molecular sieving effect.

Table 8.1 Permeability values for P6F reported by Jeong et al. and Cornelius

	Permeability (Barrers)				
	He	CO_2	O_2	N_2	CH_4
6FDA-6FpDA-8%-DABA 56K (Krych) **	178.8	83.7	36.3	10.1	6.2
PANC 5wt% mixed at 30°C	147.5	65.7	24.3	6.2	3.6
PANC 10wt% mixed at 30°C	94.4	51.2	18.5	2.1	1.2
PANC 10wt% mixed at 60°C	67.5	28.3	9.3	1.2	0.7
6FDA-6FpDA-8%-DABA 56K (Cornelius)	130.2	54.7	13.7	2.8	1.3

Table 8.2 Ideal selectivity values for P6F reported by Jeong et al. and Cornelius

	Ideal Selectivity									
	He/O_2	He/N_2	He/CH_4	He/CO_2	O_2/N_2	O_2/CH_4	N_2/CH_4	CO_2/O_2	CO_2/N_2	CO_2/CH_4
6FDA-6FpDA-8%-DABA 56K (Krych)	4.93	17.69	28.66	2.14	3.59	5.81	1.62	2.31	8.28	13.42
PANC 5wt% 30°C	6.07	23.99	41.56	2.25	3.95	6.85	1.73	2.70	10.68	18.50
PANC 10wt% 30°C	5.10	45.40	76.15	1.85	8.91	14.94	1.68	2.76	24.60	41.26
PANC 10wt% 60°C	7.29	54.85	96.37	2.39	7.53	13.23	1.76	3.05	22.98	40.39
6FDA-6FpDA-8%-DABA 56K (Cornelius)	9.53	46.17	97.16	2.38	4.84	10.19	2.10	4.00	19.38	40.79

Upon review of our work with 8MR-AlPO polymer composites it can be concluded that it is at least very difficult to create a molecular sieving membrane with this layered aluminophosphate using current methods. Most of the methods we employed to form nanocomposites with 8MR-AlPO were borrowed from the literature available for polymer clay nanocomposites (PCN). This could be a fatal flaw in our methods because 8MR-AlPO is a very different material when compared to traditional aluminosilicates used in the PCN literature. For example, the gallery space of montmorillonite (MMT) is populated by sodium ions held in place by electrostatic forces before it is ion exchanged with a surfactant. In contrast, the gallery space of 8MR-AlPO is populated with

ethylammonium ions which are hydrogen bonded in a complex network (Figure 2.11). This hydrogen bonding network appears to provide structure to the platelets of 8MR-AlPO. The sodium ions in MMT provide no structural support to the individual layers but the positioning of the ethylammonium ions in the 8MR-AlPO structure almost certainly provide support for the 8MR openings in the framework of the layers. It is unclear whether or not the removal of the ions in 8MR-AlPO would cause collapse of the 8MR openings we are counting on to provide separation properties. This is a non issue in PCNs where MMT serves as a barrier to diffusion and alteration of the structure unimportant. We think more fundamental work should be performed on the effects to the size and shape of the 8MR openings as a result of ion exchanging ethylammonium for larger surfactant ions. The forces involved in exfoliating MMT and 8MR-AlPO are likely very different. The hydrogen bonding network in the layers of 8MR-AlPO most certainly holds the layers together with more force when compared to the Na^+ ions of MMT which hold the plates together with a weaker electrostatic charge. We think it is therefore much easier to exfoliate MMT in solution when compared to 8MR-AlPO. Most of the composites we made showed poor exfoliation and dispersion of the individual platelets of 8MR-AlPO even though we followed many methods used to successfully exfoliate MMT in polymers. This is one reason why we cannot say for certain that 8MR-AlPO will never enhance separation. A fully exfoliated 8MR-AlPO in a polymer matrix is required to answer this question. Further, even if the layers are exfoliated, we are not convinced that the micropores of individual plates of 8MR-AlPO will not completely collapse if the hydrogen bonding network is removed. Literature is available on the exfoliation of 8MR-AlPO in aqueous systems; however, no work on the exfoliation of

8MR-AlPO in organic solvents is currently available. Work in this area is necessary before true 8MR-AlPO polymer nanocomposites can be formed with common engineering polymers. It is therefore our conclusion that polymer 8MR-AlPO membranes fabricated with the current methods will not result in an increase in selectivity of small gas species over larger gas species.

We have recently found a surfactant treatment that appears to exfoliate and disperse 8MR-AlPO better than the surfactant treatments we have used previously. We have always suspected that good dispersion of 8MR-AlPO could be achieved if the right solvent, surfactant, polymer system was chosen. This was the main reason we varied the surfactant treatment of 8MR-AlPO in several of our previous studies. Recently 8MR-AlPO was swollen with a two tailed surfactant mentioned in the literature review section of this dissertation. The treatment of 8MR-AlPO with dioctadecyldimethyl ammonium ($2M2HT^+$) and subsequent dispersion in polysulfone via chloroform resulted in favorable exfoliation. The dispersion and exfoliation was compared to 8MR-AlPO treated with the one tailed surfactant cetyltrimethyl ammonium ($CMTA^+$) which was also dispersed in polysulfone using chloroform as the solvent. Figure 8.1 a-b contains TEM images of the two composites and illustrates the differences in exfoliation and dispersion. Figure 8.1a is a composite of 5wt% $CMTA^+$ 8MR-AlPO dispersed in polysulfone. Large tactoids of 8MR-AlPO can be seen and the dispersion is poor. The particle shapes are block like with low aspect ratio which is not favored for the current project.

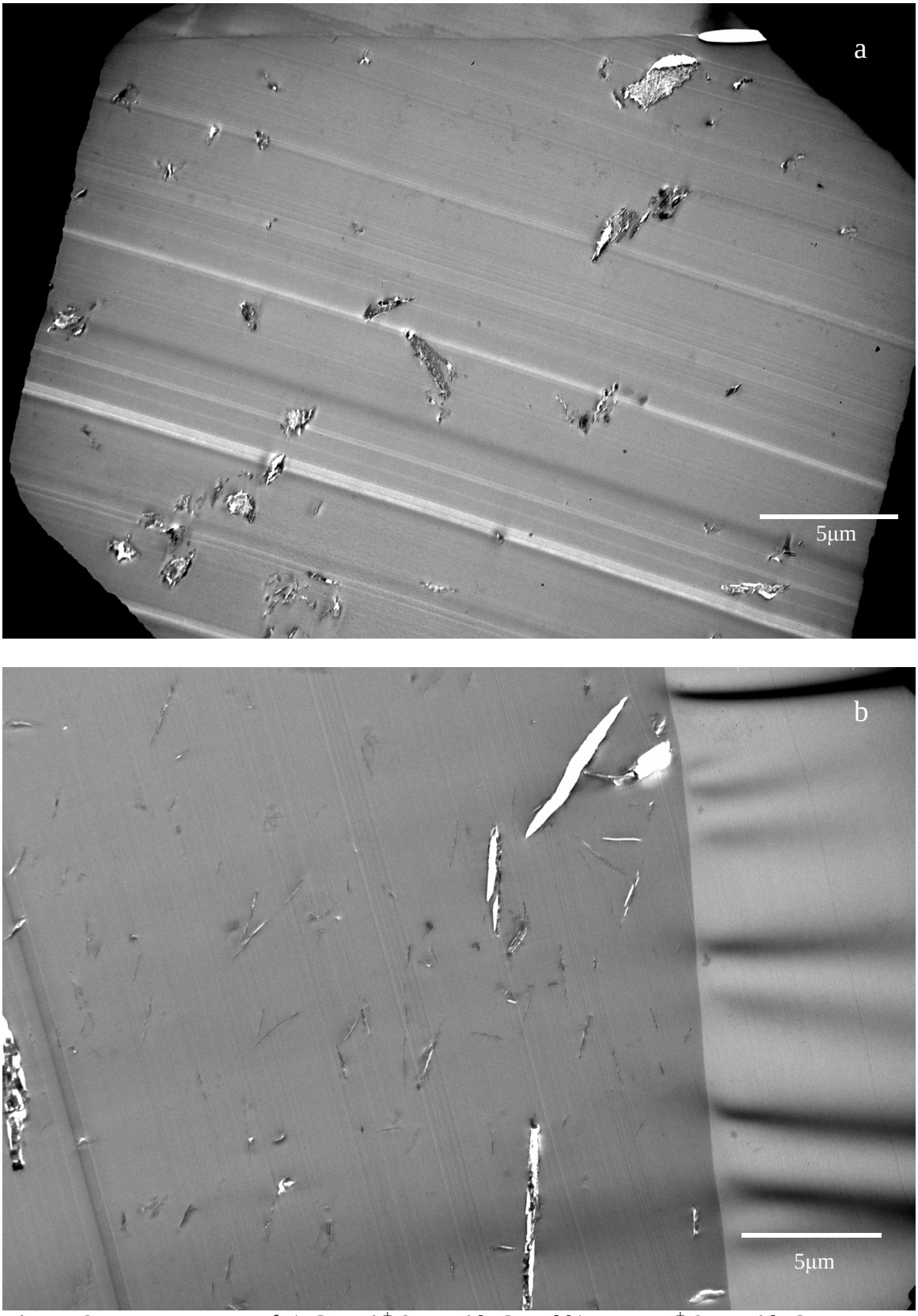

Figure 8.1 TEM images of a) $CMTA^+$ 8MR-AlPO and b) $2M2HT^+$ 8MR-AlPO polysulfone composite membranes

In contrast, Figure 8.1b shows 2wt% $2M2HT^+$ 8MR-AlPO dispersed in polysulfone using the same technique. A difference can be clearly seen. The particles are much longer and thinner and the dispersion appears more uniform. Some long thin tear out tracks can be seen where particles fell out during microtoming but many particles with large aspect ratio are still visible. This type of dispersion and exfoliation is favorable for the current application. Unfortunately the transport properties of membranes made with $2M2HT^+$ 8MR-AlPO and polysulfone were not improved. Even though there was good exfoliation the permeability increased and the selectivity dropped dramatically in this particular polymer. Efforts are currently under way to repeat the experiments with Matrimid as the polymer matrix.

Future research involving layered aluminophosphates to enhance gas selectivity should be focused on obtaining well exfoliated and dispersed nanoplatelets in polymer matrices. The improved dispersion and exfoliation mentioned above is proof that this material can be exfoliated with large aspect ratio if the right surface treatment and dispersing solvent can be matched. The next step is to find a polymer that is soluble in the dispersing solvent and chemically compatible enough with the surfactant to intercalate the gallery space and form a good bond between polymer and inorganic. Cationic polymers could be a useful route to exfoliate 8MR-AlPO because the platelets are negatively charged. We did some preliminary work in this area with a cationic butyl methacrylate derivative in THF but did not have any success. The polymer we were using contained only a small amount (5%) of charged groups and 8MR-AlPO was not swollen. Future work with an engineering polymer containing more cationic groups mixed with a swollen version of 8MR-AlPO could give better results. A plausible idea

we did not pursue also takes advantage of the negative charge on 8MR-AlPO. A cationic polymer and the negatively charged 8MR-AlPO could be combined using layer by layer deposition techniques to form a membrane. This method would only work if the 8MR-AlPO could be completely exfoliated in solution. Another possible direction could involve a water soluble cationic or nonionic polymer and 8MR-AlPO. It was mentioned in the literature review section of this dissertation that 8MR-AlPO could be exfoliated in aqueous systems. We did some preliminary work in this area using the polymer Chitosan. Chitosan is a water soluble cationic polymer with good film forming properties. We were able to disperse 8MR-AlPO in water utilizing ethylammonium as the exfoliating agent as mentioned in the literature section of this dissertation. We were also able to form composite films with Chitosan and 8MR-AlPO. We were however, unable to measure transport properties of these films because the inherent permeability of Chitosan is below the detection limits of our equipment. Because we know 8MR-AlPO can be dispersed in water, future work could involve good film forming polymers which are soluble in aqueous systems and possess measurable transport properties. The aqueous example would likely be only for proof of concept purposes because water is generally present in most separation applications and we are not aware of a method to spin water soluble polymers into hollow fiber membranes for actual use. We did not employ melt intercalation as a method to exfoliate 8MR-AlPO in a polymer matrix although the PCN literature has shown this to be a viable method. This technique could also be a route to exfoliate 8MR-AlPO and show proof of concept, for increased selectivity from the porous flakes.

Future experimental work

After discussing the results of this work with my committee several possible experiments that might advance this project to the next level emerged. All of the ideas were centered on manipulation and characterization of the inorganic component of the membranes.

One suggestion related to the sorption data collected on the 8MR-AlPO samples swollen with surfactant then treated with ozone and heating at 200°C to remove the surfactant. This treatment was the most effective of those tried and produced an increase in the sorption of most simple gases. The duration of the treatment was only 10 hours and it was suggested that a longer time may produce an even greater increases in sorption. A series of experiments could be performed where the duration of the heating is varied to determine the amount of time needed to produce the optimal sieve properties. The treated samples could be characterized with NMR to determine connectivity of the tetrahedra, XRD to asses the d-spacing and crystallinity of the material, TGA to quantify surfactant removal, and high resolution TEM to observe the porous nature of the flakes once calcined. Finally sorption of some simple gases could give insight into changes in transport properties resulting from the calcination process.

Another set of suggestions addressed the choice of surfactant used to swell 8MR-AlPO. It was suggested that DSC could be used as a probe to detect ordering of the swelling agent present in the gallery space. To reduce ordering of the surfactant in the gallery space it was suggested that a small inorganic molecule be intercalated along with a long alkyl chain surfactant. The addition of a small molecule should break up any potential ordering and allow for easier exfoliation of the platelets in solution. Another

idea discussed was to add a surfactant that survives high temperatures along with a surfactant that degrades at low temperatures. The idea involves swelling the gallery space with a combination of these surfactants and then removing the surfactant that degrades at low temperature with heating. The high temperature surfactant is anticipated to survive this process and keep the platelets separated until they could be exfoliated in solution. Along with these new treatments it was suggested that a method be developed to quantify how much surfactant is present on the 8MR-AlPO after swelling or subsequent treatments. It is believed that a method involving TGA could be used to accomplish this.

Appendix A: Chemical Structures and Nomenclature

Surfactants

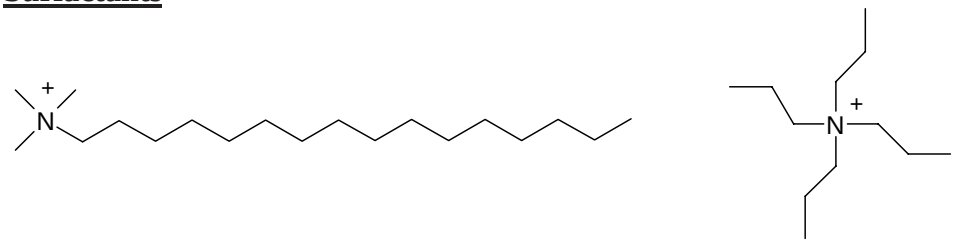

Cetyltrimethyl ammonium chloride 25 wt% solution in water, Aldrich
Tetra-n-propylammonium hydroxide 40% w/w aqueous, Alfa Aesar CAS# 4499-86-9

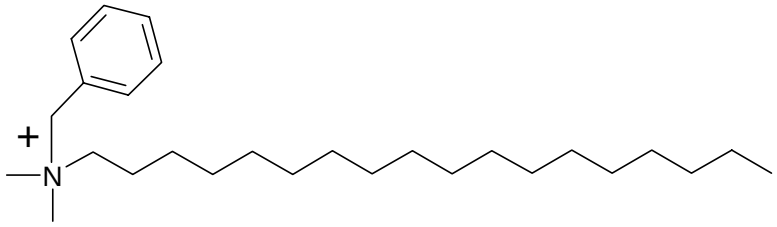

Octadecyldimethyl benzyl ammonium chloride, Pfaltz & Bauer inc, CAS# 122-19-0

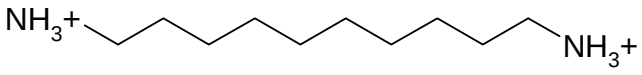

(Protonated) 1,12-diaminododecane 98%, Aldrich, CAS# 2783-17-7

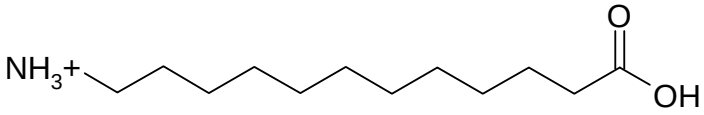

(Protonated) 12-Aminododecanoic acid 95%, Aldrich, CAS# 693-57-2

Polymers

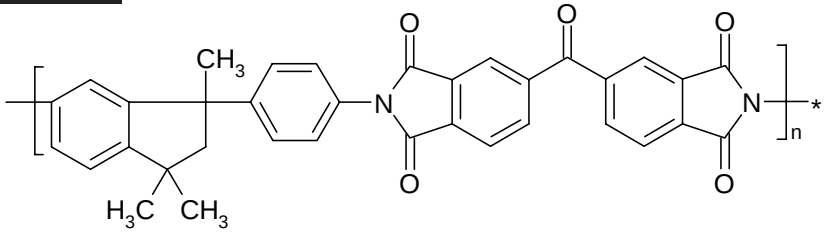

Matrimid© 5218, Vantico

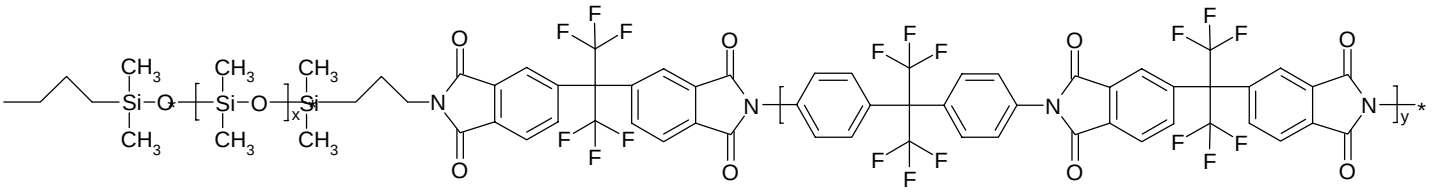

6FDA-6FpDA-PDMS co-polymer

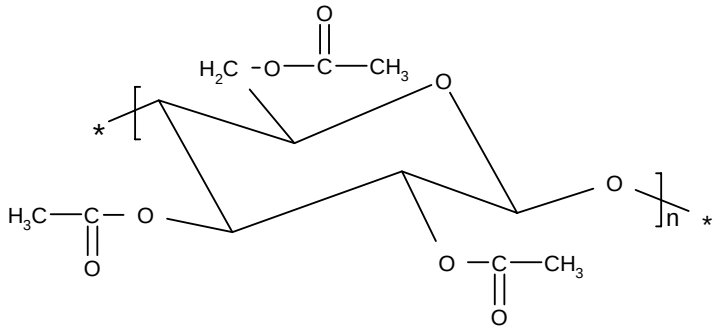

(CA) Cellulose acetate, CA-398-30, Eastman

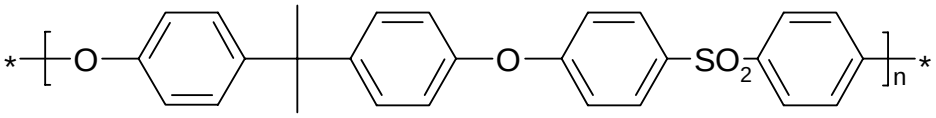

(PSF) Polysulfone, UDEL P-3500© Solvay Advanced Polymers

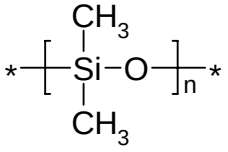

(PDMS) Polydimethylsiloxane, RTV615, GE Silicones

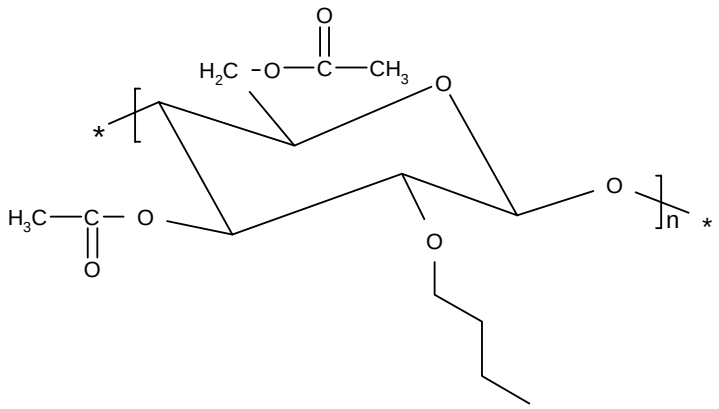

(CAB) Cellulose Acetate Butyrate, Sp^2-Scientific polymer products Inc., CAS# 9004-36-8

Solvents

(THF) Tetrahydrofuran Ultra Low Water, J.T. Baker, CAS# 109-99-9

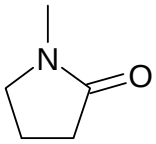

(NMP) 1-Methyl-2-pyrrolidone anhydrous 99.5%, Sigma Aldrich, CAS# 872-50-4

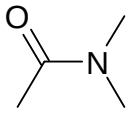

(DMAc) N,N Dimethylacetamide anhydrous 99.8%, Aldrich, CAS# 127-19-5

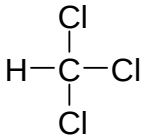

Chloroform anhydrous 99+%, Sigma Aldrich, CAS# 67-66-3

Reactants

8MR-AlPO

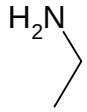

Ethylamine 70 wt% solution in water, Aldrich, CAS# 75-04-7

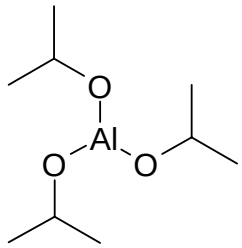

Aluminum Isopropoxide 98+%, Aldrich, CAS# 555-31-7

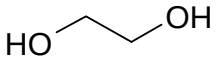

Ethylene Glycol, EM Science, CAS# 107-21-1

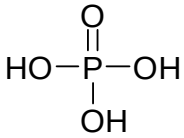

Phosphoric acid 85 wt%, Aldrich, CAS# 7664-38-2

Polyetherimide synthesis

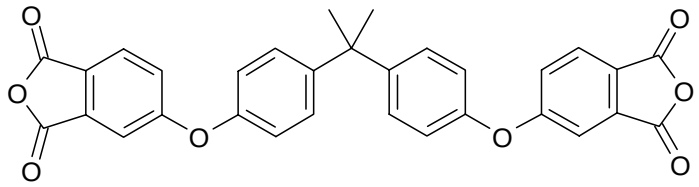

(BPADA) 4,4'-(4,4'-Isopropylidenediphenoxy) bis (phthalic anhydride) 97%, Aldrich, CAS# 38103-06-9 *used as received*

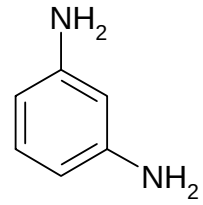

(MPD) m-Phenylene diamine flakes 99+%, Aldrich, CAS# 108-45-2 *used as received*

PDMS-6FDA-6FpDA co-polymer

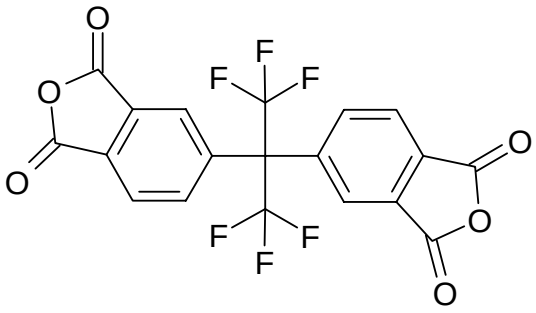

(6FDA) 2,2-bis(3,4-anhydrodicarboxyphenyl)hexafluoropropane, Clariant, CAS# 1107-00-2 *used as received*

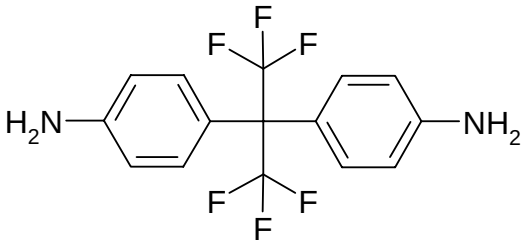

(6FpDA) 2,2 Bis(4-aminophenyl) hexafluoropropane, SynQuest Labs Inc., CAS# 1095-78-9 *sublimed before use*

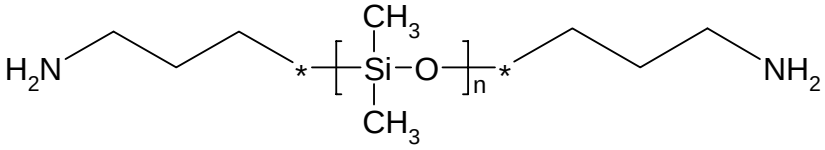

Aminopropyl terminated polydimethylsiloxane, Gelest Inc., CAS#106214-84-0 *used as received*

Benjamin Ray Vaughan was born on February 12, 1974 in Corvallis, Oregon. He moved to Christiansburg, VA at the age of seven where he spent his formidable years. In May, 1997 Ben received a Bachelors of Science in Environmental Science with a concentration in Aquatics from Virginia Tech. He spent the summer after his graduation year as a Christian missionary in Shizuoka, Japan. Following that summer he took a position as laboratory coordinator for Water Chemistry Inc. in Roanoke Virginia. While there he worked with local industry sampling and analyzing drinking water and waste water streams for various contaminants. Following several years at Water Chemistry Ben returned to Virginia Tech to work as a staff member in the Biological Systems Engineering department. He worked in the Water Lab where most of his time was spent on the Virginia rural household water quality program. This program was established to test well water samples at a reduced rate from the counties in Virginia for various contaminants and to report the results to the well owners. During his time as a staff member at Virginia Tech Ben began to take classes in the Chemistry and Chemical Engineering Departments. He resigned his staff position in BSE during the 2002-2003 academic school year to pursue the undergraduate courses in Chemical Engineering required to enter the graduate school. He was accepted to the Chemical Engineering graduate school in May, 2003 and worked that summer as a technician for Dr. Marand in the Gas Separations Lab. Following that summer he began his graduate work under the tutelage of Dr. Eva Marand in the area of gas separations with polymer aluminophosphate mixed matrix membranes. He graduated from Virginia Tech in May of 2007with a PhD in Chemical Engineering.